HIGH RESOLUTION ICE CORE RECORDS OF CLIMATE VARIABILITY AND FORCING

by

Joel B. Pedro
B. Sc., University of Western Australia
B. Antarctic Studies (Hons.), University of Tasmania

Submitted in fulfilment of the requirements for the degree of
Doctor of Philosophy
Institute for Marine and Antarctic Studies (IMAS)
University of Tasmania

June 2012

Declarations

Statement of originality

This thesis contains no material that has been accepted for a degree or diploma by the University or any other institution. The work contained in this thesis, except where otherwise acknowledged, is the result of my own investigations.

Signed:

Joel B. Pedro

Date: 6 June 2012

Statement of authority of access

This thesis may be available for loan and limited copying in accordance with the Copyright Act 1968.

Signed:

Joel B. Pedro

Date: 6 June 2012

Abstract

This thesis exploits the high temporal resolution and precise dating of ice cores from Law Dome, coastal East Antarctica, to address questions concerning climate forcings, variability and feedbacks over a range of timescales: (i) sub-annual to decadal-scale environmental influences on the ^{10}Be solar activity proxy; (ii) centennial to millennial-scale internal climate variability; and (iii) the phase relationship between Antarctic temperature and atmospheric CO_2 during the last deglaciation.

Cosmogenic ^{10}Be is a primary ice core proxy for past solar activity. However, interpretation of the ^{10}Be record is hindered by limited understanding of the physical processes governing its atmospheric transport and deposition to the ice sheets. The thesis presents a suite of monthly to annually-resolved Law Dome ^{10}Be records, which combined span 1936–2009. The records are quantitatively assessed against observed cosmic ray intensities, instrumental and reanalysis climate data and ECHAM5-HAM General Circulation Model (GCM) simulations. The seasonal variability in ^{10}Be is characterised by an (austral) summer to autumn concentration maximum and a winter concentration minimum. The GCM simulations, corroborated by earlier observations of ^{10}Be:^{7}Be ratios, link the seasonal concentration maximum to direct input of ^{10}Be from the Antarctic stratosphere to the lower levels of the Antarctic troposphere. On annual timescales, Law Dome ^{10}Be concentrations are significantly correlated to the 11-year solar cycle modulation of cosmic ray intensity, $r_{xy} = 0.54$, with 95% confidence interval (CI) $[0.31; 0.70]$. A significant correlation is also observed between annual ^{10}Be concentrations and the zonal wave three pattern of atmospheric circulation, $\mathrm{r}_{xy} = -0.36$, 95% CI $[-0.57; -0.10]$. An additional annually-resolved ^{10}Be record, from the Das2 site in southeast Greenland spanning 1936–2002, is analysed to facilitate inter-hemispheric comparisons. Das2 ^{10}Be concentrations are also significantly correlated to cosmic ray intensity, $r_{xy} = 0.45$, 95% CI $[0.22; 0.62]$ and to variability in the dominant mode of at-

mospheric circulation in the region, the North Atlantic Oscillation, $r_{xy} = -0.42$, 95% CI $[-0.64; -0.15]$. The strength and spectral coherence of the solar activity signal in ^{10}Be is enhanced, and the climate signals are reduced, when ^{10}Be records are combined from both Antarctica and Greenland. This implies that solar reconstructions are likely to be more robust when ^{10}Be records are included from multiple sites. The amplitudes of the 11-year solar cycles in the ^{10}Be records are inconsistent with the view that the ice sheets receive only ^{10}Be produced at polar latitudes, instead supporting that they sample from a globally well-mixed atmosphere. In addition, a chemical method is developed to remove the problematic ^{10}Be isobar boron-10 from Accelerator Mass Spectrometer (AMS) targets.

The last deglaciation was characterised by a 'bipolar seesaw' pattern of opposing hemispheric climate variations on millennial timescales. Precise information on the timing and sequence of these climate variations can assist in identifying the mechanisms involved. The timescale of the Law Dome ice core is synchronised throughout the deglaciation (using methane ties) with four other high-resolution Antarctic and Greenland cores. The stable water isotope signal in a composite record constructed from the synchronised Antarctic cores is interpreted as a temperature proxy for the Antarctic region. The millennial warming (and cooling) trends in the Antarctic record are matched by opposing cold (and warm) periods in Greenland. There is little-to-no time lag between climate transitions in Greenland and opposing changes in Antarctica. Such rapid signal-communication between the hemispheres supports the operation of rapid bipolar ocean and/or atmospheric teleconnections.

Two precisely dated ice core CO_2 records are synchronised to the same timescale as the Antarctic temperature proxy. These records show that the deglacial CO_2 increase lagged the Antarctic temperature increase by only 0 to 400 years. This implies a faster feedback between temperature and CO_2 than the centennial to millennial-scale lags suggested by previous studies.

Acknowledgements

I am most grateful to my advisors, Dr Tas van Ommen, Dr Mark Curran, Dr Andrew Smith and Dr Will Howard, for their support and guidance throughout my doctoral studies. Without their hard work over many years it would not have been possible to carry out this research. I thank Tas again for passing me the opportunity to work on the Law Dome records from the last deglaciation. This opened a new field to me, which it has been fascinating to begin to explore.

I would also like to thank the Antarctic Climate & Ecosystems CRC, a place where I have made many good friends and where I've had great support for my research, a fantastic place to work. Financially, I'm very grateful for the assistance that I've received from an Australian Post-Graduate Award and an Australian Institute of Nuclear Science and Engineering (AINSE) Post-Graduate Award.

Logistical support for the retrieval of ice core and snow pit records was provided by the Australian Antarctic Division (Australian Antarctic Science Projects AAS#2384, AAS#3064 and AAS#1172). The ^{10}Be measurements could not have been completed without the support of AINSE and the enthusiastic collaboration of the Isotopes in Climate Change and Atmospheric Systems (ICCAS) project at the Australian Nuclear Science and Technology Organisation (ANSTO).

In completing this research as a series of individual papers I have benefited greatly from the input of many coauthors. I sincerely thank all of them for their important contributions — Krista Simon, Dr David Child, Dr David Fink, Dr Ulla Heikkilä, Dr Andrew Moy, Dr Sarah Das, Dr Joe McConnell, Dr Sune Rasmussen, Dr Vin Morgan, Dr Jérôme Chappellaz, Dr Valerie Masson-Delmotte, Dr Mark Delmotte, Dr Andrew Smith, Dr Tas van Ommen and Dr Mark Curran (specific contributions are listed on pp. x–xii).

Chapter 2, was improved by insightful comments from Prof. William Webber and two anonymous referees. I also thank the Bartol Research Institute for provision of their McMurdo neutron record. Special thanks to Krista Simon for her help with carefully preparing so many ^{10}Be samples and to Dr Simon Wotherspoon for his advice on statistics.

Chapter 3, benefited from the assistance of Charles Mifsud, Dr Vlad Levchenko and Dr Stephan Winkler with AMS sample measurement and reprocessing and Dr Robert Ditchburn's suggestions on boron removal.

Chapter 4, could not have been completed without Dr Ulla Heikkila's enthusiastic support of my suggestion to make a new ECHAM5-HAM simulation for evaluation against the Law Dome ^{10}Be data. I thank Ulla also for hosting my visit to the Bjerknes Centre in 2008 which started our collaboration and for her endurance in helping to see the results through to publication. I'm also very grateful to Dr Andrew Klecociuk for responding to so many queries about reanalysis data. I acknowledge the German Computer Center (DKRZ) for donating the required computing time. I also thank Dr Andreas Stohl for providing insightful comments that contributed to the discussion and for generously making the FLEXPART data available.

Chapter 5, benefited from many researchers sharing their data and resources. Dr Andrew Smith contributed the DSS core for ^{10}Be measurement. Corridor discussions at the XXIX SCAR 2006 Open Science Conference resulted in Dr Joe McConnell and Dr Sarah Das generously contributing the remains of the Das2 Greenland core to the ^{10}Be cause. I thank the Australian Research Council Network for Earth System Science (ARCNESS) and the ACECRC, for contributing the funds which allowed me to travel to the Desert Research Institute (DRI) in Reno NV to sample the core. I also thank the staff and students of the DRI ice core lab for their assistance in analysing the ice cores. I'm grateful to Prof. Ilya Usoskin for providing me with the CRAC:10Be model data.

Chapter 6, owes a special thanks to Dr Sune Rasmussen who generously shared his expertise on synchronising ice core timescales – thanks also for all the laughs. Sune's visit to the ACE CRC and our collaboration could not have occurred without the support of an Inge Lehmann grant. I also acknowledge the constructive reviews provided by Prof. Ed Brook and Prof. Eric Wolff, which improved the quality of the final manuscript.

Chapter 7, was assisted by grants from the Trans-Antarctic Association and University of Tasmania that enabled me to present the work at the XVIII INQUA conference in Bern Switzerland and obtain feedback from international researchers. The final version of the manuscript was written during my subsequent visit to the Neils Bohr Institute's Centre for Ice and Climate (CIC). I thank Sune for hosting this visit and CIC and the North Atlantic INTIMATE group for providing financial assistance.

Throughout the thesis I have been encouraged and sometimes challenged by interactions with some great and generous scientist: I thank, in particular, Prof. Bill Budd, Prof. Juerg Beer, Dr Ken McCracken, Dr Dietmar Wagenbach, Prof. David Karoly and Vin Morgan.

I have experienced some wonderful and stimulating travels during my PhD. Ice coring in Antarctica in 2008/09, science out of tents at $-20°C$, was a great experience and bloody good fun. I thank Mark and Tas and the Australian Antarctic Division again for the privilege. My sincere thanks also to the Australian Academy of Science and the Council for the Lindau Nobel Laureate Meetings for inviting me to Germany in 2010 with the Australian delegation to the inspiring Lindau Meeting of Nobel Laureates.

For me, going from farm boy on the south coast of Western Australia to the world of Earth and climate science, has been a fascinating adventure. I always wanted to be a scientist and I thank my family for encouraging me on my journey. Finally, I thank Laura for all her help and care these past years.

Statement of co-author contributions

Chapters 2–7 of this thesis have all been prepared as manuscripts for submission to peer-reviewed journals. Unless otherwise specified, the design and implementation of the research, ice core dating, data interpretation, numerical analysis and manuscript writing were the responsibility of the candidate but were carried out in consultation with supervisors and with input from specialist contributors. These contributions are outlined for each chapter below.

Chapter 2: Pedro, J. B, A. M. Smith, K. J. Simon, T. D. van Ommen and M. A. J. Curran, High-resolution records of beryllium-10 in ice from Law Dome, East Antarctica: measurement, reproducibility and principal trends, *Climate of the Past*, 7, 707-721, doi:10.5194/cp-7-707-2011, 2011.

– J. B. Pedro designed the research project, led laboratory sampling and chemical preparation of the ice samples, dated the ice cores and conducted the data interpretation, numerical analysis and writing. J. B. Pedro also assisted with the AMS ^{10}Be measurements and fieldwork/ice core drilling. A. M. Smith led the AMS ^{10}Be measurements. K. J. Simon assisted with chemical preparation of the ^{10}Be samples. T. D. van Ommen advised on sample dating. M. A. J. Curran advised on ice core chemistry. All coauthors commented on the manuscript.

Chapter 3: Simon, K. J., J. B. Pedro, A. M. Smith, D. P. Child and D. Fink, Reprocessing of ^{10}B-contaminated ^{10}Be AMS targets, in review (submitted July 2011), *Nuclear Instruments & Methods in Physics Research B*.

– K. J. Simon developed the chemical technique for boron removal, with assistance from all coauthors and led the writing. J. B. Pedro led the experiments to identify the source of boron contamination. A. M. Smith and D. Fink conducted the AMS ^{10}Be measurements. All coauthors commented on the manuscript and contributed to the experimental design.

Chapter 4: Pedro, J. B., U. E Heikkilä, A. Klekociuk, A. M. Smith, T. D. van Ommen and M. A. J. Curran, Beryllium-10 transport to Antarctica: results from seasonally-resolved observations and modeling, *Journal of Geophysical Research (Atmospheres)*, 116, D23120, doi:10.1029/2011JD016530, 2011.

– J. B. Pedro proposed the project and led the data interpretation and writing. U. E. Heikkillä conducted the ECHAM5-HAM model run and advised on its interpretation. A. Klekociuk provided the tropopause-height data and advised on polar meteorology. M. A. J. Curran advised on ice core chemistry. T. D. van Ommen advised on ice core dating. All coauthors commented on the manuscript.

Chapter 5: Pedro, J. B., J. R. McConnell, T. D. van Ommen, D. Fink, M. A. J. Curran, A. M. Smith, A. D. Moy and S. B. Das, Constraining solar activity and climate influences on ice core ^{10}Be records from Antarctica and Greenland during the neutron monitor era, in review (submitted January 2012), *Earth and Planetary Science Letters*.

– J. B. Pedro conducted the ice core sampling, chemical preparation, numerical analysis, data interpretation, manuscript preparation and also assisted with the AMS ^{10}Be measurements. S. B. Das contributed the Das2 core. J. R. McConnell dated the Das2 core and led the measurement of non sea-salt-sulphur concentrations on the Das2 and DSS cores. A. M. Smith drilled the DSS core and along with D. Fink conducted the AMS ^{10}Be measurements. M. A. J. Curran advised on ice core chemistry. A. D. Moy measured the DSS and Das2 δ^{18}O records. K. J. Simon assisted with chemical preparation of the samples. All coauthors commented on the manuscript.

Chapter 6: Pedro, J. B., T. D. van Ommen, S. O. Rasmussen, V. I. Morgan, J. Chappellaz, A. D. Moy, V. Masson-Delmotte and M. Delmotte, The last deglaciation: timing the bipolar seesaw, *Climate of the Past*, 7, 671–683, 10.5194/cp-7-671-2011, 2011.

– J. B. Pedro developed the idea of a Antarctic deglacial composite, led the placement of records onto the Greenland Ice Core Chronology 2005 (GICC05) and conducted the numerical analysis, data interpretation and writing. T. D. van Ommen assisted with construction of the revised deglacial ice and gas chronologies for Law Dome. S. O. Rasmussen advised on ice core timescales. J. Chappellaz and T. D. van Ommen led the Law Dome CH_4 measurements, with assistance from J. B. Pedro in the laboratory sampling. A. D. Moy conducted new δ^{18}O measurements on the Law Dome core. All coauthors commented on the manuscript.

Chapter 7: Pedro, J. B., S. O. Rasmussen and T. D. van Ommen, Rapid coupling of Antarctic temperature and CO_2 during deglaciation, Clim. Past Discuss., 8, 621-636, doi:10.5194/cpd-8-621-2012, 2012.

– J. B. Pedro developed the idea of constraining the CO_2/Antarctic temperature phasing using the Antarctic deglacial composite and near-coastal CO_2 records. J. B. Pedro conducted the synchronisation of all records to GICC05 and led the manuscript preparation. S. O. Rasmussen advised on ice core timescales refined the lag determination technique. T. D. van Ommen gave guidance and advice at all stages of the work. All coauthors commented on the manuscript.

Contents

List of Figures

List of Tables

Chapter 1

Introduction

1.1 Ice cores as archives of past climate variability and forcing

Ice cores, extracted from the polar ice sheets, are among the richest sources of information on past climate [e.g. *Wolff*, 2000]. The thesis is focused on three important ice core parameters: the cosmogenic radionuclide beryllium-10 (^{10}Be) trapped within the ice, the oxygen isotope ratios (δ^{18}O) of the ice itself, and the CO_2 gas extracted from the ice core air bubbles. These parameters are used in reconstructions of key aspects of climate variability and forcing: from ^{10}Be, external solar forcing [e.g. *Bard et al.*, 2000; *Usoskin et al.*, 2009; *Steinhilber et al.*, 2009]; from δ^{18}O, local to regional scale temperature variations [*Dansgaard*, 1964; *Petit et al.*, 1999; *Lowe et al.*, 2008]; and from CO_2, details of the internal greenhouse gas feedback [e.g. *Fischer et al.*, 1999; *Monnin et al.*, 2001; *Wolff*, 2011]. However, there are many challenges to the reliable interpretation of such records [e.g. *Wolff*, 1996; *Jouzel et al.*, 1997; *Jones et al.*, 2009]. Foremost among these, and an overarching theme of the thesis, is the need for accurate and/or precise dating. Well-constrained dating is a prerequisite for (i) proxy evaluation against instrumental or model-derived data [e.g. *Vinther et al.*, 2003; *Abram et al.*, 2011], (ii) synthesising records from multiple sites [e.g. *Fisher et al.*, 1996; *Andersen et al.*, 2006; *Rasmussen et al.*, 2008], and (iii) identification of leads and lags in the climate system, in turn crucial for separating cause from effect (or forcing from response) [e.g. *Sowers and Bender*, 1995; *Blunier and Brook*, 2001; *Morgan et al.*, 2002; *Mudelsee*, 2003;

Ganopolski and Roche, 2009]. A second major challenge and also a common theme throughout the thesis, is separating the signal of interest from 'noise' introduced by other environmental variables, and the application of techniques to improve the signal to noise ratio [e.g. *Fisher et al.*, 1996; *White et al.*, 1997; *Vinther et al.*, 2003; *Muscheler et al.*, 2007].

High temporal resolution ice core ^{10}Be, δ^{18}O and CO_2 records are used as tools in the thesis to address these challenges. The temporal resolution achievable at an ice core site is primarily controlled by the thickness of its annual snow accumulation layers. This leads to a focus on ice cores from high-accumulation/near-coastal sites, mainly Law Dome Summit South (DSS), Coastal East Antarctica, complemented by intercomparisons with cores from other Antarctic and Greenland sites. Due to the thinning of annual ice layers with ice sheet depth, the maximum temporal resolution at which information can be extracted from the ice decreases as the depth in the ice sheet and age of the ice increase. The term high-resolution is used here in a relative sense to refer to records which are among the most finely resolved currently available for the periods under investigation.

The chapters comprising the thesis have all been prepared for, or recently published in peer-reviewed international journals. While there are common themes throughout the work, it should be made clear that the chapters focused on ^{10}Be address objectives that are distinct from those of the chapters focused on δ^{18}O and CO_2. These objectives are set out in the following sections. More detailed overviews of the literature most relevant to each chapter are provided in their respective introductory sections.

1.1.1 Ice core ^{10}Be as a solar proxy

The production rate of ^{10}Be in the Earth's atmosphere is proportional to cosmic ray intensity [*Lal and Peters*, 1967]. The physical basis for the use of ^{10}Be as a solar proxy is that cosmic ray intensity is modulated by solar (magnetic) activity, which in turn is related to changes in solar irradiance and hence climate forcing [*Cane et al.*, 1999; *Lean et al.*, 2002; *McCracken et al.*, 2004; *Steinhilber et al.*, 2009]. The physics of the solar activity control on the ^{10}Be production rate is relatively well understood and captured by models [*Masarik and Beer*, 1999; *Webber and Higbie*, 2003; *Webber et al.*, 2007; *Masarik and Beer*, 2009; *Kovaltsov and Usoskin*, 2010]. However, complexity is

introduced by the time-variable and climate-sensitive processes which transfer ^{10}Be from its point of production in the atmosphere to the ice core archive [*McHargue and Damon*, 1991; *Beer*, 2000]. Limited understanding of these non-production or 'climate effects' is arguably the largest source of uncertainty hindering the quantitative reconstruction of solar activity from the ice core record [*Muscheler et al.*, 2007; *Delaygue and Bard*, 2011]. The thesis aims to improve understanding of climate influences on ^{10}Be records and to quantify their strengths relative to production-related signals. The main questions or points of debate in current understanding of ^{10}Be records that are addressed in the thesis include the following:

- concerns regarding poor reproducibility of ^{10}Be records sampled from different locations [*Moraal et al.*, 2005];

- whether there is a significant seasonal cycle in ^{10}Be concentrations in Antarctica and if so what are the main factors driving it [*Pedro et al.*, 2006];

- the transport pathways which deliver ^{10}Be to the ice sheets, in particular, whether there is substantial stratosphere to troposphere exchange of ^{10}Be across the polar tropopause [*Wagenbach et al.*, 1988; *McHargue and Damon*, 1991];

- whether a previously reported relationship [*Pedro et al.*, 2006] between δ^{18}O and ^{10}Be observed on sub-annual timescales holds on annual timescales;

- uncertainties regarding the effect of changes in atmospheric circulation on ^{10}Be, and in particular whether long term changes in circulation may influence the ice core record, as suggested for example by *Lal* [1987], and *Field et al.* [2006], though contested by *Heikkilä et al.* [2009].

- the atmospheric source regions of the ^{10}Be deposited to the ice sheets, i.e. the extent of meridional mixing of ^{10}Be prior to deposition [*Mazaud et al.*, 1994; *Steig et al.*, 1996; *Bard et al.*, 2000; *Field et al.*, 2006; *Heikkilä et al.*, 2009];

- the efficacy of combining ^{10}Be records from different sites as a means to enhance the production signal, as used for example by *Muscheler et al.* [2007] and *Usoskin et al.* [2009].

These questions are addressed by evaluating high-resolution ^{10}Be records spanning recent decades against cosmic ray intensities, observed and reanalysis climate data, general circulation model results and various ice core parameters.

1.1.2 Ice core δ^{18}O and CO_2 records of internal climate variability and feedbacks

There is a well-documented linear relationship in the middle and high latitudes between the mean annual δ^{18}O isotope content of precipitation and the mean annual temperature at the precipitation site [*Craig*, 1961; *Dansgaard*, 1964]. This relationship, which is particularly well conformed to over Antarctica and Greenland, is the basis for using δ^{18}O in ice as a palaeo-temperature proxy [*Jouzel et al.*, 1997]. However, as with ^{10}Be, several factors complicate the interpretation of the record. For example, δ^{18}O may also be affected by evaporative origin, seasonal distribution of precipitation, site elevation and anomalous ice flow, all of which may change under different climates [e.g. *Steig et al.*, 1994; *Jouzel et al.*, 1997; *Masson-Delmotte et al.*, 2008]. By contrast, CO_2 extracted from the bubbles trapped within Antarctic ice cores serves not as a proxy but rather as a direct measurement of past atmospheric CO_2 concentrations (note that this is not necessarily the case for Greenland CO_2 records, which are affected, particularly during glacial times, by post-depositional reactions involving their high concentrations of carbonates [*Tschumi and Stauffer*, 2000]). A complicating factor in the interpretation of the CO_2 record is that diffusive and bubble trapping processes lead to an age offset (Δage) between the ice and trapped gas at a given point in the ice core. The Δage is larger and associated with greater uncertainty at ice core sites with low accumulation rates [e.g. *Loulergue et al.*, 2007].

Focus is directed here toward δ^{18}O and CO_2 records from the last deglaciation, $\sim$ 19–11 thousand years before present (ka BP). This period is the most recent example of a major naturally forced global climate change, making it a key testing ground for the use of δ^{18}O and CO_2 records to examine internal climate variability and feedbacks. The deglaciation was characterised by an overall warming in both hemispheres. However, on millennial and shorter timescales, climate evolution at northern and southern high-latitudes was very different [*Sowers and Bender*, 1995; *Blunier and Brook*, 2001; *Shakun and Carlson*, 2010]. In Greenland the deglaciation was punctuated by the abrupt Bølling-Allerød (GI-1a-e) warming which was later followed by a return to the

near glacial conditions of the Younger Dryas (GS-1) before a final abrupt warming that marked the onset of the Holocene [*Steffensen et al.*, 2008; *Lowe et al.*, 2008]. By contrast, the deglaciation in Antarctica was characterised by more gradual temperature rise interrupted by a period of cooling during the Antarctic Cold Reversal (ACR) [*Jouzel et al.*, 1995; *Blunier et al.*, 1998; *Morgan et al.*, 2002; *Stenni et al.*, 2011]. The Antarctic temperature trend was matched closely by changes in atmospheric CO_2; current estimates suggest that the deglacial temperature rise preceded the rise in atmospheric CO_2 by $\sim$ 200–1400 years [*Fischer et al.*, 1999; *Monnin et al.*, 2001].

The bipolar seesaw concept proposes that the opposing north-south climate oscillations result from oscillations in the strength and direction of heat transport in the Atlantic Ocean [*Broecker*, 1998; *Stocker and Johnsen*, 2003]. More recently, a (potentially complimentary) inter-hemispheric coupling mechanism has been proposed involving atmospheric teleconnections [*Anderson et al.*, 2009; *Toggweiler and Lea*, 2010]. Changes in physical and biogeochemical processes in the high-latitude Southern Ocean are suggested to link these mechanisms to deglacial changes in the atmospheric CO_2 concentration [*Schmittner and Galbraith*, 2008; *Skinner et al.*, 2010; *Anderson and Carr*, 2010; *Lee et al.*, 2011]. Tighter constraints on the relative timing of the changes in Antarctic and Greenland temperatures and in CO_2 can contribute to sorting out the relative roles of these mechanisms and provide more stringent test criteria for the models seeking to simulate the processes involved [*Skinner*, 2008; *Ganopolski and Roche*, 2009]. The main questions or points of current debate in the field that are addressed in the thesis include:

- the timing of the ACR onset and termination and the extent to which the ACR-timing varies between Law Dome and other Antarctic sites [*Morgan et al.*, 2002; *Stenni et al.*, 2011];
- the relative timing of the ACR onset and termination with respect to the Bølling (GI-1e) and Younger Dryas (GS-1) onsets [*Blunier and Brook*, 2001; *Morgan et al.*, 2002; *EPICA Community Members*, 2006];
- the phase relationship during deglaciation between atmospheric CO_2 and Antarctic temperature [*Fischer et al.*, 1999; *Monnin et al.*, 2001; *Ahn et al.*, 2004; *Mudelsee*, 2003].

To tackle these questions, the $\delta^{18}O$ records from Law Dome and four other high-resolution Antarctic sites are placed onto a onto a single timescale common with Green-

land ice cores and two Antarctic CO_2 records. The common timescale then permits a detailed examination of the sequence of deglacial climate change.

1.2 Approach

Chapters 2–5 detail the measurement and dating of a suite of new ^{10}Be records and then examine these records for solar and climate signals on sub-seasonal to decadal timescales. Chapters 6–7 move to the centennial-to-millennial timescales of the last deglaciation, first detailing the synchronisation of Antarctic and Greenland records and then examining the timing of the bipolar seesaw and CO_2 feedback. The research approach and questions addressed in each chapter are detailed below.

Chapter 2 presents five quasi-monthly resolved ^{10}Be records, all sampled from different locations on Law Dome Summit South (DSS). The chapter begins with a description of the techniques used in the sampling, chemical preparation and measurement of the records. Reproducibility is assessed through intercomparison of the five records. A single 10-year (1999 to 2009) composite series is constructed from these records and evaluated against observed cosmic ray intensities. A lag correlation analysis between the composite and cosmic ray intensity is used to constrain the atmospheric residence time of the ^{10}Be deposited to the site. The relationship between δ^{18}O and ^{10}Be is also examined.

Chapter 3 details a chemical method developed to remove the problematic ^{10}Be isobar boron-10 from AMS targets.

Chapter 4 continues analysis of the 10-year ^{10}Be composite, using the seasonal cycle in ^{10}Be concentrations as a tool to identify physical processes affecting ^{10}Be transport and deposition. The analysis is complemented by ECHAM5-HAM GCM simulations of ^{10}Be deposition to the site. A complete description of the seasonal cycle required accurate information on the intra-annual variability in the snow accumulation rate (see also Appendix A.). Particular attention is paid to seasonal variability in the pathways of ^{10}Be transport and the potential for exchange across the polar tropopause.

Chapter 5 presents two annually-resolved ^{10}Be records, one from DSS, Law Dome (spanning 1936–2009) and one from the high-accumulation Das2 site in southeast Greenland (spanning 1936–2002). The time-periods are selected to overlap with the instru-

mental records of cosmic ray intensity and modern observed and reanalysis climate data. Following insights into the seasonal variability of ^{10}Be gained in Chapter 4, both records are physically sampled in a way that minimises the risk of seasonal aliasing in annual average concentrations. ^{10}Be concentrations and fluxes in both records are evaluated quantitatively against cosmic ray intensities, snow accumulation rates, δ^{18}O ratios and dominant modes of atmospheric circulation. The chapter then tests whether the strength and spectral properties of the production signal in ice core ^{10}Be are enhanced in a composite record constructed from all available annually resolved ^{10}Be records spanning this period. Finally, the production source regions of the ^{10}Be deposited to the ice sheets are probed by comparing the relative amplitudes of the 11-year solar cycles in ^{10}Be concentration with model estimates of the amplitudes of the solar cycles in ^{10}Be production in the global and polar atmosphere. Potential implications of the findings for ^{10}Be-based solar activity reconstructions are discussed.

Chapter 6 directly addresses uncertainties regarding the regional trends in Antarctic climate during the deglaciation and their time-relationships with climate transitions in Greenland. The chapter begins by presenting new methane measurements on the Law Dome deep ice core. Using the rapid, and effectively globally synchronous variations in methane during the deglaciation as time markers, the Law Dome core is placed on a timescale common with Greenland cores and four other high-resolution Antarctic records. The common timescales permit construction of an Antarctic deglacial δ^{18}O composite. It is argued that the composite can be interpreted as a proxy for temperature in the Antarctic region. The composite is compared with Greenland records to assess the inter-hemispheric sequence of deglacial climate variations. Results are discussed in the context of inter-hemispheric climate coupling mechanisms, including the bipolar ocean seesaw and bipolar atmospheric teleconnections.

Chapter 7 utilises the Antarctic δ^{18}O composite from Chapter 6 to examine the timescales of the atmospheric CO_2 feedback during deglaciation. The chapter begins by placing two previously published CO_2 records onto the common GICC05 timescale. The phase relationship between the δ^{18}O composite and CO_2 rise is determined by maximising their time-lagged correlation. The sensitivity of the lag to CO_2 measurement uncertainties, differences between the two CO_2 data sets, and variations in lag determination procedure are determined by a Monte Carlo-style sensitivity analysis. The chapter finishes by commenting on the compatibility of the results with current concepts of the mechanisms controlling the deglacial CO_2 feedback.

Chapter 8 concludes the thesis by emphasising overarching themes, reiterating the main findings and suggesting future research directions.

Chapter 2

High-Resolution Records of the ^{10}Be Solar Activity Proxy in Ice from Law Dome, East Antarctica: Measurement, Reproducibility and Principal Trends

J. B. Pedro[1,2], A. M. Smith[3], K. J. Simon[3], T. D. van Ommen[2,4] and M. A. J. Curran[2,4]

Published July 2011 in *Climate of the Past*, 7, 707-721, doi:10.5194/cp-7-707-011.

[1]Institute of Marine and Antarctic Studies, University of Tasmania, Hobart, TAS, Australia
[2]Antarctic Climate and Ecosystems Cooperative Research Centre, Hobart, TAS, Australia
[3]Australian Nuclear Science and Technology Organisation, Menai, NSW, Australia
[4]Australian Antarctic Division, Kingston, TAS, Australia

Abstract

Three near-monthly resolution ^{10}Be records are presented from the Dome Summit South (DSS) ice core site, Law Dome, East Antarctica. The chemical preparation and Accelerator Mass Spectrometer (AMS) measurement of these records is described. The reproducibility of ^{10}Be records at DSS is assessed through intercomparison of the ice core data with data from two previously published and contemporaneous snow pits. We find generally good agreement between the five records, comparable to that observed between other trace chemical records from the site. This result allays concerns raised by a previous Antarctic study [*Moraal et al.*, 2005] about poor reproducibility of ice core ^{10}Be records. A single composite series is constructed from the three ice cores providing a monthly-resolved record of ^{10}Be concentrations at DSS over the past decade (1999 to 2009). To our knowledge, this is the first published ice core data spanning the recent exceptional solar minimum of solar cycle 23. ^{10}Be concentrations are significantly correlated to the cosmic ray flux recorded by the McMurdo neutron monitor ($r_{xy} = 0.64$, with 95 % CI of 0.53 to 0.71), suggesting that solar modulation of the atmospheric production rate may explain up to ∼40 % of the variance in ^{10}Be concentrations at DSS. Sharp concentration peaks occur in most years during the summer-to-autumn, possibly caused by stratospheric incursions. Our results underscore the presence of both production and meteorological signals in ice core ^{10}Be data.

2.1 Introduction

Atmospheric cosmogenic beryllium-10 (^{10}Be) in polar ice is an important proxy for past variations in solar activity and cosmic ray intensity [*Bard et al.*, 2000; *McCracken et al.*, 2004; *Vonmoos et al.*, 2006; *Steinhilber et al.*, 2009]. Ice core ^{10}Be records therefore offer great potential for use in refining our understanding of links between solar activity and climate. However, obtaining reliable information from the ^{10}Be record requires proven sample processing and measurement techniques, along with a good understanding of the sequence of environmental processes controlling production in the atmosphere and ultimate storage in the ice sheet. We have developed a methodology for accurate measurement of high-resolution, precisely-dated ice core and snow pit ^{10}Be records that can be used to improve understanding of environmental influences on ^{10}Be concentrations in ice.

^{10}Be (half-life, $(1.36 \pm 0.07) \times 10^6$ years [*Nishiizumi et al.*, 2007]) is produced in the lower stratosphere and troposphere by the spallation of N and O atoms by galactic cosmic rays (GCR) [*Lal and Peters*, 1967]. Variations in the solar magnetic field modulate the GCR flux and therefore the atmospheric production rate of ^{10}Be. Variations in the solar magnetic field are also correlated to variations in solar irradiance; it is this relationship that is the basis for using long-term variations in ^{10}Be concentrations in polar ice as proxy records of past solar irradiance [*Beer*, 2000]. Additionally, the terrestrial magnetic field also modulates the GCR, however, this occurs mainly over centennial to millennial timescales [*Muscheler et al.*, 2007] that are outside the scope of the present study.

The challenge of measuring the extremely low concentrations of ^{10}Be in polar ice (of order 10^4 atoms g^{-1}) was met by Accelerator Mass Spectrometry (AMS) techniques developed in the 1970's [e.g. *Raisbeck et al.*, 1978]. ^{10}Be records have now been produced from multiple polar ice core sites, in both Greenland (e.g., Dye 3, GRIP, GISP2, Renland [*Beer et al.*, 1990, 1991; *Yiou et al.*, 1997; *Finkel and Nishiizumi*, 1997; *Aldahan et al.*, 1998; *Heikkilä et al.*, 2008c]) and Antarctica (e.g., Dome Concordia, South Pole, Dome Fuji, Taylor Dome, Queen Maud Land, Dronning Maud Land and Law Dome [*Raisbeck et al.*, 1990; *Steig et al.*, 1996; *Aldahan et al.*, 1998; *Smith et al.*, 2000; *Moraal et al.*, 2005; *Pedro et al.*, 2006; *Horiuchi et al.*, 2008; *Pedro et al.*, 2009]). Particular care in sample preparation and measurement is required for samples from Law Dome, where ^{10}Be concentrations are the lowest of all of these sites. A major challenge to the sensitivity of AMS measurement of ^{10}Be is interference from the isobar boron (^{10}B) [e.g. *Aldahan et al.*, 1998; *Pedro et al.*, 2009]. To this end, our previous sample processing technique [*Child et al.*, 2000] has been modified by introducing several steps aimed at reducing the levels of ^{10}B in samples.

Following measurement, a number of factors complicate the interpretation of the ^{10}Be record. One of these, which is a potential issue hindering the interpretation of all ice core trace chemicals, is the physical reworking or chemical alteration of the snow pack after deposition [*Wolff*, 1996]. This may occur, for example, by removal, re-deposition and/or mixing of near-surface snow by the wind, ablation, melt, sublimation or post-depositional chemical exchange between the atmosphere and ice [*Jones et al.*, 2009]. Recently, questions have been raised about the potential for significant post-depositional influences on ^{10}Be in a study that found up to fourfold differences in ^{10}Be concentrations between two records extracted from the Queen Maud Land Ice Shelf [*Moraal et al.*, 2005]. The cause of this discrepancy was not resolved, however, it was

proposed that local scale and/or post-depositional factors were involved. This study, although not carried out at a proven ice core site, has contributed to concern about the reliability of ice core records of ^{10}Be more generally [e.g. *Webber and Higbie*, 2010]. Such concerns need to be resolved before historical ^{10}Be records can be confidently used to infer past variations in solar activity or cosmic ray intensity [*Webber and Higbie*, 2010]. Addressing this issue requires multiple ice cores from nearby locations. However, with the exception of the *Moraal et al.* [2005] study, multiple records from individual Antarctic or Greenland ice core sites have not previously been available. This has been a motivation for high-resolution study of ^{10}Be deposition at the Law Dome ice core site.

A second motivation for accessing high-resolution and well dated ^{10}Be records is to directly test the response of ^{10}Be concentrations in ice to variations in the atmospheric production rate. The parameter most suited to conducting such tests is the GCR flux recorded by ground-based neutron monitors. Neutron monitors provide a precise and high time resolution measure of the GCR that is linearly related to the ^{10}Be production rate at any point in the Earth's atmosphere [*O'Brien and Burke*, 1973]. By contrast, the sunspot record is less useful since the relationship between sunspots and ^{10}Be production is neither linear nor direct [*Lean et al.*, 2002; *McCracken et al.*, 2004]. Previously, testing the relationship between ^{10}Be and the GCR has been limited by a scarcity of ^{10}Be records that are contemporaneous with the era of neutron monitor measurements beginning in the 1950s. Of the handful of comparisons that have been made (Taylor Dome Antarctica [*Steig et al.*, 1996], Queen Maud Land Antarctica [*Moraal et al.*, 2005], GRIP and Dye 3, Greenland [*Berggren et al.*, 2009] and Renland, Greenland [*Aldahan et al.*, 1998]), in all cases, trends in ^{10}Be data consistent with the 11-year Schwabe cycle modulation of the atmospheric production rate are observed. However, each site is also affected by environmental factors unrelated to atmospheric production [*Field and Schmidt*, 2009; *Webber and Higbie*, 2010]. Constraining the strength of the production rate signal at Law Dome, and hence the sites suitability for obtaining a long-term record of past solar activity, is also an objective of the present study.

Distinguishing our work from studies at other sites is the near-monthly resolution of the Law Dome data, compared to annual and coarser at the other sites. This high resolution, combined with accurate dating also permits the investigation of short-term (monthly to seasonal) variations in ^{10}Be concentrations and their possible causes.

2.2 Methods

2.2.1 The Law Dome ice core site

Law Dome is a small ($\sim$ 200 km diameter) ice cap, situated in Wilkes Land, Coastal East Antarctica (Fig. 2.1). The icecap is separated from the flow of the main East Antarctic ice sheet and is the most northerly point on the Antarctic coast outside the Antarctic Peninsula [*Morgan et al.*, 1997]. The passage of cyclonic systems originating to the north combined with the polar easterlies and the orographic influence of Law Dome, produces exceptionally high accumulation, which is relatively uniformly distributed throughout the year with respect to other deep Antarctic ice core sites [*van Ommen and Morgan*, 1997].

The high accumulation rate at DSS (0.68 m year^{-1} ice), coupled with low annual mean wind-speed (8.3 m s^{-1}) and perennially low temperatures (summer mean: $-12.6\,^{\circ}$C) [*Morgan et al.*, 1997] results in the preservation of unambiguous annual snow layers. These thick annual layers can be reliably detected using a variety of measurement techniques and counted to produce accurate dating (Sect. 2.2.5). Hence, ice core and snow pit records from DSS are particulary suited to investigating annual to sub-annual variations in the trace chemical concentrations of snow and this has been a focus of prior glaciological work at the site e.g., [*van Ommen and Morgan*, 1997; *Curran et al.*, 1998; *Palmer et al.*, 2001].

The ^{10}Be records discussed here were taken from close to the Dome Summit South ice core drilling site (DSS: 66°46′ S 112°48′ E), 4.6 km south-southwest from the summit of the Dome (Fig. 2.1).

2.2.2 Law Dome ^{10}Be records

Three new ^{10}Be ice core records (total of 117 samples) from the DSS site, sampled at near-monthly resolution, are presented here: DSS0506-core, DSS0809-core and DSS0910-core. These new records are also compared with two previously published snow pit records: DSS0102-pit and DSS0506-pit [for sampling details refer to *Pedro et al.*, 2006; *Pedro et al.*, 2009]. The names of the records refer to the sample site ("DSS") followed by the (austral) summer during which sampling took place (e.g., "0506" refers

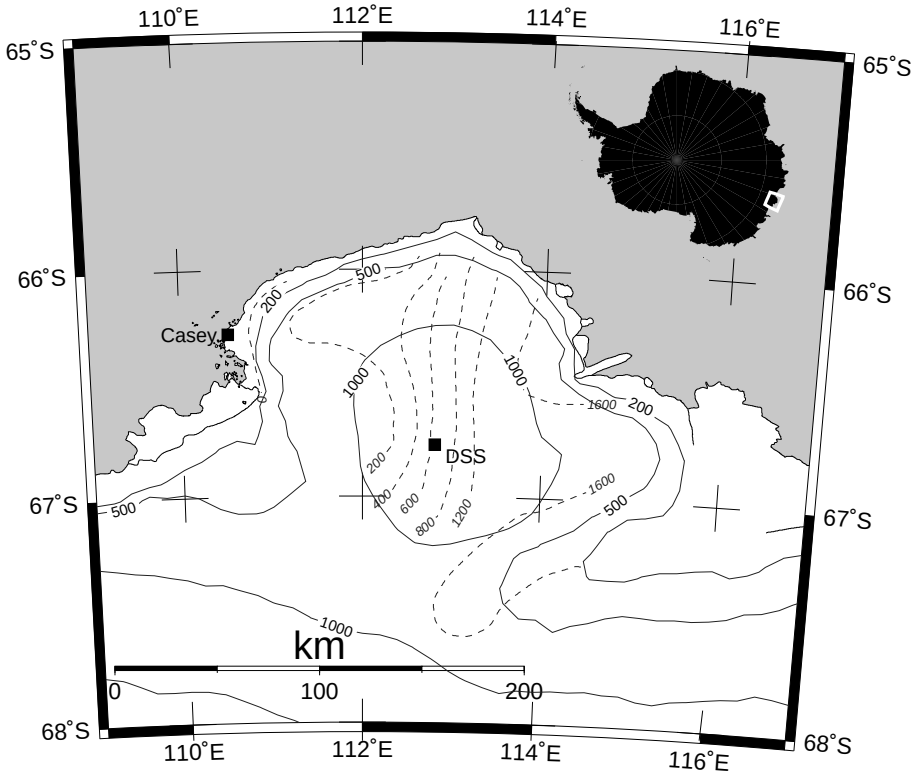

Figure 2.1: Location of the Dome Summit South (DSS) sample site, Law Dome with surface elevation contours (m, solid lines) and accumulation isopleths (mm ice equivalent, dashed lines).

to summer of 2005 to 2006).

DSS0506-core was drilled using a 195 mm diameter thermal drill [see also *Burn-Nunes et al.*, 2011], whilst DSS0809 and DSS0910-core were drilled using 79 mm diameter Polar Ice Core Office (PICO) hand augers. Three PICO cores were drilled alongside each other in order to obtain sufficient mass for ^{10}Be measurements. A summary of the key details of each ^{10}Be record discussed in the text is provided in Table 2.1.

2.2.3 Sample preparation

^{10}Be samples were cut from the ice cores continuously at the depth intervals listed in Table 2.1. For the PICO cores, ice from the three adjacent cores was combined into one sample. Sample masses ranged between 0.5 to 2.0 kg. All work took place in a HEPA-filtered cold laboratory using a stainless steel band-saw.

Detailed stable water isotope (δ^{18}O) and trace chemical records were also extracted from the cores at high resolution (ranging from 3.0 to 6.0 cm). For δ^{18}O measurements, sub-samples (0.4 ml) were equilibrated with CO_2 at 25 °C with a VG Isoprep-18 equilibration bench. δ^{18}O ratios of the equilibrated CO_2 were measured on a VG Isogas SIRA mass spectrometer at the Central Science Laboratory, University of Tasmania. The δ^{18}O values are expressed as per mil (‰) with respect to Vienna Standard Mean Oceanic Water (V-SMOW). Standard deviation of the δ^{18}O values for repeated measurements of laboratory reference water samples was less than 0.07 %. Trace chemical measurements were performed by suppressed ion chromatography following previous techniques [*Curran and Palmer*, 2001].

2.2.4 Extraction of ^{10}Be from ice and AMS measurement

A flow chart depicting the procedure for preparing ^{10}Be samples for Accelerator Mass Spectrometer (AMS) measurement is shown in Fig. 2.2. This updated procedure, which was used on the DSS0506-core, DSS0809-core and DSS0910-core, is based on the methods for extraction of ^{10}Be from aqueous samples described by *Child et al.* [2000] and *Smith et al.* [2000], with recent revisions aimed at improving efficiency and reducing levels of the isobaric AMS interferant boron (see also Chapter 3).

All equipment was rinsed with dilute HNO_3 solution and then triple rinsed with deionised

Table 2.1: Details of the high-resolution DSS, Law Dome ^{10}Be snow pit and ice core records discussed in the text.

^{10}Be record (sample type)	Location	Samples	Resolution (metres, months)	Period spanned	Mean ^{10}Be $\pm 1\sigma$ ($\times 10^3$ atoms g^{-1})
DSS0102-pit (snow pit)	66°46′09″ S 112°48′38″ E	20	0.10, 0.57	Jan 2001–Dec 2001	5.00 ± 1.91
DSS0506-pit (snow pit)	66°46′11″ S 112°48′41″ E	40	0.10, 0.78	Mar 2004–Oct 2005	5.52 ± 1.77
DSS0506-core (thermal core)	66°46′20″ S 112°48′26″ E	62	0.13, 1.07	Dec 1999–Jun 2005	4.61 ± 1.43
DSS0809-core (PICO core)	66°46′02″ S 112°48′28″ E	40	0.14, 1.25	Dec 2004–Dec 2008	7.58 ± 1.94
DSS0910-core (PICO core)	66°46′02″ S 112°48′28″ E	15	0.14, 0.93	Oct 2008–Dec 2009	6.74 ± 2.31
Full chemistry blanks	NA	16	NA	NA	0.06 ± 0.04

water ($18\,M\Omega$ cm^{-1} resistivity). Ice samples were melted inside a covered polypropylene container in the presence of ~ 0.26 g of $(1.090 \pm 0.020) \times 10^3$ mg kg^{-1} accurately weighed ^{9}Be carrier solution, prepared from the mineral beryl with a ^{10}Be:^{9}Be ratio of $< 3 \times 10^{-15}$. The absolute ^{9}Be concentration of the carrier was verified by inductively coupled plasma atomic emission spectroscopy. Due to the acidity of the carrier (it was prepared in dilute HNO_3) the samples typically had a pH of ~ 4.2 after melting. A complementary set of δ^{18}O samples (in addition to those taken directly from the cores, Sect. 2.2.3) were taken from the bulk meltwater of each ^{10}Be sample. These δ^{18}O measurements provide a record that is directly co-registered with the ^{10}Be record. For each set of ten ice samples a ^{10}Be chemistry blank sample was also prepared by adding carrier to deionised water and thereafter treating identically as for samples.

Sample meltwater was peristaltically-pumped through 41 μm (nylon) and 0.45 μm (nitrocellulose) in-series filters directly into columns containing 10 ml of cleaned and conditioned (see Fig. 2.2) Dowex 50W-X8 200 mesh cation exchange resin, which captures beryllium. The 41 μm filter removes micro-meteorites and other foreign matter, while the 0.45 μm filter removes terrestrial dust, both of which contain ^{10}Be at concentrations several orders of magnitude higher than those occurring naturally in Antarctic ice [*Baumgartner et al.*, 1997]. Beryllium was stripped from the columns by a sequence of

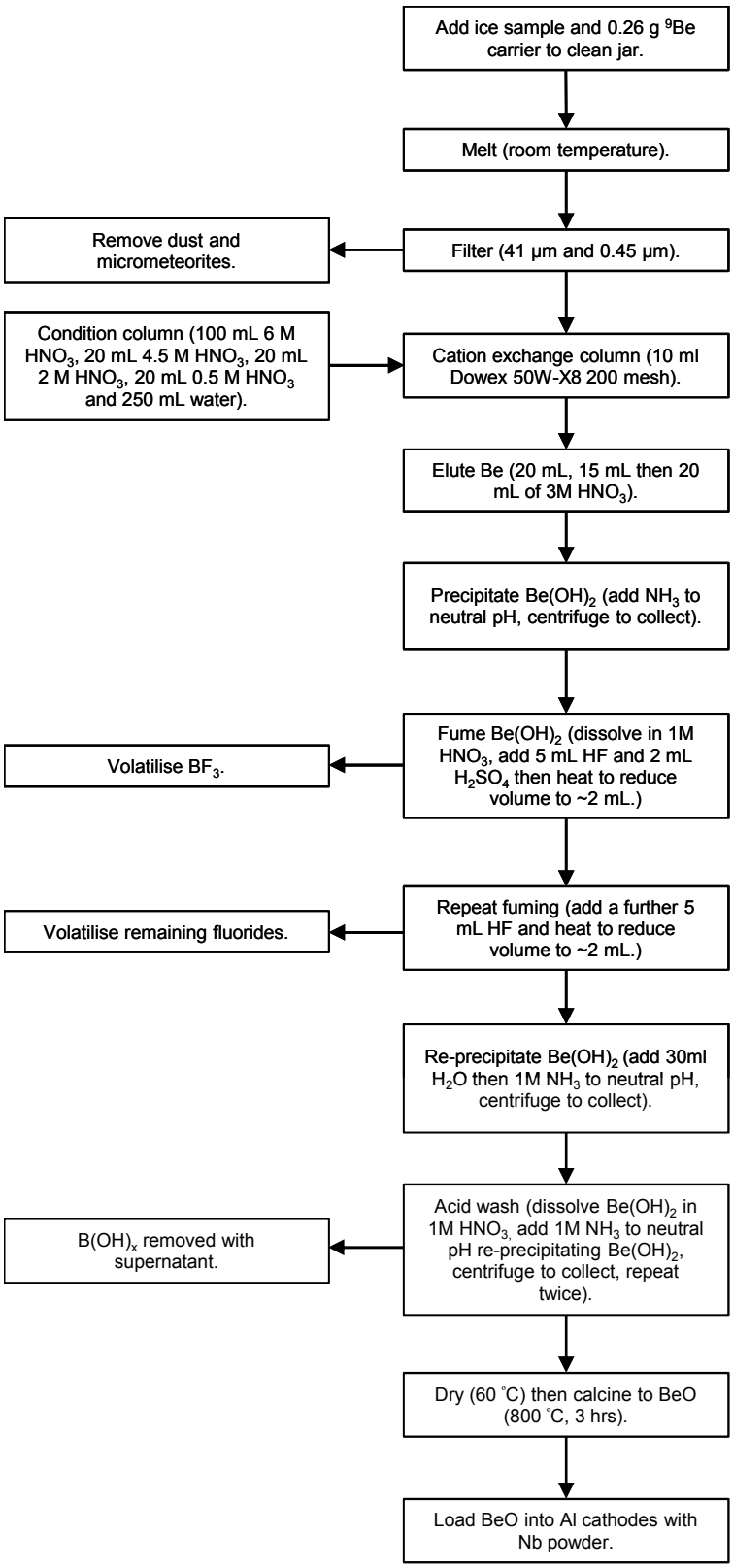

Figure 2.2: Flowchart showing the procedure used for extracting ^{10}Be from ice samples for AMS measurement.

three washes of 20 ml, 15 ml and 20 ml of 3 M HNO_3. Eluent from the first two washes was combined into a single fraction and then pH adjusted to 7.8 to 8.5 by adding concentrated NH_3. Full precipitation of beryllium (as $Be(OH)_2$) was achieved after several hours, whereupon the sample was centrifuged and the supernatant discarded. All beryllium was generally stripped from the column by the first fraction and neutralisation of the eluent from the final 20 ml "backup" fraction did not yield any precipitate. The $Be(OH)_2$ was dissolved in $\sim$ 1 ml 1 M HNO_3 then treated to remove boron by adding 2 ml concentrated H_2SO_4 and 5 ml of concentrated HF and heating to reduce the volume to 2 ml in a teflon beaker ("fuming"). This treatment volatalises the boron present in the sample as BF_3 (boiling point 101 °C). After cooling, a further 5 ml of concentrated HF was added and the fuming process was repeated. As the presence of fluorides in the sample will affect the chemical equilibria of Be cations in solution [*Child et al.*, 2000], the sample was heated for a further hour to ensure complete removal of HF. When treated in this way, ^{10}Be measurements have been completed on samples which were previously unmeasurable on the Australian National Tandem for Applied Research (ANTARES) AMS due to their high boron levels [*Simon et al.* submitted/Chapter 3].

$Be(OH)_2$was then precipitated by adjusting the sample pH to 7.8 to 8.5 using concentrated NH_3 and again collected by centrifuging. In a further step aimed at removing any boron hydroxides (which in contrast to $Be(OH)_2$ remain soluble at neutral pH *Child et al.*, 2000), the $Be(OH)_2$ was dissolved in several drops of 1 M HNO_3, re-precipitated by neutralisation with 1 M NH_3, rinsed with deionised water and centrifuged discarding the supernatant to waste (with this sequence being repeated two more times in order to thoroughly clean the $Be(OH)_2$ of soluble boron hydroxides). After drying at 60 °C, the $Be(OH)_2$ was calcined at 800 °C for 6 h in a quartz crucible to BeO. Median carrier recovery yield was 70 %, with the majority of the loss associated with the acid wash step rather than the fuming step. Finally, the BeO was mixed with 325 mesh niobium powder in an agate pestle and mortar at a mass ratio of $\sim$ 1:4 BeO:Nb. The mixture was loaded into 1.6 mm-diameter aluminium target holders and rear-pressed at a pressure of 120 kPa against a steel pin. This provides a good quality sample surface at a reproducible depth below the target face.

Measurement of the three ice core ^{10}Be records was carried out using the ANTARES AMS facility at ANSTO, following the basic method outlined in *Fink et al.* [2000]. BeO^- was injected with a terminal voltage of 6.880 MV and the 3+ charge state was selected, with $^9Be^{3+}$ currents of 2 to 6 μA and a particle transmission of $\sim$ 36 % from

the entrance of the accelerator to the detector. Fast isotope cycling was used to inject $^{9}Be^{16}O^{-}$ (1 ms) followed by $^{10}Be^{16}O^{-}$ (199 ms) for a repetition rate of 5 Hz. Samples were moved in a circular path under the primary cesium beam to minimise sample cratering and to maximise the use of sample material. The measurement proceeded by bracketing four ice samples between reference standards with measurement times of 600 s for the samples and 120 s for the standards. All ice samples were measured twice, but where necessary some were measured for a third time to obtain $\sim 2.5\,\%$ precision. The standards (typically 5) were cycled throughout the run.

All measurements were normalised to the National Institute of Standards ^{10}Be standard reference material 4325 (NIST SRM), utilising the *Nishiizumi et al.* [2007] ^{10}Be:^{9}Be ratio of $(2.79 \pm 0.02) \times 10^{-11}$. Measurements of the NIST SRM exhibited standard deviation of $< 2\,\%$. ^{10}Be:^{9}Be ratios for samples prepared from ice ranged from (234 to 992) $\times$ 10^{-15}. Chemistry procedural blanks had consistently low ^{10}Be:^{9}Be ratios. The mean for all blanks ($\pm 1\sigma$) was $(3.1 \pm 1.4) \times 10^{-15}$. The extremely low chemistry blank values demonstrate that the ^{9}Be carrier, chemistry processes and machine background did not introduce ^{10}Be at any significant level. Boron ($^{10}B^{3+}$) rates were sufficiently low that there was no interference with the measurement of $^{10}Be^{3+}$.

Knowing the quantity of ^{9}Be carrier added initially, the ^{10}Be:^{9}Be ratio is used to directly obtain the number of atoms of ^{10}Be in the original sample. Note that the chemical yields of the sample processing technique does not factor in this calculation since we are working with isotopic ratios.

Standard errors (incorporating all sources of experimental and measurement error) for the 117 ice samples ranged from 2.2 to 5.5 % with a median of 2.8 %.

2.2.5 Dating

Contiguous high-resolution (2.5 to 5.0 cm) δ^{18}O and trace chemistry measurements were carried out on the DSS0506-core and on PICO cores extracted alongside the DSS0809- and DSS0910-cores. Conversion of the ice core depth scales to timescales was carried out with reference to the clear annual cycles in δ^{18}O and trace chemistry observed in these records [*van Ommen and Morgan*, 1997; *Curran et al.*, 1998]. The boundaries of "years" were defined by the mid-summer δ^{18}O isotope maximum, which has a mean timing of 10 January at DSS [*van Ommen and Morgan*, 1997]. The timescale was developed by

interpolating between year boundaries, which assumes even snow accumulation over the course of each year. This assumption is valid for DSS when averaged over many years [*van Ommen and Morgan*, 1997]. However, in any given year, precipitation biases occur and contribute to uncertainty in the timescales. Overall, uncertainty in the dating of individual samples is estimated to be ±(1 to 2) months. This estimate of uncertainty is supported by analysis of the DSS0102-pit chronology. The pit was originally dated using automatic weather station (AWS) records of snow accumulation/ablation events, thus providing a very accurate timescale [*Pedro et al.*, 2006]; re-dating the pit by applying the same technique that was used for the ice core records (i.e., interpolating between year boundaries) results in a timescale that is consistent with the AWS-timescale within the bounds of our estimated dating uncertainty.

2.3 Results and discussion

^{10}Be concentrations in the three ice core records ranged between (2.13 and 14.08) × 10^3 atoms g^{-1}, with (mean ± 1σ) for all samples (5.92 ± 2.05) × 10^3 atoms g^{-1}.

The records are shown in Fig. 2.3a and the δ^{18}O ratios measured on the bulk meltwater of each ^{10}Be sample are shown in Fig. 2.3b. Also shown in these figures are the ^{10}Be concentrations and δ^{18}O ratios from the previously reported and contemporaneous DSS snow pit records: the DSS0102-pit and the DSS0506-pit. Note that all of these records are now calibrated to the *Nishiizumi et al.* [2007] NIST SRM ^{10}Be:^{9}Be ratio (our previous publications of the DSS0102-pit and DSS0506-pit data were calibrated to an earlier NIST value [*Pedro et al.*, 2006; *Pedro et al.*, 2009]). Since all samples are referenced to this same standard they can be directly compared.

The results and discussion are arranged as follows: Sect. 2.3.1 considers the issue of reporting concentrations versus flux; Sect. 2.3.2 analyses the level of reproducibility between all DSS ^{10}Be records; Sect. 2.3.3 constructs a 10-year monthly-resolved composite record of ^{10}Be concentrations; Sect. 2.3.4 quantifies the variability in ^{10}Be concentrations that may be explained by variations in the GCR and places new constraints on the atmospheric residence time of ^{10}Be; and finally, Sect. 2.3.6 examines meteorological influences on ^{10}Be concentrations.

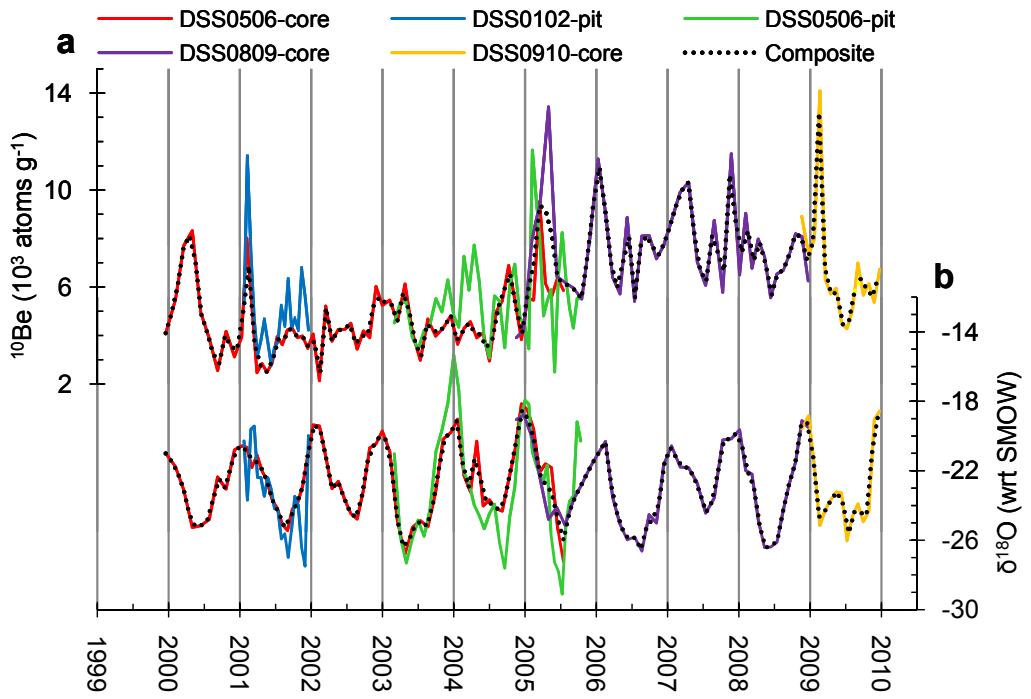

Figure 2.3: **(a)** ^{10}Be concentrations and **(b)** δ^{18}O ratios in three new high-resolution ice core records from DSS, Law Dome (DSS0506-core, DSS0809-core and DSS0910-core), and also in two previously published [*Pedro et al.*, 2006; *Pedro et al.*, 2009] snow pits (DSS0102-pit and DSS0506-pit). Composite records constructed (see Sect. 2.3.3) from the ice core series are overlain, providing a 10-year (1999 to 2009) monthly-resolved record of ^{10}Be concentrations and δ^{18}O ratios at DSS. Timescale uncertainty is estimated at $\pm$(1 to 2) months, standard ^{10}Be measurement errors are generally $< 3\,\%$.

2.3.1 Concentration and flux

Our analysis is focused on ^{10}Be concentrations in ice rather than on ^{10}Be fluxes, since concentration is the parameter directly measured in the ice. Discussing ^{10}Be variability in terms of flux would require an accurate estimate of accumulation variability. While data on an annual accumulation rate is available at DSS [*van Ommen and Morgan*, 2010], data on a monthly accumulation variability is highly uncertain and this uncertainty would transfer directly into any inferred flux values. Furthermore, ^{10}Be deposition to Law Dome is dominated by precipitation-related processes, i.e., is wet deposited [*Smith et al.*, 2000; *Pedro et al.*, 2006]. At wet deposition sites, changes in accumulation rate are not expected to have a strong influence on concentrations. This is demonstrated at Law Dome by the observation that the concentration of ^{10}Be at three ice core sites across the Dome is independent of the eightfold difference in precipitation

rate [*Smith et al.*, 2000].

2.3.2 Reproducibility

Five DSS ^{10}Be records are shown in Fig. 2.3. The most obvious difference between the records is the greater detail captured by the DSS0102-pit and DSS0506-pit when compared to DSS0506-core. This greater detail is consistent with the snow pit records being sampled at finer depth (and therefore time) resolution compared to the ice cores; comparable differences in detail are observed between the corresponding δ^{18}O records, supporting this interpretation. There are also some discrepancies in the timing and amplitude of concentration signals between the records. The clearest example of this is the concentration maximum in 2005 that is recorded by the DSS0506-pit, DSS0506-core and DSS0809-core. Between these three records, the timing of the ^{10}Be maxima varies by $\pm$(1 to 2) months and its concentration varies between (9.51 and 13.43) $\times$ 10^3 atoms g^{-1} (i.e., by up to 41 %). The variations in timing fall within the timescale uncertainty of the records (Sect. 2.2.5), however, the variations in concentration clearly exceed measurement errors (typically < 3 %). Such variations in concentration may therefore represent real differences caused by environmental factors.

An apparent offset is noticeable between ^{10}Be concentrations in the DSS0102-pit and the DSS0506-core where the records overlap. While both of these records show the same pattern, the mean concentration ($\pm 1\sigma$) in the pit, $(5.00 \pm 1.91) \times 10^3$ atoms g^{-1}, is 27 % higher than the same period in the core, $(3.95 \pm 1.4) \times 10^3$ atoms g^{-1}. In selecting a statistical test to determine if this offset is significant, information is first required about the distribution of the ^{10}Be data. Applying a Kolmogorov-Smirnov test (K-S test) for normality rejects the null hypothesis (at $p < 0.01$) that the ^{10}Be data from these records is normally distributed. Applying the K-S test to the log-transformed ^{10}Be data also rejects the null hypothesis (at $p < 0.01$) that the data is log-normally distributed (the non-normality of the data results from the sharp concentration maxima that introduce positive skew to the ^{10}Be distribution). Further K-S testing revealed that none of the five ^{10}Be series discussed in the text can be described as normally or log-normally distributed (at $p < 0.01$). Non-parametric tests are therefore preferred for treating the ^{10}Be data. We use the Wilcoxon rank-sum test, which tests the null hypothesis that two series are independent samples from identical continuous distributions with equal medians, against the alternative that they do not have equal medians. This test

Table 2.2: Intercomparison of contemporaneous sections of ^{10}Be records from DSS, Law Dome. A Wilcoxon rank-sum hypothesis test (see text) is used to test for significant difference between the pairs of records ($h = 0$ implies no evidence that the records are significantly different at the 95 % CI, i.e., where $p < 0.05$).

Records x & y	$n_x,\ n_y$	Overlap (years)	$\bar{x}(\pm 1\sigma),\ \bar{y}(\pm 1\sigma)$ ($\times 10^3$ atoms g^{-1})	Wilcoxon $h,\ p$
DSS0506-core & DSS0102-pit	14, 20	0.91	3.95(±1.40), 5.00(±1.91)	1, 0.01
DSS0506-core & DSS0506-pit	26, 35	2.35	5.00(±1.37), 5.54(±1.90)	0, 0.37
DSS0506-core & DSS0809-core	9, 7	0.68	5.97(±1.42), 7.37(±3.06)	0, 0.06
DSS0809-core & DSS0506-pit	9, 18	0.92	7.01(±2.95), 6.05(±2.23)	0, 0.08

determines that the concentration difference between the DSS0506-core and DSS0102-pit is significant ($p = 0.01$).

According to the Wilcoxon test criteria, no other overlapping sections of core are significantly different at $p < 0.05$, although in two cases (DSS0506-core and DSS0506-pit, DSS0506-pit and DSS0809-PICO), the differences do come close to this level. Differences between the average concentrations, where the records overlap, are in all cases $< 1.4 \times 10^3$ atoms g^{-1} or expressed differently, differences range between 10.8 and 24.0 %. Full results of statistical tests are provided in Table 2.2. Our identification of significant and marginally significant differences between records raises the question: do the differences between ^{10}Be records exceed the level of differences previously observed between other trace chemicals at Law Dome?

To answer this question we compared records of other trace chemicals from the corresponding cores. By way of example, the Na^+ records from the corresponding cores are shown in Fig. 2.4, and in Table 2.3 the same analysis applied to the ^{10}Be data is applied to these records. As with ^{10}Be, the Na^+ record shows broadly the same patterns, but some differences in the amplitude of signals between years. According to the Wilcoxon rank-sum test and its criteria, none of the overlapping sections of Na record may be classified as significantly different at $p < 0.05$. Nevertheless, large differences in the amplitude of signals are observed in some years, notably in 2004 and 2008. If these years are viewed in isolation then the differences between records would be classified as significant. Overall, with the possible exception of the ^{10}Be concentration offset between DSS0102-pit and DSS0506-core the level of differences between the ^{10}Be records does not appear anomalous with respect to other trace chemical records.

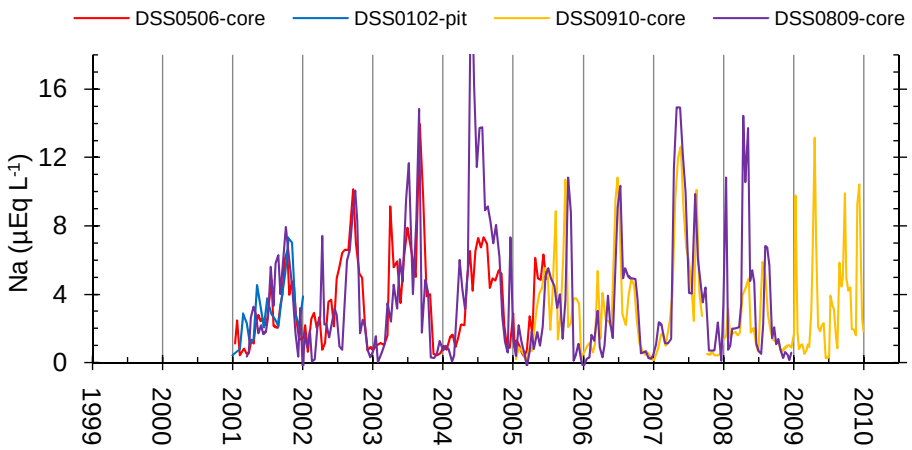

Figure 2.4: Intercomparison of Na^+ concentrations from the same ice core and snow pit records used in the analysis of ^{10}Be reproducibility. Standard measurement error in Na^+ concentrations are $\sim 15\,\%$. Note that trace chemistry was not measured on the DSS0506-pit.

Previous intercomparisons of trace chemicals from Law Dome provide insight into processes responsible for variability between records. Studies of Law Dome snow pits and firn cores have reported generally good spatial reproducibility between trace chemical and δ^{18}O records sampled up to 7.7 km apart [*McMorrow et al.*, 2001, 2002]. Differences observed between these records, particularly on a sub-seasonal scale, are attributed to small local variations in snow accumulation, snow surface topography, surface disturbance, ablation and densification between sample sites. By influencing the relative thickness of snow layers corresponding to common meteorological events, and therefore also the assumptions made during dating (of evenly distributed snow accumulation during the coarse of each year), these processes can alter the timing and amplitude of concentration signals [*McMorrow et al.*, 2001, 2002]. Hence, a certain level of variability between all trace chemical records must be regarded as unavoidable. This offers a suitable explanation for the differences between the ^{10}Be records, again with the possible exception of the apparent systematic concentration offset between DSS0102-pit and DSS0506-core.

Since there were differences in the laboratory procedure used to extract the ^{10}Be from the DSS0102-pit and DSS0506-core, the possibility cannot be excluded that the offset was due to procedural rather than site-to-site differences. Meltwater from DSS0102-pit samples was acidified with 1 ml per kg ice of concentrated HNO_3 prior to filtration [*Pedro et al.*, 2006], whereas the DSS0506-core samples were not acidified. Acidification

prior to filtration has two main effects: firstly, the undesirable effect of potentially releasing ^{10}Be atoms from any dust and/or micro meteorites present in the samples (i.e., terrestrial ^{10}Be that is not part of the atmospheric signal we are interested in) [*Smith et al.*, 2000]; and secondly, potentially reducing the loss of ^{10}Be atoms by adsorption to filters, tubing and sample bottle walls [*Finkel and Nishiizumi*, 1997; *Yiou et al.*, 1997]. Both of these procedural differences would act in the direction of increasing measured concentrations in the DSS0102-pit samples with respect to DSS0506-core, as observed. The first explanation is inadequate to explain the results, since the available fraction of ^{10}Be associated with dust and micrometeorites in Antarctic ice from the Holocene is very low [$< 2\,\%$, *Lal*, 2007; *Baumgartner et al.*, 1997]. The second explanation also appears unlikely. Both sample sets were melted in the presence of ^{9}Be carrier, which floods samples with $\sim 10^{13}$ times more ^{9}Be atoms than ^{10}Be atoms. We assume that any loss of ^{10}Be by adsorption to experimental equipment is balanced by loss of ^{9}Be carrier, such that ^{10}Be:^{9}Be ratios are unaffected. Importantly, this assumption may not hold if the carrier ^{9}Be and ice core ^{10}Be are in different chemical forms *and* there has not been sufficient time for reaction kinetics to equilibrate ^{9}Be and ^{10}Be atoms between these different forms. There is some evidence that the assumption of equilibrium does break down for Greenland ice samples from the last glacial period with high dust particle concentrations [*Finkel and Nishiizumi*, 1997; *Yiou et al.*, 1997]. This probably relates to non-equilibrium exchange (adsorption and desorption) of ^{10}Be and ^{9}Be between terrestrial dust and meltwater in ways that are not fully understood [*Baumgartner et al.*, 1997]. Importantly, Holocene ice samples, with much lower particle concentrations, were negligibly affected by this problem [*Finkel and Nishiizumi*, 1997; *Yiou et al.*, 1997]. The particle concentrations in modern DSS ice are actually among the lowest of all the polar ice core sites [*Jun et al.*, 1998]. In addition, recall from Sect. 2.2.3, that the carrier itself is an acidic solution that typically lowers the sample meltwater pH to ~ 4.2. The aqueous chemistry of Be dictates that at pH more acidic than 5.7 the dominant species of Be is the strongly hydrated Be^{2+}, which tends to remain in solution [*Everest*, 1973]. In the absence of dust, we expect the ice core ^{10}Be and carrier ^{9}Be to be in equilibrium in this Be^{2+} form. We cannot completely rule out some selective loss of ^{10}Be, however we consider it unlikely to have played any major role in the offset between the two DSS records.

An alternative explanation is that the thermal drilling process used to retrieve DSS0506-core may itself have caused some loss of ^{10}Be ions by eluting away some of the soluble

Table 2.3: Intercomparison of contemporaneous sections of Na^+ records from the same ice cores and snow pits used in the analysis of ^{10}Be reproducibility. As in Table 2.2, a Wilcoxon rank-sum hypothesis test is used to test the null hypothesis that the two series are independent samples from identical continuous distributions with equal medians ($h = 1$ implies that the null hypothesis should be rejected as $p < 0.05$). Note that trace chemistry was not measured on the DSS0506-pit.

Na^+ Records x & y	n_x, n_y	Overlap (years)	$\bar{x}(\pm1\sigma)$, $\bar{y}(\pm1\sigma)$ ($\times10^3$ atoms g^{-1})	Wilcoxon h, p
DSS0506-core & DSS0102-pit	28, 20	0.91	2.57 (±1.64), 3.11 (±1.84)	0, 0.30
DSS0506-core & DSS0708-core	111, 101	4.42	3.41 (±2.57), 3.81 (±2.76)	0, 0.37
DSS0506-core & DSS0809-core	106, 112	4.26	3.52 (±2.57), 3.88 (±4.04)	0, 0.60
DSS0809-core & DSS0910-core	107, 101	3.93	3.42 (±3.68), 3.00 (±2.88)	0, 0.99

ions in the firn with the meltwater produced during drilling. To investigate whether this may have happened, we again consider other trace chemical records. In Fig. 2.4, Na^+ records from the corresponding pits/cores are plotted. Large intra-annual variations are observed in Na^+ concentrations reflecting seasonal variability in the delivery of this sea-salt species to the ice core site [*Curran et al.*, 1998]. In most years, the agreement between the individual Na^+ records is excellent. Visually, no clear offset is observed between the DSS0102-pit and the thermally drilled DSS0506-core, nor between the DSS0809-core and DSS0506-pit, with their longer period of overlap. Applying statistical tests, no significant offset is found between these overlapping records (see Table 2.3). However, in some years discrepancies are observed, for example 2004 and 2008. These discrepancies are indicative of the level of variability inherent between contemporaneous trace chemical records from these sites. In this context, the differences between ^{10}Be records and, in particular, between the thermally drilled record and physically/mechanically sampled records do not appear anomalous.

To our knowledge there has been only one other investigation of the reproducibility of ice core ^{10}Be records [*Moraal et al.*, 2005]. This study found up to a fourfold difference in ^{10}Be concentrations between two records sampled 300 m apart. However, this study was not carried out at a proven ice core site, instead, it was an opportunistic effort to retrieve ^{10}Be samples from cargo loading ramps that are cut annually into the Queen Maud Land (QML) ice shelf for the purpose of resupply of the South African research station. *Moraal et al.* [2005] were unable to determine the reason for the ma-

jor discrepancy between these records. However, they suggested that local-scale and/or post-depositional influences may have been involved.

A number of factors may have contributed to the poor reproducibility in the QML study. The study site was not ideal for a number of reasons: (i) one of the loading ramp faces used for sampling had been exposed to the atmosphere for 1 year prior to sampling, potentially contaminating the record with chemicals (including from sea spray) that were not present at the time of snow deposition and leaving the record vulnerable to solar ablation, aeolian ablation and melt, (ii) snow accumulation at the sampling site itself is very low with most accumulation arriving as snow drift from other regions, making the record difficult to interpret and sensitive to shifts in prevailing wind patterns between years, and (iii) surface melt-layers occur annually at the site, leading to post-depositional changes to the chemistry record. All of these factors act against the preservation of reliable ice core records. The long exposure of one of the sampling faces to the atmosphere prior to sampling, may have been the critical factor; it was this exposed record that had much lower concentrations than the record sampled from the freshly cut cargo ramp. Field and laboratory studies suggest that at sites where annual melt layers are common, melt-water percolation can remove 50 to 80 % of the soluble ion fraction from the snow-pack [*Johannessen and Henriksen*, 1978; *Eichler et al.*, 2001; *Hou and Qin*, 2002]. Excessive melt of the exposed sampling face therefore offers a plausible explanation for the concentrations difference between the two QML records. When compared to the much higher level of reproducibility observed at the more controlled DSS ice core site, the QML result appears more likely to be related to problems with the sampling site and methodology rather than any inherent problem in the reproducibility of ^{10}Be records.

Overall, our results support the reproducibility of ^{10}Be records obtained from proven high resolution ice core sites. This result is encouraging from the perspective of using ^{10}Be as a solar activity proxy. However, we advise some caution in interpreting *absolute* concentration differences between different records/sites that have not been collected and prepared identically.

2.3.3 ^{10}Be composite record

A monthly resolution 10-year composite record is constructed from the DSS ^{10}Be data in order to obtain the longest possible record for intercomparison with other geophysical data series. DSS0506-core, DSS0809-core and DSS0910-core are used for the composite (all of which were sampled at similar resolution and prepared for measurement identically). All three records were resampled to even (monthly) sample spacing by linear interpolation. As monthly spacing is close to the mean resolution of the original data, the effect of this resampling is benign. For periods where there is an overlap between records, the average of the records was used. We neglect the comparatively small influence of measurement errors (typically $< 3\,\%$).

The composite record is shown in Fig. 2.3a as the dashed line overlain on the original time series. A composite δ^{18}O record was also constructed using the same technique and is shown as the dashed line in Fig. 2.3b. In constructing the composite, more complicated methods of data splicing and interpolation were also trialled, however, the resulting differences were negligible therefore the simple technique outlined above was preferred.

2.3.4 Production rate signal

Neutron monitor data is the best measured parameter against which to test modern ice core ^{10}Be data for a production rate signal [e.g. *Steig et al.*, 1996; *Berggren et al.*, 2009]. Here, we use the neutron counting rate on the McMurdo Neutron Monitor, Antarctica [from the *Bartol Research Institute*].

Figure 2.5a shows ^{10}Be concentrations alongside the monthly average McMurdo neutron counting rate. On interannual timescales there is an obvious relationship between the neutron counting rate and the ^{10}Be concentration. The strength of this relationship is explored by calculating Pearson's correlation coefficient (r_{xy}) as the lag between ^{10}Be and the neutron counting rate is varied (Fig. 2.5c. We employ a non-parametric stationary bootstrap method in the calculation (r_{xy}) and associated 95 % (bias-corrected and accelerated) confidence intervals (CI). An important advantage of this method over conventional techniques is that it yields reliable confidence intervals for (r_{xy}) when applied to serially dependent and non-normally distributed data series [*Mudelsee*, 2003]. At zero lag, a highly significant correlation is observed, $r_{\mathrm{xy}} = 0.64$ (with 95 % CI of 0.53

to 0.71), as shown in Fig. 2.5b. This indicates a production signal in the composite record coherent with Schwabe cycle modulation of the GCR. Our results suggest that the production signal accounts for $\sim 40\,\%$ of the variance in ^{10}Be concentrations over the 10-year series. Concentrations during the solar minimum years (2008, 2009) are a factor of 1.64 times those during the solar maximum years (2001, 2002, 2003). According to the Wilcoxon rank-sum test, this difference is significant at $p < 1 \times 10^{-8}$.

The concentration difference between solar maximum and solar minimum exceed the theoretical variation in the *global* atmospheric production rate over the same interval, which was a factor of 1.34 (calculated using the cosmic ray modulation strength (Φ) values of *Usoskin et al.*, 2005 and the cross-sections and alpha correction of *Masarik and Beer*, 2009). Interestingly, the concentration difference is comparable to the theoretical variation in the *polar* (i.e., 60 to 90° S) atmospheric production rate, which was a factor 1.59. The question of whether the ^{10}Be deposited to the polar regions should reflect changes in the global production rate, polar production rate, or some mixture of both is still not settled [see, *Mazaud et al.*, 1994; *Steig et al.*, 1996; *Bard et al.*, 2000; *McCracken*, 2004; *Field et al.*, 2006; *Heikkilä et al.*, 2008b]. However, given that the DSS record samples only one Schwabe cycle, it would be premature to draw too much from our result. It may be that meteorological influences that are unrelated to production variations have contributed to enhance the concentration differences above what may be attributed to global production rate changes alone. A study currently underway at DSS looking at ^{10}Be concentrations over multiple Schwabe cycles will provide greater insight into this issue.

Theoretical studies suggest that globally ∼50 to 75 % of ^{10}Be production occurs in the stratosphere [*Masarik and Beer*, 1999; *Heikkilä et al.*, 2008b]. Atmospheric residence times in the stratosphere are of order 1 to 2 years whilst residence times in the troposphere are substantially shorter, of order several weeks [*Raisbeck et al.*, 1981; *Jordan et al.*, 2003; *Heikkilä et al.*, 2009]. The behaviour of r_{xy} as lag is increased, Fig. 2.5c, provides empirical information on the atmospheric residence time of ^{10}Be. As the lag is varied beyond 10 months, r_{xy} begins to decline (Fig. 2.5c. At lag 18 months the correlation is already significantly lower (at 95 % CI) than for lags less than 10 months. When the lag is varied beyond 24 months, the correlation is not significantly different from zero. This lag-correlation analysis suggests that most ^{10}Be arriving to DSS has been produced in the atmosphere within the previous 0 to 10 months. Given that stratospheric and tropospheric lifetimes bracket this range, this result argues for appreciable

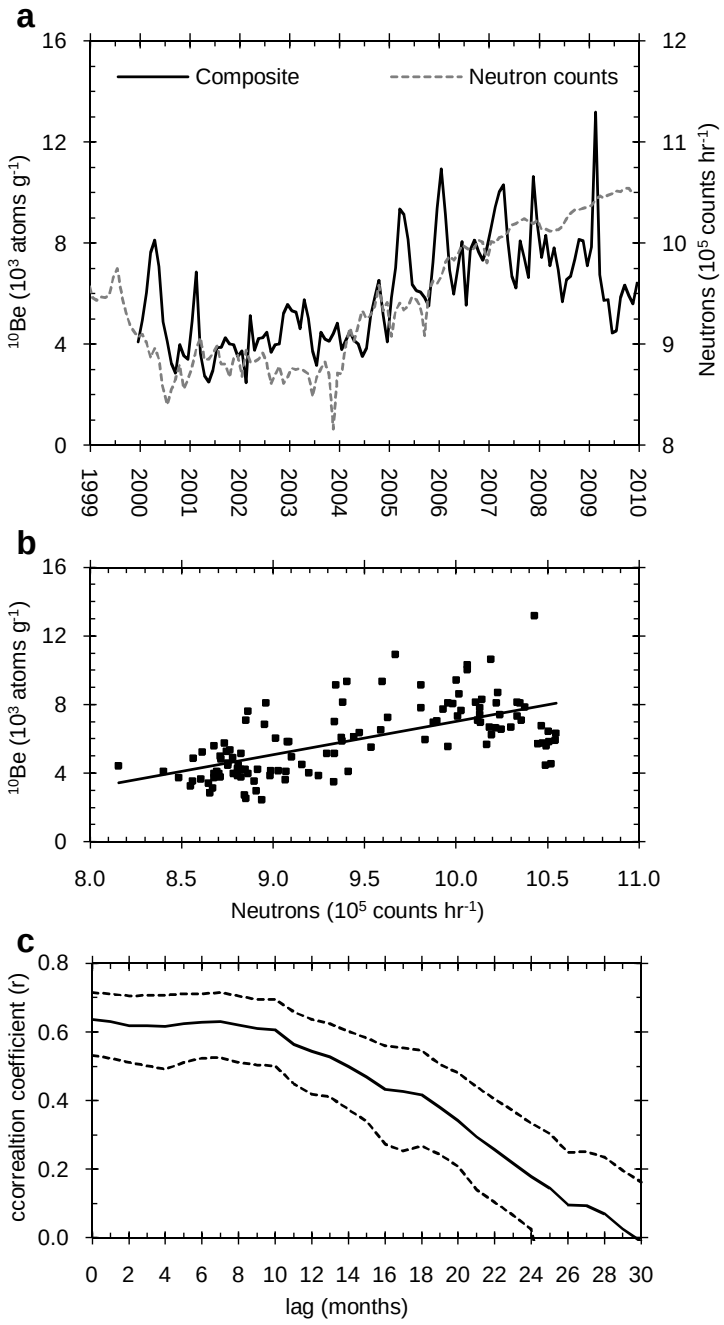

Figure 2.5: The relationship between ^{10}Be concentrations in the DSS composite record and the neutron counting rate on the McMurdo neutron monitor, Antarctica. **(a)**, Concentrations of ^{10}Be (black line) compared to the neutron counting rate (dashed grey line). **(b)**, Concentrations of ^{10}Be plotted against the neutron counting rate (at zero lag) with a linear regression line fitted to the data. **(c)**, The correlation coefficient between ^{10}Be concentration and the neutron counting rate as the lag of ^{10}Be behind neutron counts is varied (black line) and the 95 % CI around the correlation coefficient (dashed blacked lines). Measurement errors in ^{10}Be concentrations are typically < 3 %, and timescale errors are $\pm$(1 to 2) months, errors in the neutron counting rate are negligible.

contributions from both of these sources to total ^{10}Be fallout at the site. Resolving the precise contribution of each reservoir to total depositions is not yet possible empirically, however, ^{7}Be measurements now underway on snow pit samples from DSS are expected to help in this respect.

While on interannual timescales the atmospheric production emerges as a principal control on concentrations in ice, factors other than production also have considerable influence. Maximum levels for the 10-year composite are reached in the summer to autumn of 2009, however, average annual concentrations actually decline over the period 2008 to 2009. This is in contrast to neutron counting rates at high latitudes, which in 2009 actually reached their highest levels since the installation of monitors in the 1960s [*Moraal et al.*, 2009]; coinciding with the deepest solar minimum (according to various parameters) since the 1920s [*Lockwood et al.*, 2009; *Lockwood*, 2010]. These indicators imply an atmospheric ^{10}Be production rate at record high levels with respect to the same historical interval. The divergence between ^{10}Be and neutron counting rates must therefore be explained by non-production factors. Since the procedure for extraction of ^{10}Be from melt-water was identical for all of the records used in the composite, chemical processing factors do not explain the divergence. This leaves meteorological influences or local/in-situ effects (e.g., local variations in snow accumulation, snow surface topography, ablation and other forms of surface disturbance) as the most probable explanation.

2.3.5 Solar cosmic ray events

A previous paper [*Pedro et al.*, 2009] reporting results from the DSS0506-pit investigated whether the concentration peak in summer 2005 may have been a response to the 20 January 2005 solar cosmic ray event. This event was calculated to increase monthly cumulative ^{10}Be production in the polar atmosphere by $\sim 120\,\%$ above the GCR background [*Webber et al.*, 2007]. The new ^{10}Be records reported here also replicate the summer 2005 peak. However, with the benefit of these longer records it is seen that the 2005 peak is not anomalous, for example, the concentration is exceeded by the maximum in summer 2009. Careful analysis of ^{10}Be concentrations following a number of historically recorded solar cosmic ray events will now be required in order to judge whether the events can trigger short-term peaks in the ice core data.

2.3.6 Meteorological signals

2.3.6.1 Influence of stratospheric air

On monthly timescales, there are large variations in concentration that cannot be explained by production variations. Short-lived (1 to 2 months) events of particularly high concentration (more than 2σ above the mean) occur in some years, typically in summer to autumn, e.g., 2001 and 2005 to 2009. Comparable events are absent or damped during the solar maximum (neutron counting minimum) years of 2002 to 2004.

We are not aware of any monthly-resolved ^{10}Be records from other Antarctic sites with which to compare the DSS composite. However, there are at least two such records available from Greenland. The first is from a snow pit spanning 1978 to 1983 from the Dye 3 site in south Greenland [*Beer et al.*, 1991]. The second is from a snow pit spanning 1986 to 1990 from the GRIP site in central Greenland [*Heikkilä et al.*, 2008c]. Similarly to DSS, both Greenland sites experience short-lived concentration maxima. An important difference between the Antarctic and Greenland records is that the concentration maximum typically occurs during the (austral) summer to autumn in Antarctica, whereas in Greenland there is suggestion of a bimodal pattern with a primary maximum in the (boreal) summer to autumn and a secondary maximum in the (boreal) spring.

The sharp concentration peaks in the ^{10}Be data resemble features observed in a recently compiled series spanning 1975 to 2006 of ^{10}Be and ^{7}Be concentrations in ground-level air samples from two sites in Sweden [*Aldahan et al.*, 2008]. In this study, sporadic events of >2 to 3 times average concentrations were observed in some years, typically in spring to summer. The authors concluded that the sporadic peaks were likely caused by intrusions of ^{10}Be rich air from the stratosphere, they suggested further that such a mechanism may explain relative peaks in ice core ^{10}Be records. Our results appear to support this view. According to the most detailed model study yet of atmospheric transport into the polar troposphere [*Stohl and Sodemann*, 2010], and in agreement with the timing of the concentration peaks observed here, summer to autumn is the period during which there is the highest probability of encountering air of recent stratospheric origin in the Antarctic troposphere. Maximum influence of stratospheric air during the summer to autumn is also supported by signals observed in numerous other stratospheric aerosol markers at Antarctic air sampling stations [*Raisbeck et al.*, 1981; *Sanak et al.*, 1985;

Feeley et al., 1989; *Savoie et al.*, 1992; *Wagenbach*, 1996].

2.3.6.2 Relationship between ^{10}Be and δ^{18}O

Results from an earlier analysis of the DSS0102-pit suggested an important meteorological influences on ^{10}Be forced by variability in local meteorology and air mass moisture history [*Pedro et al.*, 2006]. This influence was detected in the form of a significant negative correlation ($r_{xy} = 0.57, p < 0.01$) between first-differences in δ^{18}O and ^{10}Be measurements. The relationship can now be tested over the 10-year composite.

Following the procedure in [*Pedro et al.*, 2006], first-differences in ^{10}Be concentrations are tested against first-differences in δ^{18}O. This yields $r_{xy} = -0.14$ with a 95 % CI of -0.38 to 0.02. This negative relationship is consistent with, although weaker than, that observed in the pervious study. Indeed, the 95 % CI around r_{xy} indicates that the significance of the relationship is marginal. Notably, there is no trend in δ^{18}O capable of offering an explanation for the departure of ^{10}Be concentrations from the neutron counting rate curve in 2008 and 2009.

An important difference with respect to our earlier study that may explain this weaker correlation is the sub-monthly (snowfall event scale) resolution of DSS0102-pit compared to the coarser monthly-resolution of the composite. The implication is that ^{10}Be and δ^{18}O co-vary at DSS on the snowfall event scale, but that this relationship appears to deteriorate with coarser sample resolution. This is also an encouraging result from the perspective of interpreting information about atmospheric production from ice core ^{10}Be.

2.4 Summary and conclusions

We have described the methodology used to obtain high-resolution and well-dated ice core records of ^{10}Be from the DSS ice core site and presented three new records. Combined, these datasets provide a record of near-monthly variations in the concentration of ^{10}Be over the past decade at the DSS ice core site. In comparing the records with previously reported snow pit records sampled from up to 500 m away, variations of up to 40 % between records during individual months are observed. This short-term variability is attributed to local-scale differences between sites in accumulation, ablation and

density profiles and potentially differences in the experimental procedure that applied to one of the records (DSS0102-pit). When records are averaged across their overlapping intervals (ranging from 0.91 to 2.35 years) agreement improves. For the records with the longest period of overlap the absolute difference is 0.54 $\times 10^3$ atoms g^{-1}, or 10.8 %. Overall, the agreement between ^{10}Be records is comparable to that observed between other commonly measured trace chemicals, supporting the reproducibility of ^{10}Be records sampled from the DSS site.

Our results illustrate that ^{10}Be records are more reliable when sampled from proven or carefully selected ice core sites; by contrast, sites where melt layers are common, where windblown snow contributes a large fraction of annual accumulation, where the snow pack has been disturbed or where sampling surfaces have been left open to the atmosphere should probably be avoided if the intent is to obtain a record which can inform on the atmospheric production rate. Also, caution should be taken in comparing absolute concentrations between records that have not been prepared for AMS measurement identically. Further study directed at constraining site-to-site differences between records, or differences attributable to in-situ effects on annual and greater timescales is worthwhile, and ideally would require some decades of identically prepared contemporaneous records.

A composite record spanning the past decade was constructed from the three (identically prepared) DSS ^{10}Be ice cores. Using this record, we find that the neutron counting rate, a measure of the cosmic ray flux, can explain up to ~ 40 % of the variance in ^{10}Be concentrations at the site. The phase relationship of ^{10}Be and the neutron counting rate is consistent with the bulk of the ^{10}Be arriving to Law Dome having been produced in the atmosphere during the previous 0 to 10 months.

The atmospheric production rate is responsible for the principal trend in concentrations on interannual timescales. However, the relationship appears to break down during 2008 to 2009 when neutron counting rates increase to unusually high levels whilst ^{10}Be concentrations actually decrease. In our assessment, this divergence must be caused by some unexplained meteorological influence or local/in-situ processes (e.g., local variations in snow accumulation, snow surface topography, ablation or other forms of surface disturbance).

On monthly timescales there are large variations in concentration that cannot be explained by production variations. It appears that short-term peaks in ^{10}Be concen-

trations may be associated with input of stratospheric air into the polar troposphere. Similarly, to a previous study at DSS a negative relationship is found between ^{10}Be and δ^{18}O, however the relationship is much weaker than that observed previously.

Summing up, our results allay some concerns about poor reproducibility of ^{10}Be records sampled from polar ice core sites. At suitable ice core sites, ^{10}Be records should respond primarily to changes in atmospheric production with additional influence from climate and meteorological variability. At Law Dome the atmospheric production rate is strongly represented in the concentration data. This, along with increasing understanding of climate and meteorological influences on ^{10}Be deposition, marks Law Dome as a valuable site for extraction of longer term records of ^{10}Be for investigation of past variations in solar activity and cosmic ray intensity.

The datasets are available online at the Australian Antarctic Data Centre (http://data.aad.gov.au/).

Chapter 3

Reprocessing of ^{10}B-Contaminated ^{10}Be AMS Targets

K. J. Simon[1], J. B. Pedro[2,3], A. M. Smith[1], D. P. Child[1] and D. Fink[1]

In review (submitted July 2011), *Nuclear Instruments & Methods in Physics Research B*.

[1]Australian Nuclear Science and Technology Organisation, Menai, NSW, Australia
[2]Institute of Marine and Antarctic Studies, University of Tasmania, Hobart, TAS, Australia
[3]Antarctic Climate and Ecosystems Cooperative Research Centre, Hobart, TAS, Australia

Abstract

^{10}Be accelerator mass spectrometry (AMS) is an increasingly important tool in studies ranging from exposure age dating and palaeo-geomagnetism to the impact of solar variability on Earth's climate. High levels of boron in BeO AMS targets can adversely impact the quality of ^{10}Be measurements through interference from the isobar ^{10}B. Numerous methods in chemical sample preparation and AMS measurement have been employed in order to reduce the impact of excessive boron rates. We present details of a method developed to chemically reprocess a set of a set of forty boron-contaminated BeO targets derived from modern Antarctic ice. Previously, the excessive boron levels in these samples, as measured in an argon-filled absorber cell preceding the ionisation detector, had precluded routine AMS measurement. The procedure involved removing the BeO+Nb mixture from the target holders and dissolving the BeO in hot concentrated H_2SO_4. The solution was then heated with HF to remove the boron as volatile BF_3 before re-precipitating as $Be(OH)_2$ and calcining to BeO. This was again mixed with niobium and pressed into fresh target holders. Following reprocessing, the samples gave boron rates reduced by 10–100 times, which are sufficiently low and similar to previous successful batches of ice core, snow and associated blank samples, thus allowing a successful ^{10}Be measurement in the absence of any boron correction. Overall recovery of the BeO for this process averaged 40 %. Extensive testing of relevant processing equipment and reagents failed to determine the source of the boron. As a precautionary measure, a similar H_2SO_4+HF step has been subsequently added to the standard ice processing method.

3.1 Introduction

^{10}Be is a long lived radionuclide ($t_{\frac{1}{2}} = 1.387 \pm 0.012 \times 10^6$ years [*Korschinek et al.*, 2010; *Chmeleff et al.*, 2010] of beryllium formed in the upper atmosphere by the collision of galactic cosmic rays (GCR) with N and O. ^{10}Be has found a wide-ranging field of applications, and second to ^{14}C, is the most commonly measured radioisotope by AMS [*Fink*, 2010]. ^{10}Be levels in ice-cores from polar regions can provide important insights into past changes in the factors which control the GCR intensity in the Earth's upper atmosphere, namely changes in solar activity and changes in the geomagnetic field strength [*Raisbeck et al.*, 1978; *Beer et al.*, 2000]. In-situ production of ^{10}Be in

quartz bearing Earth surface materials can provide bedrock erosion rates and moraine exposure ages that have revolutionised our understanding of landscape evolution and glacial climate change [*Gosse*, 2001; *Dunai*, 2010]. Improved ^{10}Be AMS measurement capabilities driven by demands for dating young surfaces and ice cores sites of high snow accumulation with ^{10}Be concentrations of the order of 10^3 to 10^4 atoms per gram quartz or ice. This in turn has placed increased demands for AMS BeO targets to deliver higher currents lower processing blanks with ^{10}Be:^{9}Be $< 10^{-15}$ [*Rood et al.*, 2010] and reduced boron levels.

The major interference in the analysis of ^{10}Be by AMS is the isobar ^{10}B. Since it has a higher atomic number than ^{10}Be, this isobar can be stopped in a foil or an absorber cell placed in front of the detector, still leaving sufficient energy for detection of ^{10}Be by conventional gas ionization energy loss detectors. The difficulty comes about when ^{10}B levels are sufficiently high that recoil ^{7}Be, produced by the p(^{10}B, ^{7}Be)α reaction, is misidentified as a ^{10}Be event. This can lead to an unacceptable elevation of ^{10}Be:^{9}Be ratios in procedural blanks and an overestimate of ^{10}Be:^{9}Be for unknown samples. Moreover, dead-time corrections and corrections for false ^{10}Be events due to excessive boron rates can be highly non-linear. This can be a serious issue for the measurement of samples with low ^{10}Be, as background corrections and error propagation become uncomfortably high. Annually-resolved ice samples from the high-accumulation, 0.68 m yr^{-1} ice [*Morgan et al.*, 1997], Law Dome site in coastal East Antarctica have typical ^{10}Be:^{9}Be ratios of $\sim$ 200–800 $\times$ 10^{-15}. For exposure dating, measurements of late Holocene or 'little ice age' glacial deposits using typical sample masses of tens of grams of quartz and minimum ^{9}Be carrier mass (0.2–0.3 mg) can result in ^{10}Be:^{9}Be ratios as low as 10–100 $\times$ 10^{-15}.

Various technical innovations have been devised to reduce boron rates. Stopping ^{10}B by the gas absorber cell method is the most effective and efficient method for ^{10}Be AMS systems with terminal voltages of 5 MV or more. The addition of a charge-changing post-stripper foil before a deflecting magnet or an electrostatic analyser can reduce boron rates by a factor of ten at best (^{10}Be^{3+} ions are stripped to ^{10}Be^{4+} with minimal reduction in yield whereas 70–90 % of ^{10}B^{3+} predominately populates the ^{10}B^{5+}). With the move to lower terminal voltage AMS machines, very thin ultra-homogenous Si_3N_4 energy changing foils placed before an energy dispersive device can be used to reduce ^{10}B by 4 to 5 orders of magnitude, but there is a trade-off as it inevitably results in very low overall ^{10}Be efficiencies, some 3 to 5 times lower than those measured with the gas-

absorber cell method [*Müller et al.*, 2010]. However all such systems are vulnerable to particularly high levels of boron contamination. In this paper we report on a method whereby the sputtered BeO target material found to be contaminated with boron is chemically reprocessed to reduce ^{10}B levels.

3.2 Measurement of ^{10}Be at ANTARES

Beryllium AMS targets at ANSTO are prepared typically with $\sim$ 0.25–0.50 mg of ^{9}Be from either a beryl-derived carrier solution or a commercially available 1000 ppm Be trace element analysis reference solution. The resultant BeO is mixed with -325 mesh niobium powder in the mass ratio of $\sim$ 1:4 BeO:Nb, following our discovery that niobium doubles BeO^- yields [*Fink et al.*, 2000]. The oxide-metal mix is rear-pressed into an aluminium target holder with a 1.6 mm diameter recess at 120 kPa to produce an AMS target.

The method used for ^{10}Be analysis at ANTARES is fully described in *Fink and Smith* [2007]. Efficiencies for $^{10}Be^{3+}$ transport are 30–35 % from 2–6 μA of BeO^- at 6.8 MV. Intra-run reproducibility of repeat standard measurements is 1.5 % ($\pm 1\sigma$). Full chemistry procedural blanks from our low-level beryl spike solution using our regular methods for ice and methods for purified quartz extracted from rock [*Child et al.*, 2000] range between 1 and 5×10^{-15}. This is based on 2-D software energy spectra gates at 98 % ^{10}Be cut-off (i.e. we accept 98 % of all ^{10}Be events during measurement of a standard). Reducing the integration criteria to 90 %, which we prefer not to do, lowers the ^{10}Be:^{9}Be of a procedural blank by 33–50 %. We use an argon filled absorber cell to fully stop the ^{10}B rate from entering the active multi-anode gas ionisation detector. Havar foils separate the detector gas (P-10 gas) from the Ar absorber cell gas and vacuum system. The body of the absorber cell is an aluminium tube which is biased by 200 V with respect to the entrance window. The boron-induced electron current flowing in the absorber cell, I_{Bcell}, is continuously recorded by the data acquisition system and provides a measure of the ^{10}B rate. This signal can also be used to set up the accelerator for a ^{10}Be measurement if required.

For a low-level ice or rock sample (ie for ^{10}Be:^{9}Be $< 500 \times 10^{-15}$) with acceptable boron content that does not adversely affect the ratio, I_{Bcell} is typically in the range of 50–500 nA for a corresponding $^{9}Be^{3+}$ current of 2–6 μA, measured in an off-axis

Faraday cup after the ANTARES analysing magnet. We define a 'figure of merit' (FOM) as the ratio of I_{Bcell} (in nA) to the $^{9}Be^{3+}$ current (in μA) which provides a semi-quantitative measure of the quality of a sample with respect to the purity of BeO and the boron level. The FOM for beryl full chemistry processing blanks ranges typically from 10–200(^{10}B nA:$^{9}Be^{3+}$ μA), whereas some ice and rock samples can have a FOM as high as 800. Beryl processing blanks which cover this range of FOM and I_{Bcell} do not show an increase in their measured ^{10}Be:^{9}Be ratios above the acceptable range of 2×10^{-15} to 10×10^{-15} and hence such samples do not require any corrections. Targets loaded with commercially purchased BeO powder (mixed with niobium, no chemistry) or only niobium powder, or empty aluminium targets have I_{Bcell} currents of less than 50 nA.

BeO produced from the low-level beryl solution was spiked with controlled concentrations of boron with B:Be (atom:atom) ratios of $\sim$ 50 and $\sim$ 600 ppm. These samples were used to calibrate I_{Bcell} by measuring their $^{10}B^{3+}$ current directly in a Faraday cup that can be inserted immediately in front of the absorber cell. In this way we are able to convert I_{Bcell} currents (up to $\sim 4,000\,n$A) to absolute $^{10}B^{3+}$ particle rates, and correspondingly, estimate the ^{10}B:^{9}Be ratio in the BeO target assuming similar negative ion efficiencies and transmission. For example, beryl processing blanks (FOM $\sim$ 50, $I_{Bcell} \sim 200\,n$A) correspond to $\sim$ 10 ppm B:Be in the target oxide.

3.3 Contaminated samples

In November 2005 a 4 m snow pit (DSS0506-pit) was dug near the summit of Law Dome, Antarctica, and a set of forty samples of ice were taken for ^{10}Be measurement. This work was a component of our research program to gain a more thorough understanding of the atmospheric transport and deposition of ^{10}Be to polar ice sheets [*Pedro et al.* 2009; *Pedro et al.* 2011a/Chapter 2]. The samples were melted in the presence of our low ^{10}Be beryl-derived carrier, filtered and acidified at the Antarctic Climate & Ecosystems Cooperative Research Centre (ACE-CRC) in the University of Tasmania (UTAS) in Hobart. All of the ice was consumed during processing. Additionally, full procedural blanks were prepared with high-purity deionised water and beryl carrier and treated as for the ice samples. The liquid samples were then sent to the ANSTO for further preparation to BeO and finally measurement on ANTARES.

The sample preparation method is based on *Child et al.* [2000], and is detailed in Fig. 3.1. During this preparation method, the bulk of the boron is separated by the cation exchange column, as boron is not retained on Dowex 50W-X8 at any pH [*Korkisch*, 1989]. Any remaining boron should be removed in the final step before calcining, when the $Be(OH)_2$ is rinsed with deionised water three times, as all boron species are soluble at neutral pH [*Pourbaix*, 1974]. This identical procedure had been previously employed for over 100 ice samples for measurement on ANTARES, all of which had acceptable boron levels.

However, on measurement it was found that this set of samples had become contaminated with boron. For the targets measured, the I_{Bcell} ranged from 550–5100 (average = 2700) and the FOM ranged from 440–4840 (average = 2600). These exceptionally high boron rates, coupled with the relatively low ^{10}Be:^{9}Be ratios typical for these ice samples, lead to an unacceptable increase in the ^{10}B-induced detector background. As this important sample set was collected at great expense and effort, measurement was terminated early so as to preserve the remaining BeO. Eleven of the sample targets and all of the eight procedural blanks targets were measured during this run.

Rather than relying upon a numerical correction to the ^{10}Be data, which could introduce significant errors, it was decided that a method for reprocessing the targets to decrease the boron concentration should be developed. In this paper we describe the reprocessing technique and present results demonstrating the success of the technique, as well as a series of experiments that were designed to identify the source of abnormally high boron levels in these targets.

3.4 Materials and methods

High purity (18.2 MΩ cm^{-1}) deionised water was used throughout and all reagents were analytical grade. Unless otherwise specified, the beryllium carrier used was BDH Spectrosol 1000 mg^{-1} L.

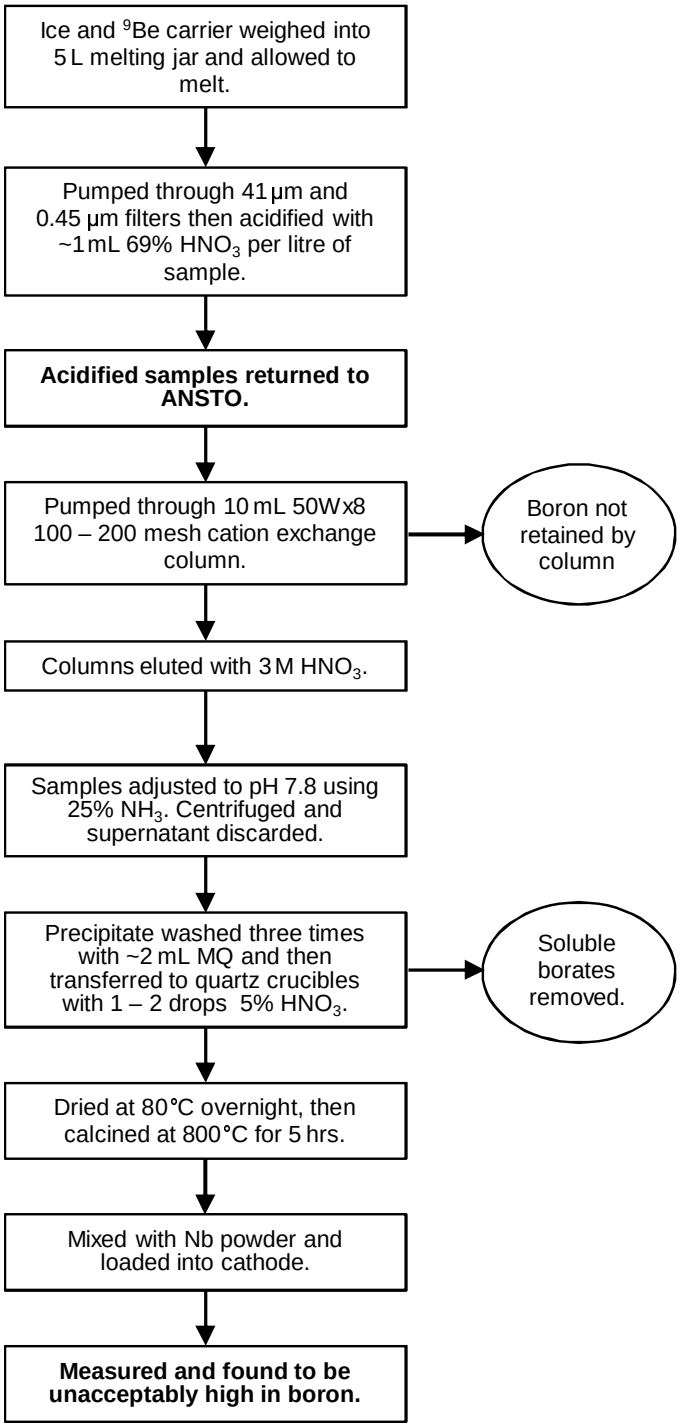

Figure 3.1: Sample preparation method for the boron-contaminated sample set.

3.4.1 Reprocessing method

Two options for removing the boron were investigated on trial samples: (1) volatilisation, where samples are heated in the in the presence of HF to liberate boron as volatile boron trifluoride, which can be represented as: $H_3BO_3 + 3HF \rightarrow BF_3(g) + 3H_2O$; and (2) reprecipitation, where (making use of the solubility of boron at high pH [*Pourbaix*, 1974]), the precipitated $Be(OH)_2$ is dissolved in dilute HNO_3 and then re-precipitated with NH_3, with the aqueous boron discarded in the supernatant. This rinses out boron that may have been trapped within the $Be(OH)_2$ precipitate.

In order to reprocess the contaminated AMS targets the BeO required dissolving. A complication is presented by the presence of the niobium which had been mixed with the BeO. Furthermore, when loading small amounts of oxide an additional 4 mg of niobium is added between the pin and the sample; this was the case for the DSS0506-pit samples. Separating the beryllium from the niobium is important as any niobium carried through into reprocessed $Be(OH)_2$ would be oxidised during the calcining step and hence dilute the BeO content reducing ion-source yield.

Both 50 % HF and 98 % H_2SO_4 were found to preferentially dissolve BeO leaving the niobium metal; H_2SO_4 was chosen for safety reasons. Any dissolved niobium remaining in solution was removed by precipitation at pH = 2.5–3.0, i.e. within the pH range that beryllium is soluble and niobium is insoluble [*Asselin et al.*, 2007]. It was assumed that any caesium introduced by the initial measurement on ANTARES was removed in the discarded supernatants, due to the high solubility of caesium salts.

A method utilising both the volatilisation and repeated precipitation options was found to be best at removing the boron. An overview of this method is depicted in Fig. 3.2. The BeO/Nb was removed from each target holder by pushing the loading pin forwards out of the sample recess and collecting the solid plug in a small centrifuge tube. For the first stage of chemical reprocessing, aimed at dissolving the BeO but leaving the bulk of the niobium, the solid was transferred into a small PTFE beaker with 2 mL of 98 % H_2SO_4 then heated and ultrasonicated for 2 hours (or until it fully disintegrated). Following this treatment, the sample was centrifuged and the supernatant returned to a small PTFE beaker. 2 mL of 50 % HF was then added to the sample, whereupon it was heated with until its volume was constant at less than 2 mL, so driving off the BF_3 and excess HF.

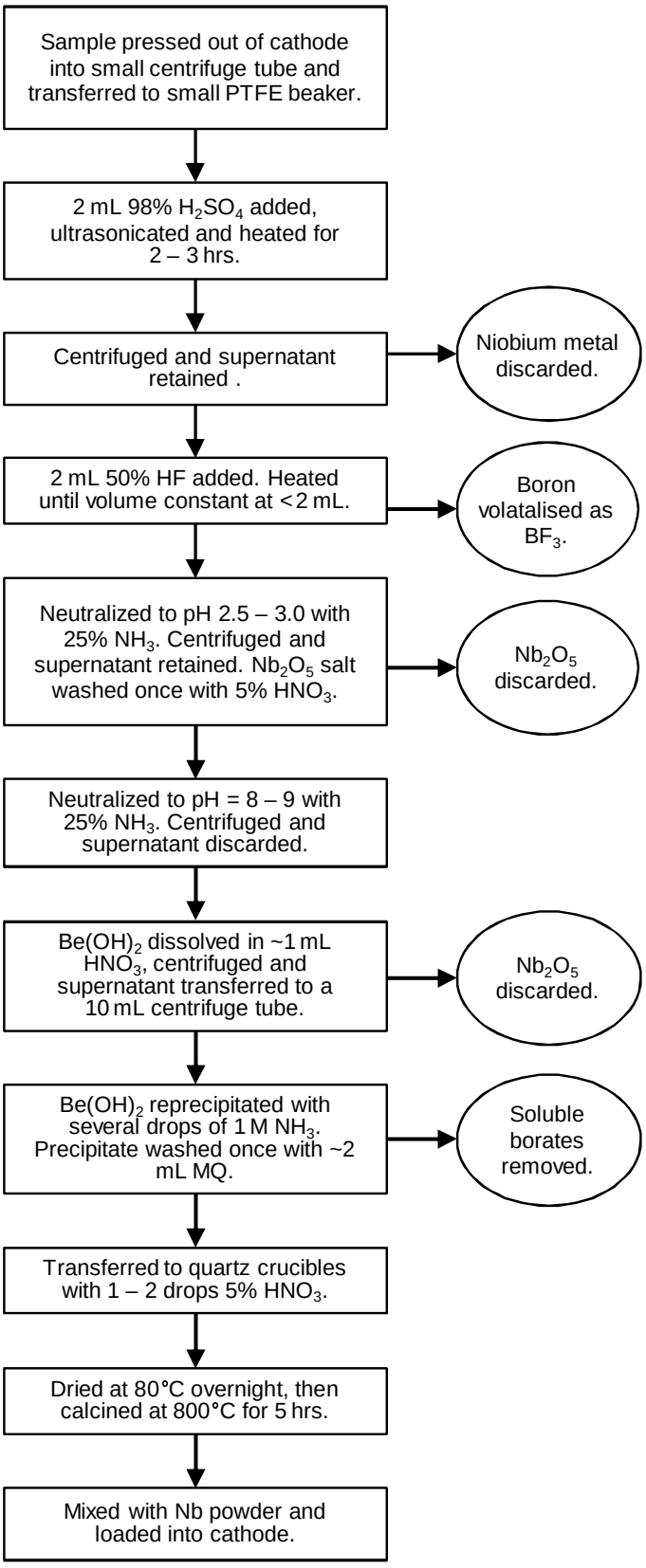

Figure 3.2: Details of the method used to reprocess the boron-contaminated AMS targets for measurement on ANTARES. 45

This solution, with the bulk of the boron now removed, was made up to 20 mL with deionised water. In an additional step aimed at removing any dissolved niobium, the pH was adjusted to 2.5–3.0 with 25 % NH_3, before allowing the sample to sit overnight to permit the Nb_2O_5 to fully precipitate. The following day, the sample was centrifuged, and the supernatant, containing the dissolved beryllium, transferred to a clean centrifuge tube. The Nb_2O_5 precipitate was rinsed once with 2 mL 5% HNO_3 to strip out any adsorbed beryllium. The pH of the supernatant was adjusted to 8–9 with 25 % NH_3, and again allowed to sit overnight to fully precipitate beryllium as $Be(OH)_2$. This precipitate was collected and the supernatant discarded. 1 mL of 1 M HNO_3 was then added to the precipitate in order to redissolve the beryllium. A small fraction of precipitate failed to redissolve, and was assumed to be Nb_2O_5. The sample was centrifuged and the supernatant (containing the beryllium) collected. The Nb_2O_5 precipitate was rinsed twice with 1 mL 1 M HNO_3 to strip out any adsorbed beryllium which was then added to the beryllium-bearing supernatant.

The $Be(OH)_2$ was then dissolved and re-precipitated a second time to further reduce boron levels; the $Be(OH)_2$ is redissolved in a few drops of 1 M HNO_3, and then neutralised with dilute NH_3 to re-precipitate the $Be(OH)_2$. The sample was centrifuged, and the supernatant containing the soluble borides discarded. A final rinse with deionised water completes this stage of the reprocessing.

Finally, the precipitate was transferred into a small quartz crucible with 1–2 drops of 5 % HNO_3, dried in a 80 °C oven overnight and then calcined at 800 °C for 5 hours to convert the hydroxide to BeO, as per our usual method. The oxides were mixed with four times their mass in niobium and rear-loaded into detachable cap target holders, which have a smaller 1 mm diameter recess, ready for measurement on ANTARES.

3.4.2 Experiments to identify the ^{10}B contamination source

The sample preparation method used for the contaminated sample set (detailed in Fig. 3.1), has been used with success in previous studies [*Smith et al.*, 2000; *Pedro et al.*, 2006], indicating that it is not our sample preparation method per se that is the problem. It was also possible to rule out UTAS and the Antarctic ice itself as the contamination source, as partial procedural blanks started using deionised water at ANSTO were similarly contaminated. This implies a contamination event(s) that

occurred during the processing of these samples at ANSTO. The contamination in the final BeO indicates that the boron was too high to be removed by the normal processing steps, or was introduced during or after the $Be(OH)_2$ precipitate was rinsed with the deionised water.

There are many potential sources of boron, even in a HEPA filtered laboratory. Previous studies have shown that the filters used in laboratory air systems can be a major source of the boron in blanks for boron isotopic analysis [*Rosner et al.*, 2005]. Boron can also be found in laboratory equipment, in particular borosilicate glass (e.g. Pyrex®), though ice samples at ANSTO are prepared using only cleaned plastics and PTFE. Furthermore, whilst analytical grade chemicals and high purity deionised water (18.2 $M\Omega\,cm^{-1}$) are used exclusively for the ice samples, boron could have been introduced by contaminated reagents, e.g. nitric acid and ammonia preparations used in chemical processing. In an effort to determine the source of the boron contamination, a series of BeO targets were prepared for measurement on ANTARES. The same equipment and chemicals used in the preparation of the contaminated samples (when available) were used in the preparation of these targets.

As the contamination was limited to the DSS0506-pit samples and procedural blanks, our testing initially focussed on the equipment and the chemicals that were specific to the preparation of these samples: new tubing (3.4.2.1) and ion exchange resin (3.4.2.2) had been purchased for the processing of these samples. Other uncontaminated ^{10}Be samples were prepared at the ANSTO cosmogenic laboratory around the same time, but these were rock samples and underwent significantly different preparative chemistry [*Child et al.*, 2000], including heating with HF, volatilising the boron as BF_3. It was therefore possible that the boron was introduced into the contaminated sample set in such a way that it was removed by the fuming step in the rock chemistry, but not by the ice chemistry. For this reason, the beryllium carrier (3.4.2.3) and the laboratory air (3.4.2.4) were also tested. There was also some concern that the contamination may have come from one of the furnaces (which was used for the ice samples, but not the rock samples) or the Macor® trays that are known to be 2 % boron, so these samples were calcined in an uncontaminated furnace and with metal trays. A separate experiment tested this furnace/tray combination (3.4.2.5).

It was not possible to test the HNO_3, NH_3 or deionised water used during the processing of the contaminated samples as the reagents had been consumed and the water system

cartridges had been replaced by the time the contamination was identified.

Replicate samples were prepared for all experiments. The test samples, described below (Sect. 3.4.2.1–3.4.2.4), were prepared for measurement on ANTARES in the following manner. The pH of the sample was increased to 7.8–8.2 with NH_3, and centrifuged to collect the precipitate. The supernatant was discarded and the precipitate washed three times with 1 mL of deionised water. The precipitate was transferred into a quartz crucible, dried overnight at 80 °C and then calcined at 800 °C for 5 hours. All the oxides were mixed with four times their weight of niobium and pressed at 120 kPa into rear pressed 1.6 mm aluminium target holders, and measured for I_{Bcell} and FOM on ANTARES.

3.4.2.1 Tubing

Samples containing 100 g deionised water, 0.3 g of beryllium carrier, and 0.06 g of 69 % HNO_3 (to represent a melted ice matrix) were prepared in 200 mL cleaned plastic beakers. The samples were circulated through new but pre-rinsed Viton ® black tubing for 16 hours. The beakers were covered in parafilm to reduce any contact with laboratory air.

3.4.2.2 Column resin

One litre samples of deionised water containing 0.3 g of beryllium carrier were added by hand (i.e. without the Viton® tubing) onto a conditioned Dowex™ 50W-X8 cation exchange column (10 mL, 100–200 mesh). The beryllium was then eluted with 55 mL 3 M HNO_3.

3.4.2.3 Laboratory air

Beryllium spiked deionised water samples were prepared in the same manner as the tubing samples. These were allowed to sit open to the laboratory air for 16 hours.

3.4.2.4 Beryllium carrier

Aliquots (1 mL) of the beryllium carrier used for the DSS0506-pit contaminated samples (Prepared from mineral beryl, ^{9}Be = 304 mg L^{-1}) were added to 30 mL of deionised water.

3.4.2.5 Furnace/trays

1 mg high purity BeO (Aldrich, 99.99%), which is used as an instrument blank on ANTARES, was weighed into quartz crucibles with 3–5 drops of deionised water. These quartz crucibles were calcined in the Macor® trays in the furnace used for the ice samples for 5 hours at 800 °C.

3.5 Results and discussion

The reprocessing of the boron contaminated targets was very successful. The dramatic decrease in boron can be seen in Fig 3.3a and b, where the I_{Bcell} and FOM for each target are plotted before and after reprocessing. The FOM shows a greater improvement than the I_{Bcell}, indicating that reprocessing also improved the BeO^- current. With the exception of one procedural blank, all reprocessed targets had FOM$<$ 400, while the average was 130 (1σ = 120), reduced from 2600 (1σ = 1300) prior to reprocessing, and I_{Bcell} of $<$ 800 with an average of 280 (1σ = 110) , reduced from 2600 (1σ = 1300). The procedural blank with high boron had a ^{10}Be:^{9}Be of 30×10^{-15} (down from 180×10^{-15}) and was not used in the data analysis. However, all the other procedural blanks measured ^{10}Be:^{9}Be ratios of $\sim 10^{-15}$, typical for ice blanks using this beryl carrier. This is a significant improvement on the initial boron contaminated measurements, which were up to 200×10^{-15}. It may be pertinent that the target with a high boron level (OZ2369) was reprocessed in the initial trials of the reprocessing method. This could mean that the contamination source was present in the laboratory during the trials, for example in one of the pre-diluted reagents, but had gone by the time the rest of the samples were reprocessed.

The average yield of the BeO for the reprocessing of the targets ranged from 6–72 % with an average of 40 %. The low yields, probably due to losses in the rinses and during

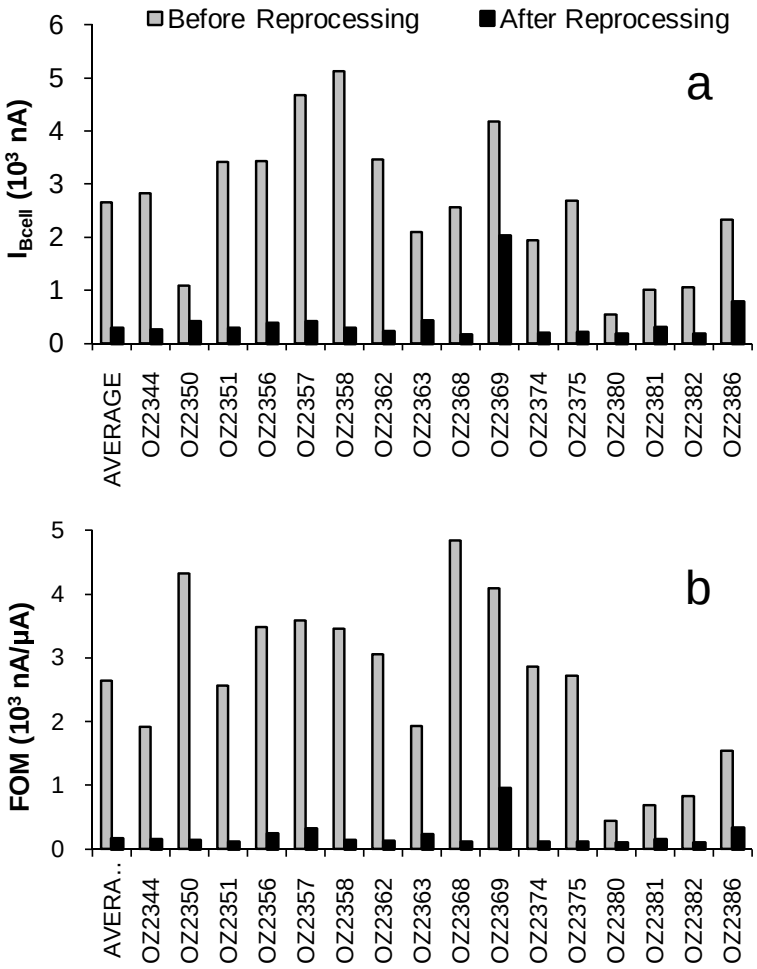

Figure 3.3: Improvement in boron levels was observed after reprocessing: **(a)** as measured in terms of the I_{Bcell} current, and **(b)** as measured in terms of the figure of merit (FOM).

Table 3.1: The measured I_{Bcell} currents and figure of merit (FOM) of the test samples from Sect. 3.4.2 investigating potential sources for the boron contamination. All the FOMs are < 400, indicating no major boron contamination.

Experimental Sample	Number of Replicates	I_{Bcell} Average (nA)	FOM Average (nA/μA
Tubing	2	800	240
Laboratory Air	2	720	180
Column Resin	3	750	200
^{9}Be Carrier	5	530	170
Furnace/Trays	2	700	240

transfers between many vessels, made it necessary to use target holders with smaller 1 mm recess diameters. However, even with the small BeO mass, the ^{10}Be:^{9}Be of the samples were measured to $< 4\,\%$ accuracy.

None of the targets prepared in Sect. 3.4.2 to investigate the source of the boron contamination had high levels of boron when measured on ANTARES. As seen in Table 3.1, each FOM was less than 300, and the I_{Bcell} currents less than 800. These values are within the normal range for samples on ANTARES, and less than even the lowest FOM measured in the contaminated sample set.

Potential sources for the contamination which could not be tested in the present experiments were the deionised water and the HNO_3 and NH_3 used on the affected sample set. Notably, the records for the deionised water system show that the cartridges were replaced just after this sample set was finished, and that, due to a scheduling error, these new cartridges were overdue by a few months.

3.6 Conclusion

We have presented a technique capable of reprocessing boron-contaminated ^{10}Be AMS targets, which were previously unmeasurable on the ANTARES AMS. The boron contaminated sample set was successfully reprocessed and meaningful results were obtained. The results from these samples were reported in *Pedro et al.* [2009], and the data used to investigate the links between concentration signals at Law Dome and solar cosmic ray events.

Frustratingly, the contamination source for the boron was never pinpointed, although most of the equipment and many of the reagents were ruled out as potential sources. The analytical grade concentrated NH_3 and HNO_3 and the deionised water used during the preparation of the sample set remain as plausible but unconfirmed sources of the boron contamination.

While the reprocessing technique is effective, it is obviously preferable to maintain low boron levels in samples during chemical processing as a matter of course. To this end, a HF/H_2SO_4 fuming step has also been added into the standard procedure for processing ice for ^{10}Be analysis. Additionally, post-stripping the $^{10}Be^{3+}$ ions from 3+ to 4+ via a thin carbon stripper foil has been developed for use on ANTARES during analysis, should any future ^{10}Be targets be found to be contaminated with boron as we have demonstrated that this technique reduces the boron rate by a factor of ~ 7. Since the implementation of these measures, there have been no issues with boron in ice samples prepared and measured for ^{10}Be at ANSTO [*Pedro et al.* 2011a/Chapter 2 and Chapter 5].

Chapter 4

^{10}Be Transport to Antarctica: Results from Seasonally-Resolved Observations and Modeling

J. B. Pedro[1,2], U. E Heikkilä[3], A. Klekociuk[4], A. M. Smith[3], T. D. van Ommen[2,4] and M. A. J. Curran[2,4]

Published December 2011 in the *Journal of Geophysical Research (Atmospheres)*, 116, D23120, doi:10.1029/2011JD016530.

[1]Institute of Marine and Antarctic Studies, University of Tasmania, Hobart, TAS, Australia
[2]Antarctic Climate and Ecosystems Cooperative Research Centre, Hobart, TAS, Australia
[3]Australian Nuclear Science and Technology Organisation, Lucas Heights, NSW, Australia
[4]Australian Antarctic Division, Kingston, TAS, Australia

Abstract

Cosmogenic ^{10}Be measured in polar ice cores has important application in the reconstruction of past solar activity. However, the processes controlling its atmospheric transport and deposition to the ice sheets are not fully understood. Here we use the seasonal changes in ^{10}Be concentrations in a 10-year monthly resolved ice core record from the Law Dome site (East Antarctica), in conjunction with ECHAM5-HAM general circulation model (GCM) simulations of ^{10}Be and ^{7}Be deposition, as tools to examine this problem. Maximum ^{10}Be concentrations are observed in the ice core during the austral late summer to early autumn (summer-autumn), while minimum concentrations are observed during the austral winter. The GCM simulations, corroborated by earlier observations of ^{10}Be:^{7}Be ratios in Antarctica from the Georg von Neumayer air sampling station, suggest that the ^{10}Be concentration maximum is linked to direct input of stratospheric ^{10}Be from the Antarctic stratosphere to the lower levels of the Antarctic troposphere during the austral summer-autumn. This result contrasts with the modeled transport of ^{10}Be to Greenland, where the seasonal maximum in stratospheric input is seen in the late winter to spring, synchronous with the timing of the seasonal maximum in mid-latitude stratosphere to troposphere exchange. Our results suggest that a different combination of processes are responsible for the transport of ^{10}Be to the Antarctic and Greenland ice sheets.

4.1 Introduction

Seasonal cycles are among the highest amplitude signals in ice core trace-chemical records. With the aid of modern instrumental data and general circulation models these seasonal cycles can be studied to uncover important details concerning the physical processes which influence the source, transport and deposition of trace-chemicals to the polar ice sheets [*Jones et al.*, 2009]. This in turn, can lead to more reliable interpretation of ice core records as indicators of paleoenvironmental change [e.g. *van Ommen and Morgan*, 1997; *Werner et al.*, 2000; *Laepple et al.*, 2011].

This paper is focused on the seasonality of the cosmogenic radionuclide ^{10}Be. Records of ^{10}Be from the polar ice sheets potentially provide information about the history of variations in solar activity and cosmic ray intensity. This history is vital for refining

understanding of the role of the sun in forcing past and present climate change [e.g. *Bard et al.*, 2000; *Vonmoos et al.*, 2006; *Muscheler et al.*, 2007; *Usoskin et al.*, 2009; *Steinhilber et al.*, 2009; *Delaygue and Bard*, 2011]. However, reliably interpreting ^{10}Be records from ice cores hinges on a thorough understanding of the physical processes that control the production, transport and deposition of ^{10}Be to the ice sheets.

The chain of processes that ultimately delivers ^{10}Be to the polar ice core sites begins with the interaction of secondary particles of the cosmic ray-induced atmospheric cascade with N and O atoms in the atmosphere [*Lal and Peters*, 1967]. The global production rate of ^{10}Be is proportional to the flux of cosmic rays to Earth, which is in turn is modulated by variations in both solar activity and the Earth's geomagnetic field (see *Lean et al.* [2002]; *Webber and Higbie* [2003]; *McCracken et al.* [2004]; *Muscheler et al.* [2007]; *Masarik and Beer* [2009]; *Kovaltsov and Usoskin* [2010] for details and complexities). Globally, 50 to 75% of ^{10}Be production occurs in the stratosphere, with the remainder in the upper troposphere [*Masarik and Beer*, 1999; *Heikkilä et al.*, 2009]. Following production, the nuclide is immediately attached to sub-micron aerosol particles and then transported with air masses [*McHargue and Damon*, 1991]. After an average atmospheric residence time of $\sim$1 year in the stratosphere and days to months in the troposphere [*Raisbeck et al.* 1981; *Jordan et al.* 2003; *Heikkilä et al.* 2009; *Pedro et al.* 2011a/Chapter 2] these particles are deposited to the Earth's surface. Deposition can occur by both wet (precipitation related) and dry (turbulent and gravitational) processes [*Davidson et al.*, 1996]. At ice core sites with relatively high precipitation rates, e.g. coastal Antarctica and most Greenland sites, the majority of ^{10}Be is wet deposited, whereas at low-precipitation sites, e.g. those on the East Antarctic Plateau, the majority is dry deposited [*Raisbeck and Yiou*, 1985; *Smith et al.*, 2000; *Field et al.*, 2006; *Heikkilä et al.*, 2009].

The measured concentration of ^{10}Be in ice is a function of interplay between the above-mentioned production, transport and deposition processes. The challenge in interpreting long term ^{10}Be records is to separate the production signal, which provides useful information on past changes in solar or geomagnetic activity, from the non-production signal, which is affected by atmospheric circulation and deposition processes. Here, we use the observed seasonality of ^{10}Be in Antarctic ice in conjunction with general circulation model (GCM) simulations of ^{10}Be production and transport as tools to examine this complex problem.

From an observational perspective, characterization of seasonality and its drivers requires precisely-dated and well-resolved ice core or snow pit records, ideally overlapping with the period of modern satellite and ground based environmental observations. Records from the Law Dome Summit South site (DSS, Fig. 4.1) in coastal East Antarctica are well suited for this task. The first indication of ^{10}Be seasonality at the site was from a sub-monthly-resolved snow pit spanning 1-year [*Pedro et al.*, 2006]. Maximum concentrations were observed in the late summer to early autumn with minimum concentrations through winter. Firm conclusions on seasonality clearly require a longer data set. Here, we analyse the monthly-resolved 10-year composite ^{10}Be series that was recently presented in *Pedro et al.* [2011a]/Chapter 2.

From a modeling perspective, simulation of ^{10}Be requires a three-dimensional model of the atmosphere, coupled with an aerosol module describing the production, transport and deposition processes of atmospheric particles. Both the GISS ModelE [*Schmidt et al.*, 2006] and the ECHAM5-HAM GCMs [*Roeckner*, 2003] have been used to simulate ^{10}Be deposition to the ice sheets [*Heikkilä et al.*, 2008c, 2009; *Field et al.*, 2006, 2009; *Field and Schmidt*, 2009]. To date, due to lack of highly resolved records, it has not been possible to test GCM performance against seasonal variations in ^{10}Be concentrations in Antarctic ice. Here we test the ability of ECHAM5-HAM to simulate the observed seasonal cycle in ^{10}Be deposition to DSS and then use the GCM data to aid interpretation of the physical processes driving the observed cycle.

4.2 Data and methods

4.2.1 DSS site characteristics and ^{10}Be composite record

Dome Summit South (DSS, 66°46.18'S 112°48.69'E, Fig. 4.1) is the main ice core drilling site on Law Dome, coastal East Antarctica (see *Morgan et al.* [1997] for site characteristics). High temporal resolution ($\sim$ monthly) ^{10}Be measurements have been carried out at DSS over a number of years, with good agreement observed between multiple records sampled up to 500 m apart [*Pedro et al.* 2011a/Chapter 2]. This indicates that variations in ^{10}Be concentrations at the site are primarily driven by production and atmospheric transport and deposition related factors and are not strongly affected by post-depositional processes. The 10-year ^{10}Be record used here is a composite derived

from three discrete, but identically processed ice cores. Full details concerning the sampling, chemical preparation, Accelerator Mass Spectrometer (AMS) measurement and construction of the composite ^{10}Be record are available elsewhere [*Pedro et al.* 2011a/Chapter 2]. Measurement uncertainties for the ^{10}Be record are small ($\sim$ 3%) and will be neglected in the analysis to follow.

The cores used in the composite record were originally sampled at an average temporal resolution of 10 samples per year. To better facilitate intercomparison with other data sets the ^{10}Be data was interpolated onto a monthly grid. The timescale has been improved (over *Pedro et al.* [2011a]/Chapter 2) through the use of reanalysis precipitation data from the European Centre for Medium-Range Weather Forecasts Interim Re-Analysis (ERA-Interim, [*Simmons et al.*, 2006; *Uppala et al.*, 2008]) to provide information on the seasonal distribution of precipitation variations within years (see Appendix A.). This technique is justified by the excellent agreement between ERA-Interim precipitation data and measured snow accumulation data from a downward pointing radar on a automatic weather station located near the site for the period 1998 to 2002 (Fig. A1). In transferring from the depth-scale to the new time-scale the information from ERA-Interim regarding the time distribution of snow fall leads to changes in the amplitude of some ^{10}Be concentration peaks relative to *Pedro et al.* [2011a]/Chapter 2 (see Fig. A2). These changes do not affect any conclusions of our previous work including the strength of the correlation between neutron counting rates and ^{10}Be concentrations.

In measuring the shared variance between time series in this paper we use the bivariate Pearson's correlation coefficient (r_{xy}), calculated using the method detailed in *Mudelsee* [2003]. This method employs the nonparametric stationary bootstrap with an average block length proportional to the maximum estimated persistence time of the data. The method is preferred over standard regression techniques since it yields robust results for r_{xy} and associated 95% confidence intervals (CIs) even for data that is autocorrelated, unevenly spaced and non-normally distributed such as the DSS ^{10}Be data.

4.2.2 ECHAM5-HAM model description and setup

For the model runs we use the ECHAM5 GCM [*Roeckner*, 2003] coupled to the HAM aerosol module [*Stier et al.*, 2005], which simulates the production, transport and depo-

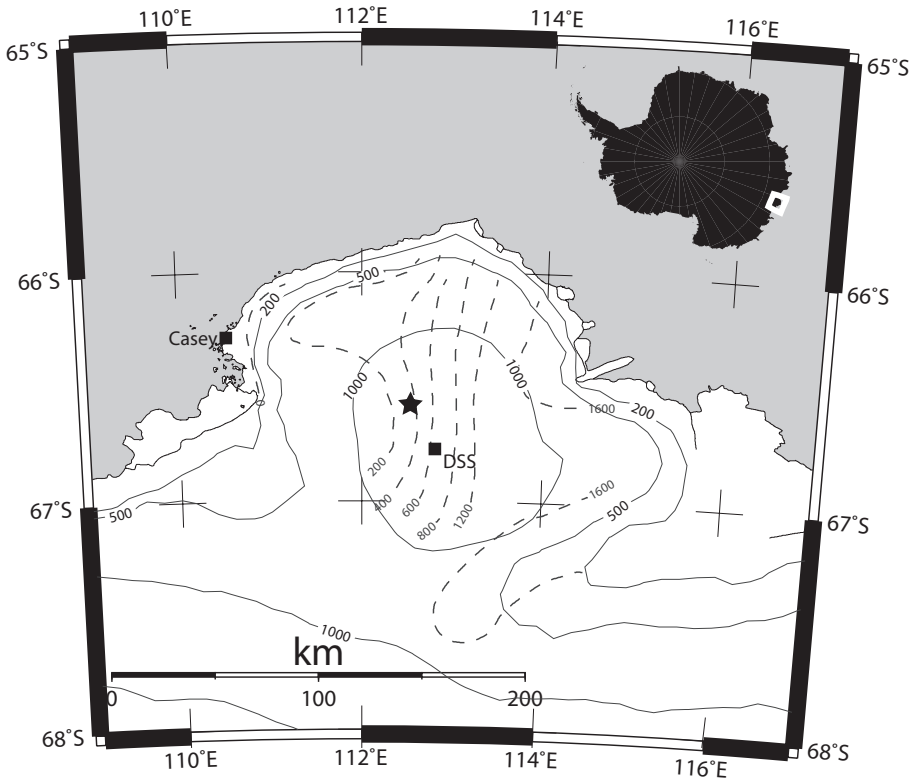

Figure 4.1: Location of the Dome Summit South (DSS) sample site, Law Dome with surface elevation contours (m, solid lines) and accumulation isopleths (mm ice equivalent, dashed lines). The centre point of the ECHAM5-HAM grid cell used in the analysis is marked by the star.

sition processes of aerosols. Solar modulation of the ^{10}Be production rate is simulated using the ^{10}Be production functions of *Masarik and Beer* [2009] and monthly-resolved values for the solar activity parameter (Φ) from [*Usoskin et al.*, 2005, available at `http://cosmicrays.oulu.fi/phi/phi.html`]. Since the period under investigation is brief, geomagnetic modulation of production is negligible and the geomagnetic field strength is held constant at the modern level. A detailed evaluation of ECHAM5-HAM's ability to simulate the general patterns of atmospheric circulation and deposition of beryllium radionuclides is provided in *Heikkilä et al.* [2008b].

For this study, the model was run on a T42L39 resolution ($\sim$ 300 km horizontal resolution, 39 vertical levels reaching up to $\sim$80 km), which is the state of the art for global models incorporating chemical modules. Including the whole stratosphere into the model domain is important for a tracer with stratospheric origin, such as ^{10}Be. The

model was run for the years 1993 to 2004. The first 5 years were used to allow ^{10}Be reach equilibrium in the atmosphere and the final 6 years (1998 to 2004) are used here in the analysis. For logistical reasons it was not possible to run the model over the full 10 years of observed data.

Model results were taken from the grid cell centered at 66°35'S 112°30'E (marked in Fig. 4.1) that covers the Law Dome site. Model resolution is a limitation for modeling coastal Antarctica as precipitation and temperature are very sensitive to the steep (sub-grid scale) gradients in elevation between the ocean and the ice sheet [*Bromwich et al.*, 2011]. The accumulation isopleths shown in Fig. 4.1 illustrate the importance of the orographic effect on snow accumulation rates at Law Dome, e.g. the accumulation rate 10 km to the east of the summit is ∼7 times higher than that observed 20 km to the west of the summit. Clearly, such sub-grid scale gradients in accumulation cannot be resolved by this model. However, the transport paths and the life time of ^{10}Be from source to sink are long and controlled mostly by large scale atmospheric processes [*Heikkilä et al.*, 2009]. To be helpful in understanding the factors driving seasonality in ^{10}Be concentrations it is more important for the model to capture these large scale processes than to describe orography in high detail.

4.3 Observational results

4.3.1 ^{10}Be concentrations and production

Fig. 4.2 (upper panel) compares observed ^{10}Be concentrations in the DSS composite against observed monthly variations in the neutron monitor counting rate on the McMurdo neutron monitor (located at 77.9°S, 166.6°E). The counting rate is proportional to the cosmic ray flux and therefore to the ^{10}Be production rate in the atmosphere [*O'Brien and Burke*, 1973]. Both the concentration and the neutron monitor counting rate clearly show the 11-year Schwabe cycle modulation of the cosmic ray flux. Pearson's correlation coefficient (r_{xy}) between annually smoothed (Gaussian filter, effective half width 12 months, dashed lines Fig. 4.2) neutron and ^{10}Be data is strong and significant: $r_{xy} = 0.90$, with 95% CI of 0.86 to 0.92 (although, given the short duration of the record these values should be interpreted with caution). If the correlation is tested on the monthly-resolved data without any smoothing (i.e. averaged over all

timescales) the relation remains significant but degrades to $r_{xy} = 0.64$, with 95% CI of 0.53 to 0.72. This weaker relation illustrates the influence of meteorologically forced variations, including seasonality, on ^{10}Be deposition on sub-annual timescales.

4.3.2 Seasonality in ^{10}Be concentrations

The seasonal cycle in ^{10}Be concentrations at DSS is determined by calculating the average value for each month of the year over the full 10-year record. The result is shown in Fig. 4.2 (lower left panel), with error bars illustrating the standard deviation in the mean for each month. A concentration maximum is observed during late austral summer to early austral autumn (hereafter summer-autumn) and a concentration minimum is observed in winter, this pattern is essentially in line with that suggested by the earlier 1-year DSS snow pit study [*Pedro et al.*, 2006]. A non-parametric Wilcoxon rank-sum test confirms that the seasonal cycle is significant: concentrations during the summer-autumn months of February, March, April ($n = 30$) are significantly higher (at $p < 0.01$) than those during the winter months of June, July and August ($n = 30$).

^{10}Be is unlike most other ice core trace chemicals in that there is no known systematic seasonal trend in its production. This is confirmed by examining the McMurdo neutron monitor counting rates over the 10-year record. Converting the counting rates to production via the relation suggested in *Moraal et al.* [2005], we find the maximum possible influence of production variability on the observed seasonal cycle is ±3%. This is negligible with respect to the observed ±20% variation in concentrations over an average seasonal cycle. Therefore, the seasonal cycle must be principally driven by variability in factors affecting deposition, including precipitation and related aerosol scavenging processes and atmospheric transport from the atmospheric source regions to the ice sheet.

4.3.3 Seasonality in snow accumulation

The monthly-resolved accumulation record at DSS over the 10-year interval corresponding to the ^{10}Be record is also shown in Fig. 4.2 (upper panel). Full details on the determination of the accumulation record are provided in Appendix A. A significant, although weak, negative relationship is observed between ^{10}Be concentrations and the

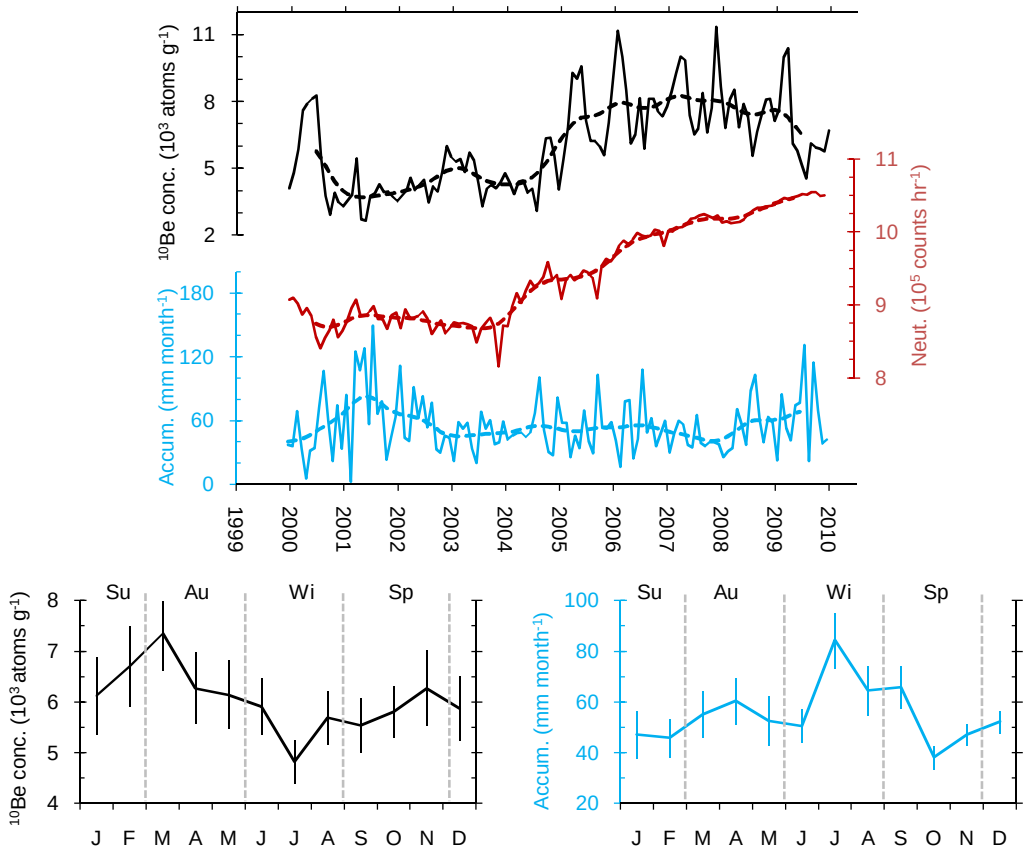

Figure 4.2: Observed data: the upper panel shows ^{10}Be concentrations in the 10-year DSS composite (adapted from *Pedro et al.* [2011a]/Chapter 2), the neutron counting rate on the McMurdo neutron monitor (proportional to the atmospheric production rate of ^{10}Be) and the accumulation at the site inferred from observations and ERA-Interim reanalysis data (see Appendix A). Dashed lines depict annually smoothed data (Gaussian filter, effective half-width 12 months). The lower panel shows the average seasonal cycles in ^{10}Be concentrations (left) and accumulation rate (right). Vertical error bars represent the standard errors in the mean value for each month.

snow accumulation rate (r_{xy} = -0.27, with 95% CI of -0.41 to -0.10). Notably, the two periods of highest accumulation rate throughout the record (in 2001 and 2009) coincide with decreases in concentrations.

To examine the potential role of accumulation variability in forcing the observed seasonal cycle in ^{10}Be concentrations we calculate the mean seasonal cycle in snow accumulation over the 10-year interval (Fig. 4.2, lower right panel). The seasonal maximum in observed accumulation occurs during the winter-spring (July to September), coinciding with the seasonal minimum in ^{10}Be concentrations. However, there is no accumulation counterpart to the summer-autumn concentration maximum. Testing the correlation between the seasonal cycles in concentration and accumulation yields r_{xy} = -0.55 with (95% CI of -0.92 to 0.21), which implies a negative relationship overall, although not significant at the 95% level.

Previous studies indicate that the relationship between precipitation rates and ^{10}Be concentrations is not straightforward [*Graly et al.*, 2011]. At sites where ^{10}Be is mainly wet deposited, such as at DSS [*Smith et al.*, 2000], precipitation events are required to scavenge aerosol-bound ^{10}Be atoms from the atmosphere and deposit them to the ice sheet. Precipitation scavenging occurs via both in-cloud processes, in which aerosol particles serve as cloud condensation nuclei or ice nuclei ('rainout'), and below cloud processes, through collision of particles with precipitation ('washout') [*Davidson et al.*, 1996]. Rainout is the dominant form of wet deposition, although in the early stages of heavy precipitation events washout is also important *Twomey* [1977]. Washout by precipitation strips beryllium radionuclides from the lower troposphere, such that their concentration in the air is progressively depleted during the precipitation event. Snow is more effective than rain at this form of scavenging [*Ishikawa et al.*, 1995]. This cleansing of the air-mass is also reflected in decreasing concentrations of beryllium radionuclides measured in the precipitation itself over the duration of the event [*Ishikawa et al.*, 1995; *Brown et al.*, 1989]. Also, *Smith et al.* [2000] observed that ^{10}Be concentrations at ice core sites to the east of the Law Dome summit, which due to the prevailing easterly atmospheric circulation are the first to receive precipitation, are higher than at sites to the west of the summit and suggested that a washout process may be responsible.

Washout and rainout also affect air masses during their transport to a sampling site. In fact, the seasonal variability in precipitation rates along the moisture transport pathway may have a more important influence on the seasonal cycle in radionuclide concentra-

tions than the precipitation rate at the site itself [*Feeley et al.*, 1989]. In line with this, *Graham et al.* [2003] observed lower ^{10}Be concentrations during periods of particularly high precipitation at several sites in New Zealand. However, *Heikkilä et al.* [2008a], did not observe any such relationship at two sites in Switzerland. Overall, the literature suggest that precipitation is one of a number of factors influencing concentrations on seasonal timescales, and its effect is likely to be stronger at sites with large seasonal variability in precipitation.

There is marked seasonal variability in precipitation within the moisture transport pathways to Law Dome. Precipitation over the oceanic moisture sources regions for the DSS site reaches a maximum in winter [*Sodemann and Stohl*, 2009], coinciding with the DSS precipitation maximum. It seems plausible then that washout processes in the transport pathways to Law Dome may link the mid winter minimum in ^{10}Be concentration to the mid winter maximum in precipitation at the site and within the transport pathways to it. However, precipitation rates at DSS offer no explanation for the timing of the ^{10}Be concentration maximum. To explain this feature we now turn to seasonal variability in atmospheric transport pathways informed by GCM modeling.

4.4 ECHAM5-HAM model results

4.4.1 Model evaluation against observations

Observed ^{10}Be concentrations in DSS ice are compared against ECHAM5-HAM modeled concentrations in Fig. 4.3a and basic statistical data is provided in Table 4.1. In the period common to both records the mean concentration ($\pm 1\sigma$) in the observed data is 4.56 ± 1.30 atoms g^{-1}, and in the modeled data is 6.85 ± 2.92 atoms g^{-1}, or a factor 1.5 times observations. Model concentrations also exhibit greater variance than observed concentrations. A factor contributing to this greater variance may be the slightly coarser temporal resolution of the observed data (originally 10 samples per year, interpolated to monthly) compared to the model data (monthly). Also, some natural smoothing of the ice core data is expected due to wind disturbance and reworking of the surface snow [*McMorrow et al.*, 2004].

The observed seasonal cycles in ^{10}Be concentration are compared with those simulated by ECHAM5-HAM in Fig. 4.3b. The cycles are calculated over the full duration of

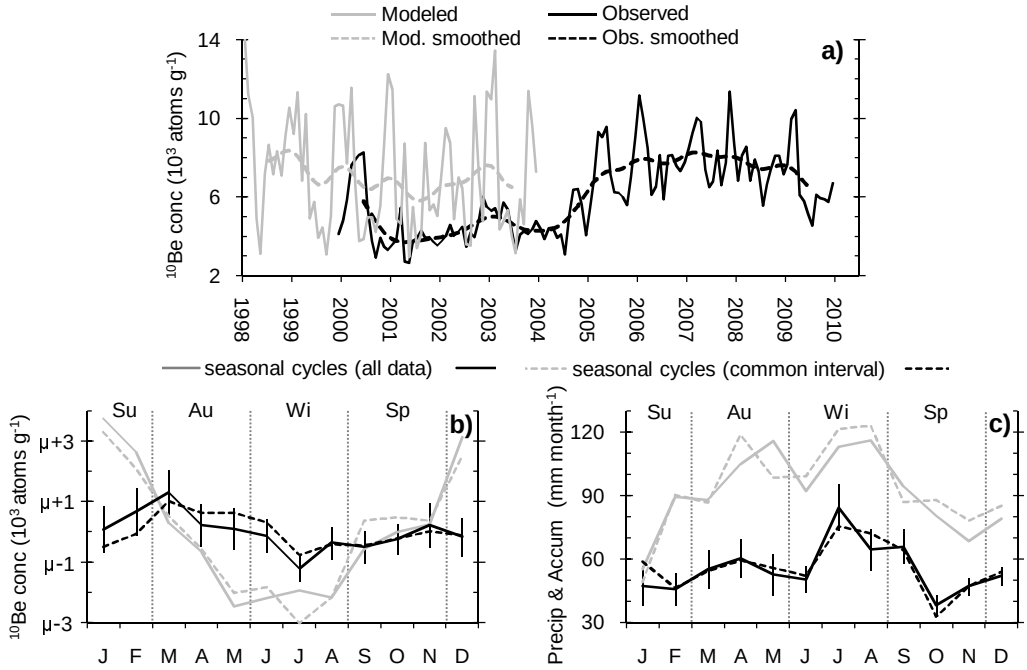

Figure 4.3: Evaluation of ECHAM5-HAM model data against observations. **a)** Observed concentrations in DSS ice and modeled concentrations at the closest grid-point. Heavy dashed lines show annually smoothed data (Gaussian filter, effective half-width 12 months). **b)** Seasonal cycles in observed and modeled ^{10}Be concentrations. Due to the offset between observed and modeled values each cycle is shown as an anomaly from its annual mean value (μ), mean values are listed in Table 4.1. **c)** Seasonal cycles in observed accumulation and modeled precipitation. Vertical error bars represent standard errors in the mean observed values for each month.

Table 4.1: Intercomparison of observed and ECHAM5-HAM-modeled values for precipitation, ^{10}Be concentration and ^{10}Be flux at DSS, Law Dome. Mean ($\pm 1\sigma$) values are calculated over both the 'complete' observed (December 1999 to December 2009) and modeled (January 1998 to December 2003) records and over the 'common interval' to both records (December 1999 to December 2003). Observed precipitation is more correctly a value for the net snow accumulation (see Appendix A).

Parameter	Complete		Common interval	
	Observed $\bar{x} \pm 1\sigma$	Modeled $\bar{x} \pm 1\sigma$	Observed $\bar{x} \pm 1\sigma$	Modeled $\bar{x} \pm 1\sigma$
Precipitation (m water year^{-1})	0.66± 0.12	1.10± 0.09	0.70± 0.17	1.12± 0.09
^{10}Be concentration (10^3 atoms g^{-1})	6.04± 2.04	7.12± 0.35	4.56± 1.30	6.85± 2.92
^{10}Be flux (atoms m^2 s^{-1})	123± 60.2	219± 82.0	95.6± 48.6	216± 82.5

the 10-year observed and 6-year modeled records. Seasonal cycles calculated over only the time intervals common to the observed and modeled records (dashed lines), are not significantly different from those calculated over the full records. Intercomparison of the observed and modeled cycles is somewhat complicated by the fact that the model overestimates the mean observed ^{10}Be concentrations. Hence, in order to focus on the timing and structure of the seasonal cycles rather than on absolute concentrations, we have shown each month of the seasonal cycle as an anomaly from the mean value of the respective record. The model correctly simulates the mid winter minimum in concentrations, however the modeled maximum precedes the observed maximum by two months.

In comparing the observed and modeled data it is important to consider how the model calculates snow concentrations. The model produces deposition fluxes of ^{10}Be from the atmosphere to the surface of the ice sheet. Snow concentrations are then calculated by dividing the interval average deposition flux by the interval average precipitation rate. Model error in precipitation rate can therefore contribute directly to model error in snow concentrations. The situation is reversed in the case of the observed data where concentration is the directly measured term and calculation of fluxes introduces error associated with uncertainties in the snow accumulation rate. Small errors in the timing and amplitude of accumulation events, particularly for highly-resolved data, can therefore lead to large uncertainties in inferred fluxes.

The observed seasonal cycle in accumulation is compared to the ECHAM5-HAM mod-

eled seasonal cycle in precipitation in Fig. 4.3c, cycles are again calculated over both the full records (solid lines) and the four years common to both records (dashed lines). The observed precipitation maximum during mid-winter is also seen in the model; however the model maximum is broader, extending to a secondary maximum in autumn. The greatest discrepancy occurs during mid summer, where the model simulates a strong precipitation minimum that it not seen in observations. The model precipitation error during summer offers an explanation for its overly early simulation of the concentration maximum. As mentioned earlier (Sect. 4.2.2), correct GCM depiction of precipitation in Antarctica is limited by model resolution, particulary in coastal regions such as Law Dome because of the importance of (sub-grid scale) orographic precipitation.

4.4.2 Stratospheric input of ^{10}Be to the polar troposphere

Aircraft sampling in polar regions ($> 60°$ S/N) finds ^{10}Be concentrations in the stratosphere that are up to 5 orders of magnitude higher than in the lower troposphere [*Jordan et al.*, 2003]. These high concentrations are a consequence of the residence time of $\sim$1 year in the stratosphere, compared to days to months in the troposphere [*Raisbeck et al.* 1981; *Jordan et al.* 2003; *Pedro et al.* 2011a/Chapter 2], and the fact that the global maximum in the ^{10}Be production rate occurs in the polar stratosphere [*Lal and Peters*, 1967]. We now use the ECHAM5-HAM to examine the role of stratospheric input to the polar troposphere as a driver of the observed seasonality in ^{10}Be concentrations. The model results are also compared against independent information on stratosphere to troposphere exchange, including observed ^{10}Be:^{7}Be ratios in Antarctic surface air and results from a recent particle dispersion model study.

Considering the model deposition flux, rather than the predicted ^{10}Be concentration, which as discussed above includes errors from the model precipitation term, allows us to focus on the larger scale processes controlling ^{10}Be transport to the site. The ECHAM5-HAM simulated seasonal cycle in total ^{10}Be deposition to DSS can be divided into the total deposition flux with a stratospheric source and the total deposition flux with a tropospheric source (Fig. 4.4a). The stratosphere is clearly the dominant source in absolute terms for ^{10}Be deposited to DSS, according to the model it accounts for on average 64% of the total deposition flux. The relative contribution of the stratosphere is seen in (Fig. 4.4b) to change throughout the year, from a maximum in summer-autumn of 68%, to a minimum in winter of 57%. These fluctuations from the mean

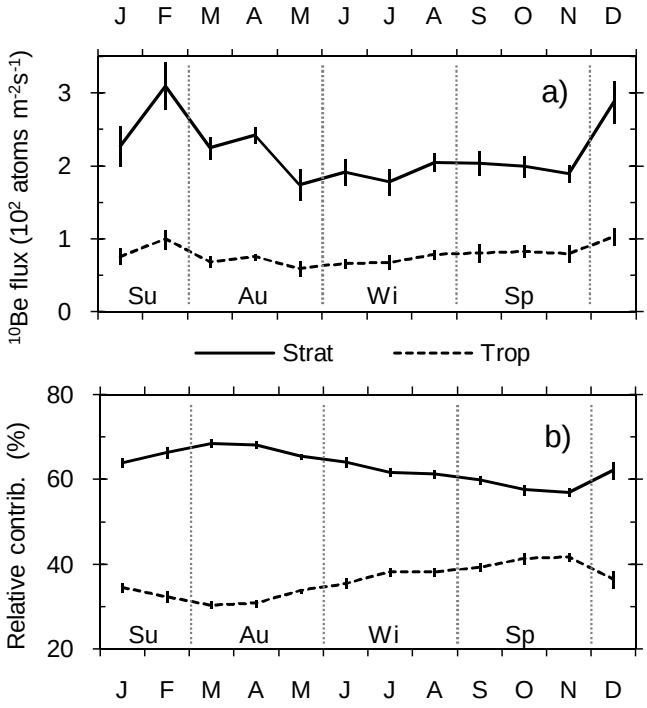

Figure 4.4: ECHAM5-HAM simulated seasonal cycles in deposition flux to DSS, showing the dominance of the stratospheric source and its seasonal variability. **a)** Seasonal cycle in the total flux to DSS broken into the stratospheric component (solid line) and tropospheric component (dashed line). **b)** Seasonal cycle in the relative contribution (%) of the stratospheric and tropospheric components to the total deposition flux. Error bars represent standard errors in the mean values for each month.

value reflect the seasonal variability in stratospheric input of ^{10}Be to the Antarctic troposphere (hereafter stratospheric input). The amplitude of the modeled seasonal variability in stratospheric input in terms of variability in total ^{10}Be deposition appears to be of order $\sim$10%.

The model depiction of stratospheric input can be compared against the seasonal timing of stratospheric input inferred from ^{10}Be:^{7}Be ratios in Antarctic surface air. ^{7}Be has a very similar source and removal distributions to ^{10}Be however it decays much more rapidly (^{7}Be $t_{1/2}$ = 53.2 days, c.f. ^{10}Be $t_{1/2} = 1.36 \pm 0.07 \times 10^6$ years [*Nishiizumi et al.*, 2007]). The two isotopes are produced at a natural ratio of ^{10}Be:^{7}Be = 0.5 (with some altitude dependent variability [*Heikkilä et al.*, 2008a]). The ratio measured in an air mass then increases with time as ^{7}Be decays, only being reset back to the natural production ratio when the air mass is cleaned of its aerosol load by a precipitation event.

This makes the ^{10}Be:^{7}Be ratio a sensitive chronometer for air mass 'age'. Stratospheric air is marked by particularly high ^{10}Be:^{7}Be ratios, due to the long mean residence times of air masses in the stratosphere and absence of cleansing precipitation events. For this reason ^{10}Be:^{7}Be ratios are particulary useful for identifying injections of stratospheric air into the troposphere [e.g. *Dibb et al.*, 1994; *Koch and Rind*, 1998; *Wagenbach*, 1996; *Jordan et al.*, 2003].

The Georg von Neumayer station in coastal Antarctica (70°39'S 8°15'W) is the only Antarctic site for which monthly-resolved ^{10}Be:^{7}Be ratios are available over multiple years (1983 to 1993) [*Wagenbach*, 1996]. Maximum ratios are reported in the summer-autumn and minimum ratios are reported in winter-spring. A recent review of the ongoing aerosol monitoring campaign at this site draws on the ^{10}Be:^{7}Be data along with a longer series of ^{7}Be:^{210}Pb data to conclude that summer-autumn is the period of maximum stratospheric input to the boundary layer at Neumayer [*Elsässer et al.*, 2011]. This timing is in close agreement with the model simulated stratospheric input to DSS, giving confidence in the model results.

The ECHAM5-HAM depiction of the seasonality in stratosphere to troposphere exchange can also be compared against recent results reported in *Stohl and Sodemann* [2010]. In this study, the particle dispersion model FLEXPART is used to calculate the mean probability (hereafter 'transport probability') that air over the Antarctic Plateau has descended from the stratosphere within the past 10 days. We use the *Stohl and Sodemann* [2010] data series, which spans 2000 to 2005 to calculate the mean seasonal cycle in transport probability. At typical cloud heights (1.5 to 3.0 km above ground level) transport probability is highest ($\sim$17%) during the late summer to autumn and lowest ($<$5%) during the winter. At lower and higher levels the seasonal pattern is similar, although absolute values increase with altitude [refer to Fig. 4 of *Stohl and Sodemann*, 2010]. The FLEXPART model, since it uses particle tracing, also explicitly identifies the transport pathway responsible for the maximum in stratospheric input: direct descent of air from the Antarctic stratosphere into the Antarctic troposphere. Importantly, this does not exclude stratospheric input to the Antarctic troposphere that takes place over longer timescales (e.g. longer range transport within the troposphere from the mid latitudes) that may not be detected by the 10-day particle tracing of the FLEXPART model. Indeed, ECHAM5-HAM suggests that the mean time between atmospheric production of beryllium radionuclides and their deposition to DSS is of order 100 days, which is similar to the residence time previously derived from

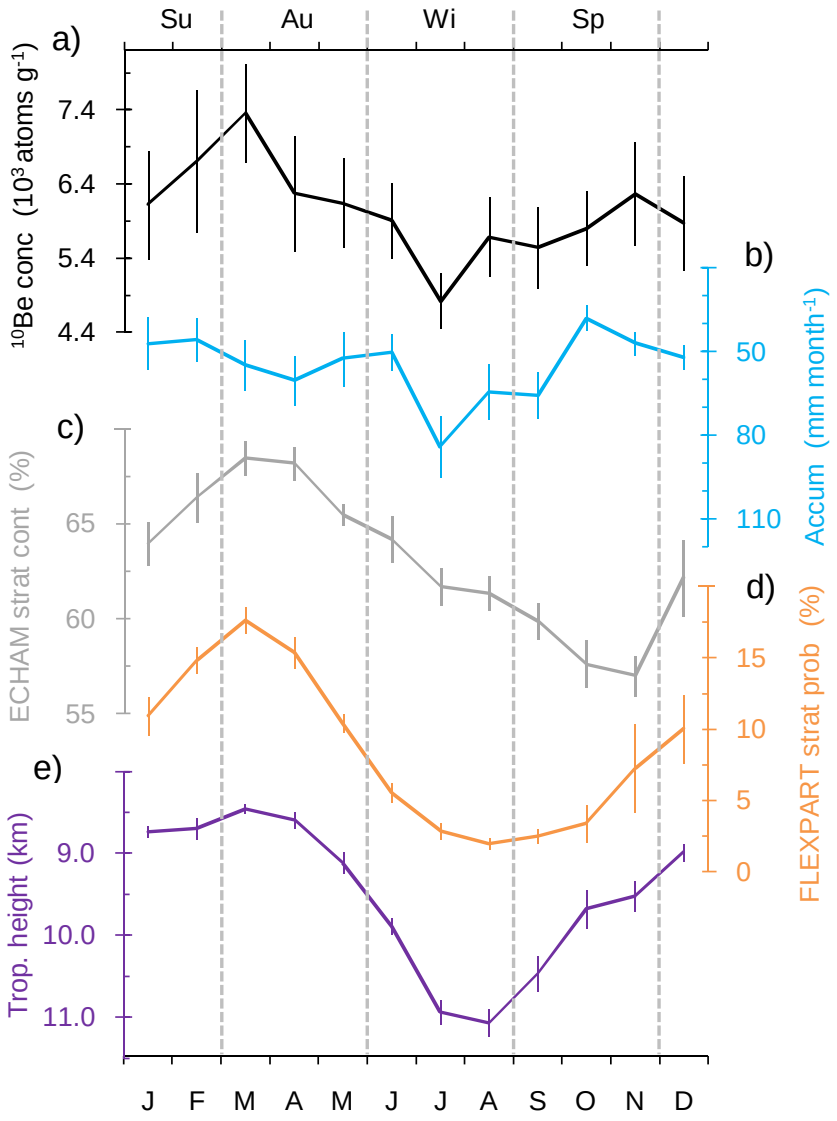

Figure 4.5: **a)** The seasonal cycle in ^{10}Be concentrations at DSS, and an overview of observed and model data suggesting factors that drive it: **b)** Seasonal cycle in accumulation rate (note that the vertical axis is reversed). **c)** ECHAM5-HAM modeled seasonal cycle in the proportion (%) of ^{10}Be atoms deposited to the site that were produced in the stratosphere. **d)** FLEXPART modeled seasonal cycle in the probability (%) that air over the Antarctic Plateau at an altitude of 1.5 to 3.0 km above ground level has come from the stratosphere within the last 10 days (data from *Stohl and Sodemann* [2010]). **e)** Seasonal cycle in the mean geopotential height of the tropopause over DSS (see Sect. 4.4.2 and note that the vertical axis is reversed). Vertical error bars represent standard errors in the mean values for each month. Seasonal cycles are calculated from monthly data over the interval contemporaneous with the ^{10}Be record with the exception of the ECHAM5-HAM (Jan 1998 to Dec 2003) and FLEXPART (Jan 2000 to Dec 2005) for which we are limited to the available data.

observational data at the site [*Pedro et al.* 2011a/Chapter 2]. Within this timescale substantial mixing of air from lower latitudes is expected.

Stohl and Sodemann [2010] note that the seasonal cycle in transport probability closely tracks that of tropopause height, lower tropopause heights are associated with increased transport probabilities (and vice-versa). To test this relationship, we evaluate the seasonal cycle in the mean monthly geopotential height of the thermal tropopause at Law Dome over the period contemporaneous with the ^{10}Be data. We use monthly-resolved data from the National Centers for Environmental Prediction (NCEP) National Center for Atmospheric Research (NCAR) Reanalysis-1 assimilation [*Kalnay et al.*, 1996] at the grid point closest to DSS and linearly interpolate geopotential height as a function of log-pressure to the log-pressure of the thermal tropopause (defined in the Reanalysis-1 assimilation using the lapse rate definition of the *World Meteorological Organisation* [1957]). The values obtained by this method are in close agreement with tropopause heights derived from radiosondes released from the nearby Casey station (not shown). The mean seasonal cycle in tropopause height (shown on an inverted axis in Fig. 4.5e) does closely match the timing of stratospheric input suggested by ECHAM5-HAM, observed ^{10}Be:^{7}Be ratios and the FLEXPART stratospheric transport probability. The tropopause descends toward the ice sheet in the summer-autumn (to a minimum geopotential height of $\sim$ 8.5 km) before ascending to its highest level ($\sim$ 11.0 km) in the winter-spring. We also evaluated, using the same technique, the seasonal cycle in tropopause height averaged over all grid-points in the polar region (60°S to 90°S), and observe the same seasonal pattern (not shown). The seasonal variation in Fig. 5e is also qualitatively consistent with that reported by *Zängl and Hoinka* [2001] for tropopause pressure obtained from ECMWF reanalysis data in the longitude range 135°W to 135°E and poleward of 80°S.

In order to visualise the timing and intensity of stratospheric input of ^{10}Be to the troposphere on a hemispheric scale, we consider the ECHAM5-HAM simulated ^{10}Be:^{7}Be ratio in deposition fluxes worldwide alongside tropopause height (Fig. 4.6). The figure suggests that in the southern hemisphere the polar and mid-latitude stratospheric input of ^{10}Be to the troposphere are controlled by different processes acting in different seasons. Over the southern polar region the highest ratios are observed in the summer-autumn, in line with observed ^{10}Be:^{7}Be ratios at Neuymayer, the maximum in direct decent of air to the polar stratosphere depicted by FLEXPART and the descent of the polar tropopause. By contrast, over the southern mid-latitudes a seasonal maximum

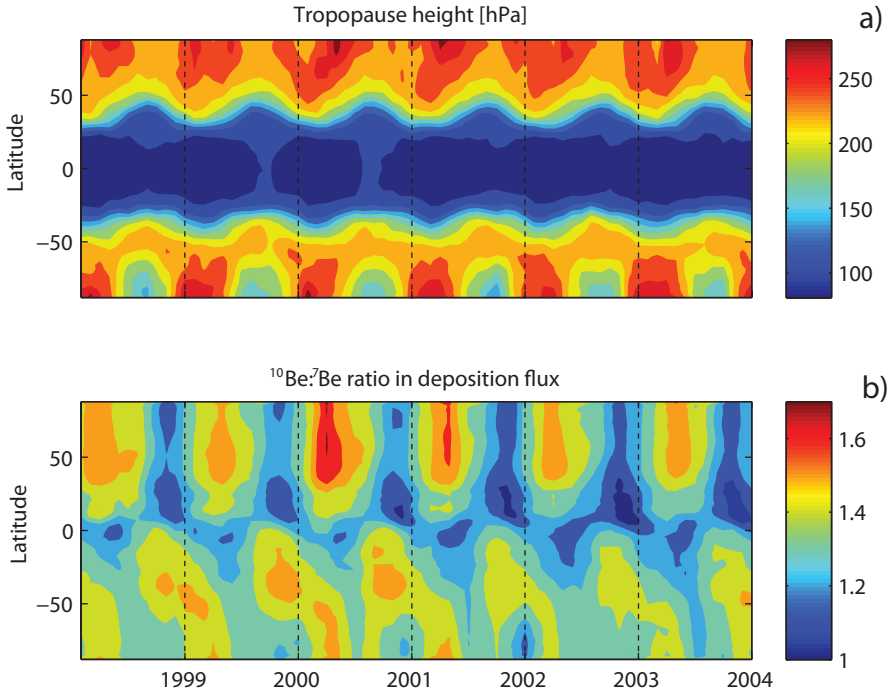

Figure 4.6: ECHAM5-HAM GCM simulations of parameters relating to temporal variability in stratospheric input into the troposphere. **a)** Tropopause height in hPa. **b)** ^{10}Be:^{7}Be ratio in deposition flux, where higher ratios imply greater influence of stratospheric air.

in modeled ^{10}Be:^{7}Be ratios is observed in the spring-summer, supported by observed ^{10}Be:^{7}Be ratios in New Zealand precipitation [*Graham et al.*, 2003]. The timing of this mid-latitude feature is associated with the combined influence of the discontinuity in the tropopause associated with the polar front jet stream (strongest in spring) and convective mixing in the troposphere driven by radiative heating (strongest in summer) [*Jordan et al.*, 2003]. This mid-latitude maximum in stratosphere to troposphere exchange cannot explain the summer-autumn maximum over Antarctica since atmospheric transport times within the troposphere from the mid-latitude to the Antarctic continent are only of order of days to weeks.

According to the GCM, the situation in northern high-latitudes is quite different. To examine the possibility of different transport pathways of stratospheric ^{10}Be to the Antarctic and Greenland ice sheets we compare the seasonal cycles in modeled ^{10}Be and ^{7}Be deposition to DSS with data from a previous ECHAM5-HAM run which sim-

ulated radionuclide deposition to the Greenland Ice Core Project (GRIP) site (72°35'N 37°38'W) [*Heikkilä et al.*, 2008c]. The modeled seasonal cycles of ^{10}Be and ^{7}Be and their ratios at GRIP and DSS are compared in Fig. 4.7. At DSS the primary peak in deposition in summer-autumn coincides with the maximum in polar stratosphere to troposphere exchange. By contrast, at GRIP the seasonal cycle in modeled ^{10}Be:^{7}Be ratios exhibits a maximum simultaneously with the maximum in mid-latitude stratosphere to troposphere exchange, in the (boreal) late winter to spring [*Heikkilä et al.*, 2008a]. An earlier FLEXPART model study also reports negligible direct stratospheric input to the Arctic troposphere during the summer-autumn [*Stohl*, 2006]. However, a short (one-year) observed record of ^{10}Be and ^{7}Be concentrations in surface air from Alert in the Canadian high-Arctic (82°N) actually suggested slightly higher ^{10}Be:^{7}Be ratios in the summer [*Dibb et al.*, 1994]. Multi-year observed ^{10}Be:^{7}Be records from Greenland are required to fully test the GCM results.

4.5 Discussion

The observed and GCM-modeled results lead to the following picture of the seasonal cycle in ^{10}Be concentrations at DSS: concentrations are highest in the late summer to autumn coinciding with a lowering of the tropopause and enhanced stratospheric input and concentrations are lowest in winter coinciding with ascent of the tropopause, decreased stratospheric input and a seasonal maximum in precipitation. The atmospheric processes that we consider to drive this pattern are now discussed.

The Antarctic continent experiences intense radiative cooling during the polar night (austral winter). This creates an extreme temperature inversion in the boundary layer, below which cold air drains from the continent [e.g. *Phillpot and Zillman*, 1970]. Where this air flows down the steep coastal slopes of the continent it forms the katabatic winds. The mass lost in katabatic outflow is replaced by general subsidence over Antarctica, which is in turn fed in the middle to upper-troposphere by the advection of warmer air from the mid-latitudes [*van de Berg et al.*, 2007]. The cyclonic vortex above Antarctica results from convergence of this mid-latitude air [*Schwerdtfeger*, 1984]. Under the influence of the vortex the height of the polar tropopause rises, reaching its maximum altitude in winter. When the vortex breaks down in spring the tropopause begins a descent toward the surface of the continent, reaching its lowest altitudes in summer-

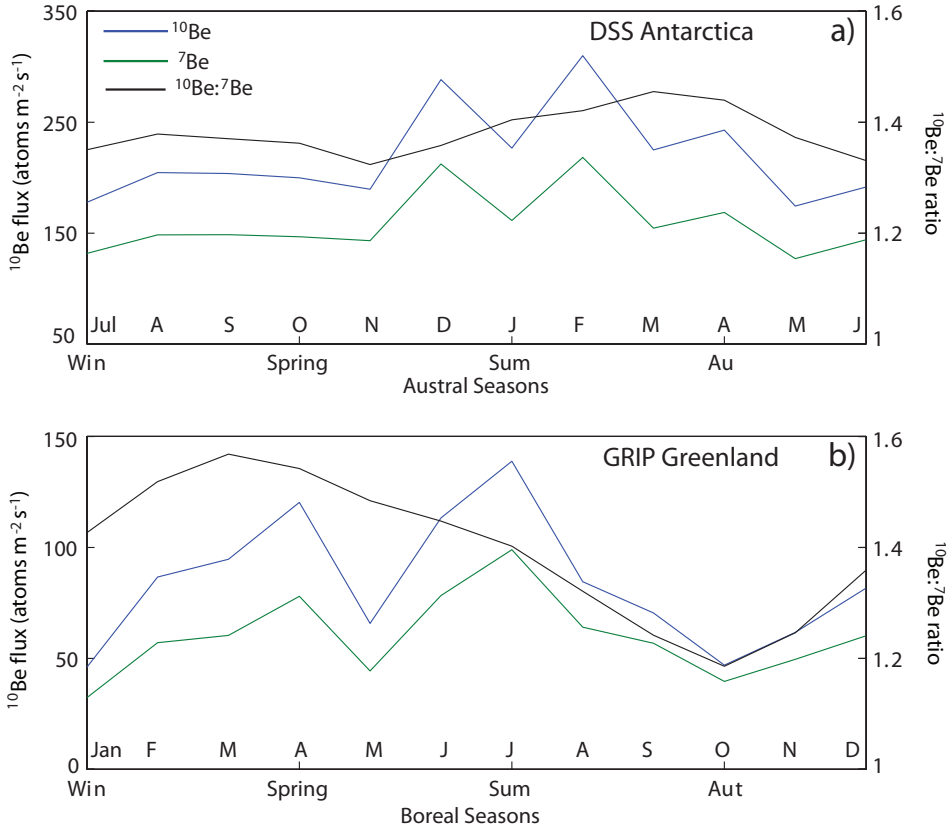

Figure 4.7: ECHAM5-HAM suggests different seasonal trends in the deposition flux of ^{10}Be and ^{7}Be to Antarctica compared to Greenland. **a)** Seasonal cycle of ECHAM5-HAM modeled ^{10}Be, modeled ^{7}Be and modeled ^{10}Be:^{7}Be ratios in deposition flux to DSS and **b)** same for GRIP, Greenland. Note that the horizontal axes are offset by six months to aid in comparing the behavior in Antarctica and Greenland during each season.

autumn (Fig. 4.5e) [see also *König-Langlo et al.*, 1998; *Randel et al.*, 2000; *Zängl and Hoinka*, 2001].

Lowering of the tropopause coincides with radiative heating, which promotes convection, reducing the static stability of the boundary layer and allowing a more direct coupling with the free troposphere above [*Wagenbach*, 1996; *Harder et al.*, 2000; *Hudson and Brandt*, 2005]. The free troposphere is in turn close to the tropopause, thus opening a route for ingress of ^{10}Be rich aerosol from the stratosphere. This is depicted by the GCM as a maximum in ^{10}Be:^{7}Be ratios in Antarctic surface air (Fig. 4.6). When these atmospheric conditions coincide with precipitation events the atmospheric signal will be deposited to the ice sheet. Averaged over many years the concentration maximum matches the timing of maximum stratospheric input (Fig. 4.5). However, the episodic nature of precipitation events (Fig. A1), leads to substantial variability between the timing of the concentration maximum in any given year (Fig. 4.2).

During winter to early-spring the situation is reversed; the static stability of the boundary layer is at its most pronounced and the input of ^{10}Be rich aerosol from the polar stratosphere is at its lowest. In addition, the precipitation rates at DSS, and in a wide region encompassing the atmospheric moisture transport pathways to the site are at their highest [*Simmonds et al.*, 2003; *Sodemann and Stohl*, 2009]. The concentration minimum is therefore explained by the limited vertical mixing within the troposphere and reduced input of ^{10}Be rich air from the stratosphere, depicted by the GCM as a minimum in ^{10}Be:^{7}Be ratios in surface air (Fig. 4.6). The minimum may also be contributed to by a washout effect, wherein higher precipitation rates lead to more regular cleansing of the incoming high latitude tropospheric air masses of their aerosol load.

Our results suggest that on seasonal timescales the ^{10}Be concentration in Antarctic ice may be interpreted as a tracer for stratospheric incursions into the polar troposphere. Seen like this, ^{10}Be concentrations may be a useful aid in interpreting other ice core trace chemicals. The complex seasonality of nitrate in Antarctica serves as an example. Nitrate accumulates in the stratosphere during the polar winter and hence, as for ^{10}Be, has an important stratospheric source. However at DSS and other Antarctic sites nitrate concentrations show a peak in the late winter to spring followed by a second larger peak in the late spring to summer [e.g. *Curran et al.*, 1998; *Wagenbach et al.*, 1998]. The absence of any clear summer-autumn signal argues that stratospheric air mass incursions are not a primary driver of these peaks. This is consistent with recent isotopic analysis

of high-resolution nitrate records which indicate that the nitrate maximum in winter-spring is associated with the sedimentation and denitrification of polar stratospheric clouds, while the maximum in spring-summer is associated with nitrate re-emission from the snow pack [e.g. *Savarino et al.*, 2007; *Frey et al.*, 2009]. Conversely, any scavenging and transport of ^{10}Be to the troposphere during polar stratospheric cloud sedimentation appears to be a relatively unimportant factor in the ^{10}Be seasonality, as argued previously by [*Wagenbach et al.*, 1998].

We now consider potential implications of this study for interpreting longer term ^{10}Be records. The seasonal change in ^{10}Be concentrations equates to a variation of $\sim$ 20% around the mean. This is comparable to the theoretical estimates of the decadal to centennial variations in ^{10}Be concentrations forced by solar modulation of cosmic rays; for instance, the production modulation over a typical Schwabe cycle is $\sim$ 20 to 50% [*Masarik and Beer*, 1999; *Webber and Higbie*, 2003; *Kovaltsov and Usoskin*, 2010]. Since the ice core ^{10}Be data used in reconstructing solar variability is typically considered at annual to decadal resolution or coarser, the seasonal cycle will be smoothed out. However, this does not mean that seasonal changes are irrelevant to interpretation of longer term data. In particular, species exhibiting large seasonal changes and relatively small long-term changes will be sensitive to variations in the seasonal distribution of precipitation [*Steig et al.*, 1994]. In practice, this implies that shifts in the seasonal distribution of precipitation may play some role in the long term variations of ^{10}Be concentrations.

A second consequence of the seasonal cycle for long term records will be dependent on the time-stability of the stratosphere to troposphere pathway identified here. Long term changes in the intensity of the pathway may affect the delivery of ^{10}Be to the ice sheet and potentially the concentration measured in ice on annual and coarser timescales. Previous GCM studies have suggested changes in stratosphere to troposphere exchange under different climate conditions [*Land and Feichter*, 2003; *Field et al.*, 2006]. An important consideration, that we are not yet able to precisely quantify, is the relative contribution of the pathway to the total deposition flux at DSS. We would estimate, based on the amplitude of the observed seasonal cycle in concentrations and the ECHAM5-HAM and FLEXPART model results, that the figure may be around 10-20%, with considerable variability between years.

It terms of reconstructing solar or production rate variability over longer timescales,

the sensitivity of reconstructions to the confounding effects of these climate/transport related factors may be reduced by combining ^{10}Be records from multiple sites, particularly sites from both hemispheres [e.g. *Steinhilber et al.*, 2009]. Another means to reduce such climate signals is to use statistical techniques to extract the common signal in ^{10}Be and radiocarbon (^{14}C), which has a very different geochemical behavior [e.g *Muscheler et al.*, 2007; *Usoskin et al.*, 2009].

Our results also offer a potential explanation for the sporadic peaks in annually resolved ^{10}Be data. Given the episodic nature of precipitation, such peaks may be expected when intervals of pronounced stratospheric input to the polar troposphere coincide with precipitation events. This basic mechanism was also put forward by *Aldahan et al.* [2008] based on their analysis of ^{10}Be isotopes in surface air in the northern hemisphere. Our results support the suggestion of *Aldahan et al.* [2008], that the solar signal in ice core ^{10}Be data may be enhanced if short term peaks in ^{10}Be concentration are regarded as transport noise and filtered out.

4.6 Summary and conclusions

The ^{10}Be concentrations at DSS show seasonal maximum concentrations during summer-autumn and minimum concentrations during winter. Results from ECHAM5-HAM GCM simulations of ^{10}Be (and ^{7}Be) deposition, corroborated by previously reported ^{10}Be:^{7}Be ratios from Antarctica [*Wagenbach*, 1996] and recent results from the FLEXPART Particle Dispersion Model [*Stohl and Sodemann*, 2010], support that the ^{10}Be concentration maximum is associated with enhanced influence of stratospheric air in the Antarctic troposphere. We propose that during summer-autumn the low Antarctic tropopause and decreased static stability of the troposphere permit a more direct coupling with the upper atmosphere, opening a path for input of polar stratospheric ^{10}Be to lower levels. By contrast in winter-spring, the tropopause rises and intense radiative cooling stratifies the lower troposphere closing this route. In addition, enhanced cyclonic activity off the Antarctic coast leads to higher precipitation rates [*Simmonds et al.*, 2003; *Sodemann and Stohl*, 2009], such that aerosol washout within the transport pathways to the site probably also contributes to the concentration minimum.

It has been conventionally assumed that the main pathway for the arrival of stratosphere produced ^{10}Be to the Antarctic troposphere is through the mid-latitude breaks

in the tropopause [e.g. *McHargue and Damon*, 1991]. Our results identify an additional important route: direct descent of ^{10}Be from the Antarctic stratosphere to the Antarctic troposphere during the summer-autumn. Interestingly, the modeled ^{10}Be and ^{7}Be data suggest this route is not important in delivering ^{10}Be to the Arctic. This adds to the large body of literature suggesting quite different atmospheric circulation and tracer transport between the northern and southern polar regions [e.g. *Holton et al.*, 1995; *Jordan et al.*, 2003; *Stohl*, 2006; *Stohl and Sodemann*, 2010].

We have obtained new insights into the processes affecting transport and deposition of ^{10}Be to the ice sheets through interpreting highly-resolved ice core measurements in conjunction with GCM data. Further improvements in simulating ^{10}Be transport and deposition to Antarctica, particularly to coastal areas, would be facilitated by improving the representation of precipitation of the GCMs. Highly-resolved ^{10}Be and ^{7}Be records from other Antarctic and Arctic sites are also required.

Chapter 5

Solar and Climate Influences on Ice Core ^{10}Be Records from Antarctica and Greenland During the Neutron Monitor Era

J. B. Pedro, J. R. McConnell, T. D. van Ommen, D. Fink, M. A. J. Curran, A. M. Smith, A. D. Moy and S. B. Das

In review (submitted January 2012), *Earth and Planetary Science Letters*

[1]Institute of Marine and Antarctic Studies, University of Tasmania, Hobart, TAS, Australia
[2]Antarctic Climate and Ecosystems Cooperative Research Centre, Hobart, TAS, Australia
[3]Australian Antarctic Division, Kingston, TAS, Australia
[4]Desert Research Institute, Reno, NV, United States
[5]Australian Nuclear Science and Technology Organisation, Menai, NSW, Australia
[6]Woods Hole Oceanographic Institution, Woods Hole, MA, United States

Abstract

Cosmogenic ^{10}Be is a primary ice core proxy for past solar activity. However, interpretation of the ^{10}Be record is hindered by limited understanding of the physical processes governing its atmospheric transport and deposition to the ice sheets. This issue is addressed by evaluating two accurately-dated, annually-resolved ice core ^{10}Be records against modern solar activity observations and instrumental and reanalysis climate data. The cores are sampled from the DSS site on Law Dome, East Antarctica (spanning 1936–2009) and the Das2 site, southeast Greenland (1936–2002), permitting inter-hemispheric comparisons. Concentrations at both DSS and Das2 are significantly correlated to the 11-year solar cycle modulation of cosmic ray intensity, $r_{xy} = 0.54$ with 95% CI [0.31; 0.70], and $r_{xy} = 0.45$ with 95% CI [0.22; 0.62], respectively. For both sites, if fluxes are used instead of concentrations then correlations with solar activity decrease. The strength and spectral coherence of the solar activity signal in ^{10}Be is enhanced when ice core records are combined from both Antarctica and Greenland. The amplitudes of the 11-year solar cycles in the ^{10}Be data appear inconsistent with the view that the ice sheets receive only ^{10}Be produced at polar latitudes. Significant climate signals detected in the ^{10}Be series include the zonal wave 3 pattern of atmospheric circulation at DSS, $r_{xy} = -0.36$ with 95% CI [−0.57; −0.10], and the North Atlantic Oscillation at Das2, $r_{xy} = -0.42$ with 95% CI [−0.64; −0.15]. The sensitivity of ^{10}Be concentrations to modes of atmospheric circulation advises caution in the use of ^{10}Be records from single sites in solar forcing reconstructions.

5.1 Introduction

The atmospheric production rate of cosmogenic ^{10}Be is proportional to cosmic ray intensity [*Lal and Peters*, 1967], which in turn is modulated by variations in solar activity and the Earth's geomagnetic field strength [*Lean et al.*, 2002; *Webber and Higbie*, 2003; *McCracken et al.*, 2004; *Masarik and Beer*, 1999; *Kovaltsov and Usoskin*, 2010]. This relationship is exploited in the use of ^{10}Be records from polar ice cores to reconstruct solar activity prior to the era of instrumental records [*Bard et al.*, 2000; *Vonmoos et al.*, 2006; *Muscheler et al.*, 2007; *Usoskin et al.*, 2009; *Steinhilber et al.*, 2009; *Delaygue and Bard*, 2011; *Shapiro et al.*, 2011]. Such reconstructions provide crucial information for assessing the role of solar forcing in past climate change [e.g.

Bard et al., 2000; *Bond et al.*, 2001; *Muscheler and Beer*, 2006] and for attributing present climate change [e.g. *Ammann et al.*, 2007].

However, different solar reconstructions are not in agreement and the reliability of ^{10}Be as a solar proxy has sometimes been questioned [*Lal*, 1987; *Webber and Higbie*, 2010]. The precise amplitude of past variations in solar activity is affected by uncertainty regarding where in the atmosphere the ^{10}Be deposited to the ice core sites has been produced [see e.g. *Bard et al.*, 2000; *McCracken et al.*, 2004; *Vonmoos et al.*, 2006; *Field et al.*, 2006; *Heikkilä et al.*, 2009; *Delaygue and Bard*, 2011]. Furthermore, non-production related signals introduced during the atmospheric transport and deposition of the isotope to the ice sheets may confound the solar activity signal [*Lal* 1987; *Pedro et al.* 2006; *Field et al.* 2006; *Field and Schmidt* 2009; *Pedro et al.* 2011b/Chapter 4]. This is important; incorrectly attributing climate-induced signals in ^{10}Be to changes in solar activity risks drawing false conclusions about solar forcing of climate. Steps can be taken to reduce this risk, for example using cosmogenic ^{14}C (recorded in tree rings) which has a very different geochemical behaviour to ^{10}Be, to help decouple the climate signal from the ^{10}Be record [e.g. *Muscheler et al.*, 2007; *Usoskin et al.*, 2009]. Nevertheless, there remains a clear need for tighter empirical constraints on the atmospheric regions from which ^{10}Be deposited to the ice sheets is sourced and on the strengths of both the solar activity (or production) and climate signals in ^{10}Be data. One means to address this issue is through direct intercomparison of high-resolution (annual) ice core ^{10}Be data with modern instrumental records.

The most suitable directly measured parameter for assessing the strength of the production signal in ^{10}Be is the cosmic ray intensity, first measured by ionisation chambers in the 1930's and then by a network of more stable ground-based neutron monitors from the 1950's [*McCracken and Beer*, 2007]. The dominant feature in these records is the modulation of cosmic ray intensity by the 11-year Schwabe cycle in solar magnetic activity. Observed and reanalysis climate data from the polar regions come online typically post $\sim$ 1950, the reliability of the reanalysis data, particularly for the Antarctic region, greatly improves post-1979 when satellite data enters the assimilations [for a review see *Bromwich et al.*, 2007]. Annually resolved ^{10}Be records spanning these recent decades, which we denote the 'neutron monitor era' are limited to: NGRIP Greenland [*Berggren et al.*, 2009], Dronning Maud Land Antarctica [*Moraal et al.*, 2005; *Aldahan et al.*, 1998], Dye 3 Greenland [*Beer et al.*, 1984] and Renland Greenland [*Aldahan et al.*, 1998]. In all of these records, trends in ^{10}Be consistent with the 11-year solar cycle are

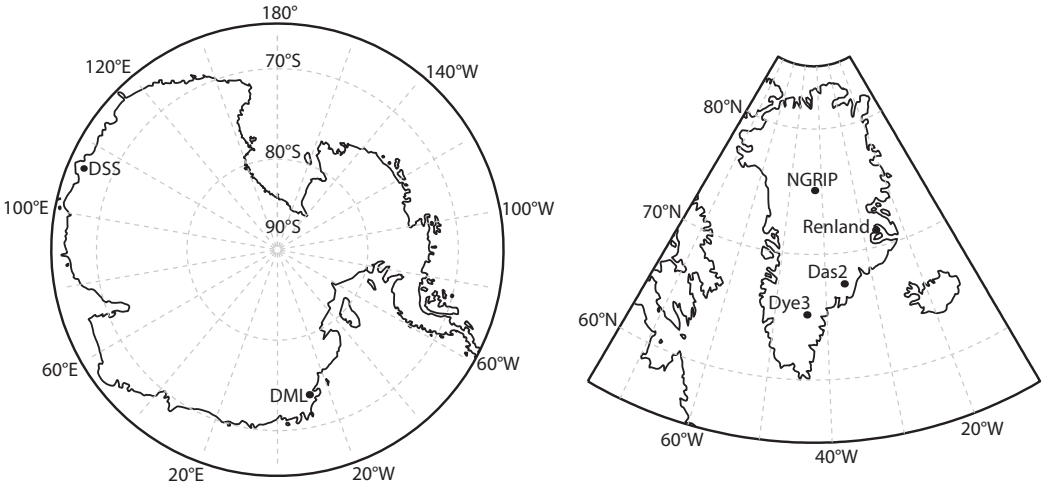

Figure 5.1: Map showing the ice core sites in Antarctica and Greenland mentioned in the text.

observed. However, each site also shows intervals where the ^{10}Be data departs from the atmospheric production rate, such that some solar cycles are poorly resolved or missed altogether. One of our objectives is to identify the particular meteorological processes responsible for this behaviour.

In this work, two new annually-resolved ^{10}Be records are introduced; one from the DSS site in Law Dome, East Antarctica and one from the Das2 site in southeast Greenland, Fig. 5.1. The exceptionally high snow accumulation rates at both sites [*Morgan et al.*, 1997; *Hanna et al.*, 2006] preserve thick and clear annual snow layers permitting unambiguous dating of annually resolved ^{10}Be records. To constrain the strength of the production signal, measured ^{10}Be concentrations and calculated ^{10}Be fluxes are evaluated against cosmic ray intensity and atmospheric ^{10}Be production rates from the CRAC:10Be model [*Kovaltsov and Usoskin*, 2010]. Potential climate signals are examined through intercomparison of the ^{10}Be data with climate variables for which there is an *a-priori* reason to suspect an influence on ^{10}Be deposition or transport to these sites: (i) observed accumulation rates; (ii) dominant modes of atmospheric circulation affecting vertical and meridional atmospheric mixing; (iii) moisture transport pathways in the southern and northern high latitudes; and (iv) ice core stable water isotope composition (δ^{18}O). Having identified significant climate signals at both sites, we test whether constructing a composite series, using ^{10}Be records from both Antarctica and Greenland, is effective in reducing the climate signals and enhancing the solar/global

production signal.

An additional question relates to the fate of recently-produced ^{10}Be. Due to its valence charge, small ionic radius and strong chemical adsorption affinity it is presumed that after production in the atmosphere ^{10}Be is rapidly scavenged by the ambient aerosol [*Kondo et al.*, 1984; *Igarashi et al.*, 1998; *Aldahan et al.*, 2008]. Since the sulphur cycle dominates the atmospheric aerosol abundance in the upper troposphere and stratosphere, where production rates of ^{10}Be are highest, it has been suggested (though not confirmed) that sulphur aerosols, primarily sulphates, are the main carriers of ^{10}Be [*McHargue and Damon*, 1991; *Field et al.*, 2006]. This consideration, and previous reports of covariability in sulphate and ^{10}Be concentrations in polar ice [*Delmas*, 1992] and low latitude rainfall [*Igarashi et al.*, 1998], motivate us to examine for a relationship between ^{10}Be and sulphur aerosol in the DSS and Das2 cores.

Finally, following *Steig et al.* [1996] and *Moraal et al.* [2005] we use the amplitudes of the 11-yr solar cycles in the ^{10}Be data to constrain the atmospheric source regions of ^{10}Be deposited to the ice sheets.

5.2 Materials and methods

The DSS ^{10}Be record was sampled from the DSS0506 ice core, drilled in November 2005 at location 66°46.33′ S 112°48.43′ E, elevation 1370 m asl. Prior work has demonstrated the suitability of this high-accumulation site, 0.68 m ice yr^{-1} [*Morgan et al.*, 1997], for the extraction of highly resolved and reproducible ^{10}Be records [*Pedro et al.* 2011a/Chapter 2].

Detailed oxygen isotope (δ^{18}O) and trace chemical records were taken from the core prior to extracting ^{10}Be samples. The continuous δ^{18}O record was physically sampled at 30–50 mm resolution and measured on a VG Isogas SIRA mass spectrometer at the Central Science Laboratory, University of Tasmania, Australia. The trace chemical analysis was carried out at $\sim$ 10 mm resolution on an ice core melter system fitted with Continuous Flow Analysis (CFA) and an Inductively Coupled Plasma Mass Spectrometer at the Desert Research Institute in Reno NV, USA [*McConnell et al.*, 2002; *McConnell et al.*, 2007]. The core was dated following established methods, in which unambiguous annual cycles in δ^{18}O are corroborated by annual cycles in trace chemi-

cals, with additional tie-point control from known volcanic events [*Palmer et al.*, 2001]. The thickness of the annual snow layers, when corrected for densification and layer thinning, was used to derive the annual accumulation for each year of the record [*van Ommen and Morgan*, 2010]. Sixty five ^{10}Be samples of average mass 2.18 kg were cut contiguously from the top 66.62 m of the core to span 1936–2000. The time series was then extended through 2000–2009 by splicing annual average ^{10}Be concentrations from a composite of DSS shallow firn cores [*Pedro et al.* 2011a/Chapter 2].

For all DSS samples, the ^{10}Be concentration integrates deposition over one complete year, defined between austral mid-winter sample boundaries. The decision to use mid-winter boundaries was guided by the previously observed seasonal cycle in ^{10}Be concentrations at the site. Sharp concentration maxima, related to the influence of polar stratospheric air [*Pedro et al.* 2011b/Chapter 4], occur during the austral summer to early autumn months of most years, whereas concentrations during winter are consistently low. By using mid-winter boundaries we avoid the possibility of including snow from two summer-autumn maxima in the one sample and thus reduce the risk of seasonal aliasing in the annual record. Previous work at DSS suggests a dating uncertainty of $\sim$ 2 months for each ^{10}Be sample throughout the length of the record [*Palmer et al.* 2001; *Pedro et al.* 2011a/Chapter 2].

The 84 m Das2 ice core was drilled in May 2003 at location 67°31.64'N, 36°03.69'W and elevation 2936 m (Fig 5.1). The snow accumulation rate at the site is also very high, 0.90 m ice yr^{-1}. Trace chemicals were measured at 10 mm resolution on the above-mentioned CFA system. Annual layer dating was completed with reference to the highly-periodic annual cycles in hydrogen peroxide. The resulting annual layer thicknesses were used previously to reconstruct annual snow accumulation rates at the site *Hanna et al.* [2006]. Sixty eight annual ^{10}Be samples of average mass 2.47 kg were extracted contiguously from the core to span 1936–2002. The available observations from snow-pit [*Beer et al.*, 1991; *Heikkilä et al.*, 2008c] and aerosol sampling studies [*Dibb et al.*, 1994] in Greenland suggest that seasonal ^{10}Be concentration maxima occur in spring and/or summer. Hence, the mid-winter minimum in hydrogen peroxide was selected as the sample boundary, which should again reduce the risk of seasonal aliasing.

The ^{10}Be samples from both sites were measured at the ANTARES AMS facility, ANSTO, Australia following previous techniques [*Fink and Smith* 2007; *Pedro et al.* 2011a/Chapter 2; *Simon et al.* submitted/Chapter 3]. During processing, $\sim$ 5 ml

δ^{18}O samples were taken directly from the bulk melt-water of each ^{10}Be sample to obtain δ^{18}O records directly co-registered with the ^{10}Be records. All ^{10}Be measurements were normalised to the National Institute of Standards and Technology USA ^{10}Be standard reference material SRM-4325, utilising the re-normalised ^{10}Be:^{9}Be ratio of $(2.79 \pm 0.02) \times 10^{-11}$ reported by *Nishiizumi et al.* [2007]. Standard errors in ^{10}Be concentrations (comprising random and systematic measurement errors) ranged from 2.0–5.8 % with a median of 2.9 % for DSS and 1.4–3.5 % with a median of 2.6 % for Das2. For both records levels of the ^{10}Be isobar boron ($^{10}B^{3+}$) were sufficiently low that there was no correction required to the ^{10}Be counting rate. Chemistry procedural blanks prepared (from low-level beryl carrier) were handled identically alongside the ice core ^{10}Be samples (one blank per batch of ten ice samples). All blanks gave ^{10}Be:^{9}Be ratios of $< 5 \times 10^{-15}$ and corresponding chemistry blank corrections (of typically $< 1 - 2$ %) were applied to the respective ^{10}Be samples.

Atmospheric production rates of ^{10}Be were calculated using the CRAC:10Be model of ^{10}Be production [*Kovaltsov and Usoskin*, 2010] and annual average values of the solar modulation constant (Φ) from *Usoskin et al.* [2011]. The Φ record is based on neutron monitor counting rates from 1951–present and on Forbush ground-based ionization chambers for 1936–1950. Larger uncertainty is associated with the ionisation chamber data, and the corresponding ^{10}Be production rates should therefore be interpreted with caution (unless specified these production rates are not used here in quantitative analysis). Centennial to millennial-scale changes in the strength and configuration of the geomagnetic field also influence production rates [*Lal and Peters*, 1967; *Muscheler et al.*, 2007], but can be neglected on annual to decadal timescales considered here. We report annual average production rates that are vertically integrated over the entire atmospheric column and averaged over all latitudes (i.e. 'global production rates'), and also columnar production rates averaged over only the geographical latitude range 60–90°S/N, (i.e. 'polar production rates'). Note that other recent models of ^{10}Be production [e.g. *Masarik and Beer*, 2009] yield production rates that are 30–40 % lower than CRAC:10Be. However, for the purpose of this study the absolute production rate is not consequential. Rather, the important detail is the relative production variation during the neutron monitor era, and on this the models are in reasonable agreement (demonstrated in Sect. 5.3.3).

Pearson's correlation coefficient (r_{xy}) is used extensively in this study to quantify the degree of (linear) correlation between the ^{10}Be series and production or climate related

variables. In calculating correlation coefficients we first linearly detrend all data to reduce the risk of spurious correlations and then employ a non-parametric stationary bootstrap. The average block-length of the bootstrap is proportional to the maximum estimated persistence time of the time series. This approach, fully detailed in *Mudelsee* [2003], is preferred over conventional techniques as it yields robust results when applied to autocorrelated, non-normally distributed and unevenly spaced data. The statistical accuracy of correlation coefficients are reported throughout in terms of their 95% confidence intervals (CI), of type bias corrected and accelerated. The CI can also be framed as a hypothesis test by evaluating whether or not it contains zero.

5.3 Results

5.3.1 Production and climate signals in ^{10}Be at DSS and Das2

The average annual ^{10}Be concentrations ($\pm 1\sigma$) are $6.07 \pm 1.33 \times 10^3$ atoms g^{-1} in the DSS record (1936–2009) and $5.91 \pm 1.25 \times 10^3$ atoms g^{-1} in the Das2 record (1936–2002). Average annual accumulation rates at the two sites over the same periods are 0.71 ± 0.14 m ice yr^{-1} at DSS and 0.90 ± 0.19 m ice yr^{-1} at Das2. Mean annual ^{10}Be fluxes, calculated from these values (as the product of the respective concentration and accumulation terms) are 125 ± 34 atoms m^{-2} s^{-1} at DSS and 151 ± 30 atoms m^{-2} s^{-1} at Das2.

Time series of the annual variations in average ^{10}Be concentration, accumulation rate and ^{10}Be flux at each site are shown in Fig 5.2. The dashed lines mark the annually resolved data and the solid lines show the data smoothed with a Gaussian filter of standard deviation 0.91 years (equivalent half-power bandwidth to a three-year running mean).

Correlation coefficients calculated between the ^{10}Be series and production or climate related variables are listed in Table 5.1 and are considered in turn below.

5.3.1.1 Cosmic ray intensity and the atmospheric production rate

The cosmic ray intensity measured by polar neutron monitors is proportional to the production rate of ^{10}Be in the atmosphere [*Obrien*, 1979]. Average annual polar neutron

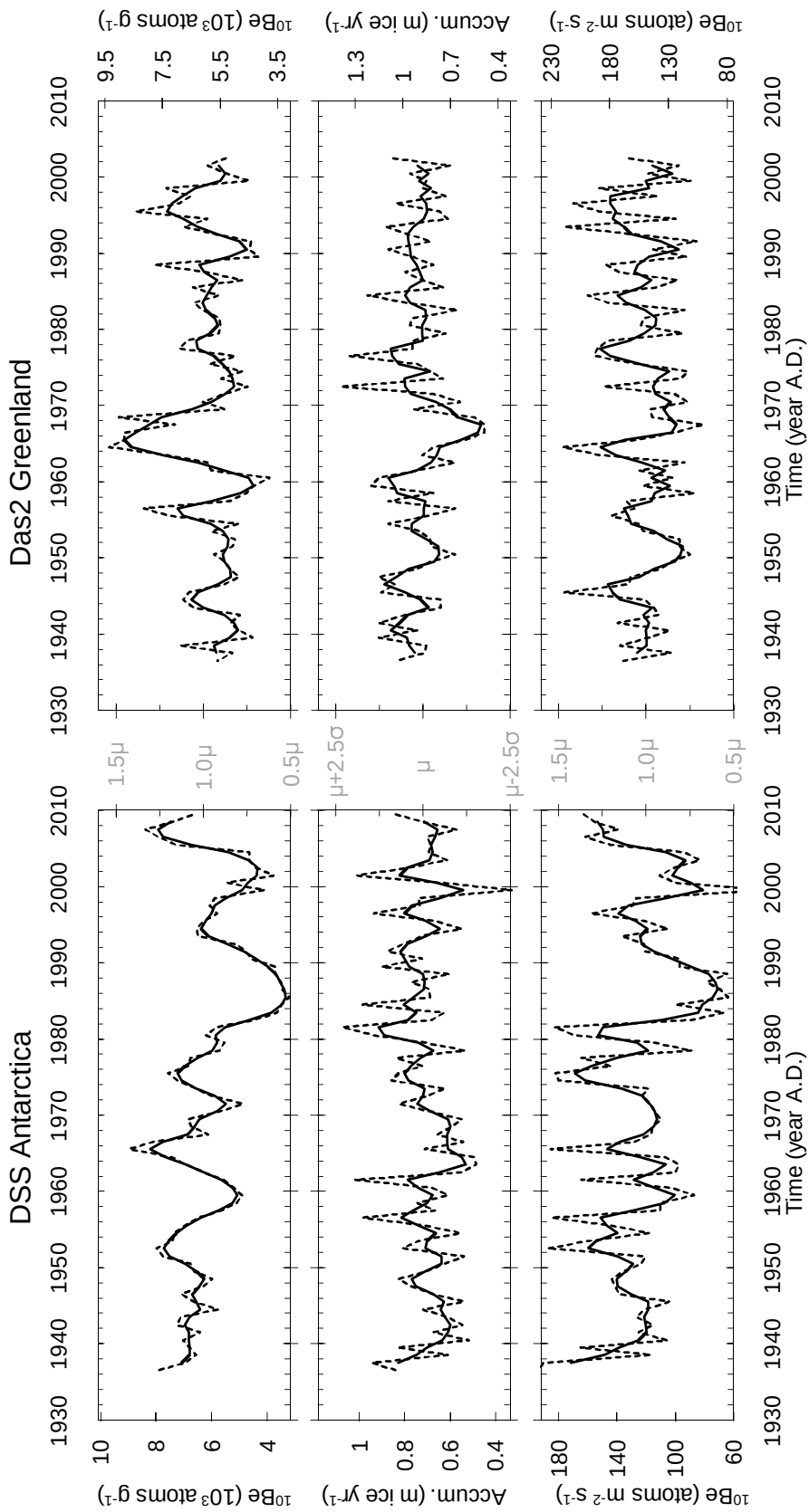

Figure 5.2: ^{10}Be concentrations (top), accumulation rates (middle) and ^{10}Be fluxes (bottom) measured in the DSS Antarctica and Das2 Greenland ice cores over recent decades. The vertical axes for concentrations and fluxes are scaled according to the mean (μ) of each record while the vertical axis for accumulation is scaled by the standard deviation (σ) for each record (as can be seen by the internal grey axes). Uncertainties in measured ^{10}Be concentrations are $\sim 3\%$. The dashed lines show annually resolved data and the solid lines show smoothed data (Gaussian filter, effective half-width 3 years).

Table 5.1: Testing for significant production and climate signals in the DSS Antarctica and Das2 Greenland ^{10}Be concentration and flux data. Pearson's correlation coefficient r_{xy} is listed for each production and climate parameter tested and the associated 95% confidence intervals are provided in parentheses. Where r_{xy} is shown in bold font the null-hypothesis of no significant relationship can be rejected (as $r_{xy} \neq 0$ at the 95% confidence level). The analysis employs the non-parametric stationary bootstrap (Sect. 5.2).

x	Time span	n	^{10}Be$_{\mathrm{Conc}}$ r$_{xy}$ [95% CI]	^{10}Be$_{\mathrm{Flux}}$ r$_{xy}$ [95% CI]
DSS Antarctica				
Production parameters				
Neut. Count.	1951–2007	57	**0.54** [0.31; 0.70]	**0.38** [0.13; 0.57]
Glob. Prod.	1951–2009	59	**0.58** [0.36; 0.73]	**0.39** [0.14; 0.58]
Glob. Prod.	1936–2009	74	**0.54** [0.33; 0.68]	0.32 [0.08; 0.49]
Snow accumulation rate				
Accum.	1936–2009	74	-0.15 [-0.34; 0.07]	**0.62** [0.45; 0.76]
Modes of atmospheric circulation				
ENSO SOI	1951–2009	59	0.06 [-0.21; 0.32]	0.13 [-0.18; 0.38]
SAM	1979–2009	31	-0.11 [-0.51; 0.28]	-0.26 [-0.60; 0.08]
ZW3	1958–2005	48	**-0.36** [-0.57; -0.10]	-0.22 [-0.51; 0.13]
DSS ice core parameters				
δ^{18}O	1936–2009	74	-0.17 [-0.39; 0.09]	0.15 [0.09; 0.38]
nssS	1936–1999	62	**0.42** [0.22; 0.60]	**0.70** [0.52; 0.81]
Das2 Greenland				
Production parameters				
Neut. Count.	1951–2002	52	**0.45** [0.22; 0.62]	**0.38** [0.15; 0.57]
Glob. Prod.	1951–2002	52	**0.44** [0.19; 0.63]	**0.36** [0.12; 0.55]
Glob. Prod.	1936–2002	67	**0.45** [0.25; 0.62]	**0.38** [0.17; 0.54]
Snow accumulation rate				
Accum.	1936–2002	66	**-0.53** [-0.67; -0.36]	**0.53** [0.34; 0.67]
Modes of atmospheric circulation				
NAO	1950–2002	53	**-0.42** [-0.64; -0.15]	-0.13 [-0.37; 0.12]
Das2 ice core parameters				
δ^{18}O	1936–2002	66	-0.05 [-0.27; 0.21]	0.16 [-0.15; 0.36]
nssS	1936–2002	66	**0.40** [0.14; 0.61]	0.26 [-0.02; 0.47]

Time spans are inclusive. For DSS nss-SO_4 there were two years of missing data (1989-90).
The time series of climate modes are from the National Center for Environmental Prediction:
ENSO: `http://www.cpc.ncep.noaa.gov/data/indices/soi`
SAM: `http://www.cpc.ncep.noaa.gov/products/precip/CWlink/daily_ao_index/aao/`
NAO: `ftp://ftp.cpc.ncep.noaa.gov/wd52dg/data/indices/tele_index.nh`

monitor counting rates [from *Usoskin et al.*, 2005] are shown for 1951–2007 in Fig. 5.3a. The 11-year Schwabe cycle modulation of cosmic ray intensity is clearly observed in the neutron data, the alternating peaked and flat topped structure of the 11-year cycle results from the 22-year Hale cycle of solar magnetic polarity [see e.g. *Webber and Lockwood*, 1988].

The agreement between the DSS ^{10}Be concentrations (Fig. 5.3b) and cosmic ray intensity is visually quite impressive, with the marked exception of their opposing trends during the 1980's. We have no evidence to suggest that this 'missing cycle' in ^{10}Be is associated with our experimental setup or measurement system, rather it is argued (in Sect. 5.3.1.3 and 5.3.1.5) that it can be linked to climate effects. The Hale cycle variations in cosmic ray intensity appear too subtle to be resolved in the ^{10}Be series. Quantitatively, the correlation between DSS concentrations and cosmic ray intensity is significant and of moderate strength, $r_{xy} = 0.54$ with 95% CI [0.31; 0.70] (hereafter expressed in the form $r_{xy} = 0.54\,[0.31;\ 0.70]$). For DSS fluxes (Fig. 5.3c), the agreement with cosmic ray intensity is visually weaker and the correlation coefficient is lower, $r_{xy} = 0.38\,[0.13;\ 0.57]$.

The correlations between cosmic ray intensity and the Das2 concentration and fluxes, Fig. 5.3d and e, are respectively $r_{xy} = 0.45\,[0.22;\ 0.62]$ and $r_{xy} = 0.38\,[0.15;\ 0.57]$. A marked feature in the Das2 concentrations is the maximum in the 1960's. While this maximum is consistent with the phase of the solar cycle, it greatly exceeds all other decadal signals. Notably, it is substantially reduced in the derived fluxes due to a corresponding pronounced minimum in the Das2 accumulation rate (Fig. 5.2, right panel).

We now assess the ^{10}Be data against the CRAC:10Be-modeled rate of ^{10}Be production in the global atmosphere. The global production rates of ^{10}Be are overlain on the DSS and Das2 concentration and flux series in Fig. 5.3b–e. Solid (grey) lines mark the production rates derived from neutron monitor data while dashed lines mark the less certain production rates derived from the pre-1951 ionisation chamber data. An advantage of considering production rates over the neutron monitor record of cosmic ray intensity is that the relative amplitudes of the production and ^{10}Be variations can be meaningfully interpreted (this is examined quantitatively in Sect. 5.3.3). Also, ^{10}Be production rates are slightly more sensitive to low energy cosmic rays than are neutron monitors and this is accounted for in the production model. During the neutron

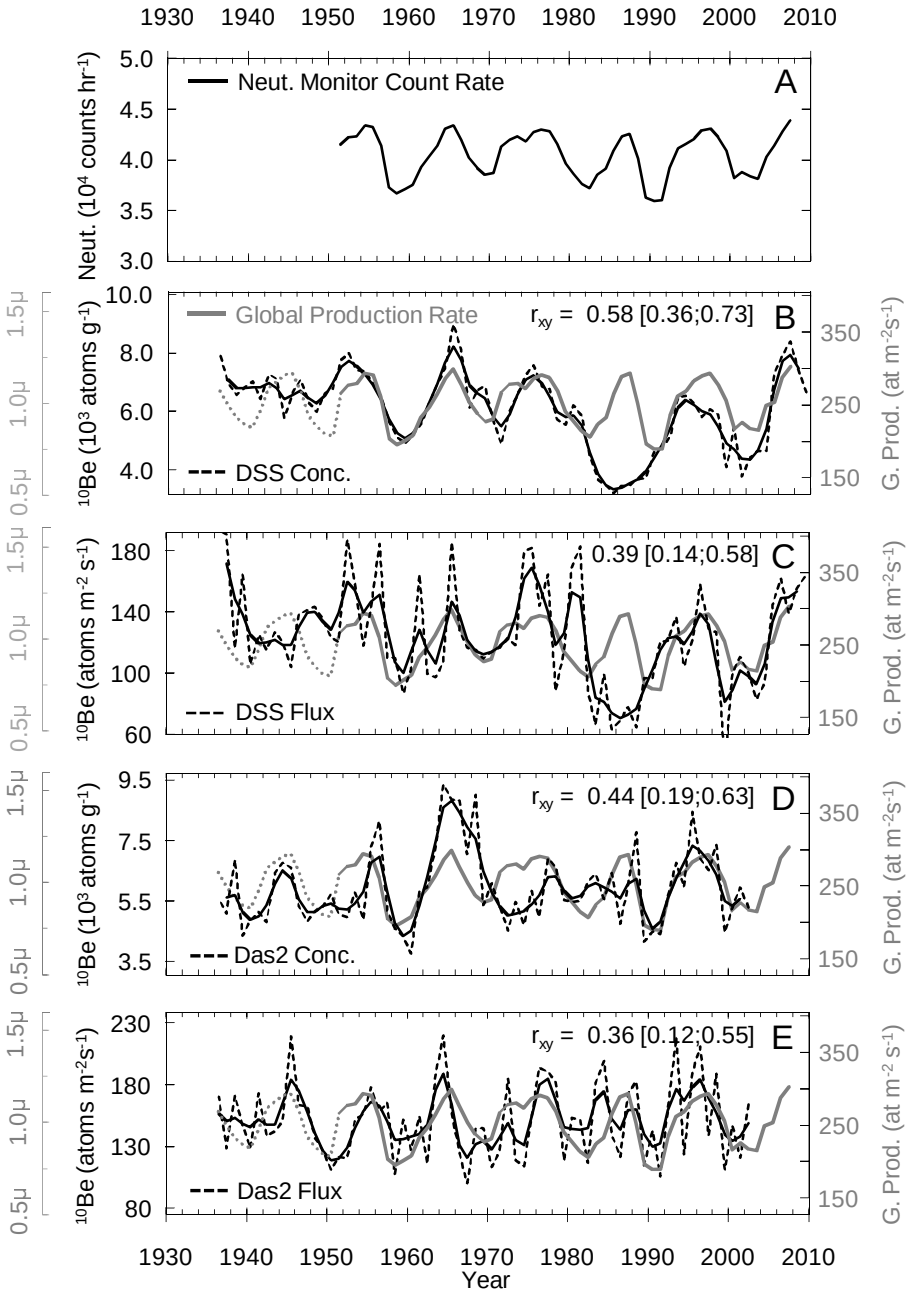

Figure 5.3: ^{10}Be concentrations and ^{10}Be fluxes at DSS Antarctica and Das2 Greenland are compared with parameters relating to cosmogenic production rates in the atmosphere. The top curve shows an index of the polar neutron monitor counting rate [from *Usoskin et al.*, 2005]. The annual average columnar production rate of ^{10}Be in the global atmosphere (solid grey lines) is overlain on the ^{10}Be concentration and flux curves from both sites. Production data for the period 1936 to 1951 (dotted grey line) is based on ionisation chamber data (see text for derivation of production rates). The axes marking ^{10}Be concentrations and global production rates are scaled according to the mean (μ) of each record (as depicted by the offset grey axes). The dashed lines show annually resolved data and the solid lines show smoothed data (Gaussian filter, effective half-width 3 years).

monitor era the correlation between global production rates and DSS concentrations is $r_{xy} = 0.58\,[0.36;\ 0.73]$. The correlation with fluxes is again lower at $r_{xy} = 0.39\,[0.14;\ 0.58]$. For Das2 concentrations and fluxes, the corresponding values are $r_{xy} = 0.44$ $[0.19;\ 0.63]$ and $r_{xy} = 0.36\,[0.12;\ 0.55]$, respectively. These correlations are very similar to those calculated using cosmic ray intensities, which should be expected given that the cosmic ray intensities are involved in the Φ reconstruction used by the production model.

The agreement between the ^{10}Be data and the ionisation chamber-based production rates (1936–1951) is relatively poor at DSS and marginally better at Das2. Correlation coefficients determined above have excluded data from this period. If the complete records are considered (1936–present) the correlations with DSS concentrations and fluxes are $r_{xy} = 0.54\,[0.33; 0.68]$ and $r_{xy} = 0.32\,[0.08;\ 0.49]$, respectively; while for Das2 they are $r_{xy} = 0.45\,[0.25;\ 0.62]$ and $r_{xy} = 0.38\,[0.17;\ 0.54]$, respectively.

There is a systematic pattern of higher correlations of cosmic ray intensity (and production rates) with ^{10}Be concentrations than with ^{10}Be fluxes: the coefficients of determination (r^2_{xy}) suggest that respectively $\sim 30\%$ and $\sim 20\%$ of the annual variance in ^{10}Be concentrations at DSS and Das2 can be predicted from the cosmic ray intensity data or from modeled production rates, compared to $\sim 15\%$ for flux at both sites. An earlier study [*Pedro et al.* 2011a/Chapter 2], utilising only the most recent 10-years of the DSS ^{10}Be record, suggested a somewhat stronger production signal in concentrations (controlling $\sim 40\,\%$ of the variance). As the present result is determined using a much longer record it must clearly be considered more robust. The stronger production signals in concentrations compared to fluxes at both DSS and Das2 may be explained in terms of ^{10}Be deposition mechanisms to the sites. Prior observations [*Smith et al.*, 2000; *Pedro et al.*, 2006], and general circulation model (GCM) studies [*Field et al.* 2006; *Heikkilä et al.* 2009; *Pedro et al.* 2011b/Chapter 4] establish that ^{10}Be is primarily ($> 90\,\%$) wet deposited to DSS, (i.e. the air to snow transfer takes place with an associated water transfer). GCM studies also suggest that wet deposition of ^{10}Be is dominant at the Das2 site [*Field et al.*, 2006; *Heikkilä et al.*, 2009], although direct observational evidence is lacking. For wet deposition sites the theory of particle deposition to ice sheets advises that the *atmospheric concentration* of a given particulate or aerosol species is more closely related to the species concentration in the ice core than it is to the species inferred flux to the ice core (the inverse is true for dry deposition sites where atmospheric concentrations are more closely related to flux) [*Alley et al.*,

1995; *Davidson et al.*, 1996]. If we assume that the atmospheric concentration of ^{10}Be is proportional to its production rate, justified at northern [*Aldahan et al.*, 2008] and southern [*Elsässer et al.*, 2011] high-latitude sites by air-sampling studies, then the stronger observed production signal in ^{10}Be concentrations than in fluxes is in line with the theory.

5.3.1.2 Accumulation rate

For DSS, the correlation between accumulation rate and ^{10}Be concentration is weak and non-significant, $r_{xy} = -0.15\,[-0.34;\ 0.07]$. However, a strong and significant positive correlation is observed between DSS flux and accumulation rate, $r_{xy} = 0.62\,[0.45;\ 0.76]$. These results are again consistent with theory [*Alley et al.*, 1995; *Davidson et al.*, 1996]: concentrations should be effectively independent of the local accumulation rate at a wet deposition site, as observed; hence calculation of fluxes (by multiplying concentrations by accumulation rate) forces an effectively spurious positive correlation with accumulation rate. In contrast, for a purely dry deposition site, little to no correlation of ^{10}Be flux with accumulation rate would be expected.

Interestingly, there is a significant negative correlation between concentration and accumulation rates at Das2, $r_{xy} = -0.53\,[-0.67;\ -0.36]$. This accumulation signal is not removed by calculating fluxes, $r_{xy} = 0.53\,[0.34;\ 0.67]$. The relationship between concentration and accumulation, in a direction that suggests dry deposition is surprising given sites near-coastal location and exceptionally high accumulation rate. While an important role for dry deposition cannot be ruled out, an alternative explanation relating to aerosol scavenging during wet deposition, can also be envisaged. Wet deposition occurs via both in-cloud processes, in which aerosol particles serve as cloud condensation nuclei or ice nuclei (rainout), and below cloud processes, through collision of particles with precipitation (washout) [*Davidson et al.*, 1996]. Washout and rainout strip beryllium radionuclides from the lower troposphere, such that their concentration in the air, and in the precipitation itself, is progressively depleted over the duration of a precipitation event [*Brown et al.*, 1989; *Ishikawa et al.*, 1995]. Results from air sampling studies demonstrate that these forms of air mass cleansing occur both at a sampling site and within the moisture transport pathways to it [*Feeley et al.*, 1989]. Hence, for the very high accumulation Das2 site, we suggest that the initial stages of large precipitation events may cleanse the atmospheric of its aerosol load while the

later stages dilute the impurity in the snowpack. This would be consistent with the observed negative correlation and appears more plausible than a major contribution of dry deposition at such a high-accumulation site.

5.3.1.3 Modes of atmospheric circulation

The DSS concentration and flux data are tested against three major modes of atmospheric variability affecting the southern high latitudes: El Ninõ Southern Oscillation Index (SOI; 1951–present); the Southern Annular Mode (SAM; 1979–present) and the zonal wave three (ZW3; 1958–present). The SOI affects an array of climate parameters in the Antarctic region [*Turner*, 2004; *Grassi et al.*, 2009] and an SOI signal has previously been observed in the shorter-lived cosmogenic ^{7}Be isotope ($t_{\frac{1}{2}} = 53.2$ days) in records from lower latitude air sampling stations [*Koch and Rind*, 1998]. SAM and ZW3 are reported to affect ice core trace chemical composition [*Goodwin et al.*, 2004] and accumulation rates at DSS [*van Ommen and Morgan*, 2010] through their influence on atmospheric circulation patterns. For the Das2 series we focus on the North Atlantic Oscillation. The NAO affects precipitation rates [e.g. *Appenzeller et al.*, 1998; *Vinther et al.*, 2003], atmospheric transport pathways [e.g. *Mosley-Thompson et al.*, 2005; *Sjolte et al.*, 2011], and stratosphere to troposphere exchange [*Baldwin et al.*, 2001] in the region. Hence it is not unexpected that an NAO signal has previously been observed in atmospheric ^{10}Be and ^{7}Be data from northern high-latitude air sampling stations [*Aldahan et al.*, 2008].

The strengths of the correlations between the ^{10}Be series and respective modes are listed in Table 5.1, the source of the time series representing each mode is also provided in the table. DSS ^{10}Be concentrations are significantly negatively correlated with the ZW3, $r_{xy} = -0.36\,[-0.57; -0.10]$. However, the correlation is weaker and non-significant with DSS fluxes. No relationship is detected with SAM or ENSO. In the north, Das2 ^{10}Be concentrations are significantly correlated with the NAO index, $r_{xy} = -0.42\,[-0.64; -0.15]$, and again the correlation with Das2 fluxes is non-significant. These relationships are illustrated in Fig. 5.4a and b and discussed in turn below.

By definition, a positive ZW3 index indicates strong meridional flow, whereas a negative index indicates weaker meridional and stronger zonal flow [*Raphael*, 2004]. A marked transition in the index from a dominant negative phase toward positive phases occurs in the 1980's [as discussed in *Raphael*, 2007]. This transition occurs close to the time

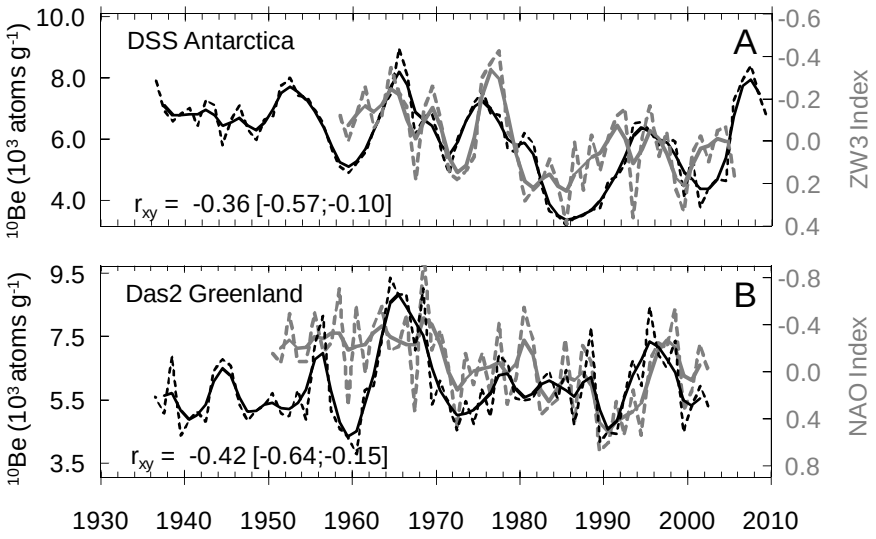

Figure 5.4: ^{10}Be concentrations are compared with modes of atmospheric circulation. (A) The southern hemisphere Zonal Wave Three (ZW3) index at the 500 mb level [annual averages from *Raphael*, 2004] overlain on ^{10}Be concentrations at DSS Antarctica. (B) The North Atlantic Oscillation (NAO) index (annual averages from the National Center for Environmental Prediction) is overlain on ^{10}Be concentrations from Das2 Greenland. Note that both indices are shown on inverted axes. The dashed lines show annually resolved data and the solid lines show smoothed data (Gaussian filter, effective half-width 3 years).

of the shift toward lower ^{10}Be concentrations through the 1980's to 90's. Interestingly, the missing cycle in ^{10}Be falls within the most strongly positive phase of ZW3 (Fig. 5.4a note the reversed axis of the index). There also appears to be similar periodicity between ZW3 and ^{10}Be in the 1960's and 70's. Note that the ZW3 index is not itself correlated with cosmic ray intensity ($r_{xy} = -0.14\,[-0.39;\,0.16]$).

A physical explanation for this relationship may be offered by the observed influence of ZW3 on atmospheric transport and regional trends in precipitation rates. During the strong positive phase of ZW3 the large scale atmospheric circulation is characterised by a clear pattern of alternating regions of poleward transport of warm mid-latitude air and equator-ward transport of cold polar air centered at around 50°S [see Fig. 1 of *Raphael*, 2004]. One of the regions of preferred poleward flow is directed toward Law Dome and is reported to influence moisture transport to the DSS site [*van Ommen and Morgan*, 2010]. Previous studies observe lower radionuclide concentrations in precipitation following intervals of enhanced precipitation in the moisture transport pathways to precipitation sites. This pattern is attributed to rainout and washout (Sect. 5.3.1.2) depleting the air mass aerosol load at and upstream of the sites [*Feeley et al.*, 1989; *Aldahan et al.*, 2001; *Graham et al.*, 2003; *Jordan et al.*, 2003; *Graly et al.*, 2011]. The effect is already observed on intra-annual timescales at Law Dome where consistently low concentrations in the austral winter have been linked to the timing of the regional precipitation maximum [*Pedro et al.* 2011b/Chapter 4]. Consistent with this line of reasoning, National Center for Environmental Prediction (NCEP) reanalysis fields depict increased precipitation in the region of warm moist air flowing toward Law Dome during the positive phase of ZW3 [see Fig. S2 and S4 of *van Ommen and Morgan*, 2010]. Hence, increased (decreased) cleansing of air masses upstream of the site by precipitation during the positive (negative) phases of ZW3 matches the direction of the observed correlation.

At Das2, Fig. 5.4b, there is a major shift toward a more positive phase of the NAO after the 1960's [e.g. *Scaife et al.*, 2005], after which similarities are seen in the two time series on both annual and decadal timescales. The ^{10}Be maximum in the mid 1960's occurs during a strong negative phase of NAO, however the two records diverge in the 1950's. Previous studies have argued that a solar activity signal is present in NAO [*Lockwood et al.*, 2010, and references therein]. However, for the period under consideration no correlation is detected between NAO and cosmic ray intensity ($r_{xy} = -0.16\,[-0.44;\,0.13]$).

A potential explanation for the NAO signal in Das2 concentrations is that moisture transport pathways are more conducive to delivering higher concentrations of ^{10}Be during the negative phase (NAO-), and lower concentrations during the positive phase (NAO+). Observational studies by *Baldwin and Dunkerton* [2001] in the northern high latitudes identified *reduced* penetration of stratospheric/upper tropospheric air mass [which has high ^{10}Be concentration, *Jordan et al.*, 2003] into the lower levels of the troposphere during NAO+. In agreement with this, *Aldahan et al.* [2008] remarked on the absence of stratospheric intrusions in beryllium radionuclide data from two high latitude sites in Sweden during the strong NAO+ between 1989 and 1992. In addition, evidence from Lagrangian-based moisture transport diagnostics suggest that moisture transport pathways to central-eastern Greenland are typically longer during NAO- [*Sodemann et al.*, 2008], thus increasing the range for aerosol scavenging, which is also consistent with the higher observed concentrations during NAO-.

The important role of NAO in precipitation rate variability in the region should also be considered [see e.g. *Appenzeller et al.*, 1998; *Vinther et al.*, 2003; *Mosley-Thompson et al.*, 2005; *Hanna et al.*, 2006]. Using data from the ECMWF ERA-15 reanalysis *Appenzeller et al.* [1998] showed that the precipitation response to NAO has pronounced spatial variability (see their Fig. 1b): on the western-central side of Greenland precipitation rates are significantly negatively correlated with the NAO, whereas on the eastern-central side (where Das2 is located) precipitation rates are significantly positively correlated with the NAO. This pattern is also seen in the output of a recent meso-scale model study [*Sjolte et al.*, 2011]. In line with these studies, the accumulation rate at Das2 is positively correlated with the NAO, $r_{xy} = 0.29$, although the significance is marginal, 95% CI $[-0.03; 0.54]$ (Fig. B1a). Since prior work indicates that the winter component of the NAO index is a stronger predictor of accumulation rate than the annual average index, we also consider the correlation between the Das2 accumulation series and the winter NAO (November to April). In this case the correlation is significant, $r_{xy} = 0.33\,[0.06; 0.53]$ (Fig. B1b). Nevertheless, the fact that the relationship between ^{10}Be concentrations and NAO is stronger than the relationship between accumulation rate and NAO (either winter or annual) suggests that this is not entirely an accumulation-driven effect. To summarise, we suggest that the directions of the observed correlations are consistent with two contributing factors: (i) an NAO modulation of accumulation rate at the Das2 site and in the moisture transport pathways to it, causing depletion of ^{10}Be concentrations in precipitation via washout

processes during the higher precipitation NAO+; and (ii) NAO controls on atmospheric transport processes including stratosphere to troposphere exchange, as outlined in the previous paragraph.

5.3.1.4 δ^{18}O

Results from an earlier sub-monthly resolved snow pit study at the DSS site found a strong and significant negative correlation between δ^{18}O ratios and ^{10}Be concentrations on sub-monthly timescales [*Pedro et al.*, 2006]. Higher (warmer) δ^{18}O values, which are typically associated with enhanced influence of warm and moist marine air, coincided with reduced ^{10}Be concentrations; whereas, lower (colder) δ^{18}O values, which are typically associated with enhanced influence of continental air, coincided with higher ^{10}Be concentrations [*Pedro et al.*, 2006, and references therein]. A negative correlation is also observed here in the annually resolved DSS concentrations, however it is weaker than that observed previously and it marginally fails a significance test $r_{xy} = -0.17\,[-0.39; 0.09]$. No correlation is apparent between Das2 concentrations and δ^{18}O. Overall it appears that the effect identified in *Pedro et al.* [2006] is strong on the snowfall event scale but relatively weak when considered on annual timescales. The weakening of the relationship in more coarsely resolved data is in line with other recent work at the site [*Pedro et al.* 2011a/Chapter 2].

5.3.1.5 Non sea salt sulphur

Figures 5.5a and b show the concentrations of non sea salt sulphur (nssS) and ^{10}Be at DSS and Das2 respectively. The nssS term reflects the sum of all sulphur containing species (predominantly sulphates, SO_4) corrected, following *McConnell et al.* [2007], for the sea salt associated sulphur species, which are mainly confined to the tropospheric boundary layer away from the ^{10}Be source region. The correlations between nssS and ^{10}Be concentrations are significant at both sites, $r_{xy} = 0.42\,[0.22; 0.60]$ at DSS, and $r_{xy} = 0.40\,[0.14; 0.61]$ at Das2. For DSS, the strengths of these correlations are slightly less than those with cosmic ray intensity/production, while for Das2 they are comparable. The relationships at both sites are considered in turn below.

The nssS signal in Antarctic ice is dominated by marine biogenic sources, with a minor contribution from anthropogenic activity, intermittent spikes from volcanic eruptions

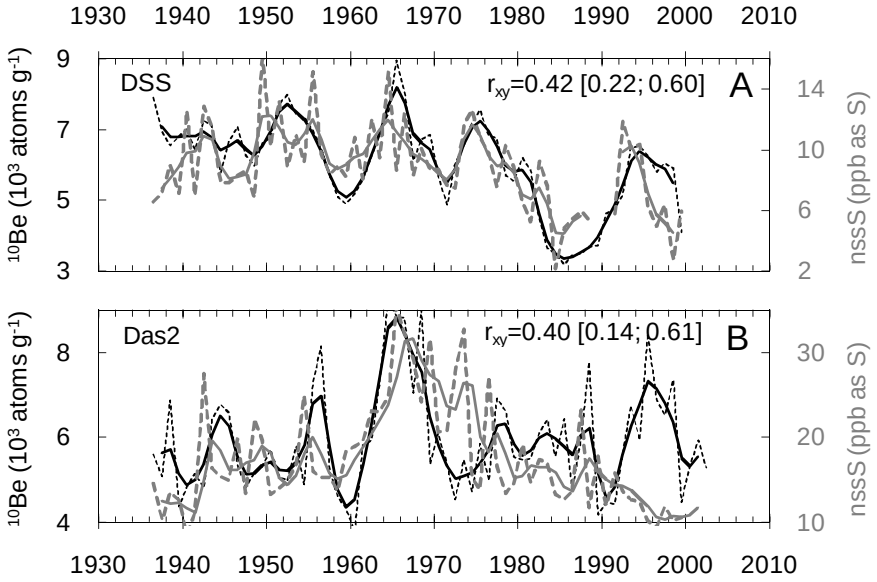

Figure 5.5: ^{10}Be concentrations are compared with nssS concentrations at (A) DSS Antarctica and (B) Das2 Greenland. The dashed lines show annually resolved data and the solid lines show smoothed data (Gaussian filter, effective half-width 3 years).

and a steady background from non-eruptive emissions [*Wagenbach*, 1996]. The similarities between nssS and ^{10}Be occur across interannual to decadal timescales (Fig. 5.5a). Despite the apparent quasi-decadal periodicity in the nssS data it is important to point out that there is no significant correlation detected between nssS and solar activity during this period, e.g. for nssS and cosmic ray intensity, $r_{xy} = 0.12\,[-0.14; 0.35]$. Remarkably, the pronounced nssS minimum in the 1980's coincides with the missing cycle minimum in ^{10}Be concentrations (take caution in visual assessment of this feature as there are two years of missing nssS data in 1989 and 1990). The nssS minimum is also seen at a site 10 km to the west (Fig. B2), confirming that the feature is not peculiar to the DSS site and that nssS levels remained low during 1989 and 1990. The common signal in nssS and ^{10}Be may be related to non-production processes jointly affecting the transport and deposition of both species. This interpretation is lent some support by the fact that DSS nssS is negatively correlated with the ZW3 index, $r_{xy} = -0.43\,[-0.65; -0.13]$ and snow accumulation rate, $r_{xy} = -0.20\,[-0.45; 0.08]$, with comparable strength and in the same direction as DSS ^{10}Be. Notably, the nssS minimum, like the missing cycle in ^{10}Be, falls within the most strongly positive phase of ZW3 (Fig. 5.4a).

For Das2, interpretation is complicated by the large contribution of anthropogenic nssS to Greenland ice. Previous analysis of sulphate in multiple Greenland cores sampled from a longitudinal transect of the ice sheet revealed a strong increase in anthropogenic sulphate from the 1940's to maximum levels in the late 1970's, followed by decreasing concentrations as emission reduction measures in Europe and the United States took affect [*Fischer et al.*, 1998]. These trends account for much of the longer-term trend in the nssS data (Fig. 5.5b). Interestingly, the marked nssS maximum at Das2 in the mid-to-late 1960's coincides with the ^{10}Be maximum yet actually precedes the maximum in anthropogenic nssS emissions. Again there is a suggestion that ^{10}Be and nssS are influenced by common climate variables. Like Das2 ^{10}Be, the nssS data is significantly negatively correlated with the snow accumulation rate, $r_{xy} = -0.41\,[-0.61;\,-0.17]$, and both the annual and winter NAO (although only the relation with the winter NAO passes a significance test, $r_{xy} = -0.38\,[-0.56;\,-0.16]$). The nssS maximum in the mid-to-late 1960's aligns with the accumulation minimum and strong NAO- phase.

The statistical significance of the relationships between nssS and ^{10}Be, and the fact that both are correlated to the same climate variables, certainly suggest that there is a real physical relationship between these species. On initial consideration this might be explained if, as suggested by *Delmas* [1992], ^{10}Be does predominantly arrive to the ice sheets attached to sulphate aerosol, in which case the transport and deposition of ^{10}Be would be influenced by the pathways of sulphate aerosols. However, it is important to avoid oversimplification: (1) as outlined above, the sources of ^{10}Be and nssS are very different, the majority of the natural and anthropogenic nssS burden is confined to the lower troposphere with a smaller fraction in the upper troposphere and stratosphere, whereas the majority of ^{10}Be is produced in the upper troposphere and stratosphere (where its scavenging by aerosols presumably first takes place); (2) the atmospheric burden of sulphate is of order Tg [*Stier et al.*, 2005], whereas that atmospheric burden of ^{10}Be is of order 10–100 g [*McHargue and Damon*, 1991], such that there should be always sufficient sulphate aerosol to scavenge the available ^{10}Be [e.g. *Field et al.*, 2006]; (3) while the agreement may be visually impressive, $< 20\,\%$ of the variance in nssS and ^{10}Be is actually shared; (4) direct experimental evidence that ^{10}Be is mainly attached to nssS aerosol is lacking. Particularly puzzling is why anthropogenic nssS at Das2, which is mainly transported in the lower troposphere, should be correlated with ^{10}Be. Some insight may be gained from a previous study which examined nssSO_4 and ^{7}Be (the shorter lived, $t_{\frac{1}{2}} = 53.24$ days, cosmogenic beryllium isotope), in precipitation collected

over four years at a site in Japan [*Igarashi et al.*, 1998]. A strong correlation between the two species was observed despite the fact that the bulk of the nssSO_4 arriving at the site was attributed to surface anthropogenic SO_2 sources. *Igarashi et al.* [1998] speculated that radionuclide 'labeled' sulphate aerosol from the upper-troposphere and stratosphere may mix well and coagulate with the 'unlabeled' sources originating from the boundary layer within the cyclonic systems that produce precipitation. A full explanation of the physical processes involved this relationship might be aided by further work on the post-production incorporation modes and precipitation scavenging mechanisms of ^{10}Be.

5.3.2 A bipolar ^{10}Be composite record

The preceding sections demonstrate that, on annual timescales, the ^{10}Be records from DSS and Das2 contain both production and climate signals of comparable strengths. In the context of using ^{10}Be as a solar proxy, we would like to enhance the production signal and reduce the climate 'noise'. A simple yet powerful technique for enhancing the signal to noise ratio in precisely-dated ice cores is to make a composite or stack of multiple records [e.g. *Fisher et al.*, 1996; *White et al.*, 1997]. The technique rests on the assumption that the signal, in this case the atmospheric production rate, is common and will be reinforced. In Fig. 5.6, the DSS and Das2 records are shown together with the other available annually resolved ^{10}Be records from the neutron monitor era: those from the Greenland sites, North GRIP, Dye 3 and Renland and the Antarctic site, Dronning Maud Land (locations in Fig. 5.1). The time series of concentrations from each site are normalised separately by dividing by their respective means over the period 1951–1984 (this period is selected as it is common to all records). Each series is overlain with the global ^{10}Be production rate, which is normalised in the same way (the issue of global versus polar mixing is addressed in the next section). The correlation coefficients and associated 95% CIs between each ^{10}Be series and the global production rate are inset on each plot. Among the individual sites, DSS has the highest correlation, followed by Das2. The attention paid here to sampling the DSS and Das2 records in a way that reduces seasonal aliasing may have contributed to their higher correlations. Among the remaining sites North-GRIP is most strongly correlated, whilst the correlations at Dye 3, Renland and DML are positive but not significantly different from zero. The weaker correlations at the later sites may be partly associated with their relatively high

Table 5.2: Assessing the strength of the solar activity and production rate signals in the multi-core ^{10}Be composite record. Pearson's correlation coefficient, r_{xy}, is listed against the polar neutron monitor counting rate (representing cosmic ray intensity), the global columnar production rate from the CRAC:10Be model, and the total solar irradiance (TSI). All correlations are significant at the 95% confidence level.

x	*Timespan*	n	r_{xy} [95% CI]
Production			
Neut. Count	1951–2002	52	**0.61** [0.44; 0.74]
Glob. Prod.	1951–2002	52	**0.62** [0.43; 0.75]
Glob. Prod.	1936–2002	67	**0.58** [0.42; 0.71]
TSI*	1979–2002	24	**-0.64** [-0.81; -0.35]

measurement uncertainties (10–15 %) [*Beer et al.*, 1984; *Aldahan et al.*, 1998], compared to uncertainties of < 5 % in the more recently measured DSS, Das2 and NGRIP records (see Sect. 5.2 and *Berggren et al.* [2009]).

The lowermost panel of Fig. 5.6 shows the average or composite of all six evenly weighted normalised records. The composite is limited to the period 1936–2002, during which there are at least two records available for averaging. In constructing the composite, annual concentrations that were more than two standard deviations away from the mean of the respective record were excluded. This form of filtering is justified by prior work linking such signals to meteorological variability, namely stratosphere to troposphere exchange events [*Aldahan et al.* 2008; *Pedro et al.* 2011b/Chapter 4], or potentially solar proton events [*Usoskin et al.*, 2006].

The composite is more strongly correlated (see Table 5.2) to the global production rate, $r_{xy} = 0.58\,[0.42;\ 0.71]$, and the cosmic ray intensity, $r_{xy} = 0.61\,[0.44;\ 0.74]$, than any of the individual cores (see Table 4.1). Furthermore, the composite is not correlated to the atmospheric modes identified earlier. For example the correlation between the composite and NAO is $r_{xy} = -0.05\,[-0.31;\ 0.27]$, and between the composite and ZW3 is $r_{xy} = -0.10\,[-0.34;\ 0.14]$. This illustrates that the signal to noise ratio has indeed been increased.

Although the period of overlap is relatively short, it is also interesting to consider the relationship between the composite ^{10}Be record and total solar irradiance (TSI), as measured by satellites since the 1970's [*Fröhlich*, 2000]. The PMOD TSI composite [*PMOD World Radiation Center*, 1979-2009] is strongly correlated with the composite

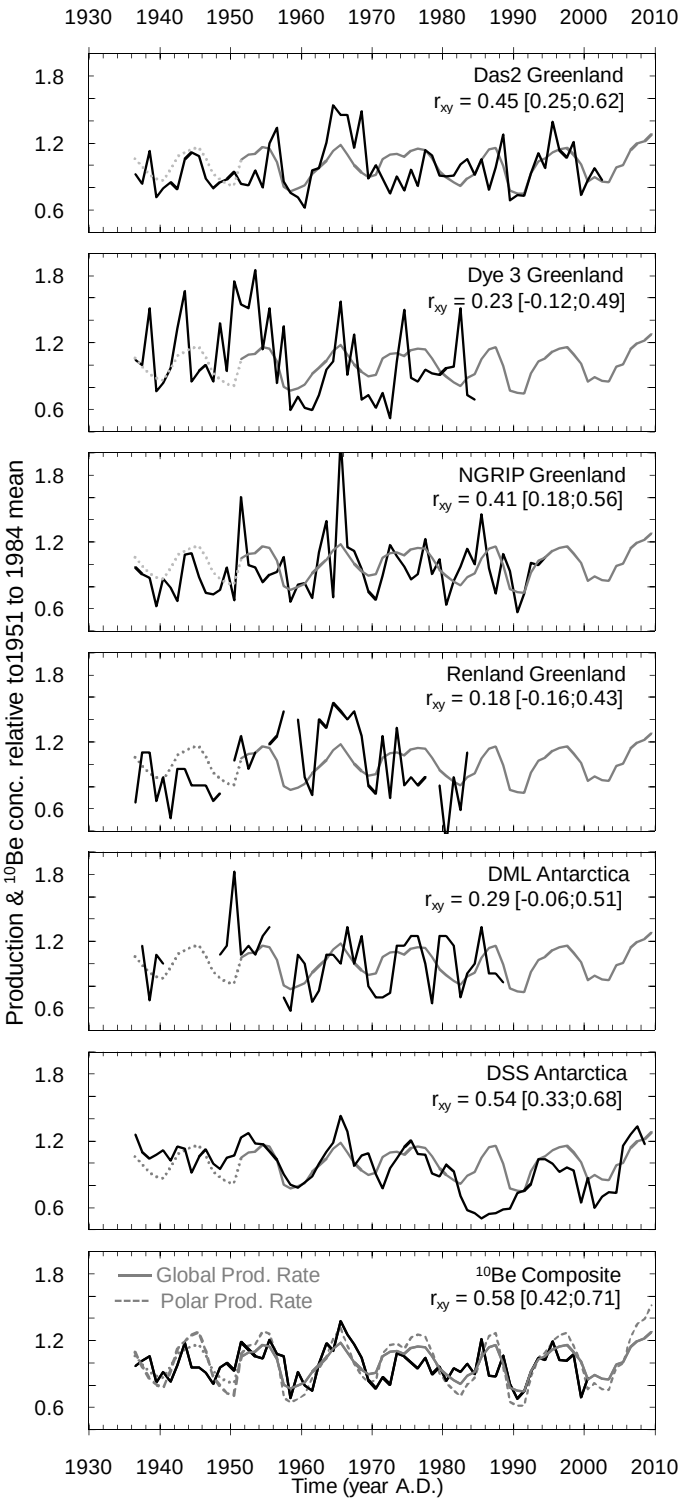

Figure 5.6: Annually resolved ^{10}Be records from Antarctic and Greenland sites during the neutron monitor era. Each record is overlain with the average global ^{10}Be production rate. The bottom panel shows a composite record constructed by stacking all of the records from the individual sites (see Sect. 5.3.2). Global average and polar average ^{10}Be production rate curves are both overlain on the ^{10}Be composite. All axis are scaled according to the mean values (μ) of the individual records over the common interval 1951–1984. The dashed lines show annually resolved data and the solid lines show smoothed data (Gaussian filter, effective half-width 3 years). Sources of the ^{10}Be series are, Dye 3 [*Beer et al.*, 1984], NGRIP [*Berggren et al.*, 2009] and Renland and Dronning Maud Land [DML; *Aldahan et al.*, 1998].

$r_{xy} = -0.64\,[-0.81; -0.35]$. The negative sign of the correlations is consistent with the association of a more active closed magnetic field (higher TSI) with a stronger open magnetic field and more shielding of cosmic rays (less ^{10}Be production) [for details see e.g. *Lean et al.*, 2002].

Spectral analysis provides additional insight into the production signal in the ^{10}Be composite. Fig. 5.7 compares the power spectrum of the ^{10}Be composite to that of the atmospheric production rate and the individual DSS and Das2 records. The power spectrum was produced using Matlab® by fast Fourier transform (FFT), employing the FFTW library [*Frigo and Johnson*, 2005] to perform the FFT computation on the linearly detrended series. The solar-cycle is clearly expressed in production rates as a peak at period 10.8 years. The ^{10}Be composite captures the period of the solar cycle very well, also showing a peak, albeit somewhat broader, at 10.8 years. By contrast in the individual cores the period of the solar cycle is poorly resolved; at DSS power is split between peaks at 10.4 and 14.6 years and at Das2 in a broad maximum between 9.4 and 16.3 years. This further supports that the fidelity of the production signal is enhanced in the composite ^{10}Be record compared to in the individual records.

5.3.3 Global or polar mixing of ^{10}Be

Cosmic rays are directed toward the geomagnetic poles leading to production rates over the polar latitudes ($> 60°$S/N) that are $\sim$ 3–20 times greater (depending on altitude) than those over the lower latitudes [*Kovaltsov and Usoskin*, 2010]. More importantly, in the context of interpreting ^{10}Be as a solar activity proxy, the *amplitude* of the solar modulation of production is greater over the polar latitudes than over the lower latitudes. This can be illustrated using the CRAC:10Be production data: throughout the neutron monitor era, the amplitudes of the 11-year cycles in columnar production variations in the polar atmosphere are on average 1.63 times those averaged over all latitudes (see Fig. 5.6, bottom panel).

The amplitudes of the 11-year cycles in the individual and composite ^{10}Be series can thus be used to address the widely debated question [*Mazaud et al.*, 1994; *Steig et al.*, 1996; *Bard et al.*, 2000; *Moraal et al.*, 2005; *Field et al.*, 2006; *Heikkilä et al.*, 2009] of whether the ^{10}Be deposited to the ice sheets is produced mainly at polar latitudes, or rather represents production in the globally well-mixed atmosphere. If the ^{10}Be in an

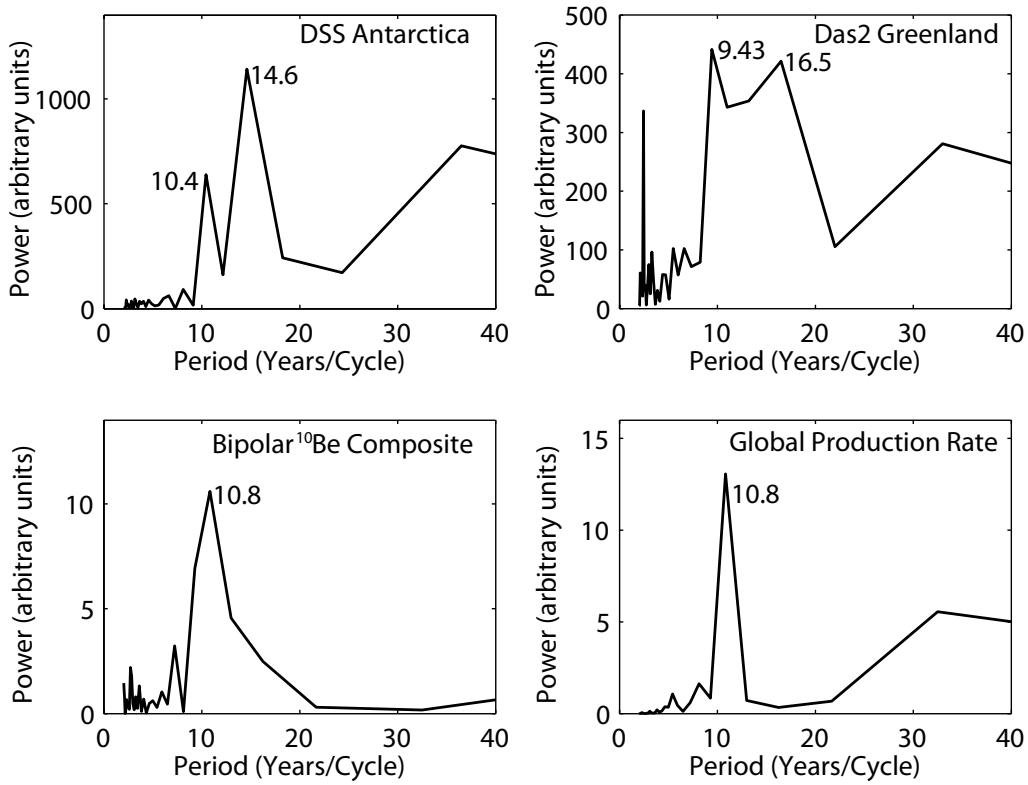

Figure 5.7: The fourier spectrums of the ^{10}Be records from DSS Antarctica (top left), Das2 Greenland (top right) are compared against the spectrums of the bipolar ^{10}Be composite (bottom left) and the global ^{10}Be production rate (bottom right). The similarity of the composite spectrum to the production rate spectrum suggests that combining multiple ^{10}Be records reduces non-production noise.

ice core record is sourced from the polar atmosphere, then the relative amplitude of the 11-year cycle should not be significantly different from that of polar production rate; whereas, if it is sourced from the globally well-mixed atmosphere, then it should not be significantly different from that of the global production rate.

Considering separately the DSS, Das2 and composite ^{10}Be records, linear regression is used to quantitatively examine the relative amplitudes and frame a statistical test, similar to the approach taken by *Steig et al.* [1996]. The ^{10}Be and production data are first normalised by dividing by their respective means over the period 1951–1984. The analysis is again restricted to the neutron monitor era (post-1951) during which the production variations are most reliable. Fig. 5.8 shows the normalised concentrations in each ^{10}Be record plotted against the normalised production rates in the global atmosphere (left column) and polar atmosphere (right column). The regression parameters in each case are estimated by non-parametric bootstrap resampling with replacement (1000 times) from the available data. This method is favored since it yields more robust confidence intervals than conventional regression, avoids assumptions about the data distribution, and accounts for auto-correlation. The critical regression parameter here is the slope; if the 95% CI around the slope contains 1 then it implies that the relative amplitude of the 11-year cycles in ^{10}Be and in the production series are not significantly different. The 95% CIs around the slopes of each regression are illustrated in Fig. 5.8 as dashed lines and are also listed inset. For all three ^{10}Be series the slope (b_1) of the regression against the global production rate is not significantly different from 1: DSS $b_1 = 0.89\,[0.55;\ 1.19]$, Das2 $b_1 = 0.75\,[0.37;\ 1.13]$ and ^{10}Be composite $b_1 = 0.74\,[0.49;\ 1.01]$. In contrast, the slopes are all significantly less than 1 for the regression against the polar production rate: for DSS $b_1 = 0.54\,[0.34; 0.73]$, for Das2 $b_1 = 0.44\,[0.22;\ 0.71]$ and for the composite $b_1 = 0.45\,[0.29;\ 0.61]$.

This result implies that the atmospheric production source region of ^{10}Be deposited to both the Antarctic and Greenland ice sheets is *not* exclusively the polar atmosphere. By contrast, *Steig et al.* [1996] reported that the amplitude of the 11-year cycle in ^{10}Be concentrations at Taylor Dome, Antarctica ($77°50'\,\mathrm{S}\ 158°40'\,E$, 2400 m asl) significantly exceeded the amplitude of the 11-year cycle in the global production rate. This led the authors to favour a polar origin for the ^{10}Be deposited to Antarctica. The difference between our results and those of *Steig et al.* [1996], warrant some examination. Several important points should be kept in mind when comparing the two studies: (1) Different production models: *Steig et al.* [1996] calculated ^{10}Be production rates using the

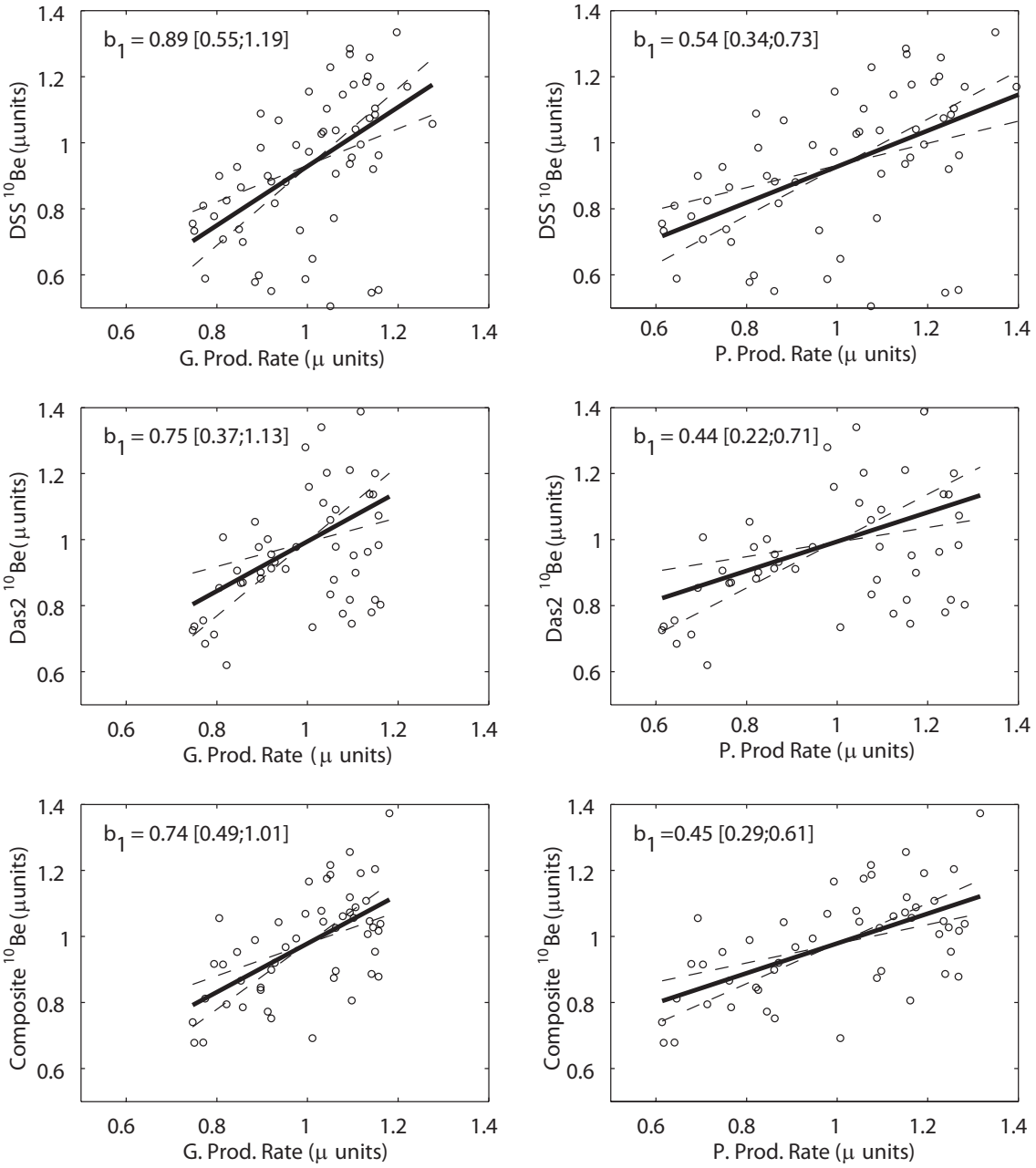

Figure 5.8: Assessing the relative amplitudes of the 11-year cycles in ^{10}Be concentrations by bootstrap linear regression against the global (left) and polar (right) production rates. Results are shown for DSS concentrations (top), Das2 concentrations (middle) and the ^{10}Be composite (bottom). Concentrations and production rates are expressed relative to the mean values (through 1951–1984) of the respective records. Solid lines show the best fit regression lines and the dashed lines show 95% confidence intervals around the regression slopes (b_1), which are also listed inset with the 95% CI in parentheses. For all three ^{10}Be records the regressions against global production rates are consistent with $b_1 = 1$ at 95% confidence, whereas the regressions against polar columar production rates yield $b_1 < 1$ at 95% confidence. Production rates are from the CRAC:10Be production model forced with the *Usoskin et al.* [2011] Φ reconstruction.

O'Brien et al. [1991] production model forced with cosmic ray intensity from the Deep River neutron monitor; whereas here we use the CRAC:10Be production model forced with the *Usoskin et al.* [2011] Φ reconstruction. (2) Different time-spans of the records: The Taylor Dome study was limited to 37-years of overlap with production rate data compared to 59-years at DSS and 52-years for both Das2 and the ^{10}Be composite. (3) Different data treatment prior to analysis: the Taylor Dome record was measured at 2–3-year resolution then resampled to annual resolution using low-degree cubic splines then filtered with a 9–13-year bandpass filter; whereas the analysis here is performed directly on annually resolved and unfiltered data. To test the sensitivity of our results to point 1 the analysis was repeated using the *Masarik and Beer* [2009] ^{10}Be production model (Fig. B3), forced as in the case of CRAC:10Be, with the *Usoskin et al.* [2011] Φ reconstruction. The same conclusions hold under the *Masarik and Beer* [2009] model, with the only difference being that the regression slopes are shifted marginally higher. With regard to points 2 and 3, the longer period of overlap, consistent results for multiple records and use of unfiltered data lend support to our conclusions. It is possible that the higher amplitude observed in the shorter Taylor Dome record may have resulted from the superposition of climate effects on the production signal, for example as appears to have occurred in the Greenland records during the 1960's (Fig. 5.6).

5.4 Discussion and conclusions

Annually resolved DSS and Das2 ^{10}Be records are significantly correlated with cosmic ray intensity and CRAC:10Be atmospheric production rates. The correlations are stronger at DSS than at Das2 and stronger with concentrations than with fluxes. The coefficients of determination imply that $\sim 30\%$ of the annual variance in ^{10}Be concentration at DSS is shared with cosmic ray intensity (and the atmospheric production rate) compared to $\sim 20\%$ at Das2 and $\sim 15\%$ for flux at both sites. The weaker signal in fluxes advises against using the flux term *at wet deposition sites* as an input for solar activity and cosmic ray intensity reconstructions. Significant portions of the variance in the ^{10}Be records was associated with non-production or climate signals. Intercomparison of the ^{10}Be records with observed and reanalysis climate data suggested some potential sources of these non-production signals. At DSS concentrations appear to be influenced by the ZW3 pattern of atmospheric circulation. At Das2 concentra-

tions appear to be influenced by the NAO and the local accumulation rate. A finding which remains difficult to explain is the significant correlations observed at both DSS and Das2 between ^{10}Be and nssS. As it stands, this result adds to prior work [*Delmas*, 1992; *Igarashi et al.*, 1998] suggesting that ^{10}Be and nssS are affected by common climate variables.

The sensitivity of the DSS and Das2 records to climate effects, particularly modes of atmospheric circulation, has potentially important implications for the interpretation of longer term records. It suggests that climate signals in ^{10}Be data may include systematic components. This can be illustrated by the NAO/^{10}Be anti-correlation at Das2. A period of relative warmth in the North Atlantic sector around the 9th–12th century AD, the 'medieval warm period' (MWP), has been associated with a prolonged positive NAO phase [e.g. *Trouet et al.*, 2009]; whereas a period of relative cold in this sector around the 16th–19th century AD, the 'little ice age' (LIA), has been associated with a prolonged negative NAO phase [*Slonosky et al.*, 2001; *Trouet et al.*, 2009]. Our results suggest that the patterns of circulation during these climate events could systematically influence ^{10}Be transport and deposition to some Greenland sites. For the Das2 site the direction of the correlation is such that it would act to exaggerate the proposed high solar activity during the MWP and the low solar activity during the LIA. It would obviously be advisable to avoid using any records affected in this way as inputs to solar forcing attribution studies. Note that the influence of NAO on the ice sheet appears to vary spatially [e.g *Appenzeller et al.*, 1998], such that the problem may affect other sites differently or not at all. Encouragingly, the NGRIP record is uncorrelated ($r_{xy} = -0.03\,[-0.27;\ 0.22]$) to the NAO at least through the interval 1950–1994. However, suitable data is currently unavailable to test whether this is also the case at the GRIP site, such a test would be useful as the GRIP record has been widely used in solar reconstructions [*Vonmoos et al.*, 2006; *Muscheler et al.*, 2007; *Steinhilber et al.*, 2009].

The potential for systematic climate influences on ^{10}Be at some sites advises caution in the interpretation of individual cores and underlines the importance of techniques to enhance the production signal. A bipolar composite record constructed using all available annually resolved ^{10}Be records from the neutron monitor era is more strongly correlated with cosmic ray intensity than any individual record. This suggests that studies which assimilate bipolar composite ^{10}Be records in solar or cosmic ray intensity reconstructions (or variants, such as the leading principal component of multiple records) [e.g. *Muscheler et al.*, 2007] are less likely to introduce spurious climate-related

signals than those assimilating ^{10}Be records from individual sites [e.g. *Bard et al.*, 2000; *Vonmoos et al.*, 2006; *Shapiro et al.*, 2011]. Using multiple ^{10}Be records in addition to cosmogenic ^{14}C from tree rings should reduce the risk of such signals even further.

The amplitude of the 11-year solar cycle in the DSS, Das2 and ^{10}Be composite records are consistent with the amplitude of the CRAC:10Be production variations in the global atmosphere. In contrast the amplitudes are significantly lower than the production variations in the polar atmosphere. This also holds when the *Masarik and Beer* [2009] production model is used in place of CRAC:10Be model, but a caveat is that it assumes the validity of the *Usoskin et al.* [2011] Φ reconstruction. This result is consistent with studies arguing that the ice sheets receive ^{10}Be from a globally well-mixed atmosphere [*Mazaud et al.*, 1994; *Heikkilä et al.*, 2009], and inconsistent with a prior study arguing that Antarctica receives ^{10}Be produced mainly in the polar atmosphere [*Steig et al.*, 1996]. A small over-representation of polar produced ^{10}Be, such as the 20 % 'polar enhancement' favoured by results from the GISS ModelE GCM study [*Field et al.*, 2006] should also not be excluded. This new empirical evidence that the ice sheets sample ^{10}Be from a globally well mixed atmosphere (or with a small polar bias) is in agreement with recent GCM studies [*Field et al.*, 2006; *Heikkilä et al.*, 2009], and with the mixing scenarios favoured by most recent ^{10}Be -based solar reconstructions [*Vonmoos et al.*, 2006; *Muscheler et al.*, 2007; *Steinhilber et al.*, 2009].

Following publication the datasets will be made available online at the Australian Antarctic Data Center (`http://data.aad.gov.au/`) and at the World Data Center for Paleoclimatology (`http://www.ncdc.noaa.gov/paleo/`).

Chapter 6

The Last Deglaciation: Timing the Bipolar Seesaw

J. B. Pedro[1,2], T. D. van Ommen[1,3], S. O. Rasmussen[4], V. I. Morgan[1,3], J. Chappellaz[5], A. D. Moy[1,3], V. Masson-Delmotte[6] and M. Delmotte[6]

Published June 2011 in *Climate of the Past*, 7, 671–683, 10.5194/cp-7-671-2011, 2011.

[1]Antarctic Climate & Ecosystems Cooperative Research Centre, Hobart, Tasmania, Australia
[2]Institute of Marine and Antarctic Studies, University of Tasmania, Hobart, TAS, Australia
[3]Australian Antarctic Division, Kingston, TAS, Australia
[4]Centre for Ice and Climate, University of Copenhagen, Copenhagen, Denmark
[5]Laboratoire de Glaciologie et Géophysique de l'Environnement, Saint Martin d'Hères, France
[6]Laboratoire des Sciences du Climat et de l'Environnement, Saclay, France

Abstract

Precise information on the relative timing of north-south climate variations is a key to resolving questions concerning the mechanisms that force and couple climate changes between the hemispheres. We present a new composite record made from five well-resolved Antarctic ice core records that robustly represents the timing of regional Antarctic climate change during the last deglaciation. Using fast variations in global methane gas concentrations as time markers, the Antarctic composite is directly compared to Greenland ice core records, allowing a detailed mapping of the inter-hemispheric sequence of climate changes. Consistent with prior studies the synchronized records show that warming (and cooling) trends in Antarctica closely match cold (and warm) periods in Greenland on millennial timescales. For the first time, we also identify a sub-millennial component to the inter-hemispheric coupling. Within the Antarctic Cold Reversal the strongest Antarctic cooling occurs during the pronounced northern warmth of the Bølling. Warming then resumes in Antarctica, potentially as early as the Intra-Allerød Cold Period, but with dating uncertainty that could place it as late as the onset of the Younger Dryas stadial. There is little-to-no time lag between climate transitions in Greenland and opposing changes in Antarctica. Our results lend support to fast acting inter-hemispheric coupling mechanisms, including recently proposed bipolar atmospheric teleconnections and/or rapid bipolar ocean teleconnections.

6.1 Introduction

The last deglaciation (ca. 19 to 11 thousand years before present (ka BP), where present is defined as 1950) is the most recent example of a major naturally forced global climate change. Previous studies confirm opposing climate trends on millennial timescales between the northern and southern mid to high-latitudes during this interval [e.g. *Sowers and Bender*, 1995; *Blunier et al.*, 1998; *Blunier and Brook*, 2001; *Shakun and Carlson*, 2010; *Kaplan et al.*, 2010]. Antarctica first warmed during the glacial conditions of Greenland stadial 2 (GS-2), then cooled during the Antarctic Cold Reversal (ACR), as Greenland experienced the warmth of the Bølling-Allerød interstadial (B-A or GI-1a-e). Antarctica then resumed warming as Greenland returned to the near-glacial conditions of the Younger Dryas stadial (YD or GS-1).

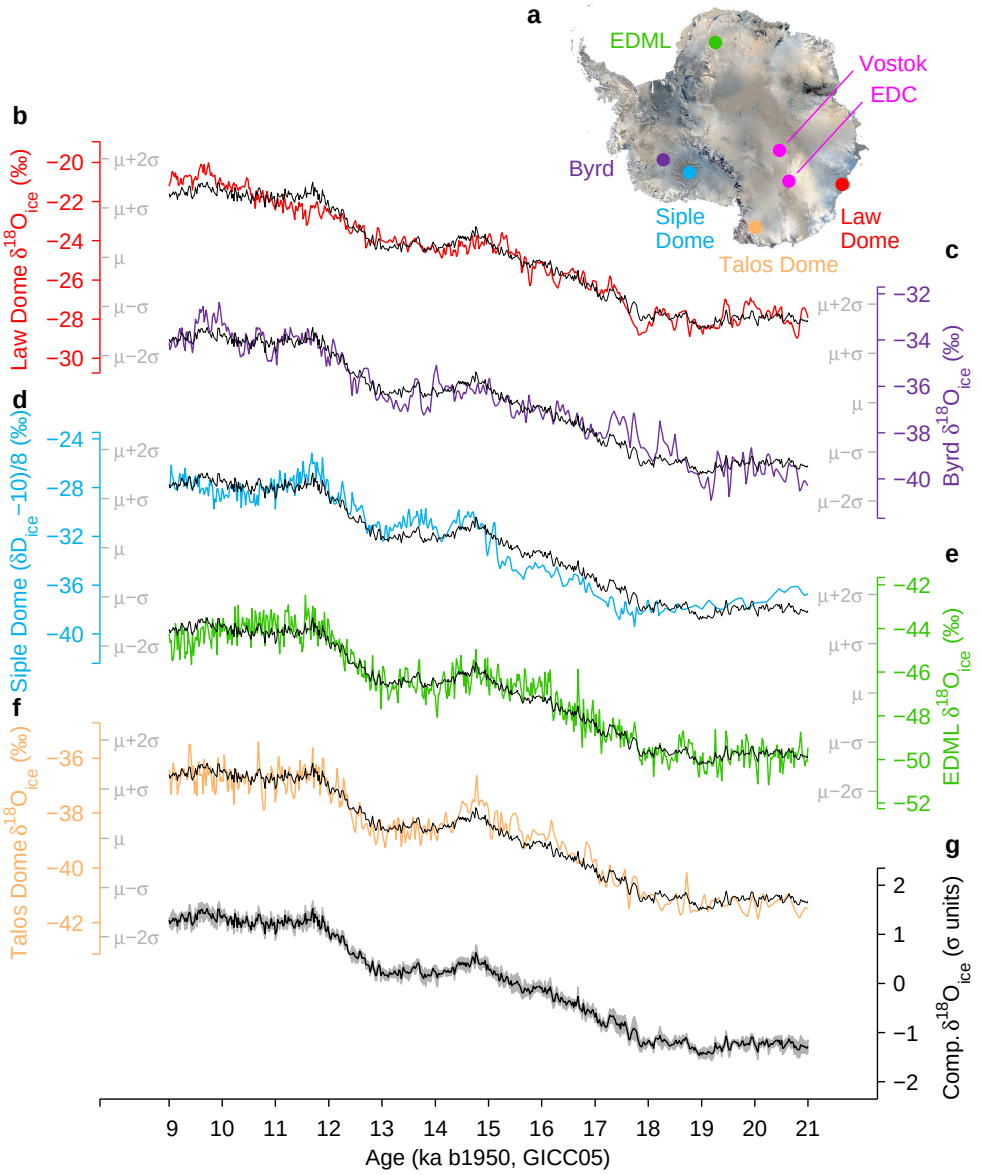

Figure 6.1: $\delta^{18}O_{ice}$ records from high-accumulation/near-coastal sites used to construct the Antarctic composite. **(a)** Map showing the location of the ice cores used and other records mentioned in the text (source: NASA). **(b)**–**(f)** Deglacial $\delta^{18}O_{ice}$ records from LD, Byrd, Siple Dome, Talos Dome, and EDML all placed on the common GICC05 timescale; the individual vertical axes are scaled according to the standard deviation of each record, as can be seen from the inner σ axis labels (in grey). **(g)** The Antarctic composite $\delta^{18}O_{ice}$ (black, also overlain in panels **(b)**–**(e)**) is shown bracketed by the standard error in the mean of the $\delta^{18}O_{ice}$ records from the five sites (grey shading). Estimated dating uncertainty in the composite (relative to GICC05) is 380, 200, and 220 years for intervals 15 to 18 ka BP, 13 to 15 ka BP, and 10 to 13 ka BP, respectively. Note that for Siple Dome the actual $\delta^{18}O_{ice}$ values were not available, so we use an appropriately scaled version of δD_{ice} (see Appendix C.).

The conventional explanation for these opposing climate trends is the bipolar ocean seesaw; it proposes that the two hemispheres are coupled via oscillations in the dominant direction of heat transport in the Atlantic Ocean due to perturbations in the meridional overturning circulation [*Broecker*, 1998]. More recently, an alternate (though potentially complimentary) mechanism has been put forward that invokes atmospheric teleconnections in forcing the bipolar coupling [*Anderson et al.*, 2009, and references therein]. Sorting out the relative contributions of oceanic and atmospheric processes is critical for understanding Earth's climate dynamics. A key role of the palaeoclimate record is to provide firm observational constraints against which these dynamical mechanisms and their timescales can be tested.

We begin by constructing a new climate chronology for the last deglaciation from the Law Dome (LD) ice core, Coastal East Antarctica, based on synchronization of fast methane variations at LD with those from Greenland (on the Greenland Ice Core Chronology 2005, GICC05 [*Rasmussen et al.*, 2008]). As with all ice core $\delta^{18}O_{ice}$ records, the LD record has been interpreted principally as a record of local temperature variations, notwithstanding that $\delta^{18}O_{ice}$ may also be influenced by changes in other variables, including temperature/humidity at the oceanic moisture source, seasonal distribution of snow fall, surface elevation, and anomalous ice flow [e.g. *Jones et al.*, 2009]. Construction of composite $\delta^{18}O_{ice}$ records from multiple ice cores has been demonstrated previously to reduce these local signals and produce reconstructions that more robustly represent regional climate trends [e.g. *White et al.*, 1997; *Andersen et al.*, 2006]. Therefore, in order to represent climate evolution in the broader Antarctic region, we construct a $\delta^{18}O_{ice}$ composite from the LD record and records from other high-accumulation/near-coastal sites: Byrd [*Blunier and Brook*, 2001], Siple Dome [*Brook et al.*, 2005], Talos Dome [*Stenni et al.*, 2011; *Buiron et al.*, 2011], and EPICA Dronning Maud Land (EDML) [*EPICA Community Members*, 2006; *Lemieux-Dudon et al.*, 2010]. These five cores are selected since they sample from a wide geographic range, including the Indian (LD), Atlantic (EDML), and Pacific (Siple Dome, Byrd, Talos Dome) sectors of the Antarctic continent (Fig. 6.1a), and because they can all be methane-synchronized with the GICC05 timescale of the central Greenland ice cores with sufficient accuracy.

The accuracy of the methane synchronization technique is limited by the offset between the age of the ice and the age of bubbles at a certain depth (i.e. the Δage; a result of the bubbles being sealed off from contact with the atmosphere at a depth of 50 to 100 m during the transformation of snow to ice). Compared to the cores from the

Table 6.1: Site characteristics and Δage values during modern, ACR, and LGM times at the Antarctic ice core sites mentioned in the text.

Site	Location	Elevation (m a.s.l.)	Distance from ocean[g] (km)	Δage modern (yr)	Δage at ACR (yr)	Δage at LGM (yr)
LD	66°46′ S, 112°48′ E	1370	100	60	350	700
Byrd[a]	80°01′ S, 119°31′ W	1530	591	270	380	480
Siple[b]	81°40′ S, 148°49′ W	621	439	242	381	815
Talos[c]	72°49′ S, 159°11′ E	2315	250	675	920	1595
EDML[d]	75°00′ S, 00°04′ E	2892	577	800	1200	2300
EDC[e]	74°39′ S, 124°10′ E	3240	912	2400	3000	4500
Vostok[f]	78°28′ S, 106°48′ E	3490	1409	3300	4400	5200

Source of Δage and elevation data: [a] *Blunier and Brook* [2001], [b] *Brook et al.* [2005], [c] *Stenni et al.* [2011], [d] *Lemieux-Dudon et al.* [2010], [e] *Parrenin et al.* [2007], [f] *Goujon et al.* [2003], [g] *Timmermann et al.* [2010] (with ice shelves considered part of the continent).

East Antarctic Plateau (e.g. EPICA Dome C (EDC) and Vostok), the relatively high accumulation records used here have more accurately constrained, and lower Δages, by up to an order of magnitude (Table 6.1), leading to greater precision in the methane synchronization.

The robust Antarctic-wide climate signal that emerges in the composite is used to provide tighter constraints on the relative timing of north-south climate variations during the deglaciation.

6.2 Methods

6.2.1 Construction of the revised Law Dome $\delta^{18}O_{ice}$ chronology

The previous LD methane record [*Morgan et al.*, 2002] is supplemented here with additional measurements that improve our timing constraints. Additional $\delta^{18}O_{ice}$ measurements were also made on the LD record, improving its temporal resolution to an average of 25 year per sample for the interval 9 to 21 ka BP.

The LD $\delta^{18}O_{ice}$ record was placed on the GICC05 timescale by synchronizing the LD CH_4 variations with GISP2 CH_4 variations on the GICC05 timescale. To ob-

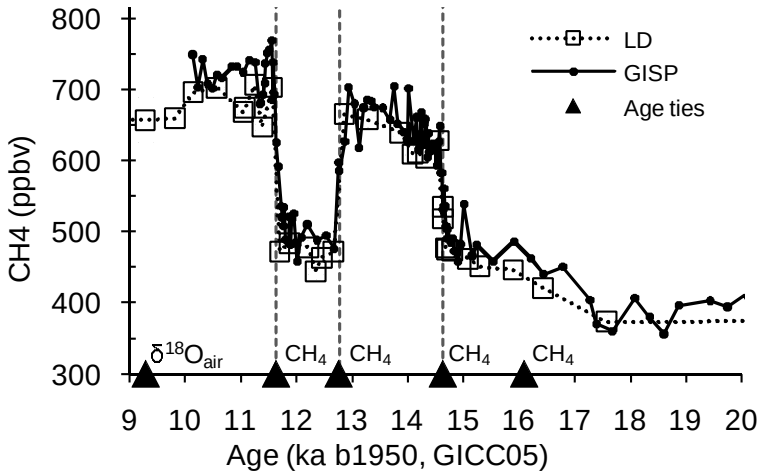

Figure 6.2: Dating of the LD ice core through the deglaciation. LD methane is synchronised with GISP2 methane [*Blunier and Brook*, 2001] on the GICC05 timescale. Timing of methane transitions at the onset of the Bølling, Younger Dryas, and Holocene are shown as dashed vertical lines. Triangles mark the position and type of the dating ties used through the deglaciation. Standard error in LD methane concentrations are ≤ 20 ppm.

tain GISP2 CH_4 on GICC05, the GISP2 CH_4 record on the ss09 timescale [reported in *Blunier and Brook*, 2001] was linearly interpolated to GRIP depths using the ss09 age-depth relation [*Johnsen et al.*, 1997], and then to GICC05 ages by linear interpolation using stratigraphical markers [*Rasmussen et al.*, 2008].

Figure 6.2 shows the GISP2 methane record and the new LD methane record. Also shown are the timings of the abrupt onsets of the Bølling, YD, and Holocene climate stages, as derived from the stable isotope records of the annually layer counted GRIP, NGRIP, and GISP2 ice cores [*Rasmussen et al.*, 2006; *Andersen et al.*, 2006; *Steffensen et al.*, 2008]. The timing of methane transitions is considered to be synchronous with the onsets of these climate stages. The LD gas age scale was tied to GICC05 at the times of these methane transitions. On the older side of the deglaciation, the mid-point of the slow deglacial rise in methane (through the interval ca. 17.5 to 15 ka BP) is used as a tie. We also used methane ties to GISP2 during Dansgaard-Oeschger events 7 and 8 (35.48 and 38.22 ka BP, respectively). On the younger side of the deglaciation we use a $\delta^{18}O_{air}$ tie to GISP2 and GRIP (9.30 ka BP).

The gas age ties were converted to ice age ties by adding an estimate of the difference between the age of the gas and the age of the ice (i.e. the Δage). We estimated Δage

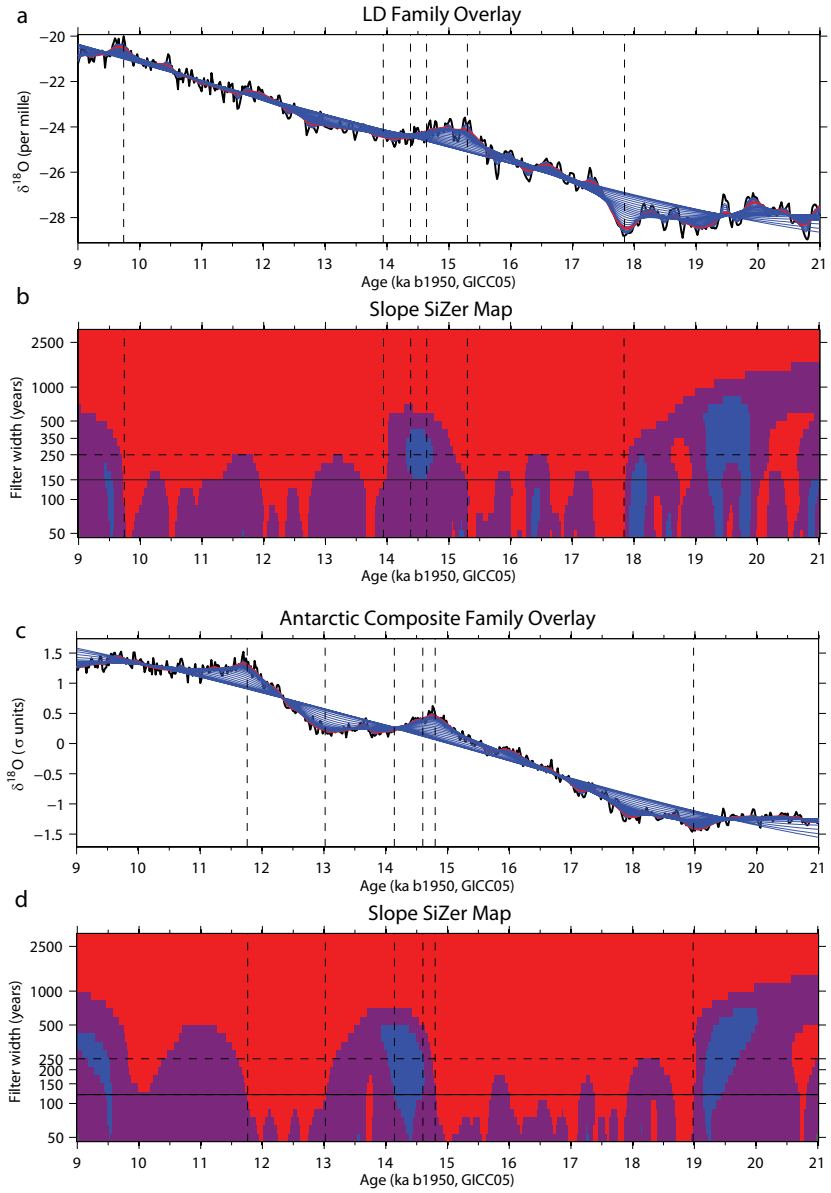

Figure 6.3: SiZer maps of the significance of features in the Law Dome and Antarctic composite records. **(a)** LD Family Overlay: blue curves show LD $\delta^{18}O_{ice}$ smoothed across a range of filter widths (40–3000 years); black curve shows the original data; red curve shows the 150 year smooth. **(b)** LD Slope Sizer Map: the significance and sign of the slope of the smoothed data is shown as filter width (vertical axis) is varied: red, significant positive slope (warming); blue, significant negative slope (cooling); purple, slope not statistically different from zero (all with respect to the 95 % CL). For instance, the significant cooling during the ACR appears as the central blue area. The timing of significant climate features at LD is interpreted from the intercepts of the 150 year smooth (horizontal solid line) with the changes in the significance and/or sign of the slope. Significant features are marked with dashed vertical lines. The timing and uncertainty of climate features are listed in Table 6.4. **(c)** Antarctic Composite Family Overlay: interpret as for LD except that the red curve shows the 120 year smooth. **(d)** Antarctic composite Slope SiZer Map: interpret as for LD except that timing of features is interpreted from the intercepts of the 120 year smooth (see Sect. 6.2.3.2).

Table 6.2: LD age ties used in construction of the deglacial chronology and their uncertainties.

Type	LD depth (m)	LD GICC05 gas age $\pm\sigma_{\text{correl}}$ (ka b1950)	Δage $\pm\sigma_{\Delta\text{age}}$ (yr)	LD ice age $\pm\sigma_{\text{ice}}$ (ka b1950)
$\delta^{18}O_{\text{air}}$	1108.64	9.30 ± 0.15	119 ± 36	9.42 ± 0.15
CH_4: Start of Holocene	1121.29	11.63 ± 0.08	148 ± 43	11.78 ± 0.09
CH_4: Start of GS-1	1125.19	12.77 ± 0.10	273 ± 82	13.04 ± 0.13
CH_4: Start of GI-1e	1129.04	14.64 ± 0.03	309 ± 93	14.94 ± 0.10
CH_4: Mid-point of deglacial rise	1131.75	15.65 ± 0.30	433 ± 130	16.09 ± 0.33
CH_4: DO7	1144.28	35.34 ± 0.18	540 ± 160	35.88 ± 0.25
CH_4: DO8	1146.70	38.34 ± 0.20	500 ± 150	38.84 ± 0.25

Note: σ_{correl} refers to the uncertainty involved in correlating the LD CH_4 record with the GISP2 CH_4 record; $\sigma_{\Delta\text{age}}$ refers to the uncertainty in Δage at LD; and σ_{ice} is calculated as the RMS sum of σ_{correl} and $\sigma_{\Delta\text{age}}$.

using the Pimienta firn densification model [*Barnola et al.*, 1991], which requires temperature and accumulation rate input. Surface temperature was estimated from $\delta^{18}O_{\text{ice}}$ by scaling of the modern temporal (seasonal) relationship between $\delta^{18}O_{\text{ice}}$ and temperature (T) at Law Dome ($\delta^{18}O_{\text{ice}}$ is proportional to $0.44\,T$) [*van Ommen and Morgan*, 1997]. Accumulation rates and ages between tie points are calculated using a simple Dansgaard-Johnsen flow model, fitted to the chosen age ties, as discussed elsewhere [*van Ommen et al.*, 2004]. The model predicts relatively low accumulation rates at Law Dome during the deglaciation, for instance ca. 20 % of modern at 15 ka BP and ca. 10 % of modern during the LGM. These model accumulation rates are the most reliable estimates available for LD and they are independently supported by measurements of the deglacial changes in $\delta^{15}N_{\text{air}}$ at LD [*Landais et al.*, 2006]. An alternate method of estimating paleoaccumulation rate from the water vapor pressure (derived from $\delta^{18}O_{\text{ice}}$) is often used at ice core sites on the East Antarctic Plateau. The water vapor pressure technique is not suited to the Law Dome site where, in contrast to the East Antarctic plateau, the accumulation rate appears to be influenced by cyclonic activity rather than by local temperature controls on the atmospheric moisture content. Problems with the assumed relation between vapor pressure and accumulation are also noted at other near coastal sites [*Monnin et al.*, 2004].

There are two main sources of error in the LD ice age ties: firstly, the uncertainty in our alignment of the fast methane transitions at Law Dome with those at GISP2 (the correlation uncertainty, σ_{correl}); and secondly, the uncertainty in the LD Δage (which

we conservatively estimate as ±30 % of Δage, $\sigma_{\Delta age}$). The gas age ties, Δages, and ice age ties together with their estimated uncertainties are listed in Table 6.2. We do not include in our error estimates the uncertainty in the GICC05 timescales for the GISP2 gas age ties; rather, we specify that the error in our age ties is relative to the GICC05 timescale.

6.2.2 Construction of the Antarctic $\delta^{18}O_{ice}$ composite record

In constructing the Antarctic composite, LD, Byrd, Siple Dome, Talos Dome, and EDML, $\delta^{18}O_{ice}$ series on their GICC05 timescales (see Appendix C.) were interpolated to 20 year time steps. Note that for Siple Dome the actual deglacial $\delta^{18}O_{ice}$ record was not available so we used an appropriately scaled version of δD_{ice} ice in its place (see Appendix C.). For simplicity, when speaking of multiple records, we continue to use the term $\delta^{18}O_{ice}$. Each series was standardized over the interval 9 to 21 ka BP to zero mean and unit standard deviation, and the mean of the five data sets was taken at each time step. Extension of the composite beyond 21 ka BP is not possible at this stage due to the lack of fast methane variations or other high-quality inter-hemispheric dating ties with which to synchronize the records. Accordingly, our focus here is only on the deglaciation, i.e. the interval beginning with the onset of a coherent Antarctic warming trend and ending with the termination of the warming trend at the start of the Holocene.

6.2.3 Statistical analysis of warming and cooling trends

A statistical approach, SiZer analysis of curvature [*Chaudhuri and Marron*, 1999], is used to objectively determine the timing of significant climate features in both the LD and Antarctic composite $\delta^{18}O_{ice}$ records during the deglaciation.

SiZer applies a series of smoothing filters to the time series (Fig. 6.3a and c) and depicts the sign of the slope as a function of time and filter width (Fig. 6.3b and d). We define the onset of deglaciation as the time at which a significant warming is first observed on all timescales (i.e. regardless of the degree of smoothing), the ACR onset is then bracketed by the end of the significant warming trend and the start of a significant cooling trend. Similarly, the ACR termination is bracketed by the end of the significant

Table 6.3: Dating uncertainties in the individual records used in the Antarctic composite during the deglaciation (Sect. 6.2.4)

	Late deglaciation (∼ 10–13 ka b1950)			Middle deglaciation (∼ 13–15 ka b1950)			Early deglaciation (∼ 15–18 ka b1950)		
Core	σ_{correl}	$\sigma_{\Delta\text{age}}$	σ_{ice}	σ_{correl}	$\sigma_{\Delta\text{age}}$	σ_{ice}	σ_{correl}	$\sigma_{\Delta\text{age}}$	σ_{ice}
LD	100	80	128	30	90	95	300	125	325
Byrd[a]	200	200	283	200	200	283	300	200	361
Siple Dome[b]	170	110	202	120	130	177	320	190	372
Talos[c]	–	–	300	–	–	300	–	–	500
EDML[d]	–	–	200	–	–	140	–	–	360
Average	–	–	223	–	–	199	–	–	384

[a] *Blunier and Brook* [2001], [b] *Brook et al.* [2005], [c] *Buiron et al.* [2011], [d] *Lemieux-Dudon et al.* [2010].

ACR cooling trend and the resumption of a significant warming trend, and the end of the deglaciation is where the significant warming trend ceases.

In using SiZer for the identification of climate features a decision must be made on the smoothing filter width that preserves a clear signal from the major millennial and sub-millennial scale climate features of interest, but is above the confounding influence of shorter term noise. Hence the optimal smoothing filter width will depend on the level of noise in the record. As it is an individual core, the level of noise in the LD record is expected to be larger than that of the 5-core Antarctic composite and therefore a wider filter is appropriate for LD compared to the Antarctic composite.

6.2.3.1 Law Dome

For the LD record at filter widths of above 250 years the deglaciation is seen, on the simplest level, as a warming interrupted by the ACR (dashed horizontal line, Fig. 6.3b). At filter widths much larger than this the timing of climate features is highly dependent on filter width, which suggests that detection is not robust. Moving to filter widths of ≤ 150 years the timing of features generally stabilises (below solid line, Fig. 6.3b). Hence, we select 150 years as the optimal filter width at which to detect climate features in the LD record (solid horizontal line, Fig. 6.3b).

6.2.3.2 Antarctic composite

For the composite record, again at filter-widths of above 250 years the major millennial scale features of the deglaciation are identified (dashed horizontal line, Fig. 6.3d). Moving to narrower filters, a threshold is seen at a width of $\leq$ 100 years, at which multiple short term signals that we regard as noise are expressed. To stay above this noise threshold we select 120 years as the optimal filter width to detect climate features of interest to this work (solid horizontal line, Fig. 6.3d).

6.2.4 Dating uncertainty in the Antarctic composite

The dating uncertainty of the Antarctic composite ($\sigma_{\text{Composite}}$) relative to GICC05 includes contributions from the dating uncertainty of the five records ($\sigma_{\text{LD ice}}$, $\sigma_{\text{Byrd ice}}$, $\sigma_{\text{Siple ice}}$, $\sigma_{\text{Talos ice}}$, $\sigma_{\text{EDML ice}}$). In the same way as for $\sigma_{\text{LD ice}}$ (Sect. 6.2.1), the individual core σ_{ice} values at Byrd and Siple Dome are calculated *Blunier and Brook* [following 2001]) as the root mean square (RMS) sum of the methane synchronisation (σ_{correl}) uncertainty and the Δage uncertainty ($\sigma_{\Delta\text{age}}$) reported by the original authors of each record [*Blunier and Brook*, 2001; *Brook et al.*, 2005, respectively]). For Talos Dome and EDML we adopt the σ_{ice} values reported with the recent publications of GICC05 consistent timescales for those cores [*Buiron et al.*, 2011; *Lemieux-Dudon et al.*, 2010, respectively]. These uncertainty terms are reported in Table 6.3.

Combining the uncertainties from the individual cores into one uncertainty value for the composite record is not straightforward: firstly, the uncertainties in the individual records vary with time during the deglaciation; secondly, it cannot be assumed that the individual uncertainties are independent; and thirdly, to our knowledge there is no formal way of combining dating uncertainty in individual records into one dating uncertainty for a composite. These complications prevent us providing any formal "standard error" value for the composite. However, a conservative estimate is that the overall uncertainty is lower than the average of the uncertainty of the individual records.

A "jack-knifing" test, in which the composite was constructed by including all and then leaving out one in turn of the five records, was used to test the robustness of the composite dating. The timing of climate features is essentially unchanged when this technique is applied. For instance, in the resulting 6 versions of the composite, the

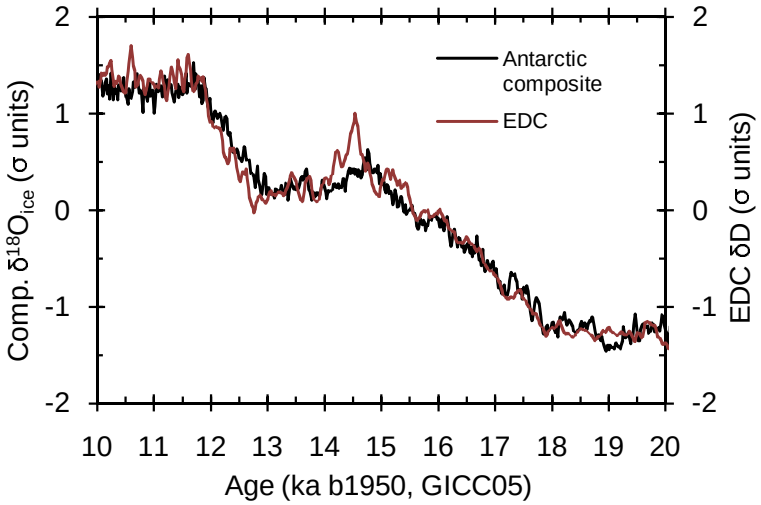

Figure 6.4: A comparison of the Antarctic composite with the EPICA Dome C (EDC) δD_{ice} record. The GICC05 consistent timescale for EDC is from *Lemieux-Dudon et al.* [2010] and δD_{ice} data are from *Jouzel et al.* [2001].

timing of the pre-ACR isotope maximum (mean$\pm 2\sigma$) is (14.76$\pm$0.02) ka BP. This result supports the robustness of the dating and the presence of a coherent Antarctic-wide climate signal within the five records.

6.3 Results and discussion

Fig 6.1b shows the LD ice core oxygen isotope record ($\delta^{18}O_{ice}$) alongside the records from Byrd, Siple Dome, Talos Dome, and EDML, all on the common GICC05 timescale. All records show a similar pattern: an overall warming trend interrupted by the millennial scale ACR. However, the precise timing of changes in climate trends differs between records. This is illustrated by apparent differences in the timing of the onset of the ACR. For instance, at LD the pre-ACR warming trend ends at 15.30$\pm$0.17 ka BP (Table 6.4), which, within timescale uncertainties, is consistent with the previously published result of *Morgan et al.* [2002]. This is considerably older than at EDML where the pre-ACR warming trend ends at 14.55$\pm$0.13 ka BP [*Lemieux-Dudon et al.*, 2010]. Such differences between cores (which are greater than dating uncertainties) represent the influence of local and/or non-climatic signals at individual sites and underscore the need for caution in interpreting the phasing of interhemispheric climate changes from single-site records.

Table 6.4: The timing of climate features in the LD and Antarctic composite $\delta^{18}O$ records derived from SiZer analysis. Dating uncertainties are the RMS sum of the dating uncertainty and uncertainty in the statistical method for picking timing of the climate feature (Sect. 6.2.3).

Climate feature	LD Age (ka b1950)	Composite Age (ka b1950)
Start deglacial warming	17.84 ± 0.32	18.98 ± 0.50
End warming (earliest ACR onset)	15.30 ± 0.17	14.80 ± 0.20
Start cooling (latest ACR onset)	14.64 ± 0.10	14.60 ± 0.20
End cooling (earliest ACR termination)	14.38 ± 0.11	14.14 ± 0.20
Start warming (latest ACR termination)	13.94 ± 0.12	13.02 ± 0.20
End deglacial warming	9.74 ± 0.15	11.76 ± 0.22

The Antarctic $\delta^{18}O_{ice}$ composite is shown superimposed on the individual records from which it is constructed in Fig. 6.1b–f, and bracketed by its standard error in Fig. 6.1g. Deviations between individual records and the composite are indicative of local, non-climatic, and/or sub-continental variations. A clear example of such a deviation is the continued rise in $\delta^{18}O_{ice}$ at LD into the Holocene (until 9.74 ± 0.15 ka BP). Air content measurements on the LD core suggest a lowering of the drill site of 100 to 300 m [*Delmotte et al.*, 1999], which would be broadly consistent with the change in $\delta^{18}O_{ice}$ relative to the other sites. Detailed evaluation of differences between the timing of climate variations in the composite and records from the East Antarctic Plateau including EDC, Vostok, and Dome Fuji is hampered by the relatively large dating uncertainties of these low accumulation records. Nevertheless, a recent revision of the EDC dating to a GICC05-consistent timescale [*Lemieux-Dudon et al.*, 2010] permits a comparison to be made (Fig. 6.4). Very close agreement between the records is observed through the onset of the deglaciation (ca. 19 to 15 ka BP); both curves show a step in the warming trend at ca. 18 ka BP and centennial-scale breaks in the warming trend centred at ca. 17.2 ka BP, and at ca. 15.8 ka BP (these features can also be seen in Fig. 6.3d, persisting at filter-widths > 120 years). The major timing differences between the records are delayed onset of the ACR and post-ACR warming at EDC compared to the composite. If real, this delay may represent a more rapid response of the near-coastal records used in the composite to the observed changes in Southern Ocean conditions [e.g. *Anderson et al.*, 2009] and/or sea ice extent [e.g. *Bianchi and Gersonde*, 2004], which can cause changes in $\delta^{18}O_{ice}$ by affecting cyclogenesis, the path of storm tracks, and the seasonal balance of precipitation [*Noone and Simmonds*, 2004].

Alternately, the timing difference between the EDC and composite curves may simply reflect timescale uncertainties. Interestingly, LD, which has the earliest ACR onset, is also the lowest latitude of the records and closest to the Southern Ocean.

Turning now to the relative timing of north-south climate variations, Fig. 6.5 shows the Antarctic composite and the North Greenland Ice Core Project (NGRIP) $\delta^{18}O_{ice}$ record [*NGRIP community members*, 2004] through the period 11 to 20 ka BP, interpreted as a proxy for climate in the broader North Atlantic region (hereafter, the "north"). We refrain from constructing a Greenland ice core composite since the main climate transitions (the onsets of which are defined in the INTIMATE climate event stratigraphy of *Lowe et al.* [2008]) are already simultaneous between the Greenland records when studied at 20 year time resolution [*Rasmussen et al.*, 2008].

Coloured vertical bands in Fig. 6.5 illustrate significant warming and cooling trends in the Antarctic composite (hereafter the "south"), the timings of these features are also listed in Table 6.4. Significant deglacial warming begins in the south at 18.98 ± 0.50 ka BP on all timescales, and we therefore define this as the start of deglaciation. However, the warming trend then falters at 18.68 ka BP, before resuming strongly and again on all timescales at 17.90 ± 0.38 ka BP. In the north, stadial conditions (GS-2) prevail until the abrupt warming of the Bølling onset at 14.64 ka BP; it has been previously proposed that the ACR onset also happened at around this time [*Blunier and Brook*, 2001; *EPICA Community Members*, 2006]. However, the issue of which came first (of critical importance in separating cause and effect) is debated [*Morgan et al.*, 2002] and has been complicated by the non-consistent timescales previously used for individual Antarctic cores. Using the composite, we see that the end of the significant deglacial warming trend in the south, at 14.80 ± 0.20 ka BP, and the start of significant ACR cooling, at 14.60 ± 0.20 ka BP, tightly bracket the Bølling onset. This synchrony of trend change in the south with transition in the north supports the view that the two events are coupled.

Progressing through the deglaciation, we find evidence for north-south climate coupling on sub-millennial timescales. The period of significant cooling within the ACR (14.60 ± 0.20 ka BP to 14.14 ± 0.20 ka BP; dark blue band, Fig. 6.5) coincides tightly with the pronounced warmth of the Bølling (GI-1e). The coherence of the southern cooling trend during this interval implies that it was communicated relatively rapidly and uniformly around the Antarctic continent. Numerical models [e.g. *Liu et al.*, 2009] and recent

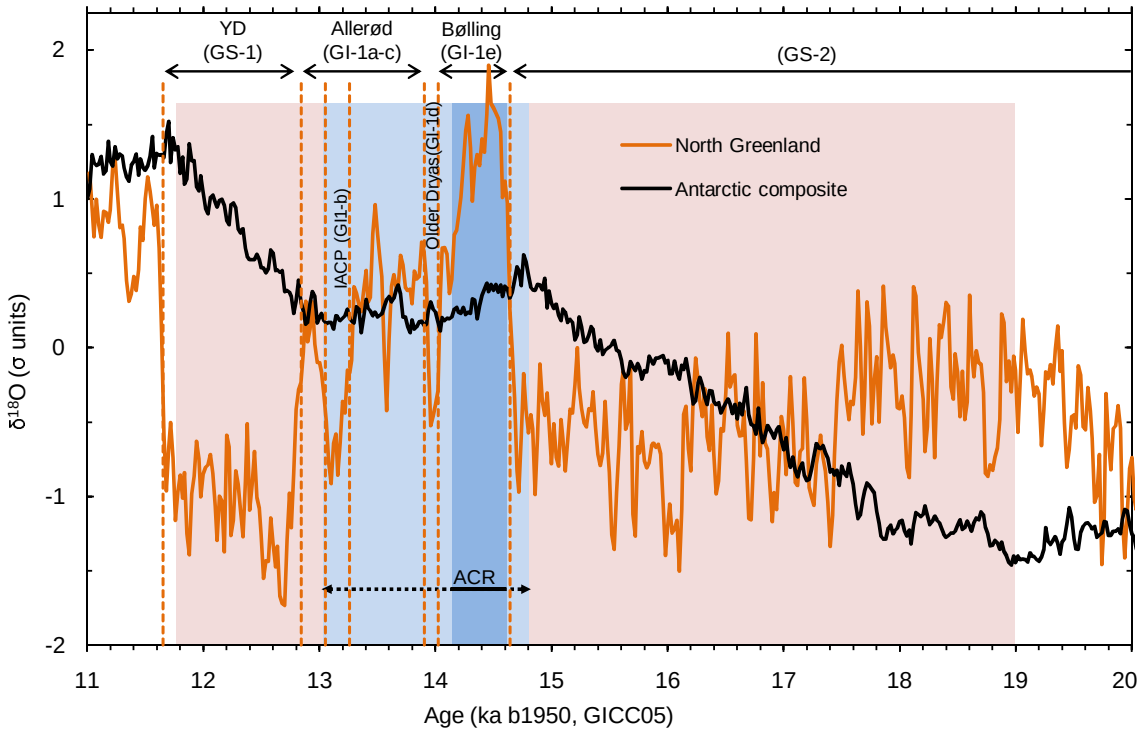

Figure 6.5: A comparison of the pattern and timing of climate change in the Antarctic and North Atlantic regions during the last deglaciation: the Antarctic composite $\delta^{18}O_{ice}$ record and the North Greenland (NGRIP) $\delta^{18}O_{ice}$ record. Vertical pink bands correspond to periods of significant Antarctic warming, vertical light blue bands correspond to a pause in Antarctic warming, and the vertical dark blue band corresponds to significant Antarctic cooling. The minimum duration of the ACR is the period spanned by the dark blue band, the maximum duration of the ACR also includes the periods spanned by the light blue bands (as marked by the solid and dashed horizontal lines below the ACR label). Dashed vertical orange lines and labels at the top of the figure show the exact timing of the North Atlantic INTIMATE climate stages [*Lowe et al.*, 2008].

proxy-based observations from a south Atlantic sediment core [*Barker et al.*, 2010] suggest that the pronounced Bølling warmth was associated with an "overshoot" of the AMOC and a southward expansion of the North Atlantic Deepwater cell. During this "overshoot", when heat release in the North Atlantic was at its strongest, our results suggest that heat flux away from the south was also at its strongest.

The initial Bølling warmth deteriorates through the Allerød and is punctuated by abrupt sub-millennial scale cooling events, including the Older Dryas (GI-1d) and the Intra-Allerød Cold Period (IACP or GI-1b) (Fig. 6.5). Results from a sediment core south of Iceland suggest that these sub-millennial cold events coincide with periods of increased meltwater flux to the North Atlantic [*Thornalley et al.*, 2010]. Changes in the trend in the Antarctic composite also occur close to the times of these sub-millennial cold events. Significant ACR cooling in the south ends around the time of the Older Dryas in the north. This is followed by a ca. 1000 year interval in the south during which there is no coherent Antarctic-wide warming or cooling trend. This interval is coincident with the Allerød stage GI-1c, which is not as warm as the Bølling (GI-1e) or the Holocene, a point we return to below. The exact timing of the resumption of post-ACR warming in the south is difficult to pinpoint and appears variable between the different cores (Fig. 6.1). Significant post-ACR warming resumes at LD at 13.94 ± 0.11 ka BP, at the start of the Allerød or possibly during the Older Dryas (GI-1d). Post-ACR warming also begins at Byrd during the Allerød (Fig. 6.1c), as noted previously by *Blunier and Brook* [2001]. Looking to the composite for the best representation of the Antarctic-wide signal, warming is first detected at the 120 year filter-width at 13.02 ± 0.20 ka BP (Fig. 6.3d). This would place the resumption of warming coincident with GI-1b (IACP) or GI-1a in the north. However, it is not until 12.74 ± 0.20 ka BP that warming is finally seen on all timescales.

According to the current concept of north-south climate coupling, the resumption of southern warming at the end of the ACR was triggered by the onset of the YD stadial in the north (at 12.85 ka BP) [e.g. *Denton et al.*, 2010; *Kaplan et al.*, 2010]. Our results, within dating uncertainties, remain consistent with this view but offer new detail. Although the entire Allerød period is generally regarded as a mild climatic period in Greenland, it is substantially cooler than the Bølling, as noted above. In fact, the NGRIP $\delta^{18}O_{ice}$ values during the IACP are similar to the pre-Bølling glacial values. Hence, the suggestion that warming may have already resumed in the south during the later stages of the Allerød, and prior to the YD, is not inconsistent with the bipolar

seesaw concept. Despite some ambiguity about the exact timing of the resumption of warming, our results show clearly that the YD does coincide with an interval of maximum warming around most of the Antarctic continent. The southern warming finally terminates at 11.76 ± 0.22 ka BP, synchronous within dating uncertainties with the abrupt Holocene onset in the north at 11.65 ka BP.

Our main results are summarized as follows: firstly, trend changes in the south are aligned with millennial and/or sub-millennial climate transitions in the north; and secondly, the coldest (warmest) stages of the deglaciation in the north are aligned with the intervals of significant warming (cooling) in the south. This opposing climate behaviour between the hemispheres is consistent with a bipolar seesaw operating with minimal time lag in the transmission of climate signals between the high latitudes of both hemispheres.

Two different (but not mutually exclusive) mechanisms have previously been advanced to explain north-south climate coupling during the deglaciation. The first calls on the bipolar ocean seesaw, whereby weakening of the AMOC during GS-2 and the YD, due to freshwater discharge into the North Atlantic [*Ganopolski and Rahmstorf*, 2001; *McManus et al.*, 2004], reduces both northward ocean heat transport and deepwater production in the North Atlantic, thereby stimulating deepwater formation and warming in the south [*Broecker*, 1998; *Stocker and Johnsen*, 2003]. A variant of this first mechanism proposes that the strengthening of the AMOC was forced from the south by freshwater perturbations to the Southern Ocean linked to sea ice retreat [*Bianchi and Gersonde*, 2004; *Knorr and Lohmann*, 2003] or freshwater discharge from the Antarctic Ice Sheet [*Weaver et al.*, 2003]. However, recent model experiments have questioned the efficacy of such "southern triggers", suggesting that freshwater forcing in the south may lead to local cooling but has little effect on the strength of the AMOC or on temperatures in the north [*Stouffer et al.*, 2007; *Swingedouw et al.*, 2009].The second mechanism invokes an atmospheric teleconnection, whereby North Atlantic cooling during GS-2 and the YD forces a southward shift of the Intertropical Convergence Zone, which in turn strengthens the southern westerlies and/or displaces them southward [*Anderson et al.*, 2009, and references therein]. Under this mechanism, the increased intensity of the westerlies is thought to warm the Southern Ocean and Antarctica through a combination of increased wind-driven upwelling, dissipation of sea ice via northward Ekman transport, and increased southward eddy transport of heat [*Denton et al.*, 2010, and references therein].

What can our results say about these mechanisms? When considering bipolar coupling during the deglaciation, division of climate in the North Atlantic into three stages (GS-2, B-A, and YD) may be too simplistic; we find evidence that the sub-millennial climate transitions within the B-A (suggested to be linked to freshwater forcing events [*Thornalley et al.*, 2010]) may also couple with climate variations in the south. Importantly, the observed timescales of north-south coupling require a mechanism capable of rapid signal transmission between the hemispheres. Fast-acting atmospheric teleconnections clearly meet this criteria. Rapid signal transmission can also be achieved via oceanic pathways through the action of internal ocean waves [e.g. *Masuda et al.*, 2010]. In the conceptual model of *Stocker and Johnsen* [2003], a rapid, wave-mediated seesaw in the Atlantic is coupled to a Southern Ocean heat reservoir. Under this "thermal bipolar seesaw", as soon as the north cools, heat begins accumulating in the south (and vice-versa). Therefore, despite the proposed 1000–1500 year time constant of the Southern Ocean heat reservoir, the changes of slope in the south that we observe to accompany the abrupt changes in the north remain consistent with the *Stocker and Johnsen* [2003] model.

Our observations do not directly resolve the question of northern or southern forcing. Indeed, in a coupled system factors in both hemispheres may be important. Interestingly, the warming trends in at least two of the individual records used in the composite weaken well in advance of the Bølling onset, at LD ca. 15.30 ka BP and at EDML ca. 16.2 ka BP [see also *Stenni et al.*, 2011], suggesting that warming in the south prior to the ACR in some parts of the continent may have reached a level at which freshwater and/or temperature forcings linked to sea ice retreat were weakening the overturning in the Southern Ocean and causing the local warming trend to falter. In this context, positive freshwater forcing due to deglacial warming in the south and reduced freshwater forcing at the end of H1 in the north may have superimposed and ultimately *both* contributed to the abrupt strengthening of the AMOC and the synchronous ACR and Bølling onsets. A similar concept was investigated in a recent model experiment [*Lucas et al.*, 2010], which found higher amplitude responses of the AMOC when freshwater forcings of opposite sign were simultaneously applied to the deepwater formation areas in both hemispheres.

6.4 Conclusions

The composite Antarctic climate record derived here is robust (i.e. insensitive to exclusion of individual records) and reflects coherent circum-Antarctic climate changes through the deglacial period. The well-constrained methane ties allow co-registration of Antarctic and Greenland ice core climate records with a ca. 200 year uncertainty.

The records confirm the operation of a bipolar temperature seesaw and provide strong evidence that the mechanism involved is rapid and operates over millennial and sub-millennial timescales; Antarctic trend changes are seen as counterparts to each of the events in the Greenland climate sequence from the Bølling and Allerød through to the Younger Dryas and the onset of the Holocene. A key result is that the period of strongest Antarctic cooling directly coincides with the period of greatest northern warmth, the Bølling (GI-1e). The high resolution of the present study indicates that significant Antarctic cooling was largely complete by the start of the sub-millennial Greenland cold stage, the Older Dryas (GI-1d). This sub-millennial scale coupling argues that in a bipolar seesaw context, division of climate in the North Atlantic into three stages (GS-2, B-A, and YD) may be too simplistic. During the Allerød, climate conditions have already cooled substantially with respect to the Bølling, and in the south post-ACR warming has begun in at least two of the Antarctic records (LD and Byrd). In the composite, we see that a coherent Antarctic-wide resumption of warming is possibly underway by the later stages of the Allerød. The YD however, does mark the period of most rapid and uniform Antarctic warming. In terms of the bipolar seesaw, this result may imply that the heat balance between the hemispheres was already tipping toward southern warming as conditions in Greenland deteriorated through the Allerød.

The Antarctic composite also provides a useful tool for evaluating the deglacial climate records of individual cores, and specifically, the more weakly dated interior East Antarctic records. For example, the younger ACR onset in the EPICA Dome C record could reflect a lag in propagation from coast to interior, different distal source and transport effects, or it may be attributed to dating uncertainties, the refinement of which could be used to reassess the Δage and accumulation relationships at these sites.

Similarly, individual site differences, such as the early cessation of the warming trend at LD (at 15.30 ka BP) argue for local or regional influences. A question which requires further investigation is whether this early signal at LD and also the early break in the

warming trend at EDML (at 16.2 ka BP) are signs of changing Southern Ocean wind or sea-ice conditions that are precursors to the later abrupt onset of the Bølling and the strong, regionally coherent ACR cooling.

The data sets are available online at the Australian Antarctic Division Data Center (http://data.aad.gov.au/) and also at the World Data Center for Paleoclimatology (http://www.ncdc.noaa.gov/paleo/).

Chapter 7

Rapid Coupling of Antarctic Temperature and Atmospheric CO_2 During Deglaciation

J. B. Pedro[1,2], S. O. Rasmussen[3] and T. D. van Ommen[1,4]

Published February 2012 in *Climate of the Past Discussions*, 8, 621-636, doi:10.5194/cpd-8-621-2012, 2012.

[1]Antarctic Climate & Ecosystems Cooperative Research Centre, Hobart, Tasmania, Australia
[2]Institute of Marine and Antarctic Studies, University of Tasmania, Hobart, TAS, Australia
[3]Centre for Ice and Climate, University of Copenhagen, Copenhagen, Denmark
[4]Australian Antarctic Division, Kingston, TAS, Australia

Abstract

During the last deglaciation atmospheric CO_2 increased by 80 parts per million by volume and Antarctic temperature increased by $\sim 10°C$. Utilising a recently developed proxy for regional Antarctic temperature, derived from five near-coastal ice cores, and two ice core CO_2 records with high dating precision, we show that the increase in CO_2 lagged the increase in regional Antarctic temperature by only 0 to 400 years. This new value for the lag, consistent for both CO_2 records, implies a faster feedback between temperature and CO_2 than the centennial to millennial-scale lags suggested by previous studies [*Fischer et al.*, 1999; *Monnin et al.*, 2001].

7.1 Introduction

The last deglaciation, 19,000 to 11,000 years before present, is the largest naturally-forced global climate change in Earth's recent climate history. Its initial impetus, as with the sequence of glacial/interglacial transitions that came before it, is most commonly attributed to orbitally induced variations in insolation at high northern latitudes [*Hays et al.*, 1976]. Amplification through climate feedback processes of the relatively weak orbital signal is then required to explain the full magnitude of the glacial-interglacial climate change [*Lorius et al.*, 1990]. Changes in the carbon cycle play a central role among these feedbacks [*Lorius et al.*, 1990; *Shackleton*, 2000]. Mounting evidence attributes a large component of the deglacial CO_2 increase to release of old CO_2 from the deep southern ocean through changes in its biogeochemistry and physical circulation [*Anderson et al.*, 2009; *Skinner et al.*, 2010]. However, there are open questions about the exact mechanisms involved and their relative contributions [*Fischer et al.*, 2010; *Sigman et al.*, 2010; *Toggweiler and Lea*, 2010]. Determining the timing of the increase in atmospheric CO_2 with respect to the increase in temperature (hereafter 'the lag'), is crucial for the models seeking to discriminate between mechanisms [*Schmittner and Galbraith*, 2008; *Ganopolski and Roche*, 2009; *Lee et al.*, 2011].

Antarctic ice cores are unique in preserving a record of both temperature variation and atmospheric CO_2 concentration. Water stable isotope ratios ($\delta^{18}O_{ice}$ and δD_{ice}) from the ice are proxies for temperature above the inversion layer at the time of snow

formation [*Jouzel et al.*, 1997], while the CO_2 is preserved in air bubbles in the ice. The transformation of snow to glacial ice isolates these bubbles at a depth of 50–100 m, leaving them younger than the surrounding ice by an amount Δage. The Δage must therefore be known for the lag between temperature and CO_2 to be accurately determined.

The most commonly cited studies constraining the lag for the last deglaciation have used ice core records from the East Antarctic Plateau (EAP) and report lags of 400–1000 years from Vostok [*Fischer et al.*, 1999] and 200–1400 years from EPICA Dome C [*Monnin et al.*, 2001]. Studies of previous deglaciations also suggest millennial-scale lags [*Fischer et al.*, 1999; *Mudelsee*, 2001; *Siegenthaler et al.*, 2005; *Caillon et al.*, 2003]. However, the low accumulation rates at these sites (2–3 g cm^{-2} $year^{-1}$) lead to lengthy intervals between deposition and bubble close off, and consequent high values for Δage : 2400–3300 years for recent times and 4500–5200 years at the last glacial maximum [*Fischer et al.*, 1999; *Monnin et al.*, 2001]. These large values are associated with uncertainties of typically 10–20%, which are comparable to the reported lag values [*Loulergue et al.*, 2007].

The contribution to the lag uncertainty from Δage can be minimised by considering ice core records from higher accumulation sites. Of the currently available CO_2 records for the deglaciation, those with the lowest Δages are the Siple Dome [*Ahn et al.*, 2004] and Byrd [*Neftel et al.*, 1988; *Staffelbach et al.*, 1991] ice cores. The Δages at these sites are 200–300 years for recent times and 500–800 years at the last glacial maximum, an order of magnitude smaller than records from the EAP. Analysis of the Siple Dome stable isotope and CO_2 records suggests lags in the 150–400 year range [*Ahn et al.*, 2004], but this result suffers from the fact that the Siple Dome deglacial isotope record contains abrupt changes not observed in other Antarctic records [*Taylor et al.*, 2004; *Brook et al.*, 2005], suggesting a local climate signal that would not be expected to correlate with CO_2 evolution.

Our approach is to compare the Siple Dome and Byrd CO_2 records to an index of regional Antarctic temperature, T_{proxy}, derived [*Pedro et al.* 2011c/Chapter 6] from a composite of high-resolution stable isotope records from the Law Dome, Siple Dome, Byrd, EPICA Dronning Maud Land and Talos Dome ice cores (Fig. 7.1a, inset shows core locations). Since T_{proxy} contains ice cores representing the Indian, Atlantic, and Pacific coastal Antarctic regions, it is expected to provide a better representation of

high-latitude Southern Ocean processes than records from single sites. This approach requires that T_{proxy} and the two CO_2 records share a common timescale. This is achieved by synchronising all records to the Greenland Ice Core Chronology 2005 (GICC05) using the rapid and effectively globally synchronous variations in CH_4 concentrations found in both Antarctic and Greenland ice cores (Sect. 7.3).

7.2 Results and discussion

Close correspondence between T_{proxy} and both CO_2 records is observed (Fig. 7.1a), supporting the hypothesis that marine processes at high southern latitudes are linked to the deglacial CO_2 increase. Visual inspection of the relative timing of the curves suggests little or no lag of CO_2 after T_{proxy}. We determine the lag quantitatively, following previous studies [*Fischer et al.*, 1999; *Mudelsee*, 2001; *Siegenthaler et al.*, 2005; *Ahn et al.*, 2004], by maximising the time-lagged correlation. Two methods are used: first by direct correlation between T_{proxy} and CO_2 and second, as used in a prior Siple Dome study [*Ahn et al.*, 2004], by correlation between the corresponding derivative curves, $\partial T_{proxy}/\partial t$ and $\partial CO_2/\partial t$.

Results are summarised as histograms in Fig. 7.1b. The widths of these four distributions reflect the sensitivity of the lag values to CO_2 measurement uncertainties, differences between the two CO_2 data sets, and variations in lag determination methodology as determined by Monte Carlo-style sensitivity analysis (see Sect. 7.3). The distributions show larger spread for the derivative method, but overall consistency between the two sites and for the two methods. Using the means and standard deviations quoted in Fig. 7.1b, we arrive at a weighted value for the lag of 163 years and the methodological uncertainty of 34 years.

Including all synchronisation, Δage, and numerical uncertainties leads to a value for the lag within the range of 0–400 years (see see Sect. 7.3). This result is substantially lower and more narrowly constrained than the previous Vostok and EPICA Dome C estimates of 200–1400 years and 400–1000 years, albeit consistent within their reported uncertainties. This short lag is supported by more recent empirical constraints indicating that EPICA Dome C Δage (and thus the CO_2-temperature lag) was significantly overestimated during the last deglaciation [*Loulergue et al.*, 2007]. It is important to emphasise that this lag represents an average for the entire deglaciation. Therefore, in

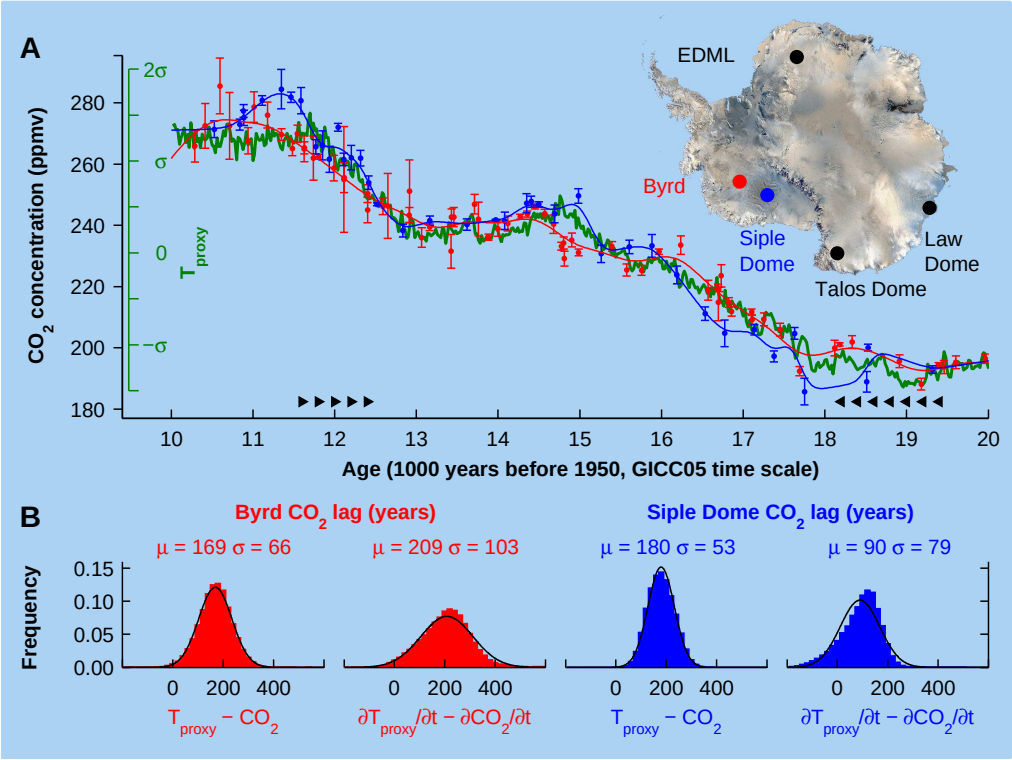

Figure 7.1: The phase relationship between regional Antarctic temperature and atmospheric CO_2. (**A**) Antarctic temperature proxy T_{proxy} (green) and CO_2 data (1σ error bars) from Byrd (red) and Siple Dome (blue) on the GICC05 timescale. In the example shown, the CO_2 curves have been smoothed with a Gaussian filter of width 105 years. (**B**) Lag histograms for the two lag determination techniques, direct correlation and correlation of derivatives, using each of the two CO_2 data sets (red, blue) and the best fit of Gaussian distributions (black curves and μ and σ values). The histogram widths reflect each lag determination's sensitivity to the degree of data smoothing, CO_2 measurement uncertainties and different choices of lag calculation data interval start and end points (black triangles in part A). The map shows the location of the Antarctic ice core sites from which data have been used (source: NASA).

a coupled system where multiple processes are likely to be involved in the CO_2 increase [*Fischer et al.*, 2010; *Sigman et al.*, 2010], this value reflects the contributions of all processes weighted by their contribution to the CO_2 increase.

This result shows that the effective combination of these mechanisms operated with little or no lag. Additional observational constraints on the mechanisms are obtained by considering in more detail the millennial and sub-millennial trends in CO_2 throughout the deglaciation. The increase in CO_2, as noted previously [*Fischer et al.*, 1999; *Monnin et al.*, 2001; *Ahn et al.*, 2004], occurs in two main steps. These steps coincide with the two periods of significant warming in T_{proxy} (pink band, Fig. 7.2) and are separated by a step down in CO_2 concentrations as T_{proxy} exhibits significant cooling within the core of the Antarctic Cold Reversal (dark blue band, Fig. 7.2). Evidence from Southern Ocean marine sediment cores directly links each of these two warming steps with release of CO_2 accumulated in the deep Southern Ocean during the last glacial period: cores from south of the Antarctic Polar Front show pulses in upwelling (represented by opal fluxes) coinciding with each warming step [*Anderson et al.*, 2009], while cores from the Atlantic sector of the Southern Ocean identify a source of old (^{14}C-depleted) carbon-rich deep water that dissipated over two corresponding intervals [*Skinner et al.*, 2010]. An explanation consistent with the reduced lag values identified here, proposes that the increases in upwelling were responsible for the simultaneous delivery of both sequestered heat and CO_2 to the atmosphere around Antarctica [*Anderson et al.*, 2009; *Skinner et al.*, 2010]. However, this raises the question of what stimulated the increases in Southern Ocean upwelling.

A clue is provided by examining the time relationship between T_{proxy} and the major millennial and sub-millennial climate events recorded by the North GRIP $\delta^{18}O_{ice}$ record (Fig. 7.2.); i.e. the timing of the well-known bipolar seesaw [*Broecker*, 1998; *Stocker and Johnsen*, 2003]. Since T_{proxy} and the CO_2 records are synchronised to GICC05, the records from both hemispheres can be directly compared. There is also little or no time lag separating the major millennial and sub millennial climate transitions in Greenland [*Lowe et al.*, 2008] from the onsets and ends of the warming and cooling trends in Antarctica [*Pedro et al.* 2011c/Chapter 6]. A picture thus emerges from the ice cores of rapid communication between Antarctic temperatures, Greenland temperatures and atmospheric CO_2.

We give attention here to two potentially complimentary mechanisms which appear

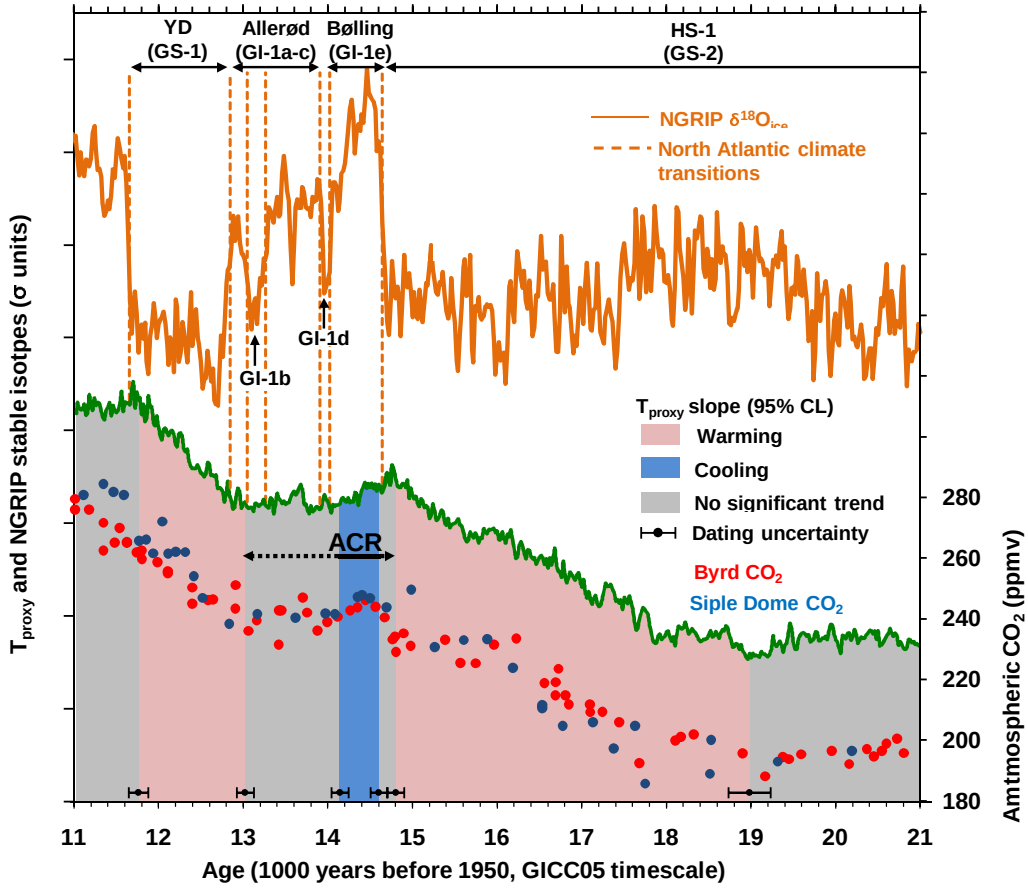

Figure 7.2: Atmospheric CO_2 and the bipolar seesaw on the GICC05 timescale. Significant warming and cooling trends in T_{proxy} are represented by coloured vertical bands, adopted from a previous study [*Pedro et al.* 2011c/Chapter 6]. Climate in the North Atlantic region is represented by the NorthGRIP ice core $\delta^{18}O$ record [*Lowe et al.*, 2008]. Changes in the slope of T_{proxy} are synchronous with climate transitions in the North Atlantic (vertical orange lines) within relative dating uncertainties (horizontal error bars). The deglacial increase in CO_2 occurs in two steps, corresponding to the significant warming trends in T_{proxy} (pink bands). A pause in the CO_2 rise is aligned with a break in the warming trend (central grey band) during the Antarctic Cold Reversal (ACR). Within the core of the Antarctic Cold Reversal significant cooling in T_{proxy} (dark blue band), coincides with an apparent decrease in CO_2. Fast-acting inter-hemispheric coupling mechanisms linking Antarctica, Greenland and the Southern Ocean are required to satisfy these timing constraints.

consistent with these observations. One mechanism supports a greater role for atmospheric pathways [*Anderson et al.*, 2009; *Toggweiler and Lea*, 2010; *Lee et al.*, 2011] while the other supports a greater role for the ocean [*Skinner et al.*, 2010; *Schmittner and Galbraith*, 2008]. Both mechanisms begin with the discharge of meltwater and ice into the North Atlantic during Greenland Stadial 2 (Heinrich Stadial 1), possibly due to orbitally driven increases in summer insolation. This causes a collapse of the Atlantic Meridional Overturning Circulation (AMOC) [*Ganopolski and Rahmstorf*, 2001; *McManus et al.*, 2004]. The atmospheric pathway proposes that rapid cooling of the North Atlantic region and sea ice expansion initiates an atmospheric reorganisation in which both the Inter Tropical Convergence Zone and the Southern Hemisphere mid-latitude westerlies are displaced south and/or intensified [*Anderson et al.*, 2009; *Toggweiler and Lea*, 2010; *Lee et al.*, 2011]. The changed westerly regime over the Southern mid- and high-latitude oceans then dissipates sea ice, displaces cold fresh surface waters, drawing up warmer deeper waters which release heat and CO_2. A recent modeling study lends support to this sequence of events and also incorporates an important role for ocean biogeochemical feedbacks [*Lee et al.*, 2011]. In line with the constraints identified here, the model supports essentially simultaneous North Atlantic cooling and atmospheric CO_2 release from the high-latitude Southern Ocean, corresponding to an atmospheric CO_2 rise of 20–60 ppm, depending on the biological response. However *Lee et al.* [2011] fail to simulate the observed response of Antarctic temperatures, possibly due to fixed Southern Hemisphere sea ice.

The ocean pathway invokes the bipolar seesaw: freshwater-induced collapse of the AMOC reduces northward ocean heat transport, thereby allowing heat to accumulate in the south [*Broecker*, 1998; *Stocker and Johnsen*, 2003]. This melts back sea ice, removing a physical barrier to the release of CO_2 and exposing the Southern Ocean surface waters to the action of the westerlies. As above, the strengthened westerlies promote upwelling and ventilation of CO_2 from the deep waters [*Skinner et al.*, 2010]. The bipolar seesaw, as originally conceived [*Broecker*, 1998], operates on the millennial timescales of ocean heat transport and hence fails to meet the timing criteria identified here. However, an ocean wave-mediated seesaw [*Stocker and Johnsen*, 2003] could be capable of sufficiently rapid signal transmission. In one model study, the bipolar-seesaw-induced changes in the circulation modes couple with changes in ocean biogeochemistry and carbon storage in the terrestrial biosphere to produce little or no lag between Greenland and Antarctic temperatures and CO_2 changes [*Schmittner*

and Galbraith, 2008]. Unlike, *Lee et al.* [2011], this model does simulate the observed seesaw-relationship between North Atlantic and Greenland temperatures. Notably, the initial (within the first 250 years) rapid response in CO_2 in *Schmittner and Galbraith* [2008] is attributed to CO_2 release from the terrestrial biosphere (triggered by cooling associated with the freshwater-induced AMOC collapse) and not to physical or biogeochemical components of the Southern Ocean carbon cycle. However, this does not dismiss the possibility of a rapid ocean CO_2 response to bipolar seesaw-related changes in ocean circulation. Recent studies emphasise the sensitivity of the timescales of ocean ventilation to model resolution; at least under modern boundary conditions, meso-scale eddy-resolving ocean models suggest much faster ventilation times than the coarser resolution models that are currently used for palaeo-simulations [*Maltrud et al.*, 2010].

Current palaeo-modeling efforts appear to be accurately simulating key components of the deglacial sequence of events. However, there is not yet a simulation which fully captures all of the observed trends and phase relationships between Antarctic and North Atlantic temperatures and atmospheric CO_2. The results presented here, with their improved timing constraints over previous studies, provide a more stringent test for future modeling efforts.

To conclude, the ice core observations point to a tightly-coupled system operating with little or no time delay between the onsets/terminations of North-Atlantic climate stages and near-simultaneous trend changes in both Antarctic temperature and atmospheric CO_2. As it stands, the observed timing of events lends support to the current concept of an atmospheric teleconnection between the northern and southern high-latitudes, which forces wind-driven CO_2 release from the Southern Ocean. However, sorting out the relative roles of atmospheric and oceanic coupling mechanisms and the interactions between them remains a major challenge. More densely sampled and higher precision CO_2 measurements from high-accumulation ice core sites may assist with constraining the time evolution of the temperature/CO_2 lag during different stages of the deglaciation. However, if the response in the Southern Hemisphere is instantaneous, then higher resolution records may not be sufficient. Further progress in understanding these mechanisms requires more work at the interface between palaeoclimate observation and Earth system modeling, in particular modeling efforts to more tightly constrain the potential timescales of bipolar seesaw-induced changes in CO_2 ventilation.

The T_{proxy} series is archived at the Australian Antarctic Data Center

(http://data.aad.gov.au/) and at the World Data Center for Paleoclimatology (http://www.ncdc.noaa.gov/paleo/). The CO_2 records on the GICC05 timescale will be similarly archived following publication.

7.3 Materials and methods

7.3.1 Record synchronisation

Ice core timescales were synchronised to the GICC05 chronology using previously published 'gas-age' depth ties from CH_4-based synchronisations of the Byrd [*Blunier and Brook*, 2001] and Siple Dome [*Brook et al.*, 2005] records with Greenland records. Byrd CO_2 data on the GRIP SS09 timescale [*Johnsen et al.*, 1997] were transferred via GRIP depth [*Blunier and Brook*, 2001] to GICC05 ages by linear interpolation using stratigraphical markers [*Rasmussen et al.*, 2008]. Siple Dome CO_2 data, on a GISP2 timescale [*Ahn et al.*, 2004] were transferred via GISP2 depth [*Meese et al.*, 1997] to GICC05 ages by linear interpolation using stratigraphical markers [*Rasmussen et al.*, 2008].

7.3.2 Lag calculation

The derivative method has smaller sensitivity to misidentification of the pre- and post-transition levels at the expense of increased sensitivity to measurement noise, especially in the sections of sparse data. Since it is not clear a priori which approach is superior, we apply both methods in parallel. Prior to the analyses, the CO_2 data are first linearly interpolated to 20-year resolution over the 9 to 21 ka interval to match the 20-year resolution of T_{proxy}. Derivatives, $\partial T_{proxy}/\partial t$ and $\partial CO_2/\partial t$, are calculated on the same grid. For both methods the data are then smoothed and the time-lagged correlation determined for lags in the -400 to $+1000$ year range. The robustness of the lag calculation to CO_2 data uncertainty is evaluated by repeating the lag determination 100 times using random realisations of the CO_2 measurements, each sampled using the published uncertainties. The lag shows some sensitivity to the degree of smoothing applied and the overall time interval chosen, and so the lag calculations are repeated for 19 different degrees of smoothing and 35 different choices of time interval. Smoothing was applied by convolution with a Gaussian filter with a standard deviation ranging

from 105 to 375 years in steps of 15 years; the data interval start and end points used for the lag calculation were varied as illustrated by the black triangles of Fig. 7.1a. This analysis generates 66,500 optimal lag values for each of the methods. The minimum width of the smoothing corresponds to the approximate sampling rate of CO_2 data in the sparsely sampled parts of the data set, and the maximum was chosen to preserve a clear Antarctic Cold Reversal signature. Similar results were obtained by replacing the Gaussian filter with a simple running mean filter of equivalent half-width. The time interval for correlation is varied within reasonable limits that encompass the overall deglaciation. Start and end ages are varied in 200 year steps: start spanning 19.4–18.2 ka (7 options) and end spanning 12.4–11.6 ka (5 options). Note that younger than around 11.5 ka both CO_2 curves have high early Holocene values that have no counterpart in the T_{proxy} record. This suggests different processes are responsible and we exclude this from the correlation interval.

7.3.3 Uncertainties in the lag-calculation

The lag uncertainty, σ_{lag}, in this study is dominated by the relative dating uncertainty between T_{proxy} and the two CO_2 records. This uncertainty comprises a component associated with synchronising CH_4 records between multiple cores, σ_{sync}, and a component associated with the Δage uncertainties of the individual cores, $\sigma_{\Delta age}$. The dating uncertainty in T_{proxy} ,$\sigma_{T_{proxy}}$, ranges from 199 to 384 years over the time interval considered, with a mean of 269 years [*Pedro et al.* 2011c/Chapter 6]. The value of σ_{lag} is smaller than $\sigma_{T_{proxy}}$ because σ_{sync} applies to both T_{proxy} and the CO_2 data and thus partially cancels (as seen in the case where data from only one core is used and σ_{sync} cancels completely). The similarity of the results from the independent lag calculation using Siple Dome and Byrd CO_2 data supports that the records are well-synchronised on centennial scales or better. We estimate the contribution to σ_{lag} from $\sigma_{\Delta age}$ and σ_{sync} to be no more than 200 years. The lag estimated from the four histograms in Fig. 7.1b is 163 years with a contribution to σ_{lag} of 34 years which is independent from the other uncertainty contributions. Combining these figures, we arrive at our final estimate that the lag value is very likely to be within the 0 to 400 year range.

Chapter 8

Conclusions

> *"Our understanding of the Earth's climate, in particular, depends foremost on the Earth's history: how past climate changed in response to changing boundary conditions."* — James E. Hansen, New York, NY, 2008.

James Hansen's words clearly express the importance of the palaeoclimate record to our understanding of the climate system. Indirectly, they also emphasise the importance of improving our understanding of individual proxies, so as to ensure that they are interpreted reliably and with the appropriate caveats; and furthermore, of efforts to extract the maximum amount of information possible from the proxy records currently available. In this context, the thesis has worked to improve the interpretation of the ice core solar activity proxy ^{10}Be, and the available high resolution deglacial records of ice core δ^{18}O and CO_2.

8.1 Summary and main findings

All of the thesis objectives raised in Chapter 1 have been addressed. High-resolution ice core ^{10}Be records overlapping with modern instrumental and reanalysis data were used in Chapters 2, 4 and 5 to advance understanding of both production (or solar related) and non-production (or climate related) signals in the ^{10}Be solar activity proxy. In addition, Chapter 3 presented a new chemical method to reduce levels of the problematic ^{10}Be isobar boron (^{10}B) in AMS targets. High-resolution records from the last deglacia-

tion were used in Chapters 6 and 7 to advance understanding of inter-hemispheric climate variability and the internal CO_2 feedback. The thesis has lent further support to the view [e.g. *Fisher et al.*, 1996] that individual proxy records should be interpreted with caution and that more robust information can be obtained through the assimilation of multiple records.

The focus throughout on high temporal resolution ice cores has facilitated precise dating. For the ^{10}Be work, precise dating was essential for meaningful intercomparison with instrumental and reanalysis data. For the deglacial δ^{18}O and CO_2 work, precise dating was essential for compositing multiple records.

The main findings are reiterated separately below for the work on ^{10}Be and deglacial δ^{18}O and CO_2, followed by suggestions for future work.

Ice core ^{10}Be

The scarcity of high-resolution ^{10}Be records spanning recent decades has previously limited opportunities for direct intercomparison of ^{10}Be records with modern observational and reanalysis data. The new ^{10}Be records presented in the thesis, covering 1936–2009 at Law Dome, Antarctica and 1936–2002 at Das2 Greenland are very valuable in this context. Chapters 2 to 5 have made use of these records resulting in the following key findings:

– *The level of agreement between multiple ^{10}Be records from Law Dome is comparable to that between other commonly measured trace chemicals at the site (Chapter 2).*

  This allays some concerns raised by a previous Antarctic study [*Moraal et al.*, 2005] about poor reproducibility of ice core ^{10}Be records. However, it also emphasises the importance of obtaining ^{10}Be records from proven or carefully selected ice core sites. Studies intending to obtain ^{10}Be records which can inform on the atmospheric production rate should avoid ice core sites where windblown snow contributes a large fraction of annual accumulation and/or where sampling surfaces have been left open to the atmosphere and/or where melt layers are common.

– *A significant seasonal cycle in ^{10}Be concentrations is observed at Law Dome,*

driven mainly by seasonal variability in the input of stratospheric ^{10}Be to the Antarctic lower troposphere (Chapter 4).

Maximum ^{10}Be concentrations occur during the (austral) late summer to early autumn and minimum concentrations occur during the winter. Comparison of the observed seasonal cycle with ECHAM5-HAM simulated ^{10}Be deposition and observed ^{10}Be:^{7}Be ratios from the Georg von Neumayer air-sampling station [*Wagenbach*, 1996; *Elsässer et al.*, 2011], strongly suggest that the timing of the seasonal maximum in ^{10}Be is associated with the input of stratospheric ^{10}Be to the lower levels of the Antarctic troposphere. Recent results from the FLEXPART Particle Dispersion Model [*Stohl and Sodemann*, 2010] also support this interpretation. The winter minimum in ^{10}Be concentrations is attributed to reduced stratospheric input of ^{10}Be and potentially also higher regional accumulation rates causing depletion (washout) of the aerosol load in incoming air-masses. The model results imply that the timing of the seasonal cycle in stratosphere to troposphere exchange does not vary widely over the Antarctic continent. Therefore, it is predicted that the seasonal cycle in ^{10}Be concentrations will be similar at other Antarctic sites.

– *Direct exchange of stratospheric air across the Antarctic stratosphere is an important pathway for ^{10}Be transport to the ice sheet (Chapter 4).*

  It has been conventionally assumed that the main pathway for the arrival of stratosphere produced ^{10}Be to the Antarctic troposphere is through the mid-latitude breaks in the tropopause [e.g. *McHargue and Damon*, 1991]. The seasonal cycle in ^{10}Be and in the model results strongly suggests that there is an additional important route: direct descent of ^{10}Be from the Antarctic stratosphere to the Antarctic troposphere during the summer-autumn. Interestingly, the ECHAM5-HAM simulations suggest this route is not important in delivering ^{10}Be to the Arctic. This adds to the large body of literature suggesting quite different atmospheric circulation and tracer transport into the northern and southern polar regions [e.g. *Holton et al.*, 1995; *Jordan et al.*, 2003; *Stohl*, 2006; *Stohl and Sodemann*, 2010].

– *The relationship between $\delta^{18}O$ and ^{10}Be observed at Law Dome on sub-monthly timescales [Pedro et al., 2006] diminishes in strength and marginally fails a significance test when assessed on monthly to annual timescales (Chapter 2 and Chapter 5).*

A strong correlation ($r_{xy} = -0.57, p < 0.01$) was previously reported between ^{10}Be concentrations and δ^{18}O ratios in a sub-monthly-resolved Law Dome snow pit. The corresponding relationships in the 10-year quasi-monthly resolved Law Dome ^{10}Be record and in the 74-year annually-resolved Law Dome record were much weaker at $r_{xy} = -0.14\,[-0.38; 0.02]$ and $r_{xy} = -0.17\,[-0.39; 0.09]$, respectively. This does not disprove the result presented in *Pedro et al.* [2006]. It appears that the meteorological processes linking ^{10}Be and δ^{18}O are important on snowfall-event timescales picked up by the snow pit, but are smoothed out when records are considered at coarser resolution.

– *^{10}Be concentrations at both Law Dome and Das2 are significantly correlated to the 11-year solar cycle modulation of cosmic ray intensity throughout the neutron monitor era (Chapter 5).*

  The correlation between observed cosmic ray intensities and ^{10}Be concentrations is $r_{xy} = 0.54$ with 95% CI $[0.31; 0.70]$ at Law Dome and $r_{xy} = 0.45$ with 95% CI $[0.22; 0.62]$ at Das2. This suggests that $\sim$ 30% and $\sim$ 20% of the annual variance in ^{10}Be concentrations at Law Dome and Das2, respectively, can be attributed to changes in the atmospheric production rate. The strength of the production signal at both sites is weaker if ^{10}Be fluxes are considered in place of concentrations. The weaker signal in fluxes advises against using the flux term *at wet deposition sites* as an input for solar activity and cosmic ray intensity reconstructions. Calculation of fluxes at such sites, by multiplying concentration and accumulation rate, essentially introduces a spurious climate-related signal to the ^{10}Be record.

– *^{10}Be concentrations at both Law Dome and Das2 are also significantly correlated to major modes of atmospheric circulation (Chapter 5).*

  Law Dome concentrations yield a correlation of $r_{xy} = -0.36$ with 95% CI $[-0.57; -0.10]$ with the zonal wave 3 index, while Das2 concentrations yield a correlation of $r_{xy} = -0.42$ with 95% CI $[-0.64; -0.15]$ with the North Atlantic Oscillation. It was argued that the modes affect ^{10}Be concentrations through their influence on moisture transport pathways (ZW3 and NAO), local to regional-scale precipitation rates (ZW3 and NAO) and stratosphere to troposphere exchange (NAO).

– *Combining ^{10}Be records from multiple Antarctic and Greenland sites enhances the strength and spectral coherence of the production signal in ^{10}Be and reduces the*

strength of climate signals (Chapter 5).

This suggests that solar or cosmic ray intensity reconstructions which assimilate multiple ^{10}Be records, particularly records from both Antarctica and Greenland [e.g. *Muscheler et al.*, 2007] are less likely to introduce spurious climate-related signals than those assimilating ^{10}Be records from only a single site [e.g. *Bard et al.*, 2000; *Vonmoos et al.*, 2006; *Shapiro et al.*, 2011]. Better still is to use multiple ^{10}Be records in conjunction with cosmogenic ^{14}C (recorded in tree rings) [e.g. *Muscheler et al.*, 2007].

– *The amplitude of the 11-year solar cycle in the Law Dome, Das2 and ^{10}Be composite records during the neutron monitor era are consistent with the amplitude of the CRAC:10Be production variations in the global atmosphere (Chapter 5) and inconsistent (significantly lower) than the amplitudes of the CRAC:10Be production variations in the exclusively polar atmosphere*

This result suggests that the ^{10}Be deposited to the ice sheets is sampled from a well-mixed global atmosphere, in agreement with recent GCM studies and with the mixing scenario favoured by most recent solar reconstructions [*Vonmoos et al.*, 2006; *Muscheler et al.*, 2007; *Steinhilber et al.*, 2009].

Ice core δ^{18}O and CO_2 records from the last deglaciation

There is strong evidence for opposing climate trends on millennial timescales between the northern and southern high latitudes during the last glacial period and deglaciation. Resolving the dynamical processes that are responsible for this north-south coupling remains a major challenge in climate science. The thesis has contributed a number of important new observational constraints on these processes.

Most previous ice core studies have examined the deglacial sequence of events based primarily on records from individual Antarctic and Greenland sites [*Blunier and Brook*, 2001; *Morgan et al.*, 2002; *Brook et al.*, 2005; *Stenni et al.*, 2011]. An important contribution of the thesis has been to bring multiple high-resolution Antarctic deglacial δ^{18}O records (Law Dome, Byrd, Siple Dome, Talos Dome, and EPICA Dronning Maud Land) onto the GICC05 chronology, common with the Greenland ice cores. All Antarctic records show a similar pattern: an overall deglacial warming trend interrupted by the millennial scale Antarctic Cold Reversal (ACR). However, the precise timing of changes

in climate trends differs between records. This is illustrated by apparent differences in the timing of the onset of the ACR. For instance, at Law Dome the pre-ACR warming trend ends at 15.30 ± 0.17 ka BP. This is considerably older than at EDML where the pre-ACR warming trend ends at 14.55 ± 0.13 ka BP [*Lemieux-Dudon et al.*, 2010]. Such differences between cores (which are greater than dating uncertainties) represent the influence of local, sub continental and/or non-climatic signals in the individual δ^{18}O records, underscoring the need for caution in interpreting the phasing of interhemispheric climate changes from single-site records. However, a robust (insensitive to the exclusion of individual records) Antarctic-wide climate signal emerges when these five records are combined into a single composite series. Interpreted alongside the NGRIP (Greenland) ice core, the composite reveals new detail about the timing of structure of the north-south climate variations during the deglaciation.

– *The Antarctic $\delta^{18}O$ composite confirms the operation of a bipolar seesaw pattern between the northern and southern high latitudes during the deglaciation (Chapter 6).*

  Break-points in the Antarctic δ^{18}O composite are seen as counterparts to each of the major events in the Greenland climate sequence. The timing of the onset of the Antarctic Cold Reversal (ACR) is one the most robust features in the composite. Within dating uncertainty (±200 years) the ACR onset is synchronous with the Bølling (GI-1e) transition in Greenland. The period of strongest Antarctic cooling within the ACR then directly coincides with the period of greatest northern warmth, the Bølling (GI-1e). Similarly, the period of strongest Antarctic warming post-ACR directly coincides with the core of the Younger Dryas cold stage (GS-2).

– *There is little-to-no time lag throughout the deglaciation between major climate transitions in Greenland and breakpoints in the Antarctic $\delta^{18}O$ composite. This implies fast acting (centennial-scale or less) inter-hemispheric coupling mechanisms (Chapter 6).*

  Fast-acting atmospheric teleconnections, as proposed by *Anderson et al.* [2009], clearly meet this criteria. However, rapid signal transmission can also be achieved via oceanic pathways through the action of internal ocean waves. The bipolar seesaw, as originally conceived [*Broecker*, 1998], operates on the millennial timescales of ocean heat transport and hence fails to meet these timing criteria. However,

an ocean wave-mediated seesaw, as proposed by [*Stocker and Johnsen*, 2003] is potentially capable of sufficiently rapid signal transmission.

In the final part of the study, two Antarctic deglacial CO_2 records (from Siple Dome and Byrd) with low Δage uncertainty were synchronised to the same timescale as the Antarctic $\delta^{18}O$ composite. The results provide new constraints on the atmospheric CO_2/temperature feedback.

– *The deglacial CO_2 increase lagged the increase in regional Antarctic temperature by only 0–400 years (Chapter 7).*

  This new value for the lag, which was consistent for both CO_2 records, implies a faster feedback between temperature and CO_2 than the centennial to millennial-scale lags suggested by previous studies.

– *Very close correspondence is observed between the Antarctic deglacial $\delta^{18}O$ composite and both CO_2 records, including the timing of trend-changes (Chapter 7).*

  This further supports the hypothesis that marine processes at high southern latitudes play a central role in the deglacial CO_2 increase [e.g. *Anderson et al.*, 2009; *Sigman et al.*, 2010; *Skinner et al.*, 2010]. Overall, the integrated consideration of high-resolution deglacial CO_2 and Antarctic and Greenland $\delta^{18}O$ records, presents a picture of a tightly coupled climate system operating with little or no time delay between North Atlantic and Southern Ocean processes.

Public debate about the significance of the historical phase relationship between temperature and CO_2 has sometimes been confused. For this reason I would stress here that the synchrony of change in Antarctic temperature and CO_2, or a centennial-scale lag between the two, is fully consistent with the idea that CO_2 played a central role as a positive feedback in the deglacial warming [see e.g. *Ganopolski and Roche*, 2009].

8.2 Future directions

Ice core ^{10}Be

^{10}Be records should continue to play a leading role in refining estimates of past solar forcing. A strong recommendation arising from the thesis is that such reconstructions

are likely to be more robust when they include data from multiple ice cores, ideally from both Antarctic and Greenland sites. Currently, the only published continuous ^{10}Be record spanning the entire Holocene is that measured on the GRIP ice core (spanning 304 to 9315 years BP at mean resolution of 5 years) [*Vonmoos et al.*, 2006]. Additional continuous Antarctic and Greenland ^{10}Be records, sampled at similar resolution, would assist in reducing uncertainty in solar forcing reconstructions for this period.

The excellent spectral coherence of the bipolar ^{10}Be composite record with the solar cycle (Chapter 5) is relevant to plans to use ^{10}Be records to investigate the temporal evolution of solar cycle periodicity; a subject with important implications for constraining the competing models of the solar dynamo. The similarity of the ^{10}Be composite's power spectrum to that of the true production signal suggests that a long-term annually-resolved composite record could be suitable for such an investigation. This would require several annually resolved ice core records with absolute dating uncertainty of $<$ 1–2 years over the past $\sim$ 1000 years, preferably incorporating records from both Antarctica and Greenland. An annually resolved record from NGRIP already exists spanning 1389–1994 [*Berggren et al.*, 2009] and could ideally be extended. Following from the work presented here, obtaining a 1000-year annually resolved Antarctic ^{10}Be record has recently been listed as a goal of the Antarctic Palaeoclimate Stream of the Australian Antarctic Science Strategic Plan 2011–12 to 2021–2022[1] . Approval is currently being sought from the Australian Antarctic Division for a drilling campaign at Law Dome in the 2012–13 season to extract such a record (Project Application 4203, 'Highly Resolved Climate Drivers & Indicators in the late Holocene'). The West Antarctic Ice Sheet (WAIS) divide site operated by the U.S. research community would also be suitable for extracting a 1000-year annually resolved ^{10}Be record.

To further improve understanding of the roles of production and climate-related factors on ice core ^{10}Be records I recently began a collaboration with University of Tasmania statistician Dr Simon Wotherspoon. Results presented in Chapters 2, 4 and 5 have primarily tested for linear relationships between ^{10}Be and environmental variables. Although more challenging to identify, non-linear interactions between these variables are also plausible. We are currently testing empirical models that permit non-linear interactions between environmental parameters (including production rate, zonal wave three, accumulation rate and tropopause height) in an attempt to further quantify and

[1] `http://www.antarctica.gov.au/__data/assets/pdf_file/0017/34208/Stream-1.4_Jan-2011.pdf`

constrain their relative contributions. Initial results indicate that up to $\sim 80\,\%$ of the variance in Law Dome ^{10}Be concentrations can be explained using these techniques. A manuscript detailing this work is currently in the early stages of preparation.

An issue which could not be completely explained in the thesis was the significant relationship between nssS and ^{10}Be in the annually-resolved Law Dome and Das2 records. It is tempting to suggest that the relationship between the species may be linked to the transport of ^{10}Be on sulphur-derived aerosol. However, the large atmospheric reservoir of sulphur (Terragrams) compared to ^{10}Be (10's of grams) strongly argues that ^{10}Be deposition should not be limited by the availability of sulphur-aerosol. I favour the interpretation that both nssS and ^{10}Be (regardless of their incorporation modes) are affected by similar environmental effects, such as washout. Research into the post-production incorporation modes of ^{10}Be may assist in resolving this issue. If it could be clearly demonstrated that the two species are affected by similar environmental effects then co-measurement of nssS or nssSO_4 concentrations with ^{10}Be might provide a means to further assist with separating production and climate signals.

Ice core δ^{18}O and CO_2 records from the last deglaciation

Chapter 6 was focused on extracting the common deglacial signal in multiple Antarctic δ^{18}O records. Comparisons were made between the resulting Antarctic δ^{18}O composite and the Law Dome and EPICA Dome C records. Additional information regarding internal variability between the Antarctic records could be obtained by a systematic evaluation of all of the individual cores against the δ^{18}O composite record. To this end, I have begun examining the residuals between the individual records and the composite. Another subject of future work is to convert the deglacial δ^{18}O composite into a quantitative regional temperature reconstruction. The δ^{18}O records from some sites have previously been converted to temperatures [e.g. *Brook et al.*, 2005]. However, such conversions raise questions about the most appropriate calibration techniques, which are currently debated and arguably vary between sites [*Masson-Delmotte et al.*, 2008; *Sime et al.*, 2009]. Progress in this area would be aided by work alongside researchers incorporating δ^{18}O into regional models and coupled ocean-atmosphere circulation models [see e.g. *Sjolte et al.*, 2011, and references therein].

Regarding Chapter 7, the next major step is to use the new constraints provided by the

lag calculation as a more stringent test for the competing models of deglacial climate dynamics. As it stands the rapid coupling reported between the Greenland and Antarctic $\delta^{18}O$ records and atmospheric CO_2 is suggestive of fast-acting atmospheric teleconnections. However, it was recently pointed out to me by Prof. Dynamical Oceanography Henk A. Dijkstra that the potential speed of oceanic teleconnections is still poorly resolved and may change as models of higher resolution come online.

One of the strongest impressions I have come away with from the thesis, particularly Chapters 6 and 7, is that the climate system is very sensitive and very tightly coupled; small initial perturbations can lead to large, rapid and globally divergent climate responses. With this in mind, I finish with the words of Prof. Wallace Broeker, who has been emphasising for decades the dangerous implications of our continued release of CO_2.

> *"The climate system is an angry beast, and we are poking at it with sticks."*
> — Wallace S. Broecker, Albuquerque, NM, c. 1991.

Appendices

A. Dating and reconstruction of monthly variations in accumulation rate at DSS

The standard technique used for dating of ice core records from DSS is to convert the ice core depth-scale to a timescale with reference to the clear annual cycles in δ^{18}O [*Palmer et al.*, 2001]. The boundaries of years at Law Dome are defined by the mid summer δ^{18}O isotope maximum. From these boundaries dating within years is estimated by linear interpolation, which assumes even snow accumulation over the course of each year. In reality, accumulation is not evenly distributed within any given year and the interpolated timescale may therefore depart from the true timescale by $\pm$(1 to 2) months [*Pedro et al.* 2011a/Chapter 2].

To reduce this uncertainty and therefore permit a more accurate representation of the seasonality of ^{10}Be at DSS, we require accurate information on the seasonal distribution of accumulation. Such information is available for some years (1998 to 2002) from an Automatic Weather Station (AWS 1181, Australian Antarctic Division, Glaciology Program) fitted with an ultra-sonic sounding device to record changes in snow height. This record was previously used to date an earlier DSS ^{10}Be record from a snow pit at the site [*Pedro et al.*, 2006] and several trace-chemical records [e.g *McMorrow et al.*, 2004]. However, as the AWS only covers several years of the ^{10}Be composite it cannot be directly used to refine dating over the full 10-years. Instead we used data from AWS 1181 to test whether reanalysis precipitation data may be used to reconstruct sub-annual accumulation variations at DSS.

Among the contemporary reanalysis products, the European Center for Medium-Range Weather Forecasts Interim Re-Analysis (ERA-Interim [*Simmons et al.*, 2006; *Uppala*

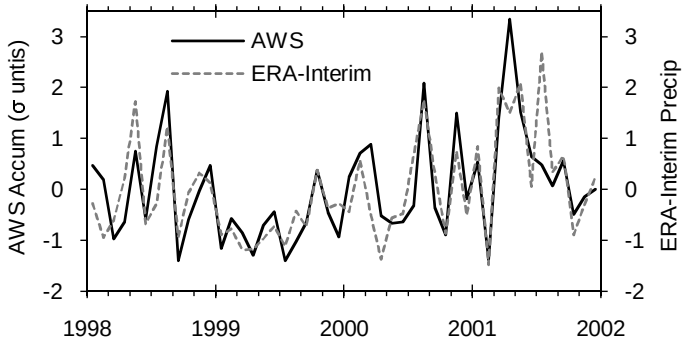

Figure A1: Gross accumulation measured by an Automatic Weather Station (AWS 1181) located at DSS is compared with ERA-Interim precipitation (monthly mean of daily means) at the closest grid point to the site. Note that both records are normalised to zero mean and unit variance over the interval 1998 to 2002.

et al., 2008]) offers the best depiction of contemporary precipitation rates over Antarctica [*Bromwich et al.*, 2011]. Compared to earlier reanalyses, ERA-Interim has relatively high horizontal ($\sim$ 80 km) and vertical resolution (60 levels). This is critical for capturing the importance of orographic precipitation on the steep coastal slopes at sites such as Law Dome. Support for the models' performance at DSS is provided by its correct representation of the strong precipitation gradient across the Dome [*Bromwich et al.*, 2011].

In comparing the AWS record with reanalysis precipitation output from ERA-Interim it must be kept in mind that accumulation refers to only that component of the total precipitation that is ultimately preserved at the ice core site. Accumulation may differ from precipitation due principally to wind removal and evaporative losses. At DSS, at least on annual scales, the precipitation signal is expected to dominate the variance in accumulation since the site is free from summer melt and experiences low wind speeds [*van Ommen and Morgan*, 2010]. An additional complexity is that converting the AWS data to an absolute accumulation series requires knowledge of variability in snow density and densification processes. Since we are interested in relative rather than absolute sub-annual variations in snow accumulation we can simplify the situation by standardising the records. Figure A1 shows monthly-binned AWS accumulation compared to the monthly ERA-Interim total precipitation (with both records normalised with respect to their own means and standard deviations over the common interval). Given the above-mentioned complications the agreement is impressive, the only major disagreement is

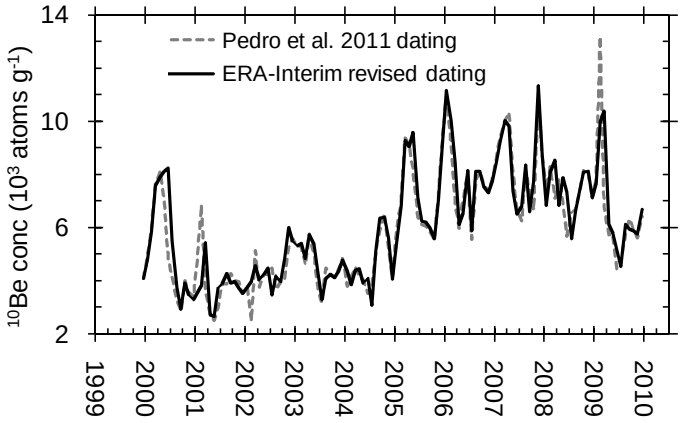

Figure A2: The 10-year DSS ^{10}Be composite record is shown on the previous timescale of *Pedro et al.* [2011a]/Chapter 2 and on the revised timescale used in this manuscript, which corrects for seasonal variability in snow accumulation using ERA-Interim monthly precipitation data.

during July 2001. Importantly, ERA-interim does not itself ingest AWS accumulation data into its assimilation system. Note that since the records are standardised the agreement implies that the size of monthly variations in accumulation scale with the size of monthly variations in precipitation, rather than that absolute values are in agreement. Testing the strength of the relation between the two series yields $r_{xy} = 0.76$ (with 95% CI, 0.60 to 0.84). The simplest explanation for the agreement is that the signals in both ERA-interim and AWS 1181 are dominated by precipitation to the site.

Figure A1 demonstrates that within any given year over this period precipitation is not evenly distributed. Dating of the ^{10}Be record and potentially other ice core records from the site can therefore be improved by refining the assumption of even accumulation throughout the year to the assumption that monthly accumulation is proportional to the ERA-Interim precipitation. Importantly, this assumption affects only sub-annual dating within years and *not* year boundaries.

Accumulation at DSS during each month (P_{month}) is inferred from the ice core derived annual accumulation (P_{year}) [*van Ommen and Morgan*, 2010] and the ERA-Interim derived monthly (b_{month}) and annual (b_{year}) precipitation, following Equation A1.

$$P_{month} = P_{year} \frac{b_{month}}{b_{year}} \tag{A1}$$

The resulting monthly accumulation series over the 10-years corresponding to the ^{10}Be composite record is shown in Figure 4.2. The revised timescale of the composite after taking into account the sub-annual variations in accumulation is shown in Figure A2 alongside the same record plotted on the previously published timescale [*Pedro et al.* 2011a/Chapter 2] that assumed even accumulation. The timescale differences are in all cases ≤ 1 month. Note that the results of our earlier study, are unaffected by this timescale revision. All of the ^{10}Be records from *Pedro et al.* [2011a]/Chapter 2 are affected equally by the timescale revision and therefore the good agreement between different records at the site still holds. Also, the correlation coefficient between ^{10}Be concentrations and the McMurdo neutron monitor counting rate on both timescales are identical.

The data sets, including the revised dating of the composite and the revised dating of the individual records from which it was composed, are available online at the Australian Antarctic Data Centre (http://data.aad.gov.au/).

B. Supporting figures for Chapter 5

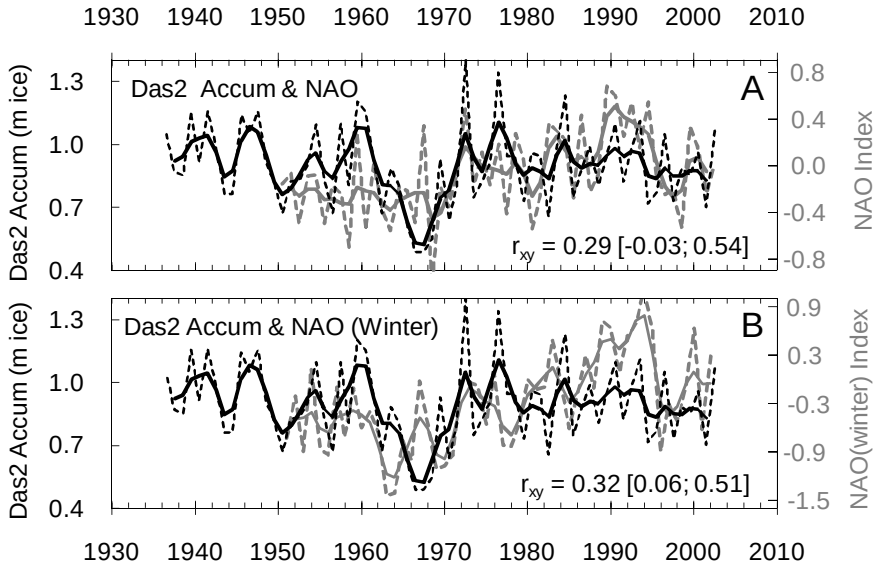

Figure B1: The accumulation rate at Das2 (black line) is compared with: (A) the average annual NAO, and (B) the winter average NAO. Correlation coefficients are listed inset. The dashed lines show annually resolved data and the solid lines show smoothed data (Gaussian filter, effective half-width 3 years).

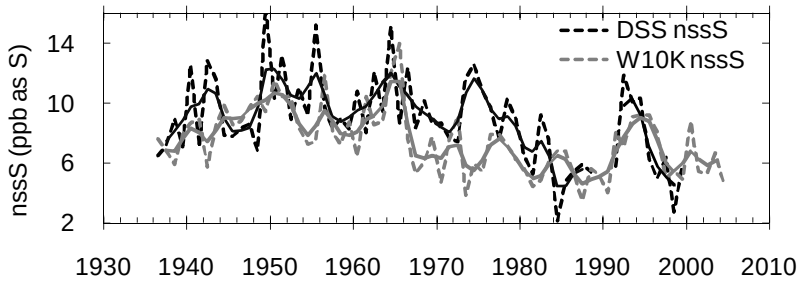

Figure B2: The nssS concentrations in the DSS0506 core are compared with those from the W10K core, located 10 km to the west. The minimum in the 1980's is observed in both records. The dashed lines show annually resolved data and the solid lines show smoothed data (Gaussian filter, effective half-width 3 years).

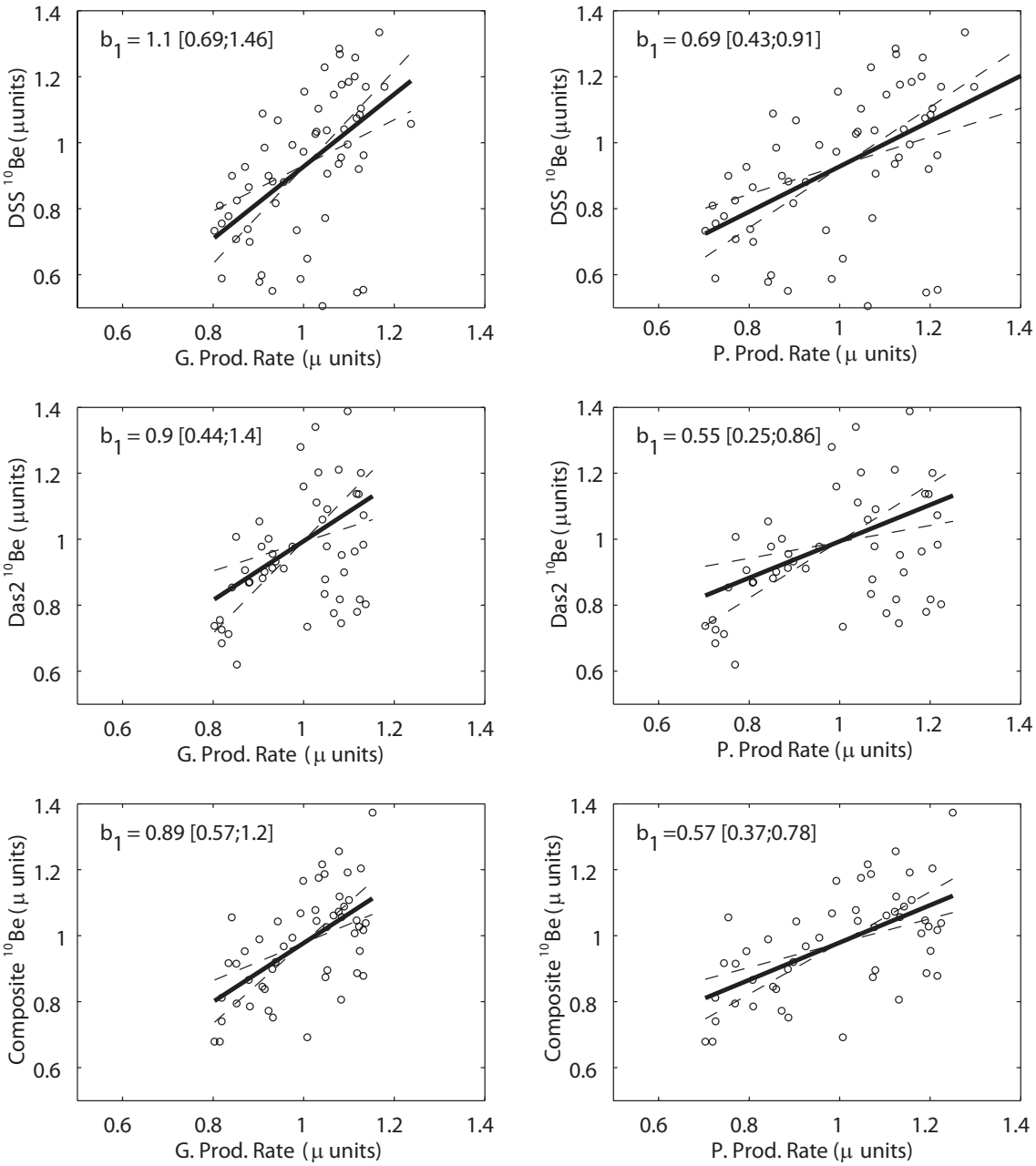

Figure B3: As for Fig. 5.8 but with production rates from the *Masarik and Beer* [2009] production model rather than the CRAC:10Be production model. Again, for DSS (top), Das2 (middle) and the ^{10}Be composite (bottom) the regressions against polar production rates are consistent with $b_1 = 1$ at 95% confidence, whereas the regressions against the polar production rate yield $b_1 < 1$ at 95% confidence.

C. Application of the GICC05 timescale to the Byrd, Siple Dome and EDML records

The Byrd, Siple Dome, Talos Dome, and EDML records were dated by previous authors by aligning variations in CH_4 with similar variations in Greenland CH_4 records from the GRIP and GISP2 ice cores. We adopt the previous dating of these records and, where necessary (Byrd and Siple Dome), transfer them to the common Greenland GICC05 timescale, as described below.

Byrd

Byrd was previously synchronised with GRIP and GISP2 using fast methane variations [*Blunier and Brook*, 2001] (data from `http://www.ncdc.noaa.gov/paleo/pubs/blunier2001/blunier2001.html`). We converted the Byrd $\delta^{18}O_{ice}$ and CH_4 records on their ss09 timescale to GICC05 in two steps:

1. converting the ss09 Byrd ages to GRIP depths via the ss09 age-depth relation [*Johnsen et al.*, 1997] (data from `http://www.iceandclimate.nbi.ku.dk/data/`);

2. converting GRIP depths to GICC05 ages by linear interpolation between the GICC05 GRIP age-depth ties [*Rasmussen et al.*, 2008] (data from `http://www.iceandclimate.nbi.ku.dk/data/`).

The resulting GICC05 timescale for Byrd $\delta^{18}O_{ice}$ was compared with an independent transfer of Byrd onto GICC05 by Thomas Blunier (personal communication, February 2010) and agreed with maximum discrepancy in the interval 9 to 21 ka BP of 36 yr and average discrepancy of 3.4 yr.

We adopt the previously reported Byrd Δage and Byrd to GISP2/GRIP CH_4 correlation errors [*Blunier and Brook*, 2001] (data from: `http://www.sciencemag.org/cgi/content/full/sci;291/5501/109/DC1`). The dating error introduced in the transfer from the GISP2 layer counted depth scale to the GICC05 timescale is negligible compared to the Δage and correlation errors, and is therefore not considered. The RMS sum of the Byrd Δage error and CH_4 correlation error during the early middle and late stages of the deglaciation are listed in Table 6.3.

The average temporal resolution of the Byrd $\delta^{18}O_{ice}$ data for the interval 9 to 21 ka BP was 41 yr.

Siple Dome

Siple Dome was previously synchronised with GISP2 using fast methane variations (data from: `http://nsidc.org/data/waiscores/pi/brook.html`) [*Brook et al.*, 2005]. As $\delta^{18}O_{ice}$ values for Siple Dome during the deglaciation were not available, we used appropriately scaled δD_{ice} i.e. (δD-10)/8 (on advice of James White and Edward Brook, pers. comm. March 2011). We converted the Siple Dome δD_{ice} and CH_4 records, which were reported on the GISP2 layer counted timescale to GICC05 in two steps:

1. converting the Siple Dome ages to GISP2 depths via the GISP2 layer counted depth scale [*Meese et al.*, 1997] (data from: `http://www.ncdc.noaa.gov/paleo/icecore/greenland/summit/document/gispdpth.htm`);
2. converting GISP2 depths to GICC05 ages by linear interpolation between the GICC05 GISP2 age-depth ties [*Rasmussen et al.*, 2008] (data from: `http://www.iceandclimate.nbi.ku.dk/data/`).

We adopt the previously reported Δage and CH_4 correlation errors [*Brook et al.*, 2005] (data from: `http://nsidc.org/data/waiscores/pi/brook.html`). The dating error introduced in the actual transfer from the GISP2 layer counted depth scale to the GICC05 timescale is negligible compared to the Δage and correlation errors, and is therefore not considered. The RMS sum of the Δage and CH_4 correlation errors in the Siple Dome data during the early middle and late stages of the deglaciation are listed in Table 6.3.

The average temporal resolution of the Siple Dome data for the interval 9 to 21 ka BP was 32 yr.

Talos Dome

The Talos Dome timescale [*Buiron et al.*, 2011] is consistent with GICC05. Standard dating errors during the early middle and late stages of the deglaciation are listed in Table 6.3.

The average temporal resolution of the Talos Dome data for the interval 9 to 21 ka BP was 39 yr.

EDML

The recently revised EDML timescale [*Lemieux-Dudon et al.*, 2010] is consistent with GICC05. The revised EDML timescale, $\delta^{18}O_{ice}$ and CH_4 data and standard dating errors were obtained from Benedicte Lemieux-Dudon (personal communication, February 2010). Standard dating errors during the early middle and late stages of the deglaciation are listed in Table 6.3.

The average temporal resolution of the EDML data for the interval 9 to 21 ka BP was 15 yr.

References

Abram, N. J., R. Mulvaney, and C. Arrowsmith, Environmental signals in a highly resolved ice core from James Ross Island, Antarctica, *J. Geophys. Res.*, *116*, D20116, doi:10.1029/2011JD016147, 2011.

Ahn, J., M. Wahlen, B. L. Deck, E. J. Brook, P. A. Mayewski, K. C. Taylor, and J. W. C. White, A record of atmospheric CO_2 during the last 40,000 years from the Siple Dome, Antarctica ice core, *J. Geophys. Res.*, *109*, D13305, doi:10.1029/2003JD004415, 2004.

Aldahan, A., G. Possnert, S. Johnsen, H. Clausen, E. Isaksson, W. Karlen, and M. Hansson, Sixty year ^{10}Be record from Greenland and Antarctica, in *Proc. Indian. Acad. Sci., Earth Planet. Sc. Lett.*, vol. 107, pp. 139–147, 1998.

Aldahan, A., G. Possnert, and I. Vintersved, Atmospheric interactions at northern high latitudes from weekly Be-isotopes in surface air, *Appl. Radiat. Isotopes*, *54*(2), 345–353, 2001.

Aldahan, A., J. Hedfors, G. Possnert, A. Kulan, A.-M. Berggren, and C. Söderström, Atmospheric impact on beryllium isotopes as solar activity proxy, *Geophys. Res. Lett.*, *35*, L21812, doi:10.1029/2008GL035189, 2008.

Alley, R. B., R. C. Finkel, K. Nishiizumi, S. Anandakrishnan, C. A. Shuman, G. R. Mershon, G. A. Zielinski, and P. A. Mayewski, Changes in continental and sea-salt atmospheric loadings in central Greenland during the most recent deglaciation: model-based estimates, *J. Glaciol.*, *41*, 503–514, 1995.

Ammann, C. M., F. Joos, D. S. Schimel, B. L. Otto-Bliesner, and R. A. Tomas, Solar influence on climate during the past millennium: Results from transient simulations with the NCAR Climate System Model, *P. Natl. Acad. Sci. USA*, *104*, 3713–3718, doi:10.1073/pnas.0605064103, 2007.

Andersen, K. K., P. D. Ditlevsen, S. O. Rasmussen, H. B. Clausen, B. M. Vinther, S. J. Johnsen, and J. P. Steffensen, Retrieving a common accumulation record from Greenland ice cores for the past 1800 years, *J. Geophys. Res.*, *111*, D15106, doi: 10.1029/2005JD006765, 2006.

Andersen, K. K., et al., The Greenland Ice Core Chronology 2005, 15 42 ka. Part 1: constructing the time scale, *Quaternary Sci. Rev.*, *25*, 3246–3257, doi:10.1016/j.quascirev.2006.08.002, 2006.

Anderson, R. F., and M.-E. Carr, Uncorking the Southern Oceans vintage CO_2, *Science*, *328*, 1117–1118, 2010.

Anderson, R. F., S. Ali, L. I. Bradtmiller, S. H. H. Nielsen, M. Q. Fleisher, B. E. Anderson, and L. H. Burckle, Wind-driven upwelling in the Southern Ocean and the deglacial rise in atmospheric CO_2, *Science*, *323*, 1443–1448, doi:10.1126/science.1167441, 2009.

Appenzeller, C., J. Schwander, S. Sommer, and T. F. Stocker, The North Atlantic Oscillation and its imprint on precipitation and ice accumulation in Greenland, *Geophys. Res. Lett.*, *25*, 1939–1942, doi:10.1029/98GL01227, 1998.

Asselin, E., T. M. Ahmed, and A. Alfantazi, Corrosion behavior of pure niobium in acidic solutions at elevated temperatures, *Corros. Sci.*, *49*(2), 694–710, 2007.

Baldwin, M. P., and T. J. Dunkerton, Stratospheric harbingers of anomalous weather regimes, *Science*, *294*, 581–584, 2001.

Baldwin, M. P., et al., The quasi-biennial oscillation, *Rev. Geophys.*, *39*, 179–230, doi:10.1029/1999RG000073, 2001.

Bard, E., G. Raisbeck, F. Yiou, and J. Jouzel, Solar irradiance during the last 1200 years based on cosmogenic nuclides, *Tellus B*, *52*, 985–992, doi:10.1034/j.1600-0889.2000.d01-7.x, 2000.

Barker, S., G. Knorr, M. J. Vautravers, P. Diz, and L. C. Skinner, Extreme deepening of the Atlantic overturning circulation during deglaciation, *Nat. Geosci.*, *3*, 567–571, doi:10.1038/ngeo921, 2010.

Barnola, J.-M., P. Pimienta, D. Raynaud, and Y. S. Korotkevich, CO_2-climate relationship as deduced from the Vostok ice core: a re-examination based on new measurements and on a re-evaluation of the air dating, *Tellus B*, *43*, 83, doi:10.1034/j.1600-0889.1991.t01-1-00002.x, 1991.

Bartol Research Institute, Neutron monitor program, McMurdo monitor data, `http://neutronm.bartol.udel.edu/`, access: December 2010.

Baumgartner, S., J. Beer, G. Wagner, P. Kubik, M. Suter, G. M. Raisbeck, and F. Yiou, ^{10}Be and dust, *NIMB B*, *123*(1-4), 296–301, doi:10.1016/S0168-583X(96)00751-3, 1997.

Beer, J., Long-term indirect indices of solar variability, *Space Sci. Rev.*, *94*, 53–66, 2000.

Beer, J., H. Oeschger, M. Andrée, G. Bonani, M. Suter, W. Wölfli, and C. C. Langway, Jr., Temporal variations in the ^{10}Be concentration levels found in the Dye 3 ice core, Greenland, *Ann. Glaciol.*, *5*, 16–17, 1984.

Beer, J., A. Blinov, G. Bonani, H. J. Hofmann, and R. C. Finkel, Use of Be-10 in polar ice to trace the 11-year cycle of solar activity, *Nature*, *347*, 164–166, doi:10.1038/347164a0, 1990.

Beer, J., W. Mende, and R. Stellmacher, The role of the sun in climate forcing, *Quaternary Sci. Rev.*, *19*(1-5), 403 – 415, doi:10.1016/S0277-3791(99)00072-4, 2000.

Beer, J., et al., Seasonal variations in the concetration of ^{10}Be, Cl^-, NO_3^-, SO_4^{2-}, H_2O_2, ^{210}Pb, ^{3}H, mineral dust, and δ^{18}O in Greenland snow, *Atmos. Environ.*, *25A*(5/6), 899–904, 1991.

Berggren, A., J. Beer, G. Possnert, A. Aldahan, P. Kubik, M. Christl, S. J. Johnsen, J. Abreu, and B. M. Vinther, A 600-year annual ^{10}Be record from the NGRIP ice core, Greenland, *Geophys. Res. Lett.*, *36*, L11,801, doi:10.1029/2009GL038004, 2009.

Bianchi, C., and R. Gersonde, Climate evolution at the last deglaciation: the role of the Southern Ocean, *Earth Planet Sci. Lett.*, *228*, 407–424, doi:10.1016/j.epsl.2004.10.003, 2004.

Blunier, T., and E. J. Brook, Timing of millennial-scale climate change in Antarctica and Greenland during the last glacial period, *Science*, *291*, 109–112, doi:10.1126/science.291.5501.109, 2001.

Blunier, T., et al., Asynchrony of Antarctic and Greenland climate change during the last glacial period, *Nature*, *394*, 739–743, doi:10.1038/29447, 1998.

Bond, G., et al., Persistent solar influence on North Atlantic climate during the Holocene, *Science*, *294*, 2130–2136, doi:10.1126/science.1065680, 2001.

Broecker, W., Palaeocean circulation during the last deglaciation: A bipolar seesaw?, *Paleoceanography*, *13*, 119–121, doi:doi:10.1029/97PA03707, 1998.

Bromwich, D. H., R. L. Fogt, K. I. Hodges, and J. E. Walsh, A tropospheric assessment of the ERA-40, NCEP, and JRA-25 global reanalyses in the polar regions, *J. Geophys. Res.*, *112*, D10111, doi:10.1029/2006JD007859, 2007.

Bromwich, D. H., J. P. Nicolas, and A. J. Monaghan, An assessment of precipitation changes over Antarctica and the Southern Ocean since 1989 in contemporary global reanalyses, *J. Climate*, *24*, 4189–4209, doi:10.1175/2011JCLI4074.1, 2011.

Brook, E. J., J. W. C. White, A. S. M. Schilla, M. L. Bender, B. Barnett, J. P. Severinghaus, K. C. Taylor, R. B. Alley, and E. J. Steig, Timing of millennial-scale climate change at Siple Dome, West Antarctica, during the last glacial period, *Quaternary Sci. Rev.*, *24*, 1333–1343, doi:10.1016/j.quascirev.2005.02.002, 2005.

Brown, L., G. J. Stensland, J. Klein, and R. Middleton, Atmospheric deposition of ^{7}Be and ^{10}Be, *Geochim. Cosmochim. Ac.*, *53*(1), 135 – 142, doi:DOI:10.1016/0016-7037(89)90280-9, 1989.

Buiron, D., et al., TALDICE-1 age scale of the Talos Dome deep ice core, East Antarctica, *Clim. Past*, *7*, 1–16, doi:10.5194/cp-7-1-2011, 2011.

Burn-Nunes, L. J., et al., Seasonal variability in the input of lead, barium and indium to Law Dome, Antarctica, *Geochim. Cosmochim. Ac.*, *75*, 1–20, doi:10.1016/j.gca.2010.09.037, 2011.

Caillon, N., J. P. Severinghaus, J. Jouzel, J.-M. Barnola, J. Kang, and V. Y. Lipenkov, Timing of atmospheric CO_2 and Antarctic temperature changes across termination III, *Science*, *299*, 1728–1731, doi:10.1126/science.1078758, 2003.

Cane, H. V., G. Wibberenz, I. G. Richardson, and T. T. von Rosenvinge, Cosmic ray modulation and the solar magnetic field, *Geophys. Res. Lett.*, *26*, 565–568, doi:10.1029/1999GL900032, 1999.

Chaudhuri, P., and J. S. Marron, SiZer for exploration of structures in curves, *J. Am. Stat. Assoc.*, *94*, 807–823, 1999.

Child, D., G. Elliott, C. Mifsud, A. M. Smith, and D. Fink, Sample processing for Earth science studies at ANTARES, *NIMB B*, *172*, 856–860, 2000.

Chmeleff, J., F. von Blanckenburg, K. Kossert, and D. Jakob, Determination of the ^{10}Be half-life by multicollector ICP-MS and liquid scintillation counting, *NIMB B*, *268*, 192–199, doi:10.1016/j.nimb.2009.09.012, 2010.

Craig, H., Isotopic variations in meteoric waters, *Science*, *133*, 1702–1703, doi:10.1126/science.133.3465.1702, 1961.

Curran, M. A. J., and A. S. Palmer, Suppressed ion chromatography methods for the routine determination of ultra low level anions and cations in ice cores, *Journal of Chromatogr. A*, *919*(1), 107–113, doi:10.1016/S0021-9673(01)00790-7, 2001.

Curran, M. A. J., T. D. van Ommen, and V. Morgan, Seasonal characteristics of the major ions in the high-accumulation Dome Summit South ice core, Law Dome, Antarctica, *Ann. Glaciol.*, *27*, 385–390, 1998.

Dansgaard, W., Stable isoptopes in precipitation, *Tellus*, *16*, 436–468, 1964.

Davidson, C. I., H. Bergin, and D. Hampden, The deposition of particles and gasses to ice sheets, in *NATO ASI Series, Vol. I 43, Chemical Exchange Between the Atmosphere and Polar Snow*, edited by E. Wolff and R. Bales, pp. 275–306, Springer, 1996.

Delaygue, G., and E. Bard, An Antarctic view of Beryllium-10 and solar activity for the past millennium, *Clim. Dynam.*, *36*(11-12), 2201–2218, doi:10.1007/s00382-010-0795-1, 2011.

Delmas, R. J., Free tropospheric reservoir of natural sulfate, *J. Atmos. Chem.*, *14*, 261–271, 1992.

Delmotte, M., D. Raynaud, V. Morgan, and J. Jouzel, Climatic and glaciological information inferred from air-content measurements of a Law Dome (East Antarctica) ice core, *J. Glaciol.*, *45*, 255–263, 1999.

Denton, G. H., R. F. Anderson, J. R. Toggweiler, R. L. Edwards, J. M. Schaefer, and A. E. Putnam, The last glacial termination, *Science*, *328*, 1652–1656, doi:10.1126/science.1184119, 2010.

Dibb, J. E., L. D. Meeker, R. C. Finkel, J. R. Southon, M. W. Caffee, and L. A. Barrie, Estimation of stratospheric input to the Arctic troposphere: ^{7}Be and ^{10}Be in aerosols at Alert, Canada, *J. Geophys. Res.*, *99*, 12,855–12,864, doi:10.1029/94JD00742, 1994.

Dunai, D. H., *Cosmogenic Nuclides: Principles, Concepts and Applications in the Earth Surface Sciences*, Cambridge University Press, 2010.

Eichler, A., M. Schwikowski, and H. W. Gaggeler, Meltwater-induced relocation of chemical species in alpine firn, *Tellus B*, *53*, 192203, doi:10.1034/j.1600-0889.2001.d01-15.x, 2001.

Elsässer, C., D. Wagenbach, R. Weller, M. Auer, A. Wallner, and M. Christl, Continuous 25-yr aerosol records at coastal Antarctica, *Tellus B*, doi:10.1111/j.1600-0889.2011.00543.x, 2011.

EPICA Community Members, One-to-one coupling of glacial climate variability in Greenland and Antarctica, *Nature*, *444*, 195–198, doi:10.1038/nature05301, 2006.

Everest, D. A., *Chap. 9, Beryllium*, pp. 531–590, Pergamon, 1973.

Feeley, H. W., R. J. Larsen, and C. G. Sanderson, Factors that cause seasonal variations in beryllium-7 concentrations in surface air, *J. Environ. Radioactivity*, *9*, 223–249, 1989.

Field, C. V., and G. A. Schmidt, Model-based constraints on interpreting 20th century trends in ice core ^{10}Be, *J. Geophys. Res.*, *114*, D12110, doi:10.1029/2008JD011217, 2009.

Field, C. V., G. A. Schmidt, D. Koch, and C. Salyk, Modeling production and climate-related impacts on ^{10}Be concentration in ice cores, *J. Geophys. Res.*, *111*, D15107, doi:10.1029/2005JD006410, 2006.

Field, C. V., G. A. Schmidt, and D. T. Shindell, Interpreting ^{10}Be changes during the Maunder Minimum, *J. Geophys. Res.*, *114*, D02113, doi:10.1029/2008JD010578, 2009.

Fink, D., AMS-11 in Rome, 2008: Past achievements, current and future trends, *NIMB B*, *268*, 1334–1342, doi:10.1016/j.nimb.2009.10.167, 2010.

Fink, D., and A. Smith, An inter-comparison of ^{10}Be and ^{26}Al AMS reference standards and the ^{10}Be half-life, *NIMB B*, *259*, 600–609, doi:10.1016/j.nimb.2007.01.299, 2007.

Fink, D., B. McKelvey, D. Hannan, and D. Newsome, Cold rocks, hot sands: In-situ cosmogenic applications in Australia at ANTARES, *NIMB B*, *172*, 838–846, 2000.

Finkel, R. C., and K. Nishiizumi, Beryllium 10 concentrations in the Greenland Ice Sheet Project 2 ice core from 3-40 ka, *J. Geophys. Res.*, *102*, 26,699–26,706, doi: 10.1029/97JC01282, 1997.

Fischer, H., D. Wagenbach, and J. Kipfstuhl, Sulfate and nitrate firn concentrations on the Greenland ice sheet 1. Large-scale geographical deposition changes, *J. Geophys. Res.*, *1032*, 21,927–21,934, doi:10.1029/98JD01885, 1998.

Fischer, H., M. Wahlen, J. Smith, D. Mastroianni, and B. Deck, Ice core records of atmospheric CO_2 around the last three glacial terminations, *Science*, *283*, 1712–1714, doi:10.1126/science.283.5408.1712, 1999.

Fischer, H., et al., The role of Southern Ocean processes in orbital and millennial CO_2 variations - A synthesis, *Quaternary Sci. Rev.*, *29*, 193–205, doi:10.1016/j.quascirev. 2009.06.007, 2010.

Fisher, D., R. M. Koerner, K. Kuivinen, H. B. Clausen, S. J. Johnsen, J.-P. Steffensen, N. Gundestrup, and C. U. Hammer, Inter-comparison of δ^{18}O and precipitation records from sites in Canada and Greenland over the last 3500 years and over the last few centuries in detail using EOF techniques, in *Climatic Variations and Forcing mechanisms of the Last 2000 Years*, *ASI Series 1: Global Environmental Change*, vol. 41, edited by P. D. Jones, R. S. Bradley, and J. Jouzel, pp. 297–328, Springer, 1996.

Frey, M. M., J. Savarino, S. Morin, J. Erbland, and J. M. F. Martins, Photolysis imprint in the nitrate stable isotope signal in snow and atmosphere of East Antarctica and implications for reactive nitrogen cycling, *Atmos. Chem. Phys.*, *9*, 8681–8696, 2009.

Frigo, M., and S. G. Johnson, The design and implementation of FFTW3, *Proceedings of the IEEE*, *93*(2), 216–231, special issue on "Program Generation, Optimization, and Platform Adaptation", 2005.

Fröhlich, C., Observations of irradiance variations, *Space Sci. Rev.*, *94*, 15–24, 2000.

Ganopolski, A., and S. Rahmstorf, Rapid changes of glacial climate simulated in a coupled climate model, *Nature*, *409*, 153–158, 2001.

Ganopolski, A., and D. M. Roche, On the nature of lead-lag relationships during glacial-interglacial climate transitions, *Quaternary Sci. Rev.*, *28*, 3361–3378, 2009.

Goodwin, I. D., T. D. van Ommen, M. A. J. Curran, and P. A. Mayewski, Mid latitude winter climate variability in the South Indian and southwest Pacific regions since 1300 AD, *Clim. Dynam.*, *22*, 783–794, doi:10.1007/s00382-004-0403-3, 2004.

Gosse, F. M., J. Phillips, Terrestrial in situ cosmogenic nuclides: theory and application, *Quaternary Sci. Rev.*, *20*, 1475–1560, doi:10.1016/S0277-3791(00)00171-2, 2001.

Goujon, C., J.-M. Barnola, and C. Ritz, Modeling the densification of polar firn including heat diffusion: Application to close-off characteristics and gas isotopic fractionation for Antarctica and Greenland sites, *J. Geophys. Res.*, *108*, 4792, doi: 10.1029/2002JD003319, 2003.

Graham, I., R. Ditchburn, and B. Barry, Atmospheric deposition of ^{7}Be and ^{10}Be in New Zealand rain, *Geochim. Cosmochim. Ac.*, *67*, 361–373, 2003.

Graly, J. A., L. J. Reusser, and P. R. Bierman, Short and long-term delivery rates of meteoric ^{10}Be to terrestrial soils, *Earth Planet Sci. Lett.*, *302*(3-4), 329–336, doi: 10.1016/j.epsl.2010.12.020, 2011.

Grassi, B., G. Redaelli, and G. Visconti, Evidence for tropical SST influence on Antarctic polar atmospheric dynamics, *Geophys. Res. Lett.*, *36*, L09703, doi:10.1029/2009GL038092, 2009.

Hanna, E., J. McConnell, S. Das, J. Cappelen, and A. Stephens, Observed and modeled Greenland Ice Sheet snow accumulation, 1958–2003, and links with regional climate forcing, *J. Climate*, *19*, 344–358, doi:10.1175/JCLI3615.1, 2006.

Harder, S., S. G. Warren, and R. J. Charlson, Sulfate in air and snow at the South Pole: Implications for transport and deposition at sites with low snow accumulation, *J. Geophys. Res.*, *105*, 22,825–22,832, doi:10.1029/2000JD900351, 2000.

Hays, J. D., J. Imbrie, and N. J. Shackleton, Variations in the Earth's orbit: Pacemaker of the ice ages, *Science*, *194*, 1121–1132, doi:10.1126/science.194.4270.1121, 1976.

Heikkilä, U., J. Beer, and V. Alfimov, Beryllium-10 and beryllium-7 in precipitation in Dübendorf (440 m) and at Jungfraujoch (3580 m), Switzerland (1998-2005), *J. Geophys. Res.*, *113*, D11104, doi:10.1029/2007JD009160, 2008a.

Heikkilä, U., J. Beer, and J. Feichter, Modeling cosmogenic radionuclides ^{10}Be and ^{7}Be during the Maunder Minimum using the ECHAM5-HAM General Circulation Model, *Atmos. Chem. Phys.*, *8*, 2797–2809, 2008b.

Heikkilä, U., J. Beer, J. Jouzel, J. Feichter, and P. Kubik, ^{10}Be measured in a GRIP snow pit and modeled using the ECHAM5-HAM general circulation model, *Geophys. Res. Lett.*, *35*, L05817, doi:10.1029/2007GL033067, 2008c.

Heikkilä, U., J. Beer, and J. Feichter, Meridional transport and deposition of atmospheric ^{10}Be, *Atmos. Chem. Phys.*, *9*, 515–527, 2009.

Holton, J. R., P. H. Haynes, M. E. McIntyre, A. R. Douglass, R. B. Rood, and L. Pfister, Stratosphere-troposphere exchange, *Rev. Geophys.*, *33*, 403–439, doi:10.1029/95RG02097, 1995.

Horiuchi, K., T. Uchida, Y. Sakamoto, A. Ohta, H. Matsuzaki, Y. Shibata, and H. Motoyama, Ice core record of ^{10}Be over the past millennium from Dome Fuji, Antarctica: A new proxy record of past solar activity and a powerful tool for stratigraphic dating, *Quat. Geocrhonology*, *3*, 253–261, 2008.

Hou, S., and D. Qin, The effect of postdepositional process on the chemical profiles of snow pits in the percolation zone, *Cold Reg. Sci. Tech.*, *34*(2), 111–116, doi:10.1016/S0165-232X(01)00065-9, 2002.

Hudson, S. R., and R. E. Brandt, A Look at the Surface-Based Temperature Inversion on the Antarctic Plateau., *J. Climate*, *18*, 1673–1696, doi:10.1175/JCLI3360.1, 2005.

Igarashi, Y., K. Hirose, and M. Otsuji-Hatori, Beryllium-7 deposition and its relation to sulfate deposition, *J. Atmos. Chem.*, *29*, 217–231, 1998.

Ishikawa, Y., H. Murakami, T. Sekine, and K. Yoshihara, Precipitation scavenging studies of radionuclides in air using cosmogenic ^{7}Be, *J. Environ. Radioactivity*, *26*(1), 19–36, doi:10.1016/0265-931X(95)91630-M, 1995.

Johannessen, M., and A. Henriksen, Chemistry of snow meltwater: Changes in concentration during melting, *Water Resour. Res.*, *14*, 615–619, doi:10.1029/WR014i004p00615, 1978.

Johnsen, S. J., et al., The δ^{18}O record along the Greenland Ice Core Project deep ice core and the problem of possible Eemian climatic instability, *J. Geophys. Res.*, *102*, 26,397–26,410, doi:10.1029/97JC00167, 1997.

Jones, P. D., et al., High-resolution palaeoclimatology of the last millennium: a review of current status and future prospects, *The Holocene*, *19*(1), 3–49, 2009.

Jordan, C. E., J. E. Dibb, and R. C. Finkel, ^{10}Be/^{7}Be tracer of atmospheric transport and stratosphere-troposphere exchange, *J. Geophys. Res.*, *108*, 4234, doi:10.1029/2002JD002395, 2003.

Jouzel, J., et al., The two-step shape and timing of the last deglaciation in Antarctica, *Clim. Dynam.*, *11*, 151–161, doi:10.1007/BF00223498, 1995.

Jouzel, J., et al., Validity of the temperature reconstruction from water isotopes in ice cores, *J. Geophys. Res.*, *1022*, 26,471–26,488, doi:10.1029/97JC01283, 1997.

Jouzel, J., et al., A new 27 ky high resolution East Antarctic climate record, *Geophys. Res. Lett.*, *28*, 3199–3202, doi:10.1029/2000GL012243, 2001.

Jun, L., T. H. Jacka, and V. Morgan, Crystal-size and microparticle record in the ice core from Dome Summit South, Law Dome, East Antarctica, *Ann. Glaciol.*, *27*, 343–348, 1998.

Kalnay, E., et al., The NCEP/NCAR 40-Year Reanalysis Project., *Bulletin of the American Meteorological Society*, *77*, 437–472, doi:10.1175/1520-0477(1996)077$\langle$$0437:TNYRP$\rangle$$2.0.CO;2, 1996.

Kaplan, M. R., et al., Glacier retreat in New Zealand during the Younger Dryas stadial, *Nature*, *467*, 194–197, doi:10.1038/nature09313, 2010.

Knorr, G., and G. Lohmann, Southern Ocean origin for the resumption of Atlantic thermohaline circulation during deglaciation, *Nature*, *424*, 532–536, 2003.

Koch, D., and D. Rind, Beryllium 10/beryllium 7 as a tracer of stratospheric transport, *J. Geophys. Res.*, *103*, 3907–3918, doi:10.1029/97JD03117, 1998.

Kondo, K., H. Muramatsu, Y. Kanda, and S. Takahara, Particle size distribution of ^{7}Be aerosols formed in high energy accelerator tunnels, *Int. J. Appl. Radiat. Isot.*, *35*, 939–944, 1984.

König-Langlo, G., J. C. King, and P. Pettré, Climatology of the three coastal Antarctic stations Dumont d'Urville, Neumayer, and Halley, *J. Geophys. Res.*, *103*, 10,935–10,946, doi:10.1029/97JD00527, 1998.

Korkisch, J., *Handbook of ion exchange resins: their application to inorganic analytical chemistry*, 3–20 pp., CRC Press, Boca Raton, 1989.

Korschinek, G., et al., A new value for the half-life of ^{10}Be by Heavy-Ion Elastic Recoil Detection and liquid scintillation counting, *NIMB B*, *268*, 187–191, doi:10.1016/j.nimb.2009.09.020, 2010.

Kovaltsov, G. A., and I. G. Usoskin, A new 3D numerical model of cosmogenic nuclide ^{10}Be production in the atmosphere, *Earth Planet Sci. Lett.*, *291*, 182–188, doi:10.1016/j.epsl.2010.01.011, 2010.

Laepple, T., M. Werner, and G. Lohmann, Synchronicity of Antarctic temperatures and local solar insolation on orbital timescales, *Nature*, *471*, 91–94, doi:10.1038/nature09825, 2011.

Lal, D., ^{10}Be in polar ice: data reflect changes in cosmic ray flux or polar meteorology., *Geophys. Res. Lett.*, *14*, 785–788, 1987.

Lal, D., Recycling of cosmogenic nuclides after their removal from the atmosphere; special case of appreciable transport of ^{10}Be to polar regions by aeolian dust, *Earth Planet Sci. Lett.*, *264*, 177–187, doi:10.1016/j.epsl.2007.09.030, 2007.

Lal, D., and B. Peters, Cosmic ray produced radioactivity on the Earth, in *Handbuch der Physik*, vol. 46, edited by S. Flugge, pp. 551–612, Springer, 1967.

Land, C., and J. Feichter, Stratosphere-troposphere exchange in a changing climate simulated with the general circulation model MAECHAM4, *J. Geophys. Res.*, *108*, 8523, doi:10.1029/2002JD002543, 2003.

Landais, A., et al., Firn-air δ^{15}N in modern polar sites and glacial interglacial ice: a model-data mismatch during glacial periods in Antarctica?, *Quaternary Sci. Rev.*, *25*, 49–62, doi:10.1016/j.quascirev.2005.06.007, 2006.

Lean, J. L., Y.-M. Wang, and N. R. Sheeley, The effect of increasing solar activity on the Sun's total and open magnetic flux during multiple cycles: Implications for solar forcing of climate, *Geophys. Res. Lett.*, *29*(24), 2224, doi:10.1029/2002GL015880, 2002.

Lee, S.-Y., J. C. H. Chiang, K. Matsumoto, and K. S. Tokos, Southern Ocean wind response to North Atlantic cooling and the rise in atmospheric CO_2: Modeling perspective and paleoceanographic implications, *Paleoceanography*, *26*, PA1214, doi: 10.1029/2010PA002004, 2011.

Lemieux-Dudon, B., E. Blayo, J.-R. Petit, C. Waelbroeck, A. Svensson, C. Ritz, J.-M. Barnola, B. M. Narcisi, and F. Parrenin, Consistent dating for Antarctic and Greenland ice cores, *Quaternary Sci. Rev.*, *29*, 8–20, doi:10.1016/j.quascirev.2009.11.010, 2010.

Liu, Z., et al., Transient simulation of last deglaciation with a new mechanism for Bølling-Allerød warming, *Science*, *325*, 310–314, doi:10.1126/science.1171041, 2009.

Lockwood, M., Solar change and climate: an update in the light of the current exceptional solar minimum, *Philos Trans. R. Soc. A.*, *466*, 303–329, doi: 10.1098/rspa.2009.0519, 2010.

Lockwood, M., A. P. Rouillard, and I. D. Finch, The rise and fall of open solar flux during the current grand solar maximum, *The Astrophysical Journal*, *700*, 937–944, doi:10.1088/0004-637X/700/2/937, 2009.

Lockwood, M., C. Bell, T. Woollings, R. G. Harrison, L. J. Gray, and J. D. Haigh, Top-down solar modulation of climate: evidence for centennial-scale change, *Environ. Res. Lett.*, *5*, 034008, doi:10.1088/1748-9326/5/3/034008, 2010.

Lorius, C., D. Raynaud, J. Jouzel, J. Hansen, and H. Le Treut, The ice-core record — Climate sensitivity and future greenhouse warming, *Nature*, *347*, 139–145, doi: 10.1038/347139a0, 1990.

Loulergue, L., F. Parrenin, T. Blunier, J.-M. Barnola, R. Spahni, A. Schilt, G. Raisbeck, and J. Chappellaz, New constraints on the gas age-ice age difference along the EPICA ice cores, 0-50 kyr, *Clim. Past*, *3*, 527–540, 2007.

Lowe, J. J., S. O. Rasmussen, S. Björck, W. Z. Hoek, J. P. Steffensen, M. J. C. Walker, and Z. C. Yu, Synchronisation of palaeoenvironmental events in the North Atlantic region during the Last Termination: a revised protocol recommended by the INTIMATE group, *Quaternary Sci. Rev.*, *27*, 6–17, doi:10.1016/j.quascirev.2007.09.016, 2008.

Lucas, M. A., J. J.-M. Hirschi, and J. Marotzke, Response of the meridional overturning circulation to variable buoyancy forcing in a double hemisphere basin, *Clim. Dynam.*, *34*, 615–627, doi:10.1007/s00382-009-0704-7, 2010.

Maltrud, M., F. Bryan, and S. Peacock, Boundary impulse response functions in a century-long eddying global ocean simulation, *Environ. Fluid Mech.*, *10*, 275–295, 2010.

Masarik, J., and J. Beer, Simulation of particle fluxes and cosmogenic nuclide production in the Earth's atmosphere., *J. Geophys. Res.*, *104*, 12,099–12,111, 1999.

Masarik, J., and J. Beer, An updated simulation of particle fluxes and cosmogenic nuclide production in the Earth's atmosphere., *J. Geophys. Res.*, *114*, D11103, doi: 10.1029/2008JD010557, 2009.

Masson-Delmotte, V., et al., A review of Antarctic surface snow isotopic composition: Observations, atmospheric circulation, and isotopic modeling, *J. Climate*, *21*, 3359, doi:10.1175/2007JCLI2139.1, 2008.

Masuda, S., et al., Simulated rapid warming of abyssal North Pacific waters, *Science*, *329*, 319–322, doi:10.1126/science.1188703, 2010.

Mazaud, A., C. Laj, and M. Bender, A geomagnetic chronology for Antarctic ice accumulation, *Geophys. Res. Lett.*, *21*, 337–340, doi:10.1029/93GL02789, 1994.

McConnell, J. R., G. W. Lomorey, S. W. Lambert, and K. C. Taylor, Continuous ice-core chemical analyses using inductively coupled plasma mass spectrometry, *Environ. Sci. Technol.*, *36*, 7–11, 2002.

McConnell, J. R., et al., 20th-Century industrial black carbon emissions altered Arctic climate forcing, *Science*, *317*, 1381–1384, 2007.

McCracken, K. G., Geomagnetic and atmospheric effects upon the cosmogenic ^{10}Be observed in polar ice, *J. Geophys. Res.*, *109*, A04101, doi:10.1029/2003JA010060, 2004.

McCracken, K. G., and J. Beer, Long-term changes in the cosmic ray intensity at Earth, 1428-2005, *J. Geophys. Res.*, *112*, A10101, doi:10.1029/2006JA012117, 2007.

McCracken, K. G., F. B. McDonald, J. Beer, G. Raisbeck, and F. Yiou, A phenomenological study of the long-term cosmic ray modulation, 850-1958 AD, *J. Geophys. Res.*, *109*, A12103, doi:10.1029/2004JA010685, 2004.

McHargue, L. R., and P. E. Damon, The global beryllium 10 cycle, *Rev. Geophys.*, *29*, 141–158, doi:10.1029/91RG00072, 1991.

McManus, J. F., R. Francois, J.-M. Gherardi, L. D. Keigwin, and S. Brown-Leger, Collapse and rapid resumption of Atlantic meridional circulation linked to deglacial climate changes, *Nature*, *428*, 834–837, doi:10.1038/nature02494, 2004.

McMorrow, A. J., M. A. J. Curran, T. D. van Ommen, V. I. Morgan, M. J. Pook, and I. Allison, Intercomparison of firn-core and meteorological data, *Antarct. Sci.*, *13*(3), 329–337, 2001.

McMorrow, A. J., M. A. J. Curran, T. D. van Ommen, V. I. Morgan, and I. Allison, Features of meteorological events preserved in a high-resolution Law Dome (East Antarctica) snow pit, *Ann. Glaciol.*, *35*, 463–470, 2002.

McMorrow, A. J., T. D. van Ommen, V. Morgan, and M. A. J. Curran, Ultra-high-resolution seasonality of trace ion species and oxygen-isotope ratios in Antarctic firn over four annual cycles, *Ann. Glaciol.*, *39*, 34–40, 2004.

Meese, D. A., A. J. Gow, R. B. Alley, G. A. Zielinski, P. M. Grootes, M. Ram, K. C. Taylor, P. A. Mayewski, and J. F. Bolzan, The Greenland Ice Sheet Project 2 depth-age scale: Methods and results, *J. Geophys. Res.*, *102*, 26,411–26,424, doi:10.1029/97JC00269, 1997.

Monnin, E., A. Indermühle, A. Dällenbach, J. Flückiger, B. Stauffer, T. F. Stocker, D. Raynaud, and J.-M. Barnola, Atmospheric CO_2 concentrations over the last glacial termination, *Science*, *291*, 112–114, doi:10.1126/science.291.5501.112, 2001.

Monnin, E., et al., Evidence for substantial accumulation rate variability in Antarctica during the Holocene, through synchronization of CO_2 in the Taylor Dome, Dome C and DML ice cores, *Earth Planet. Sci. Lett.*, *224*, 45–54, doi:10.1016/j.epsl.2004.05.007, 2004.

Moraal, H., R. Muscheler, L. du Plessis, P. W. Kubik, J. Beer, K. G. McCracken, and F. B. McDonald, ^{10}Be concentration in the Ice Shelf of Queen Maude Land, Antarctica, *S. Afr. J. Sci.*, *101*, 299–301, 2005.

Moraal, H., P. Stoker, and H. Krüger, Neutron monitor observations of the 2009 solar minimum, in *31st ICRC, Lodz*, pp. 1–4, 2009.

Morgan, V., M. Delmotte, T. van Ommen, J. Jouzel, J. Chappellaz, S. Woon, V. Masson-Delmotte, and D. Raynaud, Relative Timing of Deglacial Climate Events in Antarctica and Greenland, *Science*, *297*, 1862–1864, doi:10.1126/science.1074257, 2002.

Morgan, V. I., C. W. Wookey, J. Li, T. D. van Ommen, W. Skinner, and M. F. Fitzpatrick, Site information and initial results from deep ice drilling on Law Dome, Antarctica, *J. Glaciol.*, *43*, 3–10, 1997.

Mosley-Thompson, E., C. R. Readinger, P. Craigmile, L. G. Thompson, and C. A. Calder, Regional sensitivity of Greenland precipitation to NAO variability, *Geophys. Res. Lett.*, *322*, L24707, doi:10.1029/2005GL024776, 2005.

Mudelsee, M., The phase relations among atmospheric CO2 content, temperature and global ice volume over the past 420 ka, *Quaternary Sci. Rev.*, *20*, 583–589, doi:10.1016/S0277-3791(00)00167-0, 2001.

Mudelsee, M., Estimating Pearson's correlation coefficient with bootstrap confidence interval from serially dependent time series, *Math. Geol.*, *35*(6), 651–665, 2003.

Müller, A. M., M. Christl, J. Lachner, M. Suter, and H.-A. Synal, Competitive ^{10}Be measurements below 1 MeV with the upgraded ETH-TANDY AMS facility, *NIMB B*, *268*, 2801–2807, doi:10.1016/j.nimb.2010.05.104, 2010.

Muscheler, R., and J. Beer, Solar forced Dansgaard/Oeschger events?, *Geophys. Res. Lett.*, *33*, L20706, doi:10.1029/2006GL026779, 2006.

Muscheler, R., F. Joos, J. Beer, S. A. Müller, M. Vonmoos, and I. Snowball, Solar activity during the last 1000 yr inferred from radionuclide records, *Quaternary Sci. Rev.*, *26*, 82–97, doi:10.1016/j.quascirev.2006.07.012, 2007.

Neftel, A., H. Oeschger, T. Staffelbach, and B. Stauffer, CO_2 record in the Byrd ice core 50,000–5,000 years bp, *Nature*, *331*, 609–611, doi:10.1038/331609a0, 1988.

NGRIP community members, High-resolution record of Northern Hemisphere climate extending into the last interglacial period, *Nature*, *431*, 147–151, doi:10.1038/nature02805, 2004.

Nishiizumi, K., M. Imamura, M. W. Caffee, J. R. Southon, R. C. Finkel, and J. McAninch, Absolute calibration of ^{10}Be AMS standards, *NIMB B*, *258*, 403–413, doi:10.1016/j.nimb.2007.01.297, 2007.

Noone, D., and I. Simmonds, Sea ice control of water isotope transport to Antarctica and implications for ice core interpretation, *J. Geophys. Res.*, *109*, D07105, doi:10.1029/2003JD004228, 2004.

Obrien, K., Secular variations in the production of cosmogenic isotopes in the Earth's atmosphere, *J. Geophys. Res.*, *84*, 423–431, doi:10.1029/JA084iA02p00423, 1979.

O'Brien, K., and G. D. P. Burke, Calculated cosmic ray neutron monitor response to solar modulation of galactic cosmic rays., *J. Geophys. Res.*, *78*, 3013–3019, doi:10.1029/JA078i016p03013, 1973.

O'Brien, K., A. de La Zerda Lerner, M. A. Shea, and D. F. Smart, The production of cosmogenic isotopes in the Earth's atmosphere and their inventories, in *The Sun in Time*, edited by C. P. Sonett and M. S. Giampapa and M. S. Matthews, pp. 317–342, 1991.

Palmer, A. S., T. D. van Ommen, M. A. J. Curran, V. Morgan, J. M. Souney, and P. A. Mayewski, High-precision dating of volcanic events (A.D. 1301-1995) using ice cores from Law Dome, Antarctica, *J. Geophys. Res.*, *106*, 28,089–28,096, doi:10.1029/2001JD000330, 2001.

Parrenin, F., et al., The EDC3 chronology for the EPICA Dome C ice core, *Clim. Past*, *3*, 485–497, 2007.

Pedro, J., T. van Ommen, M. Curran, V. Morgan, A. Smith, and A. McMorrow, Evidence for climate modulation of the ^{10}Be solar activity proxy, *J. Geophys. Res.*, *111*, D21,105, doi:10.1029/2005JD006764, 2006.

Pedro, J., et al., ^{10}Be concentrations in snow at Law Dome Antarctica following the 29 October 2003 and 20 January 2005 Solar Cosmic Ray Events, in *Advances in Geosciences*, vol. 14, Solar Terrestrial (2007), edited by M. Duldig, World Scientific Publishing Company, 2009.

Pedro, J. B., A. M. Smith, K. J. Simon, T. D. van Ommen, and M. A. J. Curran, High-resolution records of the beryllium-10 solar activity proxy in ice from Law Dome, East Antarctica: measurement, reproducibility and principal trends, *Clim. Past*, *7*, 707–721, doi:10.5194/cp-7-707-2011, 2011a.

Pedro, J. B., U. E. Heikkilä, A. Klekociuk, A. M. Smith, T. D. van Ommen, and M. A. J. Curran, Beryllium-10 transport to Antarctica: Results from seasonally-resolved observations and modeling, *J. Geophys. Res.*, *116*, D23120, doi:10.1029/2011JD016530, 2011b.

Pedro, J. B., T. D. van Ommen, S. O. Rasmussen, V. I. Morgan, J. Chappellaz, A. D. Moy, V. Masson-Delmotte, and M. Delmotte, The last deglaciation: timing the bipolar seesaw, *Clim. Past*, *7*, 671–683, doi:10.5194/cp-7-671-2011, 2011c.

Petit, J. R., et al., Climate and atmospheric history of the past 420,000 years from the Vostok ice core, Antarctica, *Nature*, *399*, 429–436, doi:10.1038/20859, 1999.

Phillpot, H. R., and J. W. Zillman, The surface temperature inversion over the Antarctic continent, *J. Geophys. Res.*, *75*, 4161–4169, doi:10.1029/JC075i021p04161, 1970.

PMOD World Radiation Center, TSI composite, PMOD/WRC, Davos, Switzerland, version d41_62_1005, `ftp://ftp.pmodwrc.ch/pub/data/irradiance/composite/`, access: 29 May 2010, 1979-2009.

Pourbaix, M., *Atlas of electrochemical equilibria in aqueous solutions*, 644 pp., National Association of Corrosion Engineers, Houston, 1974.

Raisbeck, G. M., and F. Yiou, ^{10}Be in polar ice and atmospheres, *Ann. Glaciol.*, *7*, 138–140, 1985.

Raisbeck, G. M., F. Yiou, M. Fruneau, M. Lieuvin, and J. M. Loiseaux, Measurement of Be-10 in 1,000- and 5,000-year-old Antarctic ice, *Nature*, *275*, 731–733, doi:10.1038/275731a0, 1978.

Raisbeck, G. M., F. Yiou, M. Fruneau, J. M. Loiseaux, M. Lieuvin, and J. C. Ravel, Cosmogenic Be-10/Be-7 as a probe of atmospheric transport processes, *Geophys. Res. Lett.*, *8*, 1015–1018, 1981.

Raisbeck, G. M., F. Yiou, J. Jouzel, and J. R. Petit, ^{10}Be and δ ^{2}H in polar ice cores as a probe of the solar variability's influence on climate, *Philos. Trans. Soc. Lond.*, *330*, 463–469, doi:10.1098/rsta.1990.0027, 1990.

Randel, W. J., F. Wu, and D. J. Gaffen, Interannual variability of the tropical tropopause derived from radiosonde data and NCEP reanalyses, *J. Geophys. Res.*, *105*, 15,509–15,524, doi:10.1029/2000JD900155, 2000.

Raphael, M. N., A zonal wave 3 index for the Southern Hemisphere, *Geophys. Res. Lett.*, *312*, L23212, doi:10.1029/2004GL020365, 2004.

Raphael, M. N., The influence of atmospheric zonal wave three on Antarctic sea ice variability, *J. Geophys. Res.*, *112*, D12112, doi:10.1029/2006JD007852, 2007.

Rasmussen, S. O., I. K. Seierstad, K. K. Andersen, M. Bigler, D. Dahl-Jensen, and S. J. Johnsen, Synchronization of the NGRIP, GRIP, and GISP2 ice cores across MIS 2 and palaeoclimatic implications, *Quaternary Sci. Rev.*, *27*, 18–28, doi:10.1016/j.quascirev.2007.01.016, 2008.

Rasmussen, S. O., et al., A new Greenland ice core chronology for the last glacial termination, *J. Geophys. Res.*, *111*, D06102, doi:10.1029/2005JD006079, 2006.

Roeckner, E., The atmospheric general circulation model ECHAM5, Part I: Model description, *Tech. Rep. Rep. 349,*, Max Planck Inst. for Meteorology, Hamburg, Germany, 2003.

Rood, D. H., S. Hall, T. P. Guilderson, R. C. Finkel, and T. A. Brown, Challenges and opportunities in high-precision Be-10 measurements at CAMS, *NIMB B*, *268*, 730–732, doi:10.1016/j.nimb.2009.10.016, 2010.

Rosner, M., R. L. Romer, and A. Meixner, Air handling in clean laboratory environments: The reason for anormalously high boron background levels, *Anal. Bioanal. Chem.*, *382*, 120–124, 2005.

Sanak, J., G. Lambert, and B. Ardouin, Measurement of stratosphere-to-troposphere exchange in Antarctica by using short-lived cosmonuclides, *Tellus B*, *37B*, 109–115, 1985.

Savarino, J., J. Kaiser, S. Morin, D. M. Sigman, and M. H. Thiemens, Nitrogen and oxygen isotopic constraints on the origin of atmospheric nitrate in coastal Antarctica, *Atmos. Chem. Phys.,*, *7*, 1925–1945, doi:10.5194/acp-7-1925-2007, 2007.

Savoie, D. L., J. M. Prospero, R. J. Larsen, and E. S. Saltzman, Nitrogen and sulfur species in aerosols at Mawson, Antarctica, and their relationship to natural radionuclides, *J. Atmos. Chem.*, *14*, 181–204, 1992.

Scaife, A. A., J. R. Knight, G. K. Vallis, and C. K. Folland, A stratospheric influence on the winter NAO and North Atlantic surface climate, *Geophys. Res. Lett.*, *321*, L18715, doi:10.1029/2005GL023226, 2005.

Schmidt, G. A., et al., Present-day atmospheric simulations using GISS ModelE: Comparison to in situ, satellite, and reanalysis data., *J. Climate*, *19*, 153–192, doi:10.1175/JCLI3612.1, 2006.

Schmittner, A., and E. D. Galbraith, Glacial greenhouse-gas fluctuations controlled by ocean circulation changes, *Nature*, *456*, 373–376, doi:10.1038/nature07531, 2008.

Schwerdtfeger, W., *Weather and Climate of the Antarctic: Developments in Atmospheric Science 15*, 261 pp., Elsevier, Amsterdam, 1984.

Shackleton, N. J., The 100,000-year ice-age cycle identified and found to lag temperature, carbon dioxide, and orbital eccentricity, *Science*, *289*, 1897–1902, doi:10.1126/science.289.5486.1897, 2000.

Shakun, J. D., and A. E. Carlson, A global perspective on Last Glacial Maximum to Holocene climate change, *Quaternary Sci. Rev.*, *29*, 1801–1816, doi:10.1016/j.quascirev.2010.03.016, 2010.

Shapiro, A. I., W. Schmutz, E. Rozanov, M. Schoell, M. Haberreiter, A. V. Shapiro, and S. Nyeki, A new approach to the long-term reconstruction of the solar irradiance leads to large historical solar forcing, *Astron. Astrophys.*, *529*, A67, doi:10.1051/0004-6361/201016173, 2011.

Siegenthaler, U., et al., Stable carbon cycle-climate relationship during the late Pleistocene, *Science*, *310*, 1313–1317, doi:10.1126/science.1120130, 2005.

Sigman, D. M., M. P. Hain, and G. H. Haug, The polar ocean and glacial cycles in atmospheric CO_2 concentration, *Nature*, *466*, 47–55, 2010.

Sime, L., E. Wolff, K. Oliver, and J. Tindall, Evidence for warmer interglacials in East Antarctic ice cores, *Nature*, *462*, 342–345, doi:10.1038/nature08564, 2009.

Simmonds, I., K. Keay, and E.-P. Lim, Synoptic activity in the seas around Antarctica, *Mon. Weather Rev.*, *131*, 272–288, doi:10.1175/1520-0493(2003)131$\langle$$0272:SAITSA$\rangle$$2.0.CO;2, 2003.

Simmons, A., D. Uppala, D. Dee, and S. Kobayashi, New ECMWF reanalysis products from 1989 onwards, *ECMWF Newsletter No. 110*, pp. 25–35, 2006.

Simon, K. J., J. B. Pedro, A. M. Smith, D. P. Child, and D. Fink, Reprocessing of ^{10}B-contaminated ^{10}Be AMS targets, *NIMB B*, submitted.

Sjolte, J., G. Hoffmann, J. Johnsen, B. M. Vinther, V. Masson-Delmotte, and C. Sturm, Modeling the water isotopes in Greenland precipitation 1959–2001 with the meso-scale model REMO-iso, *J. Geophys. Res.*, *D18105*, D18105, doi:10.1029/2010JD015287, 2011.

Skinner, L., Facing future climate change: is the past relevant?, *Phil. Trans. R. Soc. A*, *366*, 4627–4645, doi:10.1098/rsta.2008.0228, 2008.

Skinner, L. C., S. Fallon, C. Waelbroeck, E. Michel, and S. Barker, Ventilation of the deep Southern Ocean and deglacial CO_2 rise, *Science*, *328*, 1147–1151, doi:10.1126/science.1183627, 2010.

Slonosky, V., P. Jones, and T. Davies, Instrumental pressure observations and atmospheric circulation from the 17th and 18th centuries: London and Paris, *Int. J. Climatol.*, *21*(3), 285–298, doi:10.1002/joc.611, 2001.

Smith, A. M., D. Fink, D. Child, V. A. Levchenko, V. I. Morgan, M. Curran, D. M. Etheridge, and G. Elliott, ^{7}Be and ^{10}Be concentrations in recent firn and ice at Law Dome, Antarctica, *NIMB B*, *172*, 847–855, 2000.

Sodemann, H., and A. Stohl, Asymmetries in the moisture origin of Antarctic precipitation, *Geophys. Res. Lett.*, *36*, L22803, doi:10.1029/2009GL040242, 2009.

Sodemann, H., C. Schwierz, and H. Wernli, Interannual variability of Greenland winter precipitation sources: Lagrangian moisture diagnostic and North Atlantic Oscillation influence, *J. Geophys. Res.*, *113*, D03107, doi:10.1029/2007JD008503, 2008.

Sowers, T., and M. Bender, Climate records covering the last deglaciation, *Science*, *269*, 210–214, doi:10.1126/science.269.5221.210, 1995.

Staffelbach, T., B. Stauffer, A. Sigg, and H. Oeschger, CO_2 measurements from polar ice cores - More data from different sites, *Tellus B*, *43*, 91–96, doi:10.1034/j.1600-0889.1991.t01-1-00003.x, 1991.

Steffensen, J. P., et al., High-resolution Greenland ice core data show abrupt climate change happens in few years, *Science*, *321*, 680–684, doi:10.1126/science.1157707, 2008.

Steig, E. J., P. M. Grootes, and M. Stuiver, Seasonal precipitation timing and ice core records, *Science*, *266*, 1885–1886, doi:10.1126/science.266.5192.1885, 1994.

Steig, E. J., P. J. Polissar, M. Stuiver, P. M. Grootes, and R. C. Finkel, Large amplitude solar modulation cycles of ^{10}Be in Antarctica: Implications for atmospheric mixing processes and interpretation of the ice core record, *Geophys. Res. Lett.*, *23*, 523–526, doi:10.1029/96GL00255, 1996.

Steinhilber, F., J. Beer, and C. Fröhlich, Total solar irradiance during the Holocene, *Geophys. Res. Lett.*, *36*, L19704, doi:10.1029/2009GL040142, 2009.

Stenni, B., et al., Expression of the bipolar see-saw in Antarctic climate records during the last deglaciation, *Nat. Geosci.*, *4*, 46–49, doi:10.1038/ngeo1026, 2011.

Stier, P., et al., The aerosol-climate model ECHAM5-HAM, *Atmos. Chem. Phys.*, *5*, 1125–1156, 2005.

Stocker, T. F., and S. J. Johnsen, A minimum thermodynamic model for the bipolar seesaw, *Paleoceanography*, *18*(4), 1087, doi:10.1029/2003PA000920, 2003.

Stohl, A., Characteristics of atmospheric transport into the Arctic troposphere, *J. Geophys. Res.*, *111*, D11306, doi:10.1029/2005JD006888, 2006.

Stohl, A., and H. Sodemann, Characteristics of atmospheric transport into the Antarctic troposphere, *J. Geophys. Res.*, *115*, D02,305, doi:10.1029/2009JD012536, 2010.

Stouffer, R. J., D. Seidov, and B. J. Haupt, Climate response to external sources of freshwater: North Atlantic versus the Southern Ocean, *J. Climate*, *20*, 436, doi:10.1175/JCLI4015.1, 2007.

Swingedouw, D., T. Fichefet, H. Goosse, and M. F. Loutre, Impact of transient freshwater releases in the Southern Ocean on the AMOC and climate, *Clim. Dynam.*, *33*, 365–381, doi:10.1007/s00382-008-0496-1, 2009.

Taylor, K. C., et al., Abrupt climate change around 22 ka on the Siple Coast of Antarctica, *Quaternary Sci. Rev.*, *23*, 7–15, doi:10.1016/j.quascirev.2003.09.004, 2004.

Thornalley, D. J. R., I. N. McCave, and H. Elderfield, Freshwater input and abrupt deglacial climate change in the North Atlantic, *Paleoceanography*, *25*, PA1201, doi:10.1029/2009PA001772, 2010.

Timmermann, R., et al., A consistent data set of Antarctic ice sheet topography, cavity geometry, and global bathymetry, *Earth System Science Data*, *2*, 261–273, doi:10.5194/essd-2-261-2010, 2010.

Toggweiler, J. R., and D. W. Lea, Temperature differences between the hemispheres and ice age climate variability, *Paleoceanography*, *25*, PA2212, doi:10.1029/2009PA001758, 2010.

Trouet, V., J. Esper, N. E. Graham, A. Baker, J. D. Scourse, and D. C. Frank, Persistent positive North Atlantic Oscillation mode dominated the medieval climate anomaly, *Science*, *324*(5923), 78–80, doi:10.1126/science.1166349, 2009.

Tschumi, J., and B. Stauffer, Reconstructing past atmospheric CO_2 concentration based on ice-core analyses: open questions due to in situ production of CO_2 in ice, *J. Glaciol.*, *46*, 45–53, doi:10.3189/172756500781833359, 2000.

Turner, J., The El Niño-Southern Oscillation and Antarctica, *Int. J. Climatol.*, *24*, 1–31, doi:10.1002/joc.965, 2004.

Twomey, S., *Atmospheric Aerosols*, 302 pp., Elsevier, New York, NY, United States, 1977.

Uppala, S., D. Dee, S. Kobayashi, P. Berrisford, and A. Simmons, Towards a climate data assimilation system: status update of ERA-Interim, *ECMWF Newsletter No. 115*, pp. 12–18, 2008.

Usoskin, I. G., K. Alanko-Huotari, G. A. Kovaltsov, and K. Mursula, Heliospheric modulation of cosmic rays: Monthly reconstruction for 1951–2004, *J. Geophys. Res.*, *110*, A12108, doi:10.1029/2005JA011250, 2005.

Usoskin, I. G., S. K. Solanki, G. A. Kovaltsov, J. Beer, and B. Kromer, Solar proton events in cosmogenic isotope data, *Geophys. Res. Lett.*, *33*, L08107, doi:10.1029/2006GL026059, 2006.

Usoskin, I. G., K. Horiuchi, S. Solanki, G. A. Kovaltsov, and E. Bard, On the common solar signal in different cosmogenic isotope data sets, *J. Geophys. Res.*, *114*, A03112, doi:10.1029/2008JA013888, 2009.

Usoskin, I. G., G. A. Bazilevskaya, and G. A. Kovaltsov, Solar modulation parameter for cosmic rays since 1936 reconstructed from ground-based neutron monitors and ionization chambers, *J. Geophys. Res.*, *116*, A02104, doi:10.1029/2010JA016105, 2011.

van de Berg, W. J., M. R. van den Broeke, and E. van Meijgaard, Heat budget of the East Antarctic lower atmosphere derived from a regional atmospheric climate model, *J. Geophys. Res.*, *112*, D23101, doi:10.1029/2007JD008613, 2007.

van Ommen, T. D., and V. Morgan, Calibrating the ice core paleothermometer using seasonality, *J. Geophys. Res.*, *102*, 9351–9358, doi:10.1029/96JD04014, 1997.

van Ommen, T. D., and V. Morgan, Snowfall increase in coastal East Antarctica linked with southwest Western Australian drought, *Nat. Geosci.*, *3*, 267–272, doi:10.1038/ngeo761, 2010.

van Ommen, T. D., V. Morgan, and M. A. J. Curran, Deglacial and Holocene changes in palaeoaccumulation at Law Dome, East Antarctica, *Ann. Glaciol.*, *39*, 359–365, doi:10.3189/172756404781814221, 2004.

Vinther, B. M., S. J. Johnsen, K. K. Andersen, H. B. Clausen, and A. W. Hansen, NAO signal recorded in the stable isotopes of Greenland ice cores, *Geophys. Res. Lett.*, *30*(7), 1387, doi:10.1029/2002GL016193, 2003.

Vonmoos, M., J. Beer, and R. Muscheler, Large variations in Holocene solar activity: Constraints from ^{10}Be in the Greenland Ice Core Project ice core, *J. Geophys. Res.*, *111*, A10105, doi:10.1029/2005JA011500, 2006.

Wagenbach, D., Coastal Antarctica: Atmospheric chemical composition and atmospheric transport, in *NATO ASI Series, Series I, Vol. 43, Chemical exchange between the atmosphere and polar snow*, edited by Wolff, E. W. and Bales, R. C., pp. 173–199, Spinger-Verlag, 1996.

Wagenbach, D., U. Goerlach, K. Moser, and K. O. Muennich, Coastal Antarctic aerosol - The seasonal pattern of its chemical composition and radionuclide content, *Tellus B*, *40*, 426–436, 1988.

Wagenbach, D., M. Legrand, H. Fischer, F. Pichlmayer, and E. W. Wolff, Atmospheric near-surface nitrate at coastal Antarctic sites, *J. Geophys. Res.*, *103*, 11,007–11,020, doi:10.1029/97JD03364, 1998.

Weaver, A. J., O. A. Saenko, P. U. Clark, and J. X. Mitrovica, Meltwater Pulse 1A from Antarctica as a trigger of the Bølling-Allerød warm interval, *Science*, *299*, 1709–1713, doi:10.1126/science.1081002, 2003.

Webber, W. R., and P. R. Higbie, Production of cosmogenic Be nuclei in the Earth's atmosphere by cosmic rays: Its dependence on solar modulation and the interstellar cosmic ray spectrum, *J. Geophys. Res.*, *108*, 1355, doi:10.1029/2003JA009863, 2003.

Webber, W. R., and P. R. Higbie, What Voyager cosmic ray data in the outer heliosphere tells us about ^{10}Be production in the Earth's polar atmosphere in the recent past, *J. Geophys. Res.*, *115*, A05102, doi:10.1029/2009JA014532, 2010.

Webber, W. R., and J. A. Lockwood, Characteristics of the 22-year modulation of cosmic rays as seen by neutron monitors, *J. Geophys. Res.*, *93*, 8735–8740, doi:10.1029/JA093iA08p08735, 1988.

Webber, W. R., P. R. Higbie, and K. G. McCracken, Production of the cosmogenic isotopes ^{3}H, ^{7}Be, ^{10}Be, and ^{36}Cl in the Earth's atmosphere by solar and galactic cosmic rays, *J. Geophys. Res.*, *112*, A10106, doi:10.1029/2007JA012499, 2007.

Werner, M., U. Mikolajewicz, M. Heimann, and G. Hoffmann, Borehole versus isotope temperatures on Greenland: Seasonality does matter, *Geophys. Res. Lett.*, *27*, 723–726, doi:10.1029/1999GL006075, 2000.

White, J. W. C., L. K. Barlow, D. Fisher, P. Grootes, J. Jouzel, S. J. Johnsen, M. Stuiver, and H. Clausen, The climate signal in the stable isotopes of snow from Summit, Greenland: results of comparisons with modern climate observations, *J. Geophys. Res.*, *102*(26), 425–439, 1997.

Wolff, E. W., The record of aerosol deposited species in ice cores and problems of interpretation, in *NATO ASI Series, Vol. I 43, Chemical Exchange Between the Atmosphere and Polar Snow*, edited by E. Wolff and R. Bales, pp. 1–17, Springer, 1996.

Wolff, E. W., History of the atmosphere from ice cores, in *From weather forecasting to exploring the solar system*, vol. 4, edited by C. Boutron, pp. 147–177, EDP Sciences, Les Ulis, France, 2000.

Wolff, E. W., Greenhouse gases in the Earth system: a palaeoclimate perspective, *Philos Trans. R. Soc. A.*, *369*(1943), 2133–2147, doi:10.1098/rsta.2010.0225, 2011.

World Meteorological Organisation, Meteorology - A three dimensional science: Second session of the Commission for Aerology, *WMO Bulletinb*, *4*, 134–138, 1957.

Yiou, F., et al., Beryllium 10 in the Greenland Ice Core Project ice core at Summit, Greenland, *J. Geophys. Res.*, *102*, 26,783–26,794, doi:10.1029/97JC01265, 1997.

Zängl, G., and K. P. Hoinka, The tropopause in the polar regions., *J. Climate*, *14*, 3117–3139, doi:10.1175/1520-0442(2001)014$\langle$$3117:TTITPR$\rangle$$2.0.CO;2, 2001.